Master's Thesis

Master's Programme in Theoretical and Computational Methods

From Quantum Entanglement to Interactions of Elementary Excitations in Coupled Spin Chains

An Introduction to Numerical Many-Body Physics with Matrix Product States and Tensor Networks

MARCEL NIEDERMEIER

August, 2021

Supervisor: ESKO KESKI-VAKKURI
Examiners: ESKO KESKI-VAKKURI, DAVID WEIR

University of Helsinki
Faculty of Science

HELSINGIN YLIOPISTO
HELSINGFORS UNIVERSITET
UNIVERSITY OF HELSINKI
MATEMAATTIS-LUONNONTIETEELLINEN TIEDEKUNTA
MATEMATISK-NATURVETENSKAPLIGA FAKULTETEN
FACULTY OF SCIENCE

Tiedekunta – Fakultet – Faculty	Koulutusohjelma – Utbildningsprogram – Degree programme
Faculty of Science	Master's Programme in Theoretical and Computational Methods

Tekijä – Författare – Author
Marcel Niedermeier

Työn nimi – Arbetets titel – Title
From Quantum Entanglement to Interactions of Elementary Excitations in Coupled Spin Chains

Työn laji – Arbetets art – Level	Aika – Datum – Month and year	Sivumäärä – Sidoantal – Number of pages
Master's degree	August 2021	206

Tiivistelmä – Referat – Abstract

Matrix product states provide an efficient parametrisation of low-entanglement many-body quantum states. In this thesis, the underlying theory is developed from scratch, requiring only basic notions of quantum mechanics and quantum information theory. A full introduction to matrix product state algebra and matrix product operators is given, culminating in the derivation of the density matrix renormalisation group algorithm. The latter provides a simple variational scheme to determine the ground state of arbitrary one-dimensional many-body quantum systems with supreme precision.

As an application of matrix-product state technology, the kernel polynomial method is introduced in detail as a state-of-the art numerical tool to find the spectral function or the dynamical correlator of a given quantum system. This in turn gives access to the elementary excitations of the system, such that the locations of the low-energy eigenstates can be studied directly in real space.

To illustrate those theoretical tools concretely, the ground state energy, the entanglement entropy and the elementary excitations of a simple interface model of a Heisenberg ferromagnet and a Heisenberg antiferromagnet are studied. By changing the location of the model in parameter space, the dependence of the above-mentioned quantities on the transverse field and the coupling strength is investigated. Most notably, we find that the entanglement entropy characteristic to the antiferromagnetic ground state stretches across the interface into the ferromagnetic half-chain. The dependence of the physics on the value of the coupling strength is, overall, small, with exception of the appearance of a boundary mode whose eigenenergy grows with the coupling. A comparison with a localised edge field shows however that the boundary mode is a true interaction effect of the two half-chains.

Various algorithmic and physics extensions of the present project are discussed, such that the code written as part of this thesis could be turned into a state-of-the-art MPS library with managable effort. In particular, an application of the kernel polynomial method to calculate finite-temperature correlators is derived in detail.

Avainsanat – Nyckelord – Keywords
tensor networks, matrix product states, matrix product operators, spin chains, Heisenberg model, entanglement entropy, DMRG, kernel polynomial method, computational condensed matter physics

Säilytyspaikka – Förvaringställe – Where deposited
Kumpula Campus Library

Contents

Acknowledgements

I want to thank my supervisor Esko Keski-Vakkuri for providing the initial spark which led me to the study of tensor networks and matrix product states, and for valuable discussions throughout the process of writing this thesis. The same holds true for the members of our small (virtual) group meetings: Otto Veltheim, Jani Kastikainen and Guillermo Garcia-Perez. Thanks for the interesting discussions we've had and the input you gave me! My future PhD advisors, Jose Lado and Christian Flindt, deserve my special thanks for providing additional ideas and feedback. Furthermore, I want to thank David Weir for (proof-)reading and examining this thesis at short notice. Thanks as well to my friend Alex Rawlings who proofread the whole thing (and found many typos)!

Finally, I want thank lecturers around the world who are making their lectures and lecture materials accessible online, and helped develop my understanding of tensor networks and condensed matter physics. Personally, I believe that (good) lectures are and remain a fantastic way to acquire new knowledge, and as such deserve to be shared beyond the boundaries of one's own university. Even though the Covid-19 pandemic has had the side effect of increasing the abundance and the quality of online learning materials, it is my hope that this trend continues in the future and helps unite students around the world.

Part I

Introduction and Motivation

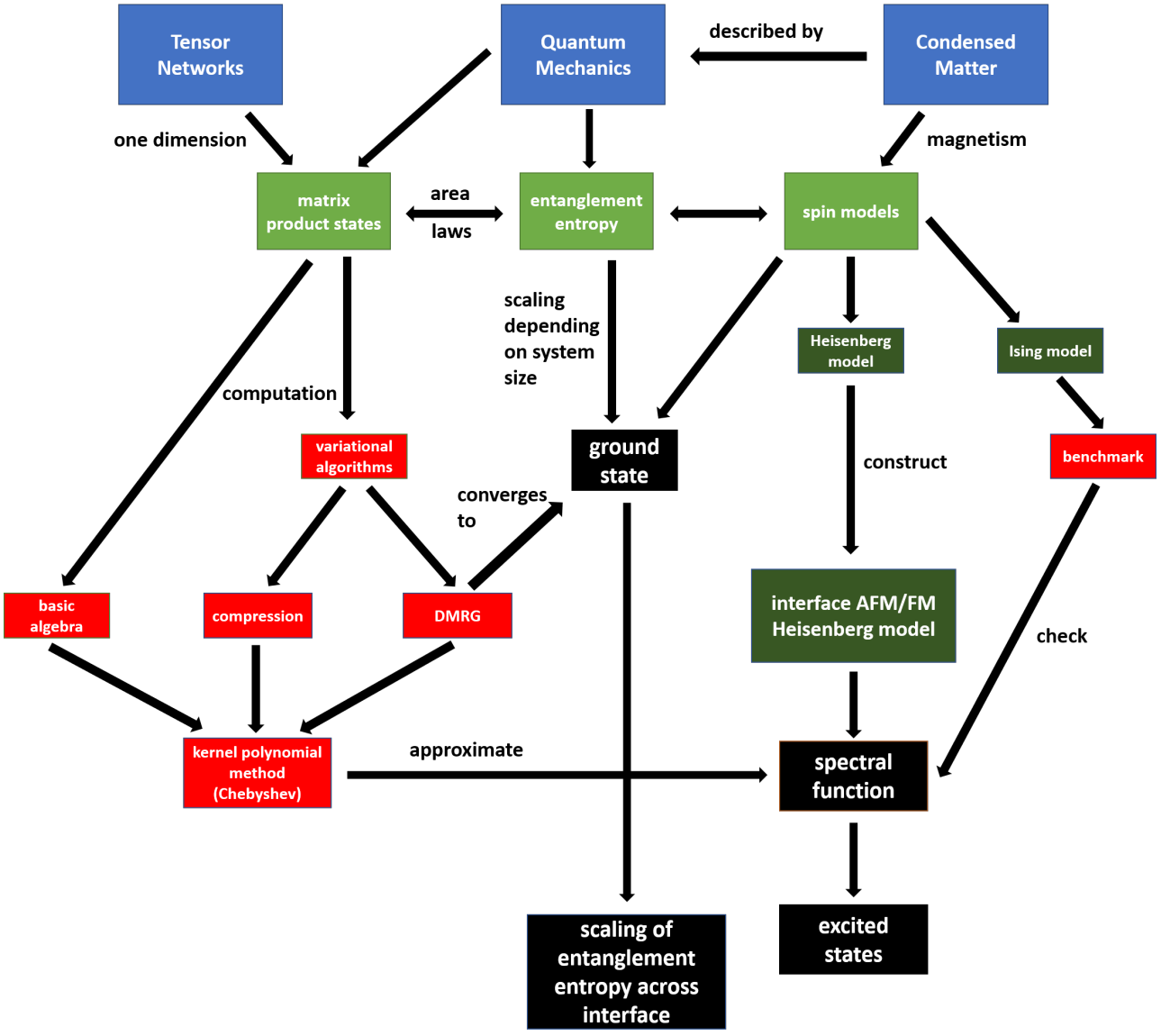

1 Introduction

Simulations of condensed matter systems are of utmost importance in both fundamental and applied physics. The need for accurate studies, capturing the effects of macroscopic numbers of interacting constituents, reaches from the engineering of new, exotic materials, such as high-temperature (cf. ref. [1]) and topological superconductors (cf. ref. [2, 3]), or topological qubits (cf. refs. [4, 5, 6]), to the understanding of the most basic properties of matter. Phenomena such as magnetism have been familiar to mankind since antiquity, but could only be explained and understood due to the advent of quantum theory, in combination with the analysis of large, interacting quantum systems.

However, studying large quantum systems is hard. In fact, it is exponentially hard, as the dimension of the Hilbert space that needs to be explored is exponential in the number of its constituent spaces. This severely limits the possibilities of solving quantum systems directly - even with the most powerful available computing resources, understanding the interactions of more than of the order of thirty to forty individual particles becomes effectively intractable, do to the exponentially large memory requirements. Different methods are therefore needed in order to explore system sizes beyond this intermediate scale, and thus to at least approximate the large-scale properties arising through the passage to the thermodynamic limit.

In recent decades, the study of quantum information theory (cf. ref. [7]) has opened a new perspective on condensed matter physics (cf. ref. [8]). Based on measures of information such as the von Neumann entropy, a classification of many-body states in terms of their entanglement entropy, i.e. their content in non-classical correlations, is now possible. The observation that for many Hamiltonians of interest, the ground state entanglement entropy tends to be significantly lower than that of a random state (cf. ref. [9]), implies that those states can efficiently be described by a much smaller number of parameters, than the exponential size of the corresponding Hilbert space would naively suggest. This fact has led to the introduction of "matrix product states" (cf. refs. [10, 11, 12]), which are constructed to approximate those low-entanglement states optimally, incurring only a minimal loss of information. Requiring a number of parameters scaling linearly with the system size (cf. ref. [13]), matrix product states therefore incite us to tackle the simulation of much larger quantum systems, and provide the crucial stepping stone in obtaining information about the behaviour of the system in the thermodynamic limit.

In this thesis, we introduce the language of matrix product states from scratch, in the hope of developing a suitable road map for newcomers in the field. We supply the necessary background in quantum mechanics and quantum information theory and study numerous examples in the simulation of one-dimensional quantum spin chains, indic-

ating links to more advanced topics of research where appropriate. Special emphasis will be given to calculating the dynamical correlator - the spectral function - of a system, which can be approximated to the desired accuracy with the kernel polynomial method (cf. ref. [14]). The latter, being a recent and versatile tool, connects introductory aspects to cutting-edge topics in modern computational condensed matter research.

As an application of the technology discussed in this thesis, we analyse an example of an antiferromagnetic Heisenberg spin chain coupled to a ferromagnetic Heisenberg spin chain in one dimension. This is a basic model of a heterogeneous material, characterised through spinon excitations in the antiferromagnetic part and magnon excitations in the ferromagnetic part. The study of such heterosystems is of great interest in current condensed matter research, as it constitutes a way of probing the presence of potentially exotic boundary modes at the interface between the two systems. Similar studies have already been realised for more complicated interfaces, such as a heterostructure of a superconductor and a quantum antiferromagnet [15], which found the existence of robust in-gap modes at the boundary. To our knowledge, albeit being a structurally much simpler model, the heterostructure defined above hasn't yet been studied in the literature, and we therefore hope it serves as a complement to the understanding of more complex interface models.

1.1 Aim of the Present Work

This thesis has multiple goals. First and foremost - as this is a research work - we want to analyse a problem relevant to current, cutting-edge condensed matter physics. Despite being a structurally simple model, the interface of a Heisenberg ferromagnet and a Heisenberg antiferromagnet doesn't admit analytical solutions, and therefore provides an ideal test subject for the numerical methods discussed in this work.

However, of almost equal importance, we want to give a pedagogical introduction to current state-of-the-art numerical methods employed in computational condensed matter studies. In particular, we expose a detailed reformulation of many-body quantum physics in terms of matrix product states and present the kernel polynomial method as a highly accurate application thereof. Unfortunately, few texts exist which help newcomers in the field in setting up their own working tensor network algorithms from scratch. In this sense, we hope to "bridge the gap" between the already existing reviews, the original research literature and the knowledge in quantum mechanics beginning graduate students typically have.

Last but not least, we also aim at presenting some important calculations relevant to introductory condensed matter problems in an accessible manner. In particular, we want

to focus on the usage of a quasiparticle-picture and investigate how it helps us to understand the spectrum of a given Hamiltonian. Often - and rightfully so -, those results are taken for granted. Nevertheless, these are important techniques at the basis of analytical condensed matter studies, and we believe that augmenting this thesis by said calculations will provide a useful guide for readers to help them navigate between analytical approaches, numerical calculations and the theoretical foundations of the latter. To keep the main body of this more concise, some of those calculations have however been deferred to the appendix.

2 Matrix Product States and Spin Chains - a Bird's Eye View

Having introduced the central goals of this thesis, it will be helpful to give a lightning summary of its contents and inter-dependencies before commencing the main body of the text. The aim of this "bird's eye view" is to supply the motivations which imply the order in which the topics are presented here, to help the reader navigate through this work.

2.1 Outline of the Thesis

We will start in **chapter 3** by introducing necessary notions from quantum mechanics and quantum information theory. Those provide the basis to describe the physics of quantum condensed matter models. In addition, we will discuss an entanglement-based state truncation prescription. **Chapter 4** directly builds on those ideas and defines the Heisenberg and Ising quantum spin chains, which are our main quantum systems of interest. For both models, we outline the analytic solutions to some detail. Especially in the case of the Ising model, this will serve us as an ideal benchmark model to test the correctness of our numerical methods. We close chapter 4 by investigating the scaling of the entanglement entropy in spin chains, which provides the motivation for a more general class of scaling laws, known as area laws. In particular, we will find that for models such as the Ising and Heisenberg models, the entanglement entropy in the ground state is "small".

Matrix product states will then be introduced in **chapter 5** as a re-parametrisation of a "full" quantum many-body state. The connection between matrix product states and quantum spin models is provided through the entanglement entropy, to which matrix product states offer a direct access. Most importantly, matrix product states are constructed such that the information contained in a many-body quantum state can be compressed ideally. Every operation from "standard" quantum mechanics can be translated into matrix product language, and we will expose the central matrix product state manipulations. To conclude chapter 6, we discuss the implementation of physically relevant Hamiltonian operators as matrix product operators. Once these basic notions have been developed, we introduce the class of variational algorithms in **chapter 6**. This gives rise in particular to the density matrix renormalisation group, which enables us to find the ground state of a given spin model with supreme accuracy. Knowledge of the ground state will furthermore allow us to calculate the spectral function of the model, which is described in **chapter 7**. There, we introduce the kernel polynomial method, which is based on recursive calculations performed on the ground state. Analysing the spectral function will then provide us with a way of studying the localisation of the elementary

excitations in real and, if one desires so, momentum space.

Having established the necessary theoretical background, **chapter 8** then provides extensive benchmark studies on the Ising and Heisenberg models, in order to assess the correct working of the matrix product state methods presented here. Furthermore, this will define suitable ranges of parameters, which we will employ in **chapter 9** to study the interface of the Heisenberg ferromagnet and Heisenberg antiferromagnet. Mainly, we will focus on determining the ground state energy, the entanglement in the ground state and the localisation of the elementary interactions, and how they depend on the parameters of the model.

We conclude this thesis by presenting a detailed outlook on further improvements and other aspects relevant for future studies in **chapter 10**. The most immediate improvement would be to study the finite-temperature spectral function, which can be found with very similar methods as the zero-temperature spectral function, and which we will calculate in a future work. **Chapter 11** presents the conclusion of this thesis.

Several further details are provided in the **appendix**. One the one hand, we present a lightning-fast review of the infinite density matrix renormalisation group, the time-evolution of matrix product states and temperature-dependent matrix product states. While these aren't employed explicitly in this work, they do provide the motivation for *why* certain algorithms we *did* use outperform their "more naive" alternatives, and therefore deserve to be at least mentioned. On the other hand, we will present some of the analytical calculations of the main body in more detail, in order to give the reader the opportunity to reproduce them. Finally, we will mention some basic aspects of programming with matrix product states and implementing exact diagonalisation methods.

2.2 Resources and Recommended Reading

Given the vast available literature about quantum spin chains, matrix product states and computational quantum physics in general, we feel that it will be useful to indicate to the reader several resources which we deem especially enlightening or rewarding. As one of our hopes is that this thesis also serves as a pedagogical introduction and road map in this field, it is only fair to highlight with special care works which have been written in a spirit similar to ours.

Furthermore, we would also like to stress that a majority of this thesis can be considered a literature review, and in this sense reflect the author's own learning process. Apart from (re-)assembling puzzle pieces in an order that we deem logical and accessible, the presentation of most of the topics here is far from original. We have therefore attempted

to not only reference our resources throughout this text, but also to indicate the main sources of each chapter in the respective opening paragraphs.

Many textbooks exist on quantum mechanics, and finding a textbook to one's liking in this area is rather a personal choice. However, there is far less quantum mechanics literature with an interface to quantum information. Our main source here was the reference work by Nielsen and Chuang [7]. For a first exposure to quantum spin chains and their analytic solutions, we recommend the book "An Introduction to Quantum Spin Systems" by Parkinson and Farnell [16]. Ideally, it is supplemented by the original literature, such as the landmark papers by Lieb, Schultz and Mattis [17] or Pfeuty [18], studying the analytical solutions of the Heisenberg XY and transverse field Ising models, respectively. Despite having reached a certain age, they remain readable and enlightening. A nice account of the Bethe ansatz to solve the Heisenberg model is furthermore presented in the review "Introduction to the Bethe Ansatz" by Karabach and Müller [19, 20, 21], which served as our main source to discuss the latter. Analytical studies of the entanglement entropy in quantum spin chains are rather recent, and the calculation presented here is modelled after the work of Latorre, Rico, Vidal and Kitaev [22, 23].

In contrast, few textbooks exist on tensor networks, and the available literature is mostly hidden in review articles. One especially good text is Schollwöcks's review [12]. Others include Orús' introduction to tensor network methods [24]. Furthermore, the lectures by Jan von Delft [25] and Guifre Vidal [26] are outstanding presentations of matrix product state and tensor network techniques. The logic behind both lecture series has had a considerable impact on the presentation in this thesis. As for the kernel polynomial method, we have exclusively employed the initial presentation by Weiße et al. [14], and the application of the method to matrix product states ("CheMPS") by Holzner et al. [27]. Both of these articles are written in a very readable and accessible manner, and we highly recommend consulting them for further details.

Part II

Theoretical Background

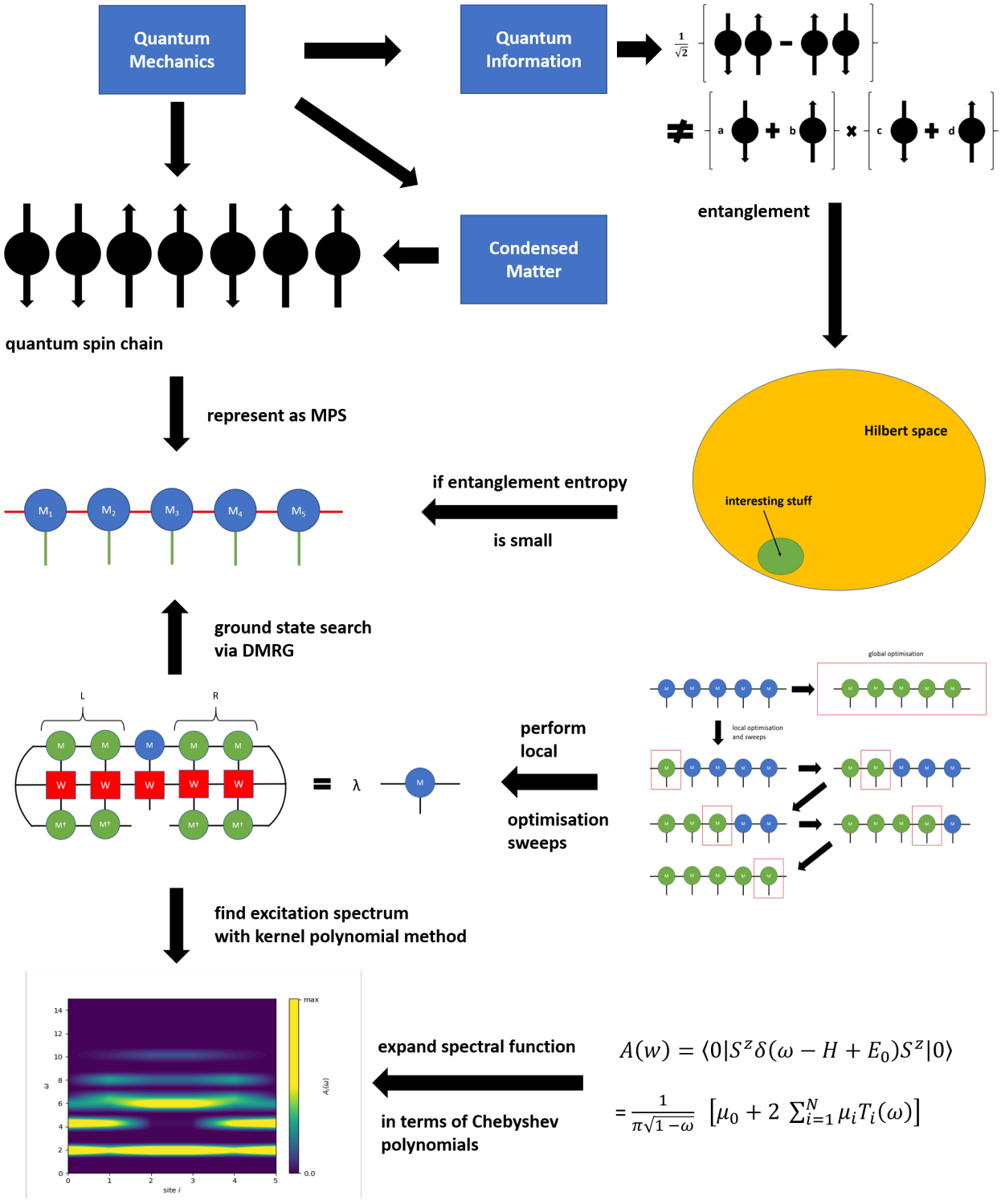

3 Notions of Quantum Mechanics and Quantum Information Theory

In this introductory chapter, we remind the reader of the notions of quantum mechanics and quantum information that will later motivate the definition (and usefulness!) of matrix product states. After introducing the basic description of quantum systems and explaining what it means to "solve" a given quantum system, we will shift our attention to many-body systems. As we will show, composing multiple quantum systems implies the existence of so-called "entangled" and "product" states. In order to quantify the amount of entanglement in a state, we will define the entanglement entropy. Using the Schmidt decomposition, we will be able to introduce a truncation prescription of states, which will turn out to be equivalent to cutting high-entanglement degrees of freedom. Finally, we remind the reader of creation and annihilation operators as the suitable language to describe (quasi-)particles in quantum systems.

Ideas in this chapter that go beyond what can be considered standard quantum mechanics knowledge are mainly based on refs. [7, 25, 28].

3.1 Basic Ideas - Solving Quantum Systems

Any well-defined quantum system can be described in a suitable **Hilbert space** $\mathcal{H}$. In this thesis, we will only work with finite-dimensional, discrete quantum systems. Fixing a basis, we can thus completely describe the N-dimensional state space as follows:

$$\mathcal{H} = \text{span}\{|i\rangle \,|1 \leq i \leq N\} \iff \dim \mathcal{H} = N. \tag{3.1}$$

A quantum state of that system is then given through any normalised linear combination of the basis vectors:

$$|\psi\rangle = \sum_{i=1}^{N} C_i \,|i\rangle\,, \quad \text{with} \quad \sum_{i=1}^{N} |C_i|^2 = 1, \tag{3.2}$$

where the coefficients C_i are called the **wave function** of the system. The **norm** of a quantum state is defined via the the inner product of the Hilbert space in question:

$$||\,|\psi\rangle\,||^2 = \langle\psi|\psi\rangle = \sum_{i,j=1}^{N} C_i^* C_j \,\langle i|j\rangle = \sum_{i=1}^{N} |C_i|^2, \tag{3.3}$$

which furthermore allows us to introduce a notion of **orthonormality**. Considering a system prepared in the general superposition state $|\psi\rangle$, one can then connect this mathematical model to the physical reality of a state by admitting that the absolute value squared $|C_i|^2$ of the coefficient C_i yields the probability p_i to measure a system in the basis state $|i\rangle$. Requiring that any well-defined probability distribution be normalised

to one on its support is therefore the physical justification for the normalisation of the quantum states:

$$\sum_{i=1}^{N} p_i = \sum_{i=1}^{N} |C_i|^2 = 1. \tag{3.4}$$

In many cases, one can immediately write down a basis determined by the setup of the system, e.g. the different spin orientations for coupled spins. This is however not necessarily the (most) suitable basis in which the physics and the dynamics of the system should be studied. The central problem of solving quantum systems is thus to identify such a suitable basis in which the state $|\psi\rangle$ can be expanded.

In order to connect this to **physical observables**, we introduce **hermitian operators** A on quantum systems as linear maps

$$A : \mathcal{H} \to \mathcal{H}. \tag{3.5}$$

The reason for restricting our attention to hermitian operators is that they always admit a spectral decomposition with real eigenvalues a_i, and their eigenbasis spans the Hilbert space which they act upon. By the **measurement postulate** of quantum mechanics, measuring an operator on a given quantum state prompts the state to collapse into one of the eigenvectors of the operator, with a probability given by the expansion coefficient of that eigenstate. We can therefore refine our above assertion: solving a finite-dimensional quantum system is equivalent to the diagonalisation of an operator of physical interest. While this is mathematically - at least in principle - a well-understood problem, actually carrying out this diagonalisation is the bottleneck for most large scale quantum computations.

Given an operator and a quantum state, the statistical **expectation value** of the outcome of measuring the operator is easily obtained by expressing the state in the (orthonormal) eigenbasis of the operator:

$$\langle\psi|A|\psi\rangle = \sum_{i,j=1}^{N} C_i^* C_j \langle i|A|j\rangle = \sum_{i,j=1}^{N} C_i^* C_j a_i \langle i|j\rangle = \sum_{i=1}^{N} |C_i|^2 a_i = \sum_{i=1}^{N} p_i a_i \equiv \langle A\rangle, \tag{3.6}$$

where the penultimate expression justifies the interpretation of the overlap $\langle\psi|A|\psi\rangle$ as a statistical expectation value $\langle A\rangle$.

The most important operator on a given Hilbert space is the **Hamiltonian operator** H, which describes the energy of the system. Its usefulness is motivated by the fact that the Hamiltonian generates time-translations of quantum systems through the **Schrödinger equation**:

$$-i\frac{d}{dt}|\psi\rangle = H|\psi\rangle. \tag{3.7}$$

For time-independent Hamiltonians, the Schrödinger equation can easily be solved by considering separable states, thus yielding the **time-evolution operator** $U(t)$:

$$|\psi(t)\rangle = e^{-iHt}\,|\psi(0)\rangle \equiv U(t)\,|\psi(0)\rangle\,, \tag{3.8}$$

where the matrix exponential $\exp(-iHt)$ is by construction a **unitary operator**. Suppose we know the spectral decomposition of the Hamiltonian; then we may expand a general quantum state in the energy eigenbasis $\{|E_i\rangle\}$:

$$|\psi\rangle = \sum_{i=1}^{N} C_i\,|i\rangle = \sum_{i=1}^{N} D_i\,|E_i\rangle\,. \tag{3.9}$$

Performing a time evolution becomes then a trivial task, as the Hamiltonian in the matrix exponential can be replaced with its respective energy eigenvalues for each state:

$$|\psi(t)\rangle = e^{-iHt}\,|\psi\rangle = \sum_{i=1}^{N} D_i e^{-iHt}\,|E_i\rangle = \sum_{i=1}^{N} D_i e^{-iE_i t}\,|E_i\rangle \equiv \sum_{i=1}^{N} D_i(t)\,|E_i\rangle\,, \tag{3.10}$$

where the whole time dependence has been absorbed in the expansion coefficients. Furthermore, the Hamiltonian is at the origin of **temperature-dependent quantum states**[1]. Intuitively speaking, the higher the temperature, the more of the lowest-lying energy eigenstates will be excited with a non-negligible statistical weight. For our purposes, "solving a quantum system" will therefore mean finding the spectral decomposition of the Hamiltonian of the system.

It is however possible to simplify this task in the presence of additional symmetries. A **symmetry** A of a Hamiltonian H is an operator that commutes with the Hamiltonian:

$$[H, A] = 0. \tag{3.11}$$

This implies that both operators share a common eigenbasis $\{|E_i, A_j\rangle\}$, such that

$$H\,|E_i, A_j\rangle = E_i\,|E_i, A_j\rangle\,, \quad A\,|E_i, A_j\rangle = A_j\,|E_i, A_j\rangle\,. \tag{3.12}$$

In this basis the Hamiltonian must therefore have a block-diagonal structure (organised in blocks of different quantum numbers A_j), as the action of H on one of the basis vectors $|E_i, A_j\rangle$ cannot change the A_j-value of this state:

$$H = \begin{bmatrix} \begin{bmatrix} A_1 \end{bmatrix} & & & 0 \\ & \begin{bmatrix} A_2 \end{bmatrix} & & \\ & & \ddots & \\ 0 & & & \begin{bmatrix} A_n \end{bmatrix} \end{bmatrix}. \tag{3.13}$$

[1] More details about how to construct a quantum state at finite temperature in the canonical ensemble are given in the appendix.

Instead of diagonalising the whole Hamiltonian matrix, one can therefore study each decoupled subspace separately.

The framework presented here is of course completely general. In practice, one first has to write down a suitable Hamiltonian before even attempting to diagonalise it. Finding the Hamiltonian, however, is in most cases not the difficult part, as microscopic interactions and couplings between quantum systems are often well-understood.

3.1.1 Density Operators

Before passing to many-body systems, we will the define the important notion of a **density operator**. The language of density operators is an entirely equivalent description of a given quantum system in comparison to the language of quantum states. In addition, however, it allows us to also describe **statistical mixtures** of quantum states.

If we consider a given quantum state $|\psi\rangle$, its corresponding density operator ρ is defined through the outer product

$$\rho \equiv |\psi\rangle\langle\psi| = \left[\sum_{i=1}^{N} C_i |i\rangle\right]\left[\sum_{j=1}^{N} C_j^* \langle j|\right] = \sum_{i,j=1}^{N} C_i C_j^* |i\rangle\langle j| \equiv \sum_{i,j=1}^{N} \rho_{ij} |i\rangle\langle j|, \tag{3.14}$$

where the matrix elements ρ_{ij} in a given basis follow immediately from the decomposition of the state in that basis. Now imagine a situation where one doesn't know which quantum state one has to deal with; such as a photon source emitting different photon states with different probabilities. The best possible description of the system is then to write down a linear combination of the corresponding density matrices, as follows:

$$\rho = \sum_i p_i |\psi_i\rangle\langle\psi_i|, \quad \text{with} \quad \sum_i p_i = 1. \tag{3.15}$$

Such a state is referred to as a **mixed state**, as opposed to a **pure state** for which only one of the probabilities p_i is non-trivial (and thus equal to one).

From the definition of the density operator, one can immediately show that it is hermitian and has a trace equal to one. One can furthermore express all the standard notions of quantum mechanics in density operator language; the expectation value of an operator A in the state ρ follows for instance as

$$\langle A\rangle = \mathrm{Tr}\,(\rho A). \tag{3.16}$$

3.2 Many-Particle Systems

Now we will introduce **combined and coupled quantum systems**, whose study is of course motivated by the fact that many physically relevant systems arise through the interplay of their constituents, such as atoms or elementary particles. In the following, we

will always work with two coupled systems, so-called **bipartite systems**, as any product of more systems can always be reduced to a succession of subsequent bipartite products.

Consider two different quantum systems, $\mathcal{H}_A$ and $\mathcal{H}_B$, of dimension N and M, respectively:

$$\mathcal{H}_A = \text{span}\{|a_1\rangle, |a_2\rangle, ..., |a_N\rangle\}, \quad \mathcal{H}_B = \text{span}\{|b_1\rangle, |b_2\rangle, ..., |b_M\rangle\}. \tag{3.17}$$

For each basis state of $\mathcal{H}_A$, $\mathcal{H}_B$ can be in any of its basis states. Thus the combined quantum system is $N \cdot M$-dimensional. Mathematically speaking, the **tensor product** of vector spaces provides exactly the product-like structure that we need to combine quantum systems[2]. We say that our quantum states live in a **product space**, and are acted on by **product operators**. The joint basis is therefore entirely specified by enumerating all possible combinations of the basis vectors:

$$\mathcal{H}_A \otimes \mathcal{H}_B = \text{span}\{|a_i\rangle \otimes |b_j\rangle \equiv |a_i b_j\rangle \,|1 \leq i \leq N;\, 1 \leq j \leq M\}. \tag{3.18}$$

Every state in the new system can now be expressed as a linear combination of those basis vectors:

$$|\psi_{AB}\rangle = \sum_{i=1}^{N}\sum_{j=1}^{M} C_{ij} |a_i b_j\rangle . \tag{3.19}$$

Similarly, operators can be denoted as tensor products as well:

$$U_{AB} = U_A \otimes U_B. \tag{3.20}$$

This notation is to be understood such that U_A only acts on states living in $\mathcal{H}_A$, whereas U_B acts on the states in $\mathcal{H}_B$. Letting U_{AB} act on the general bipartite state, we obtain

$$U_{AB} |\psi_{AB}\rangle = U_A \otimes U_B \sum_{i=1}^{N}\sum_{j=1}^{M} C_{ij} |a_i b_j\rangle = \sum_{i=1}^{N}\sum_{j=1}^{M} C_{ij} U_A |a_i\rangle \otimes U_B |b_j\rangle . \tag{3.21}$$

This equation now only contains operators in a single Hilbert space acting on single basis vectors, whose images we suppose are known by the definition of the operators.

While the notation to describe composite quantum system becomes somewhat more cumbersome, it is important to realise that we haven't changed the way in which quantum mechanics works, in comparison to the general principles described before. Indeed, one could equally well redefine the index pairs (i, j) as a single composite index α, which runs from 1 to $N \cdot M$:

$$|\psi_{AB}\rangle = \sum_{\alpha=1}^{N\cdot M} C_\alpha |\alpha\rangle , \tag{3.22}$$

and thus recover the "single-space" picture.

[2] As opposed, for instance, to the direct sum of vector spaces.

3.2.1 Subsystems and Reduced Density Operators

Whenever we are dealing with composite quantum systems, it can be interesting to study only a certain **subsystem** - think, for instance, of a principal system coupled to a reservoir, and we somehow want to "average" over the degrees of freedom of the reservoir. In general, we can consider an arbitrary state, spanned by two coupled quantum systems $\mathcal{H}_A$ and $\mathcal{H}_B$:

$$|\Psi_{AB}\rangle = \sum_{i,j} C_{i,j} |i_A\rangle |j_B\rangle \iff \rho = |\Psi_{AB}\rangle \langle\Psi_{AB}| \tag{3.23}$$

What we would like to do is to perform a measurement on only one of the systems, say, system A. Defining an operator that is non-trivial only on A by $O_A \equiv O \otimes I$, we obtain its expectation value as:

$$\begin{aligned}
\langle O_A\rangle &= \mathrm{Tr}(\rho O_A) = \sum_{i,j} \langle j_B| \langle i_A| \rho O_A |i_A\rangle |j_B\rangle \\
&= \sum_{i,j}\sum_{k,l} \langle j_B| \langle i_A|\rho|k_A\rangle |l_B\rangle \langle l_B| \langle k_A|O_A|i_A\rangle |j_B\rangle \\
&= \sum_{i,j}\sum_{k,l} \langle j_B| \langle i_A|\rho|k_A\rangle |l_B\rangle \langle k_A|O|i_A\rangle \delta_{jl} \\
&= \sum_i \langle i_A| \underbrace{\left[\sum_j \langle j_B|\rho|j_B\rangle\right]}_{\rho_A} O |i_A\rangle \equiv \sum_i \langle i_A| \underbrace{\rho_A O}_{\in \mathcal{H}_A} |i_A\rangle = \mathrm{Tr}_A(\rho_A O).
\end{aligned} \tag{3.24}$$

In the last term, we have defined the **reduced density operator**:

$$\rho_A = \sum_j \langle j_B|\rho|j_B\rangle = \mathrm{Tr}_B(\rho). \tag{3.25}$$

Tracing over the B-basis - "tracing out" the system B - thereby defines an object which behaves exactly like the "full" density operator, but without the degrees of freedom relative to the other subsystem. This operation of including only one of the systems in the trace is called "taking the **partial trace**".

3.2.2 The Schmidt Decomposition

Aside - Singular Value Decomposition

Let A be a $N \times M$ matrix. Then there exists the **singular value decomposition** (SVD):

$$A = USV^\dagger. \tag{3.26}$$

It has the following properties:

- The transformation matrices U and $V^\dagger$ obey the relations $U^\dagger U = I$ and $V^\dagger V = I$; however $UU^\dagger = I$ and $VV^\dagger = I$ do *not* hold in general (they are not unitary).
- S is a square and diagonal matrix:

$$S = \text{diag}(s_1, s_2, ..., s_r, 0, 0, ..., 0).$$

  The diagonal entries s_i of S are the **Schmidt coefficients**, and the number of non-zero Schmidt coefficients in the **Schmidt rank**. They are positive and ordered by magnitude in decreasing order.
- The dimensions and shapes of the three matrices depend on the dimensions and shape of A. If $N \leq M$, then U and S are of dimension $N \times N$, whereas $V^\dagger$ is rectangular of dimension $N \times M$. In contrast, if $N \geq M$, then U is rectangular of dimension $N \times M$, whereas S and $V^\dagger$ are square of dimension $M \times M$ Fig. 1 represents this pictorially.

Considering again a state in a bipartite quantum system,

$$|\Psi_{AB}\rangle = \sum_{i,j} C_{ij} |i_A\rangle |j_B\rangle , \tag{3.27}$$

we note at this point that there is a way of rewriting this decomposition which is more useful for many considerations we will discuss in the next chapters. The derivation of this so-called **Schmidt decomposition** is an easy exercise of applying an SVD to the coefficient matrix C_{ij}:

$$|\Psi\rangle = \sum_{i,j} \sum_{k} \overbrace{U_{ik} S_{kk} V^\dagger_{kj}}^{C_{ij}} |i_A\rangle |j_B\rangle = \sum_{i,j} \sum_{k} U_{ik} s_k V^\dagger_{kj} |i_A\rangle |j_B\rangle , \tag{3.28}$$

where the diagonal entries of S can be replaced by the Schmidt coefficients s_k. Absorbing the transformation matrices U and $V^\dagger$ into the basis vectors, we thus obtain:

$$|\Psi\rangle = \sum_{k=1}^{r} s_k \left(\sum_i U_{ik} |i_A\rangle \right) \left(\sum_j V^*_{jk} |j_B\rangle \right) \equiv \sum_{k=1}^{r} s_k |k_A\rangle |k_B\rangle . \tag{3.29}$$

This way of rewriting a bipartite quantum state has multiple advantages. First, note that the new bases $\{|k_A\rangle\}$ and $\{|k_B\rangle\}$ are orthonormal:

$$\langle k_A | j_A \rangle = \left(\sum_i \langle i_A | U^*_{ik} \right) \left(\sum_l U_{lj} |l_A\rangle \right) = \sum_{i,l} U^*_{ik} U_{lj} \underbrace{\langle i_A | l_A \rangle}_{=\delta_{il}} = \sum_i U^\dagger_{ki} U_{ij} = \delta_{kj}, \tag{3.30}$$

and similarly for $\{|k_B\rangle\}$. We can thus imagine that the Schmidt values "sit" on the boundary between the two systems, which are each guaranteed to have an orthonormal basis.

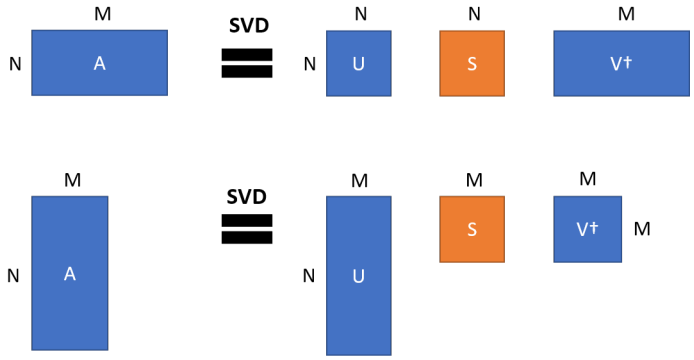

Figure 1: Shape of the matrices in a singular value decomposition, pictorial representation.

Second, the Schmidt decomposition gives us a direct access to the eigenvalues of the reduced density matrices of both subsystems. To see how, let's calculate the reduced density operator of subsystem A:

$$\begin{aligned}\rho_A &= \mathrm{Tr}_B\left[\sum_{k,l} s_k s_l^* \left|k_A\right\rangle \left|k_B\right\rangle \left\langle l_B\right| \left\langle l_A\right|\right] = \sum_m \left\langle m_B\right| \left[\sum_{k,l} s_k s_l^* \left|k_A\right\rangle \left|k_B\right\rangle \left\langle l_B\right| \left\langle l_A\right|\right] \left|m_B\right\rangle \\ &= \sum_m \sum_{k,l} s_k s_l^* \delta_{mk}\delta_{ml} \left|k_A\right\rangle \left\langle l_A\right| = \sum_m s_m^2 \left|m_A\right\rangle \left\langle m_A\right| .\end{aligned} \tag{3.31}$$

The eigenvalues of the reduced density matrix are thus simply given by the singular values squared. We can repeat the above calculation, but this time calculate the reduced density operator of the subsystem B:

$$\begin{aligned}\rho_B &= \mathrm{Tr}_A\left[\sum_{k,l} s_k s_l^* \left|k_A\right\rangle \left|k_B\right\rangle \left\langle l_B\right| \left\langle l_A\right|\right] = \sum_m \left\langle m_A\right| \left[\sum_{k,l} s_k s_l^* \left|k_A\right\rangle \left|k_B\right\rangle \left\langle l_B\right| \left\langle l_A\right|\right] \left|m_A\right\rangle \\ &= \sum_m \sum_{k,l} s_k s_l^* \delta_{mk}\delta_{ml} \left|k_B\right\rangle \left\langle l_B\right| = \sum_m s_m^2 \left|m_B\right\rangle \left\langle m_B\right| .\end{aligned} \tag{3.32}$$

This proves that the two reduced density operators of a bipartite quantum system have a common set of eigenvalues[3].

Lastly, we show how the Schmidt decomposition enables us to find a numerically cheap **approximation of a given bipartite quantum state**. Let $|\psi\rangle$ be such a quantum state and define the truncated state $|\phi\rangle$ as

$$\left|\psi\right\rangle = \sum_{k=1}^{r} s_k \left|k_A\right\rangle \left|k_B\right\rangle \quad \Rightarrow \quad \left|\phi\right\rangle = \sum_{k=1}^{r'} s_k \left|k_A\right\rangle \left|k_B\right\rangle \tag{3.33}$$

[3]Do note, however, that the resulting reduced density matrices are not the same mathematical object - they merely have the same eigenvalues. Indeed, the orthonomal bases used for both systems in the Schmidt decomposition could be entirely different.

with $r' < r$, i.e. we have truncated the $r - r'$ smallest singular values[4] from the sum. To see what **truncation error** this entails, we calculate the difference in norm of the two states:

$$\begin{aligned}\Delta_{\text{trunc}} &\equiv || \, |\psi\rangle - |\phi\rangle \, ||^2 = \langle\psi|\psi\rangle + \langle\phi|\phi\rangle - 2\,\mathrm{Re}\,\langle\phi|\psi\rangle \\ &= \sum_{k,l=1}^{r} s_k s_l \, \langle k_A| \, \langle k_B|l_B\rangle \, |l_A\rangle + \sum_{k,l=1}^{r'} s_k s_l \, \langle k_A| \, \langle k_B|l_B\rangle \, |l_A\rangle - 2 \sum_{k,l=1}^{r'} s_k s_l \, \langle k_A| \, \langle k_B|l_B\rangle \, |l_A\rangle \\ &= \sum_{k=r'+1}^{r} (s_k)^2\end{aligned} \tag{3.34}$$

As the singular values are ordered by magnitude and positive, we notice directly that the truncation error decreases monotonically with the number of singular values kept. In this sense, it is an optimal truncation procedure to approximate a state by a numerically cheaper state. Finally, note that the truncated state has to be renormalised explicitly:

$$|\phi\rangle \to \frac{1}{\sum_{i=1}^{r'} (s_i)^2} \sum_{k=1}^{r'} s_k \, |k_A\rangle \, |k_B\rangle \, . \tag{3.35}$$

At the end of the next section, we will show that this truncation offers not only a numerical advantage, but also has a clear physical interpretation.

3.3 Entanglement and Entanglement Entropy

The fact that the composition of multiple quantum systems requires the mathematical structure of a tensor product has an important consequence on the factorisation of multi-particle states into single-particle contributions. In short, there exist states in a composite Hilbert space which cannot be written as a product of states living in each of the separate Hilbert spaces. This **entanglement** between their single-particle contributions induces a non-classical class of correlations, which is a central aspect of modern quantum information science. In the following, we can only scratch the surface of the study of entanglement. Our main goals are to give a clear definition of what entanglement is and to introduce measures of entanglement. Those notions will be sufficient background for our later study of matrix product states.

[4] Typically, those can be of the order of 10^{-8} or less, depending on the degree of truncation one wants to achieve.

3.3.1 Motivation and Definition

To motivate the idea of entanglement, consider the following state in the product space $\mathcal{H}_A \otimes \mathcal{H}_B$ of two two-state quantum systems $\mathcal{H}_A$ and $\mathcal{H}_B$:

$$|\psi\rangle = \frac{1}{\sqrt{2}} \underbrace{[|0_A\rangle\,|0_B\rangle + |0_A\rangle\,|1_B\rangle]}_{\in \mathcal{H}_A \otimes \mathcal{H}_B}. \tag{3.36}$$

This is a superposition of the basis states $|00\rangle$ and $|01\rangle$ of $\mathcal{H}_A \otimes \mathcal{H}_B$. We may easily factorise it into two single-particle states:

$$|\psi\rangle = \frac{1}{\sqrt{2}} \underbrace{|0_A\rangle}_{\in \mathcal{H}_A} \otimes \underbrace{[|0_B\rangle + |1_B\rangle]}_{\in \mathcal{H}_B}. \tag{3.37}$$

Without any difficulty, we may find another valid state in $\mathcal{H}_A \otimes \mathcal{H}_B$ which does *not* factorise in this fashion. Consider for instance the state

$$|\Psi\rangle = \frac{1}{\sqrt{2}}[|0_A\rangle\,|1_B\rangle + |1_A\rangle\,|0_B\rangle]. \tag{3.38}$$

Its wave function has two non-zero coefficients: $C_{0,1} = C_{1,0} = \frac{1}{\sqrt{2}}$. To verify our claim, let's expand $|\Psi\rangle$ in terms of generic single-particle states and find what conditions their respective expansion coefficients must obey:

$$\begin{aligned} |\Psi\rangle &= [c_0^A\,|0_A\rangle + c_1^A\,|1_A\rangle] \otimes [c_0^B\,|0_B\rangle + c_1^B\,|1_B\rangle] \\ &= c_0^A c_0^B\,|0_A\rangle\,|0_B\rangle + c_0^A c_1^B\,|0_A\rangle\,|1_B\rangle + c_1^A c_0^B\,|1_A\rangle\,|0_B\rangle + c_1^A c_1^B\,|1_A\rangle\,|1_B\rangle\,. \end{aligned} \tag{3.39}$$

If this is to reproduce the exact expression we wrote down for $|\Psi\rangle$ above, the following system of equations must have a solution:

$$c_0^A c_0^B = c_1^A c_1^B = C_{0,1} = C_{1,0} = \frac{1}{\sqrt{2}}, \quad c_0^A c_1^B = c_1^A c_0^B = 0. \tag{3.40}$$

From this we immediately conclude that either c_0^A or c_1^B, and similarly either c_1^A or c_0^B must be zero. In any of those cases, the two former equations cannot have a solution as they require *all* four coefficients to have non-zero values! Hence our initial assumption - writing the state $|\Psi\rangle$ as a product of two single-system states - must have been incorrect: $|\Psi\rangle$ is indeed an entangled state.

Despite the simplicity of this example, it captures the idea of what entanglement means precisely. From here, it is straightforward to generalise it to an arbitrary multipartite quantum state. Consider an N-partite product space

$$\mathcal{H} = \bigotimes_{i=1}^{N} H_i, \quad \dim H_i = d_i \tag{3.41}$$

and let

$$|\Psi\rangle = \sum_{i_1=1}^{d_1} \sum_{i_2=1}^{d_2} ... \sum_{i_N=1}^{d_N} C_{i_1 i_2 ... i_N} |i_1\rangle_1 |i_2\rangle_2 ... |i_N\rangle_N . \tag{3.42}$$

If the wave function $C_{i_1 i_2 ... i_N}$ factorises into single-particle contributions as

$$C_{i_1 i_2 ... i_N} = C_{i_1} C_{i_2} ... C_{i_N} = \prod_{j=1}^{N} C_{i_j} \Rightarrow |\Psi\rangle = \bigotimes_{j=1}^{N} \left(\sum_{i_j=1}^{d_i} C_{i_j} |i_j\rangle_j \right), \tag{3.43}$$

the state is a product state, otherwise it is entangled.

3.3.2 Measures of Entanglement

While this definition is clear and allows one to assess whether a state is entangled or not, it is of limited operational use - verifying the factorisation properties of states in large product spaces is certainly not feasible in practice. Furthermore, it doesn't give us any information about *how much* entanglement there is in a given state. To answer the question whether there are states that are "more entangled" than others, we will need a **measure of entanglement**. For this, we will proceed in two steps: first, we introduce a general measure of the information content of a quantum state below. Building on this, we will show how this measure can be employed to quantify the entanglement in a bi-partite system.

The most common way of introducing a measure of information is the **von Neumann entropy**. Given a density operator describing a quantum state, is it defined by

$$S[\rho] = -\operatorname{Tr}(\rho \ln(\rho)) = -\sum_k \lambda_k \ln(\lambda_k), \tag{3.44}$$

where the λ_k's are the eigenvalues of the density operator. Motivating *why* this definition is a good choice is beyond the scope of this text and needs more ideas from information theory. Suffice it to say, it is constructed such that for a pure state, we get $S[\rho] = 0$ (as there is only one eigenvalue, $\lambda_1 = 1$, and $\ln(1) = 0$), whereas for a mixed state we obtain some non-zero value. This is related to the fact that if we are working with a pure state, we know exactly what state the system is in, i.e. no information is to be gained from a potential distinction of multiple states. Conversely, if our state is a mixed state, there are several possibilities which quantum state we are dealing with, and we need information to determine the state. The von Neumann entropy $S[\rho]$ puts a label on how much information we need. For instance, in the case of a **maximally mixed** state, all of the eigenvalues of ρ are $\lambda_k = 1/D$, where D is the total number of states. In that case, the von Neumann entropy evaluates to

$$S[\rho] = -\sum_{i=1}^{D} \frac{1}{D} \ln\left(\frac{1}{D}\right) = \ln(D), \tag{3.45}$$

which can be interpreted as the number of binary decisions required to distinguish between D alternatives.

Aside - General Measures of Entropy - Rényi Entropy

The von Neumann entropy is not the only measure of entropy one can consider. Different measures exist and may be more appropriate for certain setups. From an axiomatic point of view, one would rather start by writing down a "wish list" of properties that a useful measure of entropy $S[\rho]$ should satisfy. Two (out of many) such properties are:

- A pure state should have an entropy of zero:

$$S[\rho] = 0 \iff \rho = |\psi\rangle \langle\psi| \,. \tag{3.46}$$

- **Additivity** for product states:

$$S[\rho_A \otimes \rho_B] = S[\rho_A] + S[\rho_B]. \tag{3.47}$$

  This can also be generalised to the **strong subadditivity**:

$$S[\rho_{AB}] \leq S[\rho_A] + S[\rho_B], \tag{3.48}$$

  if ρ_{AB} isn't necessarily a product state, i.e. $\rho_{AB} \neq \rho_A \otimes \rho_B$.

One can show, for instance, that the **Rényi entropy** (cf. ref. [29]), defined by

$$S^{\alpha}_{\text{Rényi}}[\rho] = \frac{1}{1-\alpha} \log \left(\sum_{i=1} \lambda_i^{\alpha} \right), \tag{3.49}$$

satisfies those properties. Here, the λ_i's are again the eigenvalues of the density operator and α is a non-zero (and $\alpha \neq 1$) parameter. In the limit $\alpha \to 1$ the Rényi entropy becomes equivalent to the von Neumann entropy, and is therefore a generalisation of the latter.

3.3.3 Bipartite Entanglement and Entanglement Entropy

In order to use the von Neumann entropy to quantify entanglement, we will have to go one step further. Recall how we defined entanglement as a factorisation property of a quantum state into given subsystems - a valid measure of the entanglement must therefore be a well-defined expression depending on the bipartition into two subsystems. Given a splitting of a composite system into subsystems $\mathcal{H}_A$ and $\mathcal{H}_B$, the **entanglement entropy** between them is defined as the von Neuman entropy of either of the reduced density matrices:

$$S_{\text{entanglement}}[\rho_A] = -\operatorname{Tr}\left(\rho_A \ln(\rho_A)\right). \tag{3.50}$$

The reason why this definition is well-defined is that, as we have shown in the previous section, the two reduced density matrices ρ_A and ρ_B have a common spectrum of eigenvalues:

$$\rho_A = \sum_m s_m^2 \left|m_A\right\rangle \left\langle m_A\right|, \quad \rho_B = \sum_m s_m^2 \left|m_B\right\rangle \left\langle m_B\right|, \tag{3.51}$$

which is guaranteed through the Schmidt decomposition.

To convince ourselves that the von Neumann entropy of a reduced density matrix provides a consistent measure of entanglement, we show that for a bipartite product state, it indeed evaluates to zero, as it should. Let $|\Psi\rangle$ be a product state:

$$|\Psi\rangle = \sum_{i,j} C_{ij}^{AB} \left|i_A\right\rangle \left|j_B\right\rangle = \left(\sum_i C_i^A \left|i_A\right\rangle\right) \otimes \left(\sum_j C_j^B \left|j_B\right\rangle\right) \equiv \left|\phi_A\right\rangle \otimes \left|\phi_B\right\rangle, \tag{3.52}$$

Its density operator is then given by

$$\left|\Psi\right\rangle \left\langle\Psi\right| = \sum_{i,j} \sum_{k,l} C_{ij}^{AB} (C_{kl}^{AB})^* \left|i_A\right\rangle \left|j_B\right\rangle \left\langle l_B\right| \left\langle k_A\right|. \tag{3.53}$$

Tracing out the B-system, we obtain the reduced density operator of system A:

$$\begin{aligned} \rho_A = \mathrm{Tr}_B(\rho) &= \sum_m \left\langle m\right| \left[\sum_{i,j} \sum_{k,l} C_{ij}^{AB} (C_{kl}^{AB})^* \left|i_A\right\rangle \left|j_B\right\rangle \left\langle l_B\right| \left\langle k_A\right|\right] \left|m\right\rangle \\ &= \sum_m \sum_{i,j,k,l} C_{ij}^{AB} (C_{kl}^{AB})^* \delta_{mj} \delta_{ml} \left|i_A\right\rangle \left\langle k_A\right| = \sum_m \sum_{i,k} C_{im}^{AB} (C_{km}^{AB})^* \left|i_A\right\rangle \left\langle k_A\right|. \end{aligned} \tag{3.54}$$

Now we use the condition that our initial state was a product state, allowing us to factorise the coefficients:

$$\begin{aligned} \rho_A &= \sum_m C_m^B (C_m^B)^* \sum_{i,k} C_i^A (C_k^A)^* \left|i_A\right\rangle \left\langle k_A\right| = \sum_m |C_m^B|^2 \sum_{i,k} C_i^A (C_k^A)^* \left|i_A\right\rangle \left\langle k_A\right| \\ &= \sum_{i,k} C_i^A (C_k^A)^* \left|i_A\right\rangle \left\langle k_A\right|, \end{aligned} \tag{3.55}$$

where in the final step we have used the normalisation of the C^B's. Reordering the sums, we thus obtain

$$\rho_A = \sum_{i,k} C_i^A (C_k^A)^* \left|i_A\right\rangle \left\langle k_A\right| = \left(\sum_i C_i^A \left|i_A\right\rangle\right) \left(\sum_k (C_k^A)^* \left\langle k_A\right|\right) = \left|\phi_A\right\rangle \left\langle\phi_A\right|. \tag{3.56}$$

Therefore, the reduced density operator of the subsystem A is the density operator of a pure state! As we have seen just before, this means that its von Neumann entropy is zero, and hence the entanglement entropy of the combined system is zero, too.

3.3.4 Physical Interpretation of Truncated States

To conclude this section, we connect the entanglement entropy to the Schmidt decomposition and the state truncation prescription described before. We will show that this gives us a concrete physical interpretation of the state truncation, which is the ultimate justification for its usefulness.

Consider again the bipartite state $|\psi\rangle$ and its truncated version $|\phi\rangle$:

$$|\psi\rangle = \sum_{k=1}^{r} s_k |k_A\rangle |k_B\rangle , \quad |\phi\rangle = \sum_{k=1}^{r'} s_k |k_A\rangle |k_B\rangle . \tag{3.57}$$

As we have shown, the singular values s_k are the square roots of the eigenvalues of the corresponding reduced density matrices, λ_k. We can therefore equivalently express these states as

$$|\psi\rangle = \sum_{k=1}^{r} \sqrt{\lambda_k} |k_A\rangle |k_B\rangle , \quad |\phi\rangle = \sum_{k=1}^{r'} \sqrt{\lambda_k} |k_A\rangle |k_B\rangle . \tag{3.58}$$

This allows us to directly read off the entanglement entropy over the bipartition as

$$S[|\psi\rangle] = -\sum_{i=1}^{r} \sqrt{\lambda_k} \log\Big(\sqrt{\lambda_k}\Big), \quad S[|\phi\rangle] = -\sum_{i=1}^{r'} \sqrt{\lambda_k} \log\Big(\sqrt{\lambda_k}\Big). \tag{3.59}$$

In complete analogy to the truncation error

$$\Delta_{\text{trunc}} = || \, |\psi\rangle - |\phi\rangle \, ||^2 = \sum_{k=r'+1}^{r} \lambda_k, \tag{3.60}$$

we can thus calculate the difference in entanglement entropy directly as

$$\Delta S_{\text{trunc}} = S[|\psi\rangle] - S[|\phi\rangle] = -\sum_{i=r'+1}^{r} \sqrt{\lambda_k} \log\Big(\sqrt{\lambda_k}\Big). \tag{3.61}$$

Truncating a state by discarding a given number of Schmidt coefficients in its Schmidt decomposition is therefore equivalent to reducing the entanglement contained in the state!

Note, however, that that this truncation prescription does - a priori - in general *not* guarantee that the truncated state $|\phi\rangle$ contains the same physics as the initial state $|\psi\rangle$. Indeed, it could be that the low- as well as high-entanglement degrees of freedom are equally important to describe a certain situation. We will however show in the next chapter that for an important class of condensed matter models, this approximation is indeed an accurate way of compressing the physics contained in the state.

3.4 Quasiparticles: Understanding Energy Excitations

As the final topic of this chapter, we will introduce the quantum mechanical description of **particles and quasiparticles**, which uses the language of creation and annihilation operators. This will have two major consequences: first, the corresponding Hamiltonian is automatically diagonal and therefore gives access to the full energy spectrum of the model. Second, and most importantly, it will allow us to understand other classes of quantum models from a different perspective, by transforming the defining operators into suitable quasiparticle operators. In particular, we will be able to apply this method to understand the energy spectrum of spin chains, to which this section provides the stepping stone.

We define **creation and annihilation operators** by

$$a^\dagger |n\rangle = |n+1\rangle\,, \quad a\,|n\rangle = |n-1\rangle \qquad \text{(bosons)}; \tag{3.62}$$

$$c^\dagger |0\rangle = |1\rangle\,, \quad c\,|1\rangle = |0\rangle \qquad \text{(fermions)}, \tag{3.63}$$

omitting possible normalisation factors. This implies a representation of the corresponding quantum multi-particle states as

$$|\Psi_{boson}\rangle = \prod_{i=1}^{N} \frac{(a_i^\dagger)^{n_i}}{\sqrt{n_i!}} |0\rangle \equiv |n_1, n_2, ...n_N\rangle\,, \tag{3.64}$$

$$|\Psi_{fermion}\rangle = \prod_{i=1}^{N} (c_i^\dagger)^{n_i} |0\rangle \equiv |n_1, n_2, ...n_N\rangle\,, \tag{3.65}$$

where the last equality introduces the **occupation number representation** of the corresponding states. Imposing the **bosonic (fermionic) (anti-)symmetry** under particle exchange on the thus defined states yields the **bosonic (fermionic) (anti-)commutation relations**:

$$[a_i, a_j^\dagger] = \delta_{ij} \quad \text{(bosons)}, \quad \{c_i, c_j^\dagger\} = \delta_{ij} \quad \text{(fermions)}. \tag{3.66}$$

Those can equivalently also be regarded as the definition of the creation and annihilation operators, which allows us to interpret the quantum mechanical representation of particles from an axiomatic perspective (an excellent exposition of this perspective can be found in ref. [28]).

Consider the following fermionic Hamiltonian:

$$H = \sum_i \epsilon_i c_i^\dagger c_i. \tag{3.67}$$

This model describes free, non-interacting fermionic excitations and is diagonal by con-

struction. To see why, we apply it to a generic many-body state:

$$\begin{aligned} H\left|n_1, n_2, ..., n_N\right\rangle &= \sum_i \epsilon_i c_i^\dagger c_i \left|n_1, n_2, ..., n_N\right\rangle = \left(\sum_i \epsilon_i n_i\right) \left|n_1, n_2, ..., n_N\right\rangle \\ &\equiv E_{n_1,n_2,...,n_N} \left|n_1, n_2, ..., n_N\right\rangle , \end{aligned} \tag{3.68}$$

where the energy $E_{n_1,n_2,...,n_N}$ of the state follows as a simple sum over the energies of all occupied levels. The factor ϵ_i therefore describes how much energy we need to pay to put a fermion in the i^{th} state[5]. In conclusion, if we manage to transform a given Hamiltonian to a free-fermion Hamiltonian, we have solved the model. Any kind of state and its associated energy can then be constructed by putting particles into the corresponding energy slots and by summing over those energies.

In most cases, transforming a given quantum model to fermions will not result in the free fermion Hamiltonian as given above. One possibility is for instance a quadratic Hamiltonian

$$H = \sum_{i,j} \epsilon_{ij} c_i^\dagger c_j, \tag{3.69}$$

which "connects" the different states i and j. We can however understand the excitations of this Hamiltonian, too, by performing a transformation to another fermionic system. To show how this transformation must be defined in order to yield a valid fermionic system, we start by writing down new operators d_i which are linear combinations of the existing c_i:

$$d_i = \sum_j U_{ij} c_j. \tag{3.70}$$

In order for those operators to be fermionic, they must satisfy themselves the fermionic anti-commutation relation. Evaluating this will enable us to constrain the form of the transformation coefficients U_{ij}:

$$\left\{d_i, d_j^\dagger\right\} = \left\{\sum_k U_{ik} c_k, \sum_l U_{jl}^* c_l^\dagger\right\} = \sum_{k,l} U_{ik} U_{jl}^* \left\{c_k, c_l^\dagger\right\} = \sum_k U_{ik} U_{jk}^* = \sum_{k,l} U_{ik} (U^\dagger)_{kj} = \delta_{ij}. \tag{3.71}$$

We conclude that a linear combination of a given set of fermionic operators defines a new set of fermionic operators in its own right if the coefficients are unitary matrices. Inserting this in our general quadratic Hamiltonian, we find

$$H = \sum_k \sum_{i,j} \sum_l \left[(U^\dagger)_{ki} \epsilon_{ij} U_{jl}\right] d_k^\dagger d_l. \tag{3.72}$$

Now using the fact that the matrix ϵ_{ij} must be hermitian by construction (as H must be hermitian), we know that we can always (unitarily) diagonalise it. This in turn enables

[5] "State" is to be interpreted in an abstract sense here. It can refer to a real-space position state - i.e. location i - but may very well also represent a momentum state.

us to choose the transformation matrices U such that they perform this sought-after similarity transformation. Hence, without loss of generality we may write

$$\sum_{i,j}(U^\dagger)_{ki}\epsilon_{ij}U_{jl} \equiv \gamma_k\delta_{kl} \quad \Rightarrow \quad H = \sum_k \gamma_k d_k^\dagger d_k, \tag{3.73}$$

where the γ_k's now specify the energies of the new quasi-particles, and therefore, the eigenenergies of the system. It is however important to stress that the "new" quasiparticles are by no means "less valid" or "more abstract" than the "old" quasiparticles. From a mathematical point of view, the fermionic operators associated to both are subject to the same algebra, which is really all that is required. Alternatively, one can also imagine having written down the "correct" linear combination of operators to begin with, and simply skip the additional transformation. At any rate, applying this procedure means that we can view the diagonalisation of a given Hamiltonian as the diagonalisation of a new matrix in the abstract fermion space. This matrix is however much smaller than the original matrix representation of the "full" Hamiltonian, which makes the problem easier to solve.

The idea of working with bosonic and fermionic operators really shines when we are working with quantum systems that are defined from different, a priori unrelated operators. If we manage to define fermionic or bosonic operators as functions of the initial operators, we gain a completely new perspective on the structure of the energy excitations of the system. This is most easily illustrated by considering the simple quantum harmonic oscillator

$$H = \frac{p^2}{2m} + \frac{m\omega^2}{2}x^2, \tag{3.74}$$

where ω denotes the frequency of oscillations. By defining the two conjugate operators

$$a = \sqrt{\frac{\hbar}{2m\omega}}\left(x + \frac{i}{m\omega}p\right), \quad a^\dagger = \sqrt{\frac{\hbar}{2m\omega}}\left(x - \frac{i}{m\omega}p\right), \tag{3.75}$$

one can immediately show that they obey a bosonic canonical commutation relation:

$$[a, a^\dagger] = 1. \tag{3.76}$$

Furthermore, this allows us to rewrite the Hamiltonian as:

$$H = \hbar\omega a^\dagger a + \frac{\hbar\omega}{2} = \hbar\omega\left(a^\dagger a + \frac{1}{2}\right). \tag{3.77}$$

By the above reasoning, this is a diagonal Hamiltonian, whose eigenstates can be understood in terms of quasiparticles with energy $\hbar\omega$.

Similar techniques can be applied to understand the spectrum of quantum spin chains, as the Jordan-Wigner transformation provides a mapping from spin operators to fermionic operators.

4 Quantum Spin Chains

Whereas the previous chapter was centred on introducing abstract notions of quantum mechanics, in this chapter we will discuss several models describing the "real physics" of condensed matter systems. In particular, we will focus on models giving rise to magnetic effects, which are microscopically due to the exchange interaction between coupled spins, introduced in the first section. Building on this, we will then discuss the most important models of condensed matter physics, with a focus on the Heisenberg and Ising models. These are the simplest realisation of a - potentially macroscopically - large number of interacting spins. For the one-dimensional versions of both of these models, we will expose existing analytic results in some detail. Apart from being important results of theoretical condensed matter physics in their own right, they will provide ideal benchmarks for the numerical tools introduced subsequently.

This chapter is mainly based on refs. [16, 17, 18, 19, 20, 22].

4.1 Coupled Spins and Exchange Interaction

In this first short section, we will introduce a microscopic model for magnetism at the atomic level, the exchange interaction between spins. To set the stage, we briefly remind the reader of the angular momentum algebra and the relevant operators, before writing down an appropriate Hamiltonian for spin-spin interactions. By promoting this interaction to a larger scale in the subsequent sections with the introduction of quantum spin chains, we will be able to precisely define the microscopic models at the heart of the modelling of magnetism.

4.1.1 Spin Algebra and Definition

We define a set of **angular momentum operators** in quantum mechanics as operators J_i obeying the algebra

$$[J_i, J_j] = i\epsilon_{ijk}J_k, \quad i,j,k \in \{x,y,z\}. \tag{4.1}$$

By noting that the total angular momentum squared $\vec{J}^2$ commutes with any single component J_i, we may denote the angular momentum states by the eigenvalues of $\vec{J}^2$ and, conventionally, J_z:

$$\vec{J}^2 \left|j,m\right\rangle = j(j+1)\left|j,m\right\rangle, \quad J_z \left|j,m\right\rangle = m\left|j,m\right\rangle. \tag{4.2}$$

Using only the defining algebra, one can show that the action of the operators J_+ and J_-, defined as

$$J_+ = J_x + iJ_y, \quad J_- = J_x - iJ_y, \tag{4.3}$$

leads to new eigenstates of the total angular momentum, however with a z-projection in- or decreased by one unit:

$$J_+ |j,m\rangle \propto |j,m+1\rangle\,, \quad J_- |j,m\rangle \propto |j,m-1\rangle\,. \tag{4.4}$$

Proceeding in this fashion, it is easy to prove that the allowed values for the z-projection m must run in integer steps between $-j$ and j.

While the above definitions are completely general and do not pose any constraints on the origin or the nature of the angular momentum operators, the easiest representation of the angular momentum algebra is given by the Pauli matrices. Those define a spin-$1/2$ system[6]:

$$S^x = \frac{1}{2}\begin{bmatrix} 0 & 1 \\ 1 & 0 \end{bmatrix}, \quad S^y = \frac{1}{2}\begin{bmatrix} 0 & -i \\ i & 0 \end{bmatrix}, \quad S^z = \frac{1}{2}\begin{bmatrix} 1 & 0 \\ 0 & -1 \end{bmatrix}, \tag{4.5}$$

where the basis is chosen to describe the z-component of the spin as

$$|\uparrow\rangle \equiv |\text{up}\rangle = \begin{bmatrix} 1 \\ 0 \end{bmatrix}, \quad |\downarrow\rangle \equiv |\text{down}\rangle = \begin{bmatrix} 0 \\ 1 \end{bmatrix}. \tag{4.6}$$

Correspondingly, the spin raising and lowering operators in this basis follow immediately as

$$S^+ = \begin{bmatrix} 0 & 1 \\ 0 & 0 \end{bmatrix}, \quad S^- = \begin{bmatrix} 0 & 0 \\ 1 & 0 \end{bmatrix}. \tag{4.7}$$

We can convince ourselves that they indeed work as desired:

$$S^+ |\text{up}\rangle = \begin{bmatrix} 0 & 1 \\ 0 & 0 \end{bmatrix}\begin{bmatrix} 1 \\ 0 \end{bmatrix} = 0, \quad S^+ |\text{down}\rangle = \begin{bmatrix} 0 & 1 \\ 0 & 0 \end{bmatrix}\begin{bmatrix} 0 \\ 1 \end{bmatrix} = 1 \cdot \begin{bmatrix} 1 \\ 0 \end{bmatrix} = 1 \cdot |\text{up}\rangle \tag{4.8}$$

and

$$S^- |\text{up}\rangle = \begin{bmatrix} 0 & 0 \\ 1 & 0 \end{bmatrix}\begin{bmatrix} 1 \\ 0 \end{bmatrix} = 1 \cdot \begin{bmatrix} 0 \\ 1 \end{bmatrix} = 1 \cdot |\text{down}\rangle\,, \quad S^- |\text{down}\rangle = \begin{bmatrix} 0 & 0 \\ 1 & 0 \end{bmatrix}\begin{bmatrix} 0 \\ 1 \end{bmatrix} = 0. \tag{4.9}$$

Similarly, one could construct spin operators representing the angular momentum algebra for systems with higher spins, however in the context of this work we will only need the spin-$1/2$ representation.

4.1.2 Spin Couplings and Exchange Interaction

As magnetic moments - and thus magnetic effects - are associated with angular momentum, the microscopic origin of quantum magnetism can be found in the interaction

[6] We have omitted prefactors of $\hbar$ from here on.

of the most basic angular momenta: spins. We will assume as given that the **exchange interaction**

$$H_{\text{exchange}} = J\vec{S_1}\cdot\vec{S_2} = J\left[S_1^x S_2^x + S_1^y S_2^y + S_1^z S_2^z\right] \tag{4.10}$$

provides an accurate way of describing real physical interactions of two spins[7]. Alternatively, one can also write this coupling in terms of the spin raising and lowering operators:

$$H_{\text{exchange}} = J\vec{S_1}\cdot\vec{S_2} = J\left[S_1^z S_2^z + \frac{1}{2}\left(S_1^+ S_2^- + S_1^- S_1^+\right)\right]. \tag{4.11}$$

This latter form is especially useful to evaluate the action of the exchange Hamiltonian on the basis states, which are

$$\mathcal{H} = \text{span}\{|\uparrow\uparrow\rangle, |\uparrow\downarrow\rangle, |\downarrow\uparrow\rangle, |\downarrow\downarrow\rangle\}. \tag{4.12}$$

Applying the Hamiltonian to those yields

$$\begin{aligned}
H_{\text{exchange}}|\uparrow\uparrow\rangle &= \frac{J}{4}|\uparrow\uparrow\rangle \\
H_{\text{exchange}}|\uparrow\downarrow\rangle &= -\frac{J}{4}|\uparrow\downarrow\rangle + \frac{J}{2}|\downarrow\uparrow\rangle \\
H_{\text{exchange}}|\downarrow\uparrow\rangle &= -\frac{J}{4}|\downarrow\uparrow\rangle + \frac{J}{2}|\uparrow\downarrow\rangle \\
H_{\text{exchange}}|\downarrow\downarrow\rangle &= \frac{J}{4}|\downarrow\downarrow\rangle .
\end{aligned} \tag{4.13}$$

We recognise that the states with aligned spins are eigenstates, whereas the antialigned states are not. With this knowledge it is however easy to construct the respective eigenstates:

$$|\psi_2\rangle \equiv \frac{1}{\sqrt{2}}\big(|\uparrow\downarrow\rangle + |\downarrow\uparrow\rangle\big), \quad |\psi_3\rangle \equiv \frac{1}{\sqrt{2}}\big(|\uparrow\downarrow\rangle - |\downarrow\uparrow\rangle\big). \tag{4.14}$$

It then immediately follows that

$$H_{\text{exchange}}|\psi_2\rangle = \frac{J}{4}|\psi_2\rangle, \quad H_{\text{exchange}}|\psi_3\rangle = -\frac{3J}{4}|\psi_3\rangle \tag{4.15}$$

This eigenbasis is called the **coupled basis**, as opposed to the **uncoupled basis**. We furthermore apply the operators S^z_{tot} and $\vec{S}^2_{\text{tot}}$ to the coupled basis states:

$$S^z_{\text{tot}}|\uparrow\uparrow\rangle = +1|\uparrow\uparrow\rangle, \qquad \vec{S}^2_{\text{tot}}|\uparrow\uparrow\rangle = 2|\uparrow\uparrow\rangle \tag{4.16}$$

$$S^z_{\text{tot}}|\psi_2\rangle = 0|\psi_2\rangle, \qquad \vec{S}^2_{\text{tot}}|\psi_2\rangle = 2|\psi_2\rangle \tag{4.17}$$

$$S^z_{\text{tot}}|\downarrow\downarrow\rangle = -1|\downarrow\downarrow\rangle, \qquad \vec{S}^2_{\text{tot}}|\downarrow\downarrow\rangle = 2|\downarrow\downarrow\rangle \tag{4.18}$$

$$S^z_{\text{tot}}|\psi_3\rangle = 0|\psi_3\rangle, \qquad \vec{S}^2_{\text{tot}}|\psi_3\rangle = 0|\psi_3\rangle . \tag{4.19}$$

[7]The form of the exchange Hamiltonian can also be "derived" by considering the Pauli principle and the fermionic wavefunction antisymmetry (cf. ref. [30]). For the present discussion it is however sufficient to simply take the given Hamiltonian for granted.

Given that the eigenvalues of $\vec{S}^2$ are of the structure $s(s+1)$, we see that the eigenvectors decouple into a sector with total spin $s = 1$, and a sector with total spin $s = 0$. For the $s = 1$ sector, we have three different states with z-projections of $-1, 0, +1$, as we should. One may therefore denote the coupled basis elements as

$$\begin{aligned} &\{|\uparrow\uparrow\rangle, |\psi_2\rangle, |\downarrow\downarrow\rangle\} = \{|s=1, m=+1\rangle, |s=1, m=0\rangle, |s=1, m=-1\rangle\} \\ &\{|\psi_3\rangle\} = \{|s=0, m=0\rangle\}. \end{aligned} \tag{4.20}$$

It is however no coincidence that the eigenstates of the Hamiltonian decouple into a spin-1 and a spin-0 subspace. Ultimately, this follows immediately from the fact that the Hamiltonian H, S^z_{tot} and $\vec{S}^2_{\text{tot}}$ mutually commute:

$$[H, S^z_{\text{tot}}] = [H, \vec{S}^2_{\text{tot}}] = [S^z_{\text{tot}}, \vec{S}^2_{\text{tot}}] = 0. \tag{4.21}$$

The common eigenbasis is then of course the coupled basis, whose explicit form we have just derived. According to our general discussion in the previous chapter, we have therefore *solved* the quantum system of two coupled spins, and could now proceed to calculate its dynamics, its properties at finite temperature etc.

To close this introductory presentation, let us remark that, despite knowing the exact form of the eigenstates, the ground state of the exchange Hamiltonian depends on the choice of the sign of the parameter J. A particularly easy way to see this is to rewrite the exchange Hamiltonian once again as

$$H_{\text{exchange}} = J\vec{S}_1 \cdot \vec{S}_2 = \frac{J}{2}\vec{S}^2_{\text{tot}} - \frac{3J}{4}. \tag{4.22}$$

If $J < 0$, the energy is minimised by the states in the $s = 1$ sector, and the ground state is therefore three-fold degenerate. In contrast, for $J > 0$, the minimum energy is reached in the $s = 0$ sector.

In contrast to what the presentation in the previous chapter might have suggested, solving this quantum system did not require the explicit construction of a Hamiltonian matrix and its diagonalisation[8]. Indeed, many of the ideas presented above generalise readily to the case of a large number N of coupled spins, where an explicit matrix diagonalisation would be doomed to failure from the outset.

4.2 The Heisenberg Spin Chain

The Heisenberg model (cf. ref. [31]) is the realisation of the exchange interaction of coupled spins in a macroscopic model, and as such one of the most important models in theoretical condensed matter physics. After defining the Heisenberg model and some

[8] Implying that, luckily, there is more to quantum mechanics than just linear algebra.

variations derived from it, we will discuss how its solutions can be obtained by counting the number of flipped spins with respect to an aligned state. Constructing suitable superpositions of these spin-flip states will yield the corresponding energy eigenstates, and furthermore allow us to calculate the ground state energy of the antiferromagnetic Heisenberg model analytically (cf. refs. [19, 20]).

4.2.1 Definition and Variants

In its most basic form, the **Heisenberg model** is simply a generalisation of the spin coupling discussed in the previous section, but for a (potentially macroscopically) large number of coupled spins:

$$H = J \sum_{\langle i,j \rangle} \vec{S}_i \cdot \vec{S}_j = J \sum_{\langle i,j \rangle} \left[S_i^z S_j^z + \frac{1}{2} \left(S_i^+ S_j^- + S_i^+ S_j^- \right) \right], \tag{4.23}$$

where in the second equality we have employed the very useful rewriting in terms of spin raising and lowering operators. Here, we have already introduced a model with several simplifications, by taking the coupling J to be constant and uniform. Furthermore, we have restricted the interactions to nearest neighbour interactions, commonly denoted by the summation over $\langle i, j \rangle$. Considering only a one-dimensional chain, the model in its simplest form becomes

$$H = J \sum_{i=1}^{N} \vec{S}_i \cdot \vec{S}_{i+1} = J \sum_{i=1}^{N} \left[S_i^z S_{i+1}^z + \frac{1}{2} \left(S_i^+ S_{i+1}^- + S_i^+ S_{i+1}^- \right) \right]. \tag{4.24}$$

The parameter J regulates the interaction strength of the spins, and is usually taken to be of unit magnitude. Crucially, one has to distinguish between positive and negative values of J: the former prompt spins to antialign - thus defining an **antiferromagnet** - whereas the latter will lead to a preferred alignment of the spins, modelling a **ferromagnet**. Despite being a seemingly small difference, this sign is at the heart of the physics of the Heisenberg model and will lead to surprisingly different results, depending on the case considered. Finally, let us mention that the Heisenberg model as defined above exhibits an $\mathrm{SU}(2)$ symmetry in its spin orientation, and has therefore no preferred spatial direction.

If desired, this symmetry can be lifted by adding a transverse field of strength h, conventionally applied in the z-direction:

$$H = J \sum_{i=1}^{N} \vec{S}_i \cdot \vec{S}_{i+1} - h \sum_{i=1}^{N} S_i^z. \tag{4.25}$$

Another variant of the Heisenberg model, the so-called **X-Y model**, considers a spin coupling only in the $x - y$ plane:

$$H = J \sum_{\langle i,j \rangle} \left[\frac{1+\gamma}{2} S_i^x S_j^x + \frac{1-\gamma}{2} S_i^y S_j^y \right] - h \sum_i S_i^z. \tag{4.26}$$

This is an often studied toy model in the literature (cf. refs. [32, 33, 34, 35]), as tuning the anisotropy parameter γ gives rise to several interesting limiting cases. The most important of these limiting cases - $\gamma = 1$ - defines the **Ising model** (cf. ref. [36]):

$$H = J \sum_{\langle i,j \rangle} S_i^x S_j^x - h \sum_i S_i^z. \tag{4.27}$$

We will come back to the Ising model in the next section in much more detail; here it is only mentioned for the sake of completeness.

To study those spin models, we need to define a basis of the corresponding Hilbert space. Straightforwardly, we can simply consider the tensor product of all the constituent single spin spaces, which are each completely described in the basis of their z-projections. The total Hilbert space for a spin chain with N spins is given by

$$\mathcal{H} = \text{span}\{|i_1\rangle \otimes |i_2\rangle \otimes ... \otimes |i_N\rangle \, | i_j = \uparrow, \downarrow, \ 1 \leq j \leq N\}. \tag{4.28}$$

This is of course not necessarily an eigenbasis of the Hamiltonians defined above. Solving the Heisenberg model therefore means constructing all the eigenvectors of the Hamiltonian H and the corresponding eigenenergies explicitly from the above basis vectors.

Aside - Heisenberg from Hubbard

One of the most important models of condensed matter physics is the **Hubbard model** (cf. ref. [37]). It describes the interactions of electrons and their spins on a given lattice, but allows the electrons to hop between different sites, which requires a kinetic energy t. Furthermore, the Pauli principle is taken care of by introducing an on-site repulsion term, which only allows electrons of different spins to occupy the same orbital (by paying the potential energy U to overcome the Coulomb repulsion):

$$H_{Hubbard} = t \sum_{\langle i,j \rangle} \sum_{\sigma = \uparrow, \downarrow} \left(c_{i\sigma}^\dagger c_{j\sigma} + c_{j\sigma}^\dagger c_{i\sigma} \right) + U \sum_i c_{i\uparrow}^\dagger c_{i\uparrow} c_{i\downarrow}^\dagger c_{i\downarrow}. \tag{4.29}$$

The Hubbard model is therefore one more example of a model that is easy to write down - due to our understanding of microscopic interactions -, yet extremely hard to solve. Depending on the choice of the parameter U/t, one can derive the limiting cases of strongly localised freely moving electrons from the Hubbard model. Incidentally, treating the former case is equivalent to doing perturbation theory in the small parameter t/U. Evaluating this limit carefully reproduces nothing but the antiferromagnetic Heisenberg model (cf. ref. [38]) ,

$$H = J \sum_{i=1}^{N} \left[S_i^z S_{i+1}^z + \frac{1}{2} \left(S_i^+ S_{i+1}^- + S_i^+ S_{i+1}^- \right) \right], \tag{4.30}$$

with a coupling strength of $J = 4t^2/U$. In retrospect, this is therefore a further

justification for the fact that the Heisenberg model is indeed deeply rooted in the study of condensed matter systems, and not merely an academic example.

4.2.2 The Ferromagnetic Ground State, Spin Flips and Magnons

For what follows, we consider the "basic" Heisenberg model

$$H = J \sum_{i=1}^{N} \vec{S}_i \cdot \vec{S}_{i+1} \tag{4.31}$$

in one dimension and in the spin-$1/2$ representation. Furthermore, we assume that periodic boundary conditions hold, such that $i + N \equiv i$. One can understand the quantum mechanics of the spin-$1/2$ Heisenberg model by constructing states with a given number of spin flips, starting from a fully aligned initial state $|\Psi_0\rangle$:

$$|\Psi_0\rangle = |\uparrow\uparrow \ ... \ \uparrow\rangle \, . \tag{4.32}$$

The reason why this is a valid approach is that the Hamiltonian H, the total spin z-projection S^z_{tot} and the total spin squared $\vec{S}^2_{tot}$ all mutually commute:

$$[H, S^z_{tot}] = \left[H, \vec{S}^2_{tot}\right] = \left[S^z_{tot}, \vec{S}^2_{tot}\right] = 0. \tag{4.33}$$

This yields the more practical alternative way of enumerating our basis states by writing down all the states belonging to a *fixed* value of the total spin in z-direction. Evidently, the fully aligned state has a total spin in z-direction of $N \times 1/2$. Flipping single spins then decreases this value by one for each spin flip, leading to the set

$$S^z_{tot} \in \left\{ \frac{N}{2}, \frac{N}{2} - 1, \frac{N}{2} - 2, ..., \frac{N}{2} - j, ..., -\frac{N}{2} \right\} \quad \left(\text{for } \frac{N}{2} \text{ even} \right) \tag{4.34}$$

of accessible z-projections. We denote a state with spin flips in positions $i_1 \leq i_2 \leq ... \leq i_j$ as

$$\left| \uparrow \ ... \uparrow \underset{i_1}{\downarrow} \uparrow \ ... \uparrow \underset{i_2}{\downarrow} \uparrow \ ... \uparrow \underset{i_j}{\downarrow} \uparrow \ ... \uparrow \right\rangle \equiv |i_1, i_2, ..., i_j\rangle \, . \tag{4.35}$$

For a given number $0 \leq j \leq N$ of spin flips, there are $\binom{N}{j}$ ways of choosing the spins. Making use of the binomial theorem we immediately find that there is a total of

$$\sum_{j=0}^{N} \binom{N}{j} = 2^N \tag{4.36}$$

states, as expected. The decoupling of the Heisenberg Hamiltonian into sectors of different spin-projection in z-direction implies that the Hamiltonian may be represented as a block matrix:

$$H = \begin{bmatrix} \left[\ S^z_{tot} = \frac{N}{2} \ \right] & & & 0 \\ & \left[\ S^z_{tot} = \frac{N}{2} - 1 \ \right] & & \\ & & \ddots & \\ 0 & & & \left[\ S^z_{tot} = -\frac{N}{2} \ \right] \end{bmatrix}, \tag{4.37}$$

which follows immediately from a suitable (re-)ordering of the "spin-flip" basis states.

Using this formalism will enable us to successively construct the eigenstates of the Heisenberg Hamiltonian, by considering each of the decoupled subspaces separately. Unsurprisingly, the easiest sector to study is the first sector with no spin flips, thus containing only the fully aligned state $|\Psi_0\rangle$. We can therefore recognise it as the first energy eigenstate (as the "diagonalisation" of a 1×1 matrix is trivial):

$$H\,|\Psi_0\rangle = \frac{JN}{4}\,|\Psi_0\rangle \equiv E_0\,|\Psi_0\rangle\,. \tag{4.38}$$

An important point to note is that, for the ferromagnetic ($J < 0$, thus energetically favouring aligned spins) Heisenberg model, $|\Psi_0\rangle$ is the ground state. All other states with a non-zero number of spin flips would therefore correspond to excited states. In contrast, in the case of the antiferromagnetic ($J > 0$) Heisenberg model $|\Psi_0\rangle$ corresponds to the highest energy state, due to its having the least possible number of antialigned spins (namely zero).

Next, we consider "one-flip" sector, that is the set $\{|j\rangle\,|1 \leq j \leq N\}$. We immediately find that those are not energy eigenstates, but obey the equation

$$H\,|j\rangle = E_0\,|j\rangle + J\left[\frac{1}{2}\,|j-1\rangle + \frac{1}{2}\,|j+1\rangle - |j\rangle\right]. \tag{4.39}$$

Our task is now to find N different energy eigenstates $|\Psi_1(k)\rangle$ constructed as superpositions of states $|j\rangle$ and obeying the above equation. Defining the general superposition

$$|\Psi_1(k)\rangle \equiv \sum_{j=1}^{N} a_j(k)\,|j\rangle\,, \tag{4.40}$$

we can solve the Schrödinger equation

$$H\,|\Psi_1(k)\rangle = E_1(k)\,|\Psi_1(k)\rangle \tag{4.41}$$

to obtain an equivalent difference equation

$$J\left[\frac{1}{2}a_{j+1}(k) + \frac{1}{2}a_{j-1}(k) - a_j(k)\right] = (E_1(k) - E_0)\,a_j(k) \equiv \epsilon_1(k)a_j(k). \tag{4.42}$$

A plane wave ansatz $a_j(k) \equiv c(k)e^{ikj}$ yields the desired dispersion relation

$$J\left[\frac{1}{2}e^{ik} + \frac{1}{2}e^{-ik} - 1\right] = J\left[\cos(k) - 1\right] = \epsilon_1(k). \tag{4.43}$$

Note that the periodic boundary conditions imply

$$a_j(k) \stackrel{!}{=} a_{j+N}(k) \iff e^{ikN} \stackrel{!}{=} 1 \iff k = 2\pi\frac{l}{N}, \quad 0 \leq l \leq N-1. \tag{4.44}$$

To summarise (and imposing normalisation), the energy eigenstates living in the $S^z_{tot} = N/2 - 1$ sector are given by:

$$|\Psi_1(k)\rangle = |S^z_{tot} = N/2 - 1, k\rangle = \frac{1}{\sqrt{N}} \sum_{j=1}^{N} e^{ikj} |j\rangle \,, \quad k = 2\pi \frac{l}{N} \tag{4.45}$$

with eigenenergy

$$\epsilon_1(k) = J\left[\cos(k) - 1\right]. \tag{4.46}$$

In the case of the ferromagnetic Heisenberg model, those (true) excitations above the ground state are called **magnons**.

Similarly, one can consider each accessible sector of given number of spin flips and determine the linear combinations of spin-flip states that define the corresponding energy eigenstates. Ultimately, this leads to the **Bethe ansatz** (cf. ref. [39]), which gives a closed set of relations defining the corresponding quantum numbers. To motivate the form of the Bethe ansatz equations, it is instructive to consider the "two-flip" sector, leading to several additional complications, such as interactions between magnons.

The general construction is similar to the previously discussed "one-flip" sector. However, applying the Hamiltonian to a "two-flip" state $|j_1 j_2\rangle$ (with $j_1 < j_2$) now leads to two different equations, depending on the "spacing" between the j's. If $j_2 \neq j_1 + 1$ or $j_1 \neq 1$ and $j_2 \neq N$, i.e. if the two spin flips are not adjacent, then

$$H\,|j_1 j_2\rangle = J\left(\frac{N}{4} - 2\right)|j_1 j_2\rangle + \frac{J}{2}\big[\,|j_1 - 1, j_2\rangle + |j_1 + 1, j_2\rangle + |j_1, j_2 - 1\rangle + |j_1, j_2 + 1\rangle\,\big] \tag{4.47}$$

holds. In contrast, if the spacing between the spins flips is one, i.e. $j_2 = j_1 + 1$ or $j_1 = 1$ and $j_2 = N$, we obtain the following relation instead:

$$H\,|j_1 j_2\rangle = J\left(\frac{N}{4} - 1\right)|j_1, j_2 + 1\rangle + \frac{J}{2}\big[\,|j_1 - 1, j_2 + 1\rangle + |j_1, j_2 + 2\rangle\,\big]. \tag{4.48}$$

As in the case of single spin flips, we write the energy eigenstates as general superpositions

$$|\Psi_2(k_1, k_2)\rangle \equiv \sum_{j_2 > j_1} a_{j_1 j_2}(k_1, k_2)\,|j_1 j_2\rangle \,, \tag{4.49}$$

where the coefficients are taken to obey a general plane wave structure:

$$a_{j_1 j_2}(k_1, k_2) \equiv A e^{i(k_1 j_1 + k_2 j_2)} + B e^{i(k_1 j_2 + k_2 j_1)}. \tag{4.50}$$

Plugging the ansatz into the Schrödinger equation then yields two different equations, implicitly defining the energy eigenstates:

$$\begin{aligned} &\big(E_0 - E_2(k_1, k_2) - 2J\big) a_{j_1 j_2}(k_1, k_2) \\ &+ \frac{J}{2}\big(a_{j_1 - 1, j_2}(k_1, k_2) + a_{j_1 + 1, j_2}(k_1, k_2) + a_{j_1, j_2 - 1}(k_1, k_2) + a_{j_1, j_2 + 1}(k_1, k_2)\big) = 0 \end{aligned} \tag{4.51}$$

for $j_2 > j_1$ and

$$\big(E_0 - E_2(k_1,k_2) - J\big)a_{j_1,j_1+1}(k_1,k_2) + \frac{J}{2}\big(a_{j_1-1,j_1+1}(k_1,k_2) + a_{j_1,j_1+2}(k_1,k_2)\big) = 0 \quad (4.52)$$

for $j_2 = j_1 + 1$. Equivalently, we may regard the first relation to be true for all pairs (j_1, j_2), and impose the second equation as a condition on the coefficients $a_{j_1 j_2}(k_1, k_2)$. The most useful form of this condition is obtained by subtracting the lower equation from the upper one, yielding

$$2a_{j_1 j_1+1}(k_1,k_2) = a_{j_1 j_1}(k_1,k_2) + a_{j_1+1 j_1+1}(k_1,k_2). \quad (4.53)$$

To find the energy of a state with (k_1, k_2), it is then sufficient to evaluate the upper equation for the corresponding plane wave coefficients, which gives

$$\begin{aligned} &Ae^{i(k_1 j_1 + k_2 j_2)}\left[2(E_2(k_1,k_2) - E_0) - J\left(4 - e^{-ik_1} - e^{ik_1} - e^{-ik_2} - e^{ik_2}\right)\right] \\ =&Be^{i(k_1 j_2 + k_2 j_1)}\left[2(E_2(k_1,k_2) - E_0) - J\left(4 - e^{-ik_1} - e^{ik_1} - e^{-ik_2} - e^{ik_2}\right)\right]. \end{aligned} \quad (4.54)$$

This relation can only be true for arbitrary coefficients A, B and wavevectors k_1, k_2, if the second factor evaluates to zero. We thus immediately find the dispersion relation

$$E_2(k_1,k_2) - E_0 \equiv \epsilon_2(k_1,k_2) = J\left[2 - \cos(k_1) - \cos(k_2)\right]. \quad (4.55)$$

Invoking the additional constraint on $a_{j_1 j_2}(k_1, k_2)$ now allows us to relate the coefficients A and B:

$$\frac{A}{B} = \frac{e^{i(k_1+k_2)} + 1 - 2e^{ik_1}}{e^{i(k_1+k_2)} + 1 - 2e^{ik_2}} \equiv e^{i\Theta(k_1,k_2)} = e^{-i\Theta(k_2,k_1)}. \quad (4.56)$$

The dependence of $\Theta(k_1, k_2)$ on k_1 and k_2 may also be expressed more succinctly as

$$2\cot\left(\frac{\Theta(k_1,k_2)}{2}\right) = \cot\left(\frac{k_1}{2}\right) - \cot\left(\frac{k_2}{2}\right). \quad (4.57)$$

Finally, we then find that the coefficients of the energy eigenstates are determined by

$$a_{j_1 j_2}(k_1,k_2) = c\left(e^{ik_1 j_1}e^{ik_2 j_2}e^{i\Theta(k_1,k_2)/2} + e^{ik_2 j_1}e^{ik_2 j_1}e^{-i\Theta(k_1,k_2)/2}\right) \quad (4.58)$$

with an (unimportant) normalisation constant c. Taking the periodic boundary conditions into account by requiring $a_{j_1 j_2}(k_1,k_2) \stackrel{!}{=} a_{j_1 j_2+N}(k_1,k_2)$ then yields the discrete wavevectors

$$Nk_1 = 2\pi l_1 + \Theta(k_1,k_2), \quad Nk_2 = 2\pi l_2 + \Theta(k_1,k_2), \quad 0 \leq l_1, l_2, \leq N-1. \quad (4.59)$$

Summarising, the energy eigenstates with two spin flips are described in closed form as superpositions

$$|\Psi_2(k_1,k_2)\rangle = |S^z_{tot} = N/2 - 2, k_1, k_2, \phi\rangle = \sum_{j_1<j_2} a_{j_1 j_2}(k_1,k_2)\,|j_1 j_2\rangle \quad (4.60)$$

with coefficients

$$a_{j_1 j_2}(k_1, k_2) = c\left(e^{ik_1 j_1} e^{ik_2 j_2} e^{i\Theta(k_1,k_2)/2} + e^{ik_2 j_1} e^{ik_2 j_1} e^{-i\Theta(k_1,k_2)/2}\right) \tag{4.61}$$

and eigenenergies

$$\epsilon_2(k_1, k_2) = J\left[2 - \cos(k_1) - \cos(k_2)\right]. \tag{4.62}$$

The parameters k_1, k_2 and $\Theta(k_1, k_2)$ are related through

$$\begin{cases} 2\cot\left(\frac{\Theta(k_1,k_2)}{2}\right) = \cot\left(\frac{k_1}{2}\right) - \cot\left(\frac{k_2}{2}\right) \\ k_1 = 2\pi\frac{l_1}{N} + \frac{\phi}{N} \\ k_2 = 2\pi\frac{l_2}{N} + \frac{\phi}{N}, \end{cases} \tag{4.63}$$

and completely specified by choosing a pair of integers (l_1, l_2). Finding the energy eigenstates in this subspace is therefore equivalent to listing all possible pairs[9] of integers (l_1, l_2). This completes our derivation of the Bethe ansatz equations in the "two-flip" sector.

Aside - Classes of States: Bound States and Free Magnons

Depending on the choice of the quantum numbers l_1, l_2, or equivalently the wavevectors k_1, k_2, the resulting two-magnon energy eigenstates can be classified into different categories (cf. ref. [19]):

- If $l_1 = 0$ and $l_2 \in 0, ..., N-1$, both k_1 and k_2 admit real solutions.
- If both l_1 and l_2 are not equal to zero, but chosen such that $l_2 - l_1 > 1$, the solutions for k_1 and k_2 are still real.
- In all remaining cases, i.e. $l_1 = l_2$ or $l_2 - l_1 = 1$, the solutions for k_1 and k_2 are potentially complex.

The first two classes can be interpreted as "free" or "nearly free" magnons. In contrast, the third category describes bound states of two magnons.

4.2.3 The Bethe Ansatz

As motivated by considering the "two-flip" eigenstates of the Heisenberg Hamiltonian, deriving the eigenstates becomes increasingly more complicated once multiple magnon excitations are present in the system. A general solution, the Bethe ansatz (cf. refs. [19, 39]), can however be cast in the exact same structure. Considering the sector with n spin

[9] One can prove that there are $\frac{N(N-1)}{2}$ such pairs yielding (distinct) solutions to the Bethe ansatz equations, as there should be.

flips, the eigenstates with $S^z_{tot} = N/2 - n$ have eigenenergies

$$\epsilon_n(k_1, ..., k_n) = J \sum_{i=1}^{n} [1 - \cos(k_i)] \,. \tag{4.64}$$

The wavenumbers and phases between the different magnon pairs now obey

$$\begin{cases} 2\cot\left(\frac{\Theta(k_i,k_j)}{2}\right) = \cot\left(\frac{k_i}{2}\right) - \cot\left(\frac{k_j}{2}\right) \\ k_i = 2\pi\frac{l_i}{N} + \sum_{i\neq j}\frac{\Theta(k_i,k_j)}{N}, \quad l_i \in \{0, 1, ..., N-1\} \end{cases} \tag{4.65}$$

in complete analogy with the "two-flip" sector. Solving those equations to find the energy eigenstates in the "n-flip" sector is then again equivalent to listing all sets of Bethe quantum numbers $\{l_1, ..., l_n\}$ that give a solution of the Bethe ansatz equations.

Let us remark that **integrability** - the property of being analytically solvable - only holds for a small set of simple systems. It is for this reason that systems like the Heisenberg model are of huge interest for the benchmarking of numerical methods, as the results can easily be compared to the analytical predictions. Moreover, as those analytical predictions usually only hold in the thermodynamic limit, they give a good way of assessing the finite-size scaling properties of numerical solutions.

4.2.4 The Antiferromagnetic Ground State

A beautiful application of the Bethe ansatz is the calculation of the ground state energy of the antiferromagnetic Heisenberg model, which we will turn to next. For a more detailed derivation, consult ref. [20]. Let us note first that, naively, the **Néel state**

$$|\Psi_{Neel}\rangle \equiv |\uparrow\downarrow\uparrow\downarrow \ ... \ \uparrow\downarrow\rangle \tag{4.66}$$

seems like a perfect candidate for the antiferromagnetic ground state, for it is entirely build from anti-aligned spins. However, it is *not* an eigenstate of the Heisenberg Hamiltonian. This can easily be seen by considering the action of the spin flip terms in the Hamiltonian on the Néel state:

$$S^+_i S^-_{i+1} \left| ... \ \underset{i}{\uparrow}\underset{i+1}{\downarrow} \ \uparrow \ \downarrow \ ... \right\rangle = \left| ... \ \underset{i}{\uparrow}\underset{i+1}{\uparrow} \ \downarrow \ \downarrow \ ... \right\rangle , \tag{4.67}$$

evidently violating the defining property of the Néel state. Therefore, we have to construct the ground state using the machinery introduced before.

As a starting point, we will assume that the ground state has a total spin in z-direction of 0 (as does the Néel state), and therefore lives in the "$N/2$-flip" sector. We will therefore have to solve the Bethe ansatz equations for the lowest energy state in this sector, which

we reproduce here for the ease of reading:

$$\begin{cases} 2\cot\left(\frac{\Theta(k_i,k_j)}{2}\right) = \cot\left(\frac{k_i}{2}\right) - \cot\left(\frac{k_j}{2}\right) \\ k_i = 2\pi\frac{l_i}{N} + \sum_{i\neq j}\frac{\Theta(k_i,k_j)}{N}, \quad l_i \in \{0,1,...,N-1\}. \end{cases} \tag{4.68}$$

The lowest energy state in this sector is defined through a specific choice of the $N/2$ Bethe numbers $\{l_1,...,l_{N/2}\}$, which can be shown (cf. ref. [20]) to be

$$\{l_1,l_2,...,l_{N/2}\} = \{1,3,...,N-1\}. \tag{4.69}$$

Solving the Bethe ansatz equations with the above quantum numbers is quite an involved calculation, and not of immediate relevance in the scope of the present thesis. Suffice it to say that finding a solution for the energy of the state defined through $\{l_1,l_2,...,l_{N/2}\}$ is equivalent to solving the Bethe ansatz equations for the different wavevectors k_i. Once we have obtained those solutions, the energy would follow as

$$\epsilon_{N/2}(k_1,...,k_{/2}) = J\sum_{i=1}^{N/2}\left[\cos(k_i)-1\right]. \tag{4.70}$$

When the dust settles, after multiple substitutions and a passage to the thermodynamic limit, one obtains the surprisingly simple result

$$\epsilon_{N/2}(k_1,...,k_{/2}) = -JN\ln(2). \tag{4.71}$$

The ground state energy of the antiferromagnetic Heisenberg model is therefore given by

$$E_0^{AFM} = E_0 + \epsilon_{N/2}(k_1,...,k_{/2}) = -JN\ln(2) + \frac{JN}{4}. \tag{4.72}$$

As we assume $N \gg 1$ in the above expression, the more useful quantity to consider is the ground state energy per spin,

$$\frac{E_0^{AFM}}{N} = -J\ln(2) + \frac{J}{4}. \tag{4.73}$$

This final expression can be directly compared to the result of numerical finite-size calculations.

4.2.5 Spinons

In a similar spirit to the ground state calculation, one can use the Bethe ansatz to find the eigenstates and energies of excitations above the antiferromagnetic ground state, which are known as **spinons**. One proceeds again by identifying a suitable set of Bethe quantum numbers in the "$N/2 \pm 1$ flip" sector, and solving the Bethe ansatz equations for this choice. Discussing the exact solution in detail is again beyond the scope of this

thesis. It is however worth quoting the result (cf. ref. [20]), which consists of a continuum of states, bounded by the (again beautifully simple) energies

$$\frac{J\pi}{2}\sin(k) \leq \epsilon_1(k) \leq J\pi \sin\left(\frac{k}{2}\right), \tag{4.74}$$

where $\epsilon_1(k)$ is the excitation energy above the ground state.

4.3 The Ising Model

We have defined the Ising model (cf. ref. [36]) as a simplified variant of the Heisenberg model in the previous section. Most often, one studies the transverse field Ising model, whose definition[10] we recall here as

$$H = J\sum_{i=1}^{N} S_i^x S_{i+1}^x - h\sum_{i=1}^{N} S_i^z. \tag{4.75}$$

Similarly to the Heisenberg model, one can distinguish ferromagnetic ($J < 0$) and antiferromagnetic ($J > 0$) interactions in the Ising model. Despite seeming like a "stripped off" version of the Heisenberg model, the Ising model is a powerful toy model. One of its most important features is that it has a quantum critical point (cf. ref. [40]). Crossing this point in the J-h-parameter space leads to a quantum phase transition. Being able to accurately capture this quantum phase transition is a further benchmark for a numerical model, and will be our primary application of the Ising model. Finally, working at or off-criticality has important consequences for the entanglement entropy contained in the ground state of the Ising model. Those latter observations will ultimately motivate the study of entanglement entropy in quantum spin chains in general, which provides the stepping stone towards the definition of matrix product states.

4.3.1 Ground State Energy

The transverse field Ising model can be solved in quite a different way, compared to the Heisenberg model (cf. refs. [17, 18]). Instead of finding an explicit prescription to enumerate the energy eigenstates, we will directly rewrite the Ising Hamiltonian in terms of fermionic excitations. This representation is however not yet in diagonal form; and two subsequent transformations on the Hamiltonian have to be performed in fermion space. Once this fermionic battle is fought, we will recover a Hamiltonian in the form of the free fermion gas, whose energy spectrum follows immediately. Throughout this section, we will again work in the thermodynamic limit. A more detailed version of this

[10] One also often finds the equivalent definition $H = J\sum_{i=1}^{N} S_i^z S_{i+1}^z - h\sum_{i=1}^{N} S_i^x$, which follows by a simple rotation in spin space.

calculation can be found in the appendix.

The starting point for the solution of the Ising model is the observation that we can define a set of spinless fermionic operators from the Pauli spin matrices:

$$c_j = \left(\bigotimes_{l<j} S_l^z\right) \otimes S_j^+, \quad c_j^\dagger = \left(\bigotimes_{l<j} S_l^z\right) \otimes S_j^-, \tag{4.76}$$

which is known as the **Jordan-Wigner transformation** (cf. ref. [41]). By construction, the new operators obey the fermionic commutation relations

$$\{c_i, c_j^\dagger\} = \delta_{ij}, \quad \{c_i, c_j\} = 0. \tag{4.77}$$

It is especially convenient to express pairs of spin operators in x-direction, as well as the spin operator in z-direction as a product of these fermionic operators

$$S_i^x S_{i+1}^x = c_i^\dagger c_{i+1} + c_i^\dagger c_{i+1}^\dagger - c_i c_{i+1} - c_i c_{i+1}^\dagger, \quad S_i^z = c_i c_i^\dagger - c_i^\dagger c_i. \tag{4.78}$$

Inserting these in the Ising Hamiltonian, we obtain

$$H = J \sum_{i=1}^{N-1} (c_i^\dagger c_{i+1} + c_i^\dagger c_{i+1}^\dagger - c_i c_{i+1} - c_i c_{i+1}^\dagger) + 2h \sum_{i=1}^{N} c_i^\dagger c_i, \tag{4.79}$$

where we have implicitly assumed a thermodynamic limit, and dropped a constant term. Next, we transform the Hamiltonian to momentum space via the discrete Fourier transforms

$$d_k = \frac{1}{\sqrt{N}} \sum_l c_l e^{-ikl}, \quad d_k^\dagger = \frac{1}{\sqrt{N}} \sum_l c_l^\dagger e^{ikl}. \tag{4.80}$$

Simplifying the Hamiltonian and doing the real space sum then yields

$$H = -\sum_k \left[(2J\cos(k) - 2h) d_k^\dagger d_k + iJ\sin(k)(d_k^\dagger d_{-k}^\dagger + d_k d_{-k}) \right], \tag{4.81}$$

which is not yet completely diagonal. The final step is therefore an additional diagonalisation in the fermion space - a unitary transformation of the d_k's - to find the "right" set of fermionic operators. This **Bogoliubov transformation** (cf. refs. [42, 43]) is most easily achieved by rewriting the Hamiltonian in matrix form:

$$H = -\sum_k \begin{bmatrix} d_k^\dagger & d_{-k} \end{bmatrix} M(k) \begin{bmatrix} d_k \\ d_{-k}^\dagger \end{bmatrix}, \tag{4.82}$$

with

$$M(k) = \begin{bmatrix} J\cos(k) - h & iJ\sin(k) \\ -iJ\sin(k) & -(J\cos(k) - h) \end{bmatrix}. \tag{4.83}$$

Diagonalising the hermitian matrix $M(k)$ unitarily yields

$$H = -\sum_k \begin{bmatrix} d_k^\dagger & d_{-k} \end{bmatrix} U(k) D(k) U^\dagger(k) \begin{bmatrix} d_k \\ d_{-k}^\dagger \end{bmatrix}, \quad D(k) = \begin{bmatrix} -\epsilon(k) & 0 \\ 0 & \epsilon(k) \end{bmatrix}, \tag{4.84}$$

where the unitary matrix $U(k)$ assumes the form

$$U(k) = \begin{bmatrix} \frac{i\sqrt{a(k)-\epsilon(k)}}{\sqrt{2\epsilon(k)}} & \frac{i\sqrt{a(k)+\epsilon(k)}}{\sqrt{2\epsilon(k)}} \\ \frac{b(k)}{\sqrt{2\epsilon(k)(\epsilon(k)-a(k))}} & \frac{b(k)}{\sqrt{2\epsilon(k)(\epsilon(k)+a(k))}} \end{bmatrix}, \quad \begin{cases} a(k) = J\cos(k) - h \\ b(k) = J\sin(k) \end{cases} \tag{4.85}$$

with a dispersion relation

$$\epsilon(k) = \sqrt{J^2 - 2Jh\cos(k) + h^2}. \tag{4.86}$$

If we now redefine the "true" fermionic quasiparticle operators f_k and $f_k^\dagger$ as

$$U(k) \begin{bmatrix} d_k \\ d_{-k}^\dagger \end{bmatrix} \equiv \begin{bmatrix} f_k \\ f_{-k}^\dagger \end{bmatrix}, \tag{4.87}$$

we find the transformed Hamiltonian

$$H = \sum_k 2\epsilon(k) f_k^\dagger f_k - \sum_k \epsilon(k). \tag{4.88}$$

Finally, the ground state energy is given by doing the second sum in the Hamiltonian, which upon transformation to the thermodynamic limit becomes

$$E_0 = -\frac{1}{2\pi} \int_{-\pi}^{\pi} dk \, \sqrt{J^2 - 2Jh\cos(k) + h^2}. \tag{4.89}$$

No closed analytic form exists for the above integral, but one may of course solve it numerically to the desired precision.

4.3.2 Ground State Magnetisation

Knowledge of the relationship between spin operators and the quasiparticle operators describing the true excitations of the Ising model ($S_i \rightarrow$ Jordan-Wigner $\rightarrow$ Fourier $\rightarrow$ Bogoliubov $\rightarrow f_k$) allows us to calculate ground state expectation values. The simplest example is the magnetisation in z-direction, which we will evaluate now. Calculations of this type have been developed by Lieb, Schultz, Mattis (cf. ref. [17]), and in particular Pfeuty (cf. ref. [18]) for the transverse field Ising model. More details are again provided in the appendix.

One defines the magnetisation in the direction of the transverse field as the vacuum expectation value

$$\langle M^z \rangle = \sum_l \langle 0 | S_l^z | 0 \rangle . \tag{4.90}$$

Rewriting the spin operator S_i^z in terms of its Jordan Wigner transforms c_i and $c_i^\dagger$, and performing a subsequent Fourier transform into momentum space yields

$$\langle M^z \rangle = \sum_l \Big[\langle 0 | c_l c_l^\dagger | 0 \rangle - \langle 0 | c_l^\dagger c_l | 0 \rangle \Big] = \sum_k \Big[1 - 2 \langle 0 | d_k^\dagger d_k | 0 \rangle \Big] \tag{4.91}$$

If we now rewrite the final ground state expectation value in terms of the true quasiparticle operators as[11]

$$d_k = -\frac{i\sqrt{a(k)-\epsilon(k)}}{\sqrt{2\epsilon(k)}} f_k + \frac{b(k)}{\sqrt{2\epsilon(k)(\epsilon(k)-a(k))}} f^\dagger_{-k}, \tag{4.92}$$

we can immediately evaluate $\langle 0|d_k^\dagger d_k|0\rangle$. As the f_k's are the creation and annihilation operators of the ground state $|0\rangle$, this leaves us with only a single contribution:

$$\langle M^z\rangle = \sum_k \left[1 - 2\,\frac{b^2(k)}{2\epsilon(k)(\epsilon(k)-a(k))}\right] = -\sum_k \frac{a(k)}{\epsilon(k)} = \sum_k \frac{h - J\cos(k)}{\sqrt{J^2 - 2Jh\cos(k) + h^2}}. \tag{4.93}$$

Transforming to the thermodynamic limit, we then find the ground state magnetisation as

$$\langle M^z\rangle = \frac{1}{\pi}\int_0^\pi dk\, \frac{1 - \frac{J}{h}\cos(k)}{\sqrt{1 - \frac{2J}{h}\cos(k) + \left(\frac{J}{h}\right)^2}}. \tag{4.94}$$

This integral can again be evaluated numerically.

4.4 Entanglement Entropy in Quantum Spin Chains

As the final topic in this chapter, we will (superficially) discuss the entanglement entropy in quantum spin chains. The main result of this section is that an important class of Hamiltonians have ground states which have a "low"[12] entanglement entropy, in comparison with random states. Recalling from the previous chapter that the Schmidt decomposition and the subsequent truncation of the Schmidt values can be interpreted as a truncation of the entanglement entropy, we are thus prompted to believe that this truncation can be used for the faithful representation of a ground state, with only minimal loss of information. This is indeed the basic idea behind the matrix product state construction, which we will formalise in the next chapter. For completeness, we close this chapter by briefly discussing area laws, which generalise the above-mentioned scaling of entanglement entropy to systems of higher dimensions.

4.4.1 Entanglement Entropy in the Ground State of the Ising Model

Below, we will sketch how one could analytically calculate the entanglement entropy of a subsystem of L neighbouring spins in the Ising model, such as illustrated in fig. 2. This generalises the calculation of the previous section, and builds on the fact that knowledge of the quasiparticle operators of the Ising model enables us to evaluate arbitrary ground

[11] Note that one has to take the hermitian conjugate of the matrix $U(k)$ to obtain the coefficients.

[12] To be more precise, an entanglement entropy that scales at worst logarithmically with the system size, as we will explain shortly.

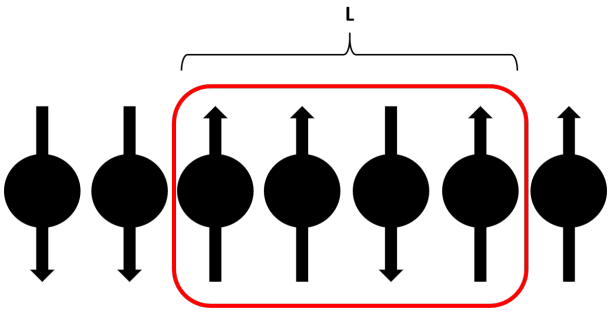

Figure 2: Subsystem of length L of a given spin chain, whose entanglement entropy we want to calculate.

state expectation values. The sole purpose of this section is to present the logic of the calculation, without dwelling on the details. For those, we refer the reader to the original publications, refs. [22, 23], and the short summary ref. [44].

In general, the reduced density matrix of this "window" of spins may be expanded in the basis of L-partite tensor products of Pauli matrices as

$$\rho_L = \sum_{i_1,\ldots,i_L} \rho_{i_1\ldots i_L} S_1^{i_1} \otimes \ldots \otimes S_L^{i_L}, \quad S_j^{i_j} \in \{E, S^x, S^y, S^z\}. \tag{4.95}$$

In this basis, the coefficients of the reduced density matrix ρ_L are then immediately found as the ground state expectation values

$$\rho_{i_1\ldots i_L} \equiv \langle 0|S_1^{i_1} \otimes \ldots \otimes S_L^{i_L}|0\rangle = \langle 0|S_1^{i_1}\ldots S_L^{i_L}|0\rangle\,. \tag{4.96}$$

Recalling the calculation of the ground state magnetisation should prompt us to express the string of Pauli matrices in terms of the elementary excitations of the Ising model, which then in turn enables us to evaluate the expectation value directly.

Aside - Majorana Operators

Majorana operators are a special class of fermions (cf. ref. [45]), and represent their own antiparticles. In addition to obeying the fermionic anticommutation relations, they must therefore also be hermitian operators:

$$\{a_i, a_j\} = 2\delta_{ij}, \quad a_i^\dagger = a_i. \tag{4.97}$$

Vidal et al. propose to study the Ising model in terms of Majorana operators, which in analogy to the Jordan-Wigner transformation are defined as

$$a_{2j-1} \equiv \left(\bigotimes_{l<j} S_l^z\right) \otimes S_j^x, \quad a_{2j} \equiv \left(\bigotimes_{l<j} S_l^z\right) \otimes S_j^y, \tag{4.98}$$

such that expectation values of spin operators are now related to expectation values of Majorana operators:

$$\langle 0|SS\ldots S|0\rangle \iff \langle 0|aa\ldots a|0\rangle\,. \tag{4.99}$$

However, the Majoranas a do not yet diagonalise the Ising Hamiltonian. A further set of transformations is needed to define another set of Majorana operators b:

$$b_p \equiv \sum_m W_{pm} a_m, \tag{4.100}$$

where the transformation matrix W follows from the form of the Ising Hamiltonian in terms of the a-operators. The b-Majoranas have the property of being linear combinations of the true excitations, and as such allow us to evaluate ground state expectation values. One finds:

$$\langle 0|b_p b_q|0\rangle = \delta_{pq} + i\Gamma^B, \quad \text{with} \quad \Gamma^B \equiv \bigoplus_k \begin{bmatrix} 0 & 1 \\ -1 & 0 \end{bmatrix}. \tag{4.101}$$

Knowledge of the b-correlators allows us to infer the a-correlators, as the latter follow through a simple linear transformation of the b's:

$$\langle 0|a_p a_q|0\rangle = \delta_{pq} + i\Gamma^A, \quad \text{with} \quad \Gamma^A = W^T \Gamma^B W. \tag{4.102}$$

Performing this transformation for the Ising model yields

$$\Gamma^A = \begin{bmatrix} \Pi_0 & \Pi_1 & \dots & \Pi_{N-1} \\ -\Pi_1 & \Pi_0 & \dots & \Pi_{N-2} \\ \vdots & & \ddots & \\ -\Pi_{N-1} & \dots & & \Pi_0 \end{bmatrix}, \quad \Pi_l \equiv \begin{bmatrix} 0 & g_l \\ -g_{-l} & 0 \end{bmatrix} \tag{4.103}$$

with

$$g_l \equiv \frac{1}{2\pi} \int_0^{2\pi} d\phi \, e^{-il\phi} \frac{\cos(\phi) - h - i\sin(\phi)}{|\cos(\phi) - h - i\sin(\phi)|}, \tag{4.104}$$

which holds in the thermodynamic limit.

This implies the following recipe to calculate the elements of an arbitrary reduced density matrix:

- Define a block of length L and define the coefficients $\rho_{i_1 \dots i_L}$ as expectation values $\langle 0|S_1^{i_1} \dots S_L^{i_L}|0\rangle$.
- Express the expectation values $\langle 0|SS \dots S|0\rangle$ in terms of a-operators as $\langle 0|aa \dots a|0\rangle$, by using the corresponding transformation rule.
- Use Wick's theorem (cf. ref. [46]) to re-express L-point correlators as sums/ products of 2-point correlators, and calculate the latter by evaluating $\langle 0|a_p a_q|0\rangle = \delta_{pq} + i\Gamma^A$.

Finally, the entanglement entropy follows by plugging the reduced density matrix into the formula for the von Neumann entropy,

$$S(L) \equiv S(\rho_L) = -\operatorname{Tr}\left(\rho_L \ln(\rho_L)\right). \tag{4.105}$$

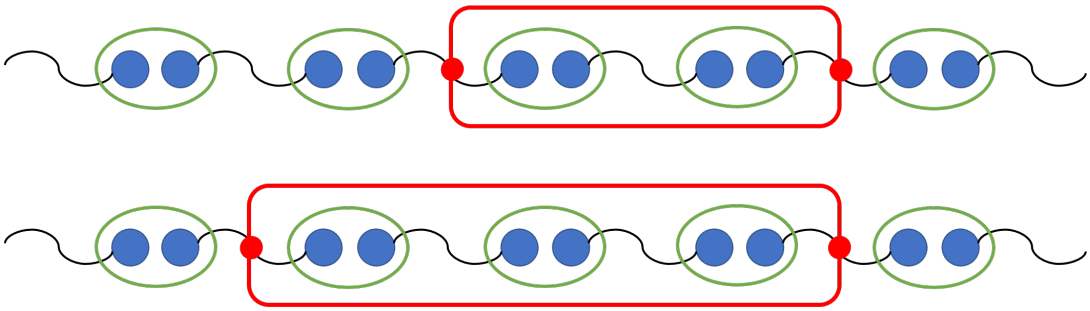

Figure 3: Toy model of a spin chain, whose state has a constant entanglement entropy between subsystems of any size and the rest of the chain.

Note that in ref. [22], Vidal et al. present a second method based on yet another transformation to a new set of Majorana operators to evaluate the entanglement entropy more directly. While being slightly less practical, the method presented here is however equally valid, and closer in spirit to the quasiparticle picture discussed in this thesis. For certain special cases, it is furthermore possible to calculate the integral defining g_l in closed form. The "worst" scaling is found at the critical value of the transverse field $h = 1$, where the entanglement entropy rises monotonically with the subsystem length:

$$S(L) \propto \frac{c}{3} \log_2(L). \tag{4.106}$$

Here, c represents the central charge of the conformal field theory of the same universality class, and is known to be $c = 1/2$ (cf. [22] and references therein). Off-criticality, the entanglement entropy quickly saturates to a constant value instead. We can therefore summarise the scaling laws as

$$S(L) \propto \begin{cases} \text{const.}, & h \neq 1 \,(\text{gapped}^{13}, \text{non-critical system}) \\ \frac{c}{3} \log_2(L), & h = 1 \,(\text{gapless, critical system}). \end{cases} \tag{4.107}$$

4.4.2 Area Laws

The result of the previous section - the fact that the entanglement entropy in the Ising scales only "slowly" with the subsystem size, if at all - is no coincidence. Indeed, Hastings proved (cf. ref. [9]) that for gapped one-dimensional quantum systems with local interactions, the entanglement entropy in the ground state admits an upper bound, and thus asymptotically scales like a constant. To get a flavour for how this type of scaling can arise, consider the spin chain model[14] in fig. 3, where we consider two subsystems of different lengths. Each pair of coupled blue dots represents a singlet state built from spin-1/2 states, i.e. the state $|\psi\rangle = 1/\sqrt{2}\,(|\uparrow\downarrow\rangle - |\downarrow\uparrow\rangle)$, and each green oval corresponds

[13] "Gapped" refers to a (non-zero) energy gap between the ground state and the first excited state.

[14] Adapted from a similar calculation in Vidal's lectures on "Explorations in Condensed Matter Physics", see ref. [26].

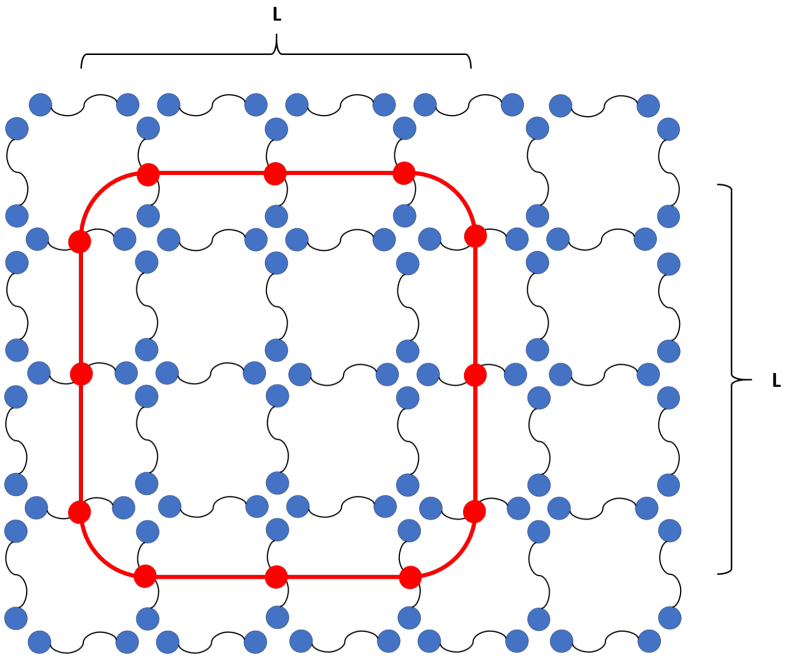

Figure 4: Example of an area law in a two-dimensional toy model. The "volume" of the subsystem corresponds to its area ($L \times L$), but the number of cut bonds is proportional to its circumference, $4 \times L$ (its "area").

to one physical site. Calculating the reduced density matrix of the subsystem gives

$$\rho_L = \frac{I}{2} \otimes \left(\bigotimes_{i=1}^{L-1} |\psi\rangle \langle\psi| \right) \otimes \frac{I}{2}, \tag{4.108}$$

where $\frac{I}{2}$ is the reduced density matrix of a cut spin singlet. By the additivity of the von Neumann entropy, the tensor products turn into a sum of the associated entropies, and we therefore get

$$S(\rho_L) = S\left(\frac{I}{2}\right) + \underbrace{\sum_{i=1}^{L-1} S\left(|\psi\rangle \langle\psi|\right)}_{=0} + S\left(\frac{I}{2}\right) = 2S\left(\frac{I}{2}\right) = 2. \tag{4.109}$$

The middle term evaluates to zero irrespective of its length, as it solely consists of pure states, which by definition have an entanglement entropy of zero. Therefore, the entanglement entropy in this model only depends on the number of cut bounds, which in one dimension is always equal to two. Corrections to this constant scaling would occur if additional entanglement between structures of multiple singlets - i.e. long-range entanglement - were present in the state.

This type of a scaling law is known as an **area law**. In general - and especially in higher dimensions - this refers to a scaling of the entanglement entropy with the *area* of the

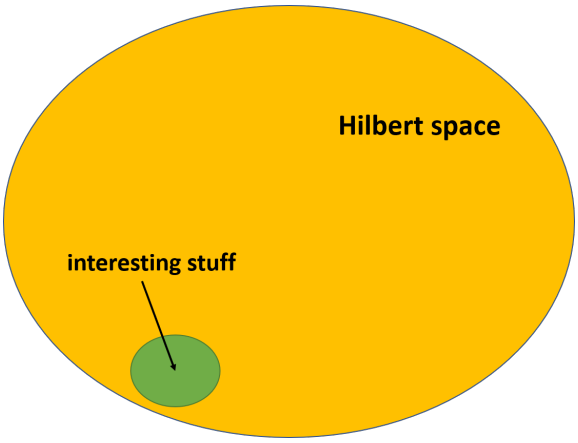

Figure 5: Visualisation of the small low-entanglement corner in Hilbert space, which is of interest for ground state calculations.

subsystem under consideration, and not its *volume* (as one might intuitively expect):

$$S(\rho_L) \propto \begin{cases} L^{D-1} \\ L^{D-1}\log(L). \end{cases} \tag{4.110}$$

Here, L is the characteristic subsystem size, for a model living in D dimensions. As in the one-dimensional case, logarithmic corrections may arise in higher dimensions, too. An area in two dimensions in shown in fig. 4. One of the famous examples of the study of area laws in physics (in a similar context) is Srednicki's calculation of the entanglement entropy of a black hole (see ref. [47]), establishing that the latter is proportional to its surface area. Numerous other examples of area laws have been found and studied. Ref. [48] provides a thorough overview.

We summarise the present theory section pictorially in fig. 5: for many systems of interest, the entanglement entropy in the ground state is "small", as guaranteed by the corresponding area laws. This in turn means that the ground state and states close to the ground state occupy only a very small corner of the total Hilbert space, and do not requite exponentially many degrees of freedom for an efficient description. As we have seen in the previous chapter, there exists a truncation prescription for quantum states which specifically reduces the entanglement contained in those states - the existence of area laws therefore provides the missing link, showing that those truncated, low-entanglement states indeed describe valid physics. Our job is then to devise an efficient parametrisation of quantum states, targeted at the description of the low-entanglement corner of Hilbert space: enter matrix product states.

5 Matrix Product States

In this chapter, we will introduce the class of matrix product states (MPS). On a formal level, this is nothing but an application of the general many-body formalism introduced in the first section. We will start by defining MPS as a decomposition of a general many-body quantum state, which proves that they provide an equivalent representation of the state. Afterwards, we will introduce different canonical forms and the concept of transfer operators, which will allow us to calculate arbitrary overlaps of states efficiently. Then, we will define matrix product operators (MPO), which are the natural counterpart to MPS. This will allow us to evaluate expectation values and correlators. Once all of those more basic notions have been explained, we will investigate some more formal aspects, by studying how bipartite entanglement is captured by MPS. Most importantly, MPS provide the optimal structure to restrict the entanglement contained in a state, building on the idea of state truncations defined in the first chapter. This provides the link to the final section of the last chapter, promoting MPS to the method of choice to represent "area law states" efficiently. To conclude this chapter, we will discuss some examples of representations of physically relevant states and Hamiltonians, and introduce a general principle for the construction of MPO representations of local operators.

This chapter is mainly based on the review article by Schollwöck (cf. ref. [12]), and the lecture series by von Delft and Vidal [25, 26]. If not indicated more specifically, all the information discussed below can be found there. We highly encourage the reader to consult those and the references therein for further details.

5.1 Definition of Matrix Product States

Suppose we are considering the quantum mechanics of N d-dimensional systems, such as N coupled spins. The basis of each "single" space thus consists of d elements and to specify an arbitrary quantum state in the product space, we have to supply $d^N - 1$ (complex) numbers[15]:

$$|\Psi\rangle = \sum_{\sigma_1,\sigma_2,...,\sigma_N} C^{\sigma_1\sigma_2...\sigma_N} |\sigma_1, \sigma_2, ..., \sigma_N\rangle , \quad 1 \leq \sigma_i \leq d. \tag{5.1}$$

In anticipation of the usage of this state for the description of different spin models, we are now indexing the basis vectors with σ's.

Aside - Tensors

In general, a tensor T of rank (n, m) is a multilinear map:

$$T : V_1 \otimes ... \otimes V_n \otimes \tilde{V}_1 \otimes ... \otimes \tilde{V}_m \to \mathbb{C}, \tag{5.2}$$

[15] The normalisation of the state lifts one degree of freedom.

where the V's are vector spaces and the $\tilde{V}$ dual vector spaces (with potentially different dimensions). The map thus needs to be supplied with n vectors and m dual vectors, which are then mapped to a (complex) scalar. Given a basis of the product space,

$$V_1 \otimes ... \otimes V_n \otimes \tilde{V}_1 \otimes ... \otimes \tilde{V}_m = \text{span}\{|e_{i_1}\rangle \otimes ... \otimes |e_{i_n}\rangle \otimes \langle \tilde{e_{j_1}}| \otimes ... \otimes \langle \tilde{e_{j_m}}|\}, \quad (5.3)$$

the components of the tensor in this basis follow as

$$T\left(|e_{i_1}\rangle \otimes ... \otimes |e_{i_n}\rangle \otimes \langle \tilde{e_{j_1}}| \otimes ... \otimes \langle \tilde{e_{j_m}}|\right) = T^{i_1 ... i_n}_{j_1 ... j_m}. \quad (5.4)$$

The wave function $C^{\sigma_1 \sigma_2 ... \sigma_N}$ here can be interpreted as a rank-N tensor, or simply a container for d^N numbers. We can however also view C as a $d \times d^{N-1}$-dimensional matrix, simply by artificially splitting off the first index. This means in turn that we can also use an SVD on that matrix, and thus rewrite C as

$$C^{\sigma_1 \sigma_2 ... \sigma_N} = C^{\sigma_1, [\sigma_2 ... \sigma_N]} = \sum_{k_1=1}^{r_1} U^{\sigma_1}_{k_1} S_{k_1 k_1} \left(V^\dagger\right)^{\sigma_2, \sigma_3 ... \sigma_N}_{k_1}. \quad (5.5)$$

Here, k_1 runs up to $r_1 \equiv d$. We can now reabsorb the singular value matrix S to its right, which defines a new C:

$$C^{\sigma_1 \sigma_2 ... \sigma_N} = \sum_{k_1=1}^{r_1} U^{\sigma_1}_{k_1} C^{\sigma_2, \sigma_3 ... \sigma_N}_{k_1}. \quad (5.6)$$

Next, we repeat this step by reshaping the new C, this time into a $k_1 d \times d^{N-2}$-dimensional matrix, and performing a new singular value decomposition:

$$C^{\sigma_2 \sigma_3 ... \sigma_N}_{k_1} = \sum_{k_2=1}^{r_2} U^{\sigma_2}_{k_1 k_2} S_{k_2 k_2} \left(V^\dagger\right)^{\sigma_3, \sigma_4 ... \sigma_N}_{k_2}. \quad (5.7)$$

Note that, as the first dimension of the matrix has increased to $k_1 d$, the sum over k_2 now may run up to $r_2 \equiv k_1 d$. Again, we can define a new coefficient matrix C by multiplying S into $V^\dagger$:

$$C^{\sigma_2 \sigma_3 ... \sigma_N}_{k_1} = \sum_{k_2=1}^{r_2} U^{\sigma_2}_{k_1 k_2} C^{\sigma_3, \sigma_4 ... \sigma_N}_{k_2}. \quad (5.8)$$

Plugging this into the previous decomposition, we find that the coefficient tensor C now becomes

$$C^{\sigma_1 \sigma_2 ... \sigma_N} = \sum_{k_1=1}^{r_1} \sum_{k_2=1}^{r_2} U^{\sigma_1}_{k_1} U^{\sigma_2}_{k_1 k_2} C^{\sigma_3, \sigma_4 ... \sigma_N}_{k_2}. \quad (5.9)$$

This game can be continued in the same fashion: next, one reshapes C again into a $k_2 d \times d^{N-3}$-dimensional matrix, applies an SVD, absorbs the S matrix into $V^\dagger$ to the right, and so on and so forth. In the end, we may therefore rewrite the wave function of the many-body quantum state as

$$C^{\sigma_1 \sigma_2 ... \sigma_N} = \sum_{k_1=1}^{r_1} \sum_{k_2=1}^{r_2} ... \sum_{k_{N-1}=1}^{r_N} U^{\sigma_1}_{k_1} U^{\sigma_2}_{k_1 k_2} ... U^{\sigma_N}_{k_{N-1}}, \quad (5.10)$$

or equivalently the whole state $|\Psi\rangle$ as

$$|\Psi\rangle = \sum_{k_1=1}^{r_1} \sum_{k_2=1}^{r_2} ... \sum_{k_{N-1}=1}^{r_N} U_{k_1}^{\sigma_1} U_{k_1 k_2}^{\sigma_2} ... U_{k_{N-1}}^{\sigma_N} |\sigma_1, \sigma_2, ..., \sigma_N\rangle \equiv U_{k_1}^{\sigma_1} U_{k_1 k_2}^{\sigma_2} ... U_{k_{N-1}}^{\sigma_N} |\sigma_1, \sigma_2, ..., \sigma_N\rangle \tag{5.11}$$

which is nothing but a product of matrices - hence the name matrix product state[16].

Incidentally, this is the proof that any arbitrary many-body state may always be rewritten in the structure of an MPS[17]. In this sense, MPS are nothing but a decomposition of an object we already know, but will turn out to have very useful properties. Do note, however, that we haven't gotten rid of any of the exponentially many components of the wave function: the complexity is now hidden in the summation indices $k_1, k_2, ..., k_{N-1}$. At each iteration step, we add another factor of d to the "left indices" of the matrix C which we are decomposing. Hence, the summation index of the Schmidt matrix S also increases by a factor of d. This increase continues until the middle of the system, where k can run up to $d^{N/2}$. Afterwards, the range of the k's decreases again, which is is due to the fact that the dimensionality of the singular value matrix is given through the *minimum* of the two dimensions of the matrix to be decomposed.

Furthermore, note that this decomposition is of very limited practical interest, as here we supposed that we already know the exponentially many components of the wave function. We will rather turn the construction upside-down, and *start* by writing down an MPS. Our claim is then that this indeed provides a valid approximation to the full state.

Our general ansatz for an MPS is thus

$$|\Psi\rangle = M_{1k_1}^{\sigma_1} M_{k_1 k_2}^{\sigma_2} ... M_{k_{N-1}1}^{\sigma_N} |\sigma_1, \sigma_2, ..., \sigma_N\rangle , \tag{5.12}$$

with generic rank-3 tensors $M_{k_{i-1}k_i}^{\sigma_i}$. From now on, we will omit explicit summations in most cases, unless they serve to highlight certain properties in particular. The indices k_i which are contracted are called **bond indices**, whereas the indices referring to the basis elements are known as **physical indices**. Often, on represents the first and last tensors with a one-dimensional "dummy index", in order to retain the rank-3 structure of the bulk tensors[18].

The central problem when working with MPS is then to find a state which approximates a given physical situation best. By fixing the bond dimension to an upper value, usually

[16] By constructing the state from the left we have obtained a so-called left-canonical form of a matrix product state. For the present discussion, however, this doesn't have any further relevance, and we will discuss canonical forms further below.

[17] MPS are **dense** in Hilbert space.

[18] This is a bit of condensed matter jargon. "Bulk" means all the elements "somewhere in the system", i.e. not at the boundaries.

denoted by χ or D, we define a manifold of MPS of a given bond dimension. Typically, one employs variational algorithms to reduce the distance to another quantum state as much as possible. A detailed discussion follows in the next chapter.

Let us remark that the idea of MPS came up at several points in history, for instance in refs. [10, 49]. Schollwöck gives a lightning-fast overview of other papers of historic relevance (cf. ref. [12]).

5.2 Gauge Transformations and Canonical Forms

In general, a **gauge transformation** is a mathematical transformation one can perform on a physics object without changing the physics described by the object. This becomes especially useful when certain gauged versions of the same object can be used more easily than the initial object itself. Similar principles hold true for MPS: a given MPS is not uniquely specified! This can easily be seen by inserting a matrix identity $I = XX^{-1}$ between any two tensors on a chain, and contracting them to the left and to the right, respectively:

$$\begin{aligned} C^{\sigma_1\sigma_2\ldots\sigma_N} &= M^{\sigma_1}_{1\alpha_1}\ldots M^{\sigma_i}_{\alpha_{i-1}\alpha_i} M^{\sigma_{i+1}}_{\alpha_i\alpha_{i+1}}\ldots M^{\sigma_N}_{\alpha_{N-1}1} = M^{\sigma_1}_{1\alpha_1}\ldots \underbrace{M^{\sigma_i}_{\alpha_{i-1}k_i} X_{k_i l_i}}_{\equiv D} \underbrace{X^{-1}_{l_i\alpha_i} M^{\sigma_{i+1}}_{\alpha_i\alpha_{i+1}}}_{\equiv E} \ldots M^{\sigma_N}_{\alpha_{N-1}1} \\ &= M^{\sigma_1}_{1\alpha_1}\ldots D^{\sigma_i}_{\alpha_{i-1}\alpha_i} E^{\sigma_{i+1}}_{\alpha_i\alpha_{i+1}}\ldots M^{\sigma_N}_{\alpha_{N-1}1}. \end{aligned} \tag{5.13}$$

One most useful application of this gauge freedom is the possibility to transform MPS into the so-called **canonical forms**, which are much more convenient to work with when it comes to the evaluation of overlaps and expectation values.

In this section, we will introduce the left-, right- and site-canonical forms. Later on, we will pick up the topic again by studying bond-canonical forms and Vidal's Gamma-Lambda form, which will be particularly useful for evaluating the bipartite entanglement in an MPS.

5.2.1 Left- and right-canonical form

First we consider bringing an MPS in **left-canonical** form. Consider a generic MPS:

$$C^{\sigma_1\sigma_2\ldots\sigma_N} = M^{\sigma_1}_{1\alpha_1} M^{\sigma_2}_{\alpha_1\alpha_2}\ldots M^{\sigma_N}_{\alpha_{N-1}1}. \tag{5.14}$$

Similarly to the construction of an MPS from an arbitrary quantum state as discussed before, we can perform an SVD on the first tensor:

$$C^{\sigma_1\sigma_2\ldots\sigma_N} = U^{\sigma_1}_{1\lambda} \underbrace{S_{\lambda\lambda'}(V^\dagger)_{\lambda'\alpha_1} M^{\sigma_2}_{\alpha_1\alpha_2}}_{\equiv M'} \ldots M^{\sigma_N}_{\alpha_{N-1}1}. \tag{5.15}$$

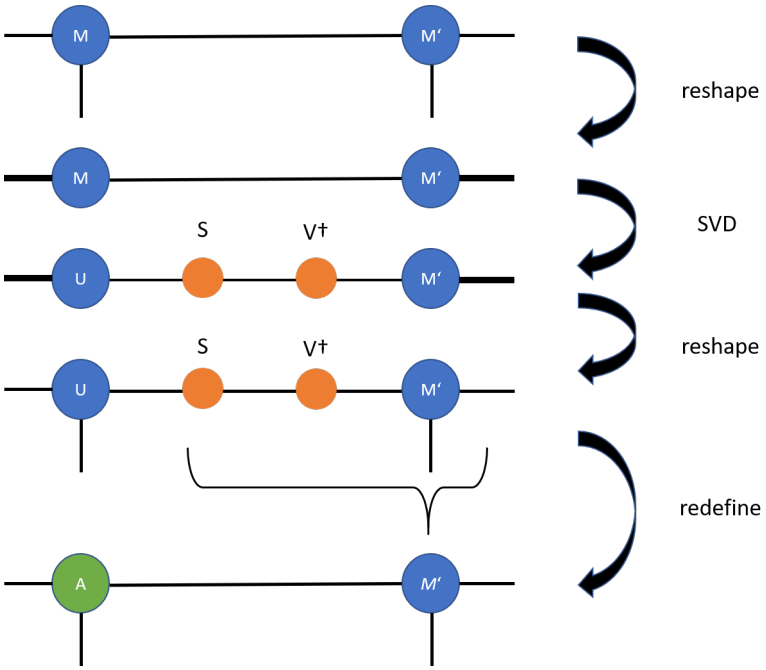

Figure 6: Iteration step during the left-normalisation of a MPS.

By contracting S and $V^\dagger$ into the next tensor on the chain, we can define the new tensor $M' = SV^\dagger M$ (suppressing the involved indices), which leaves the tensor U on the first site. It is customary to call the left-normalised tensor A, and our MPS thus assumes the form

$$C^{\sigma_1\sigma_2\ldots\sigma_N} = A^{\sigma_1}_{1\lambda}(M')^{\sigma_2}_{\alpha_1\alpha_2}\ldots M^{\sigma_N}_{\alpha_{N-1}1}. \tag{5.16}$$

This procedure continues in the same way: next we decompose the new tensor M', absorb its S and $V^\dagger$ into the third tensor in the chain, and so on and so forth. We end up with an MPS entirely built from A-tensors:

$$C^{\sigma_1\sigma_2\ldots\sigma_N} = A^{\sigma_1}_{1\lambda}A^{\sigma_2}_{\alpha_1\alpha_2}\ldots A^{\sigma_N}_{\alpha_{N-1}1}. \tag{5.17}$$

The corresponding iteration step of the algorithm is shown in fig. 6.

Converting a given MPS to **right-canonical** form is very similar to the above algorithm for the left-canonical form, only now we are normalising the chain of tensors starting from the right side. Furthermore, we rename $V^\dagger$ to be the normalised tensor, and absorb U and S in the tensor on the left before moving on:

$$\begin{aligned} C^{\sigma_1\sigma_2\ldots\sigma_N} &= M^{\sigma_1}_{1\alpha_1}\ldots M^{\sigma_{N-1}}_{\alpha_{N-3}\alpha_{N-2}}M^{\sigma_N}_{\alpha_{N-1}1} = M^{\sigma_1}_{1\alpha_1}\ldots M^{\sigma_{N-1}}_{\alpha_{N-3}\alpha_{N-2}}U_{\alpha_{N-2}\lambda}S_{\lambda\lambda'}(V^\dagger)^{\sigma_N}_{\lambda'1} \\ &= M^{\sigma_1}_{1\alpha_1}\ldots(M')^{\sigma_{N-1}}_{\alpha_{N-3}\alpha_{N-2}}B^{\sigma_N}_{\lambda'1} = \ldots = B^{\sigma_1}_{1\alpha_1}\ldots B^{\sigma_{N-1}}_{\alpha_{N-3}\alpha_{N-2}}B^{\sigma_N}_{\alpha_{N-1}1} \end{aligned} \tag{5.18}$$

Fig. 7 shows the corresponding iteration step, where it is again customary to denote the right-normalised matrices under construction by B.

Finally, note that the same left- and right-normalisation procedures can equally as well be carried out by using QR decompositions instead of SVDs. Doing this, one gains some

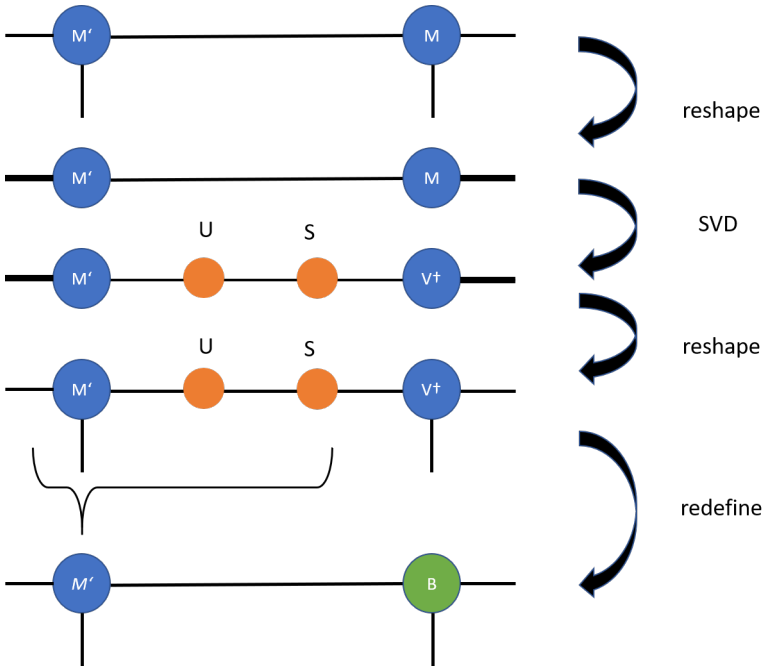

Figure 7: Iteration step during the right-normalisation of a MPS.

numerical performance, but loses the ability to control the bond dimensions during the normalisation. Hence, if one works with MPS which only have small bond dimensions which are furthermore expected to remain small in a given situation, normalisation based on QR decompositions might be a good alternative. Otherwise, the SVD method should be preferred.

Aside - QR decomposition

Let A be a $N \times M$ matrix, with $N \geq M$. Then there exists the **QR decomposition**:

$$A = QR \equiv Q \begin{bmatrix} R \\ 0 \end{bmatrix}. \tag{5.19}$$

It has the following properties:

- Q is a unitary matrix of dimensions $N \times N$.
- R is an upper triangular matrix of dimensions $M \times M$, and "0" fills in the remaining zero entries (with dimension $N - M \times M$).

Various other parametrisations of this decomposition exist.

5.2.2 Site-canonical form

The **site-canonical form** combines the left- and right-canonical forms, leaving one tensor on the chain "highlighted". Furthermore, it allows us to expand the MPS on an orthonormal basis, an idea which will again become most relevant when considering Schmidt

decompositions of MPS.

First, note that that if we naively split an MPS in left-canonical form into a left and a right subsystem:

$$\begin{aligned} |\Psi\rangle &= A^{\sigma_1}...A^{\sigma_l}A^{\sigma_{l+1}}...A^{\sigma_N}\,|\sigma_1...\sigma_l\sigma_{l+1}...\sigma_N\rangle \\ &= \underbrace{(A^{\sigma_1}...A^{\sigma_l})_{1\lambda_l}\,|\sigma_1...\sigma_l\rangle}_{|\lambda_l\rangle_A}\,\underbrace{(A^{\sigma_{l+1}}...A^{\sigma_N})_{\lambda_l 1}\,|\sigma_{l+1}...\sigma_N\rangle}_{|\lambda_l\rangle_B} \\ &= \sum_{\lambda_l} |\lambda_l\rangle_A\,|\lambda_l\rangle_B\,, \end{aligned} \tag{5.20}$$

only the basis pertaining to the left subsystem will be an orthonormal basis, as we can straightforwardly show by calculating the corresponding inner products:

$$\begin{aligned} \langle\lambda_l|\kappa_l\rangle_A &= \sum_{\sigma_1...\sigma_l} (A^{\sigma_1}...A^{\sigma_l})^*_{1\lambda_l}\,(A^{\sigma_1}...A^{\sigma_l})_{1\kappa_l} = \sum_{\sigma_1...\sigma_l} (A^{\sigma_1}...A^{\sigma_l})^\dagger_{\lambda_l 1}\,(A^{\sigma_1}...A^{\sigma_l})_{1\kappa_l} \\ &= \sum_{\sigma_1...\sigma_l} \left(A^{\dagger\sigma_l}... \underbrace{A^{\dagger\sigma_1}A^{\sigma_1}}_{=I} ...A^{\sigma_l} \right)_{\lambda_l\kappa_l} = \sum_{\sigma_2...\sigma_l} \left(A^{\dagger\sigma_l}... \underbrace{A^{\dagger\sigma_2}A^{\sigma_2}}_{=I} ...A^{\sigma_l} \right)_{\lambda_l\kappa_l} \\ &= \delta_{\lambda_l\kappa_l}. \end{aligned} \tag{5.21}$$

In the second equality, we have simply converted the complex conjugate to a hermitian conjugate by transposing the matrices, and then evaluated the hermitian conjugate for every tensor in the left bracket, which reverses the order. After this, the chain successively collapses by the virtue of $A^\dagger A = I$, leaving us with a Kronecker delta. In contrast, this isn't true in the case of the right subsystem:

$$\begin{aligned} \langle\lambda_l|\kappa_l\rangle_B &= \sum_{\sigma_{l+1}...\sigma_N} (A^{\sigma_{l+1}}...A^{\sigma_N})^*_{\lambda_l 1}\,(A^{\sigma_{l+1}}...A^{\sigma_N})_{\kappa_l 1} \\ &= \sum_{\sigma_{l+1}...\sigma_N} (A^{\sigma_{l+1}}...A^{\sigma_N})_{\kappa_l 1}\,(A^{\sigma_{l+1}}...A^{\sigma_N})^*_{\lambda_l 1} \\ &= \sum_{\sigma_{l+1}...\sigma_N} (A^{\sigma_{l+1}}...A^{\sigma_N})_{\kappa_l 1}\,(A^{\sigma_{l+1}}...A^{\sigma_N})^\dagger_{1\lambda_l} \\ &= \sum_{\sigma_{l+1}...\sigma_N} \left(A^{\sigma_{l+1}}... \underbrace{A^{\sigma_N}A^{\dagger\sigma_N}}_{\neq I} ...A^{\dagger\sigma_{l+1}} \right)_{\kappa_l\lambda_l} \neq \delta_{\kappa_l\lambda_l}. \end{aligned} \tag{5.22}$$

Here, the crucial step was to invert the order of the brackets in the first equality, which we may always do as they just denote matrix entries. The rest of the calculations is analogous to above, with the exception that we now end up with expressions like $AA^\dagger \neq I$. A similar reasoning holds for the transformation into the right-canonical form, the only

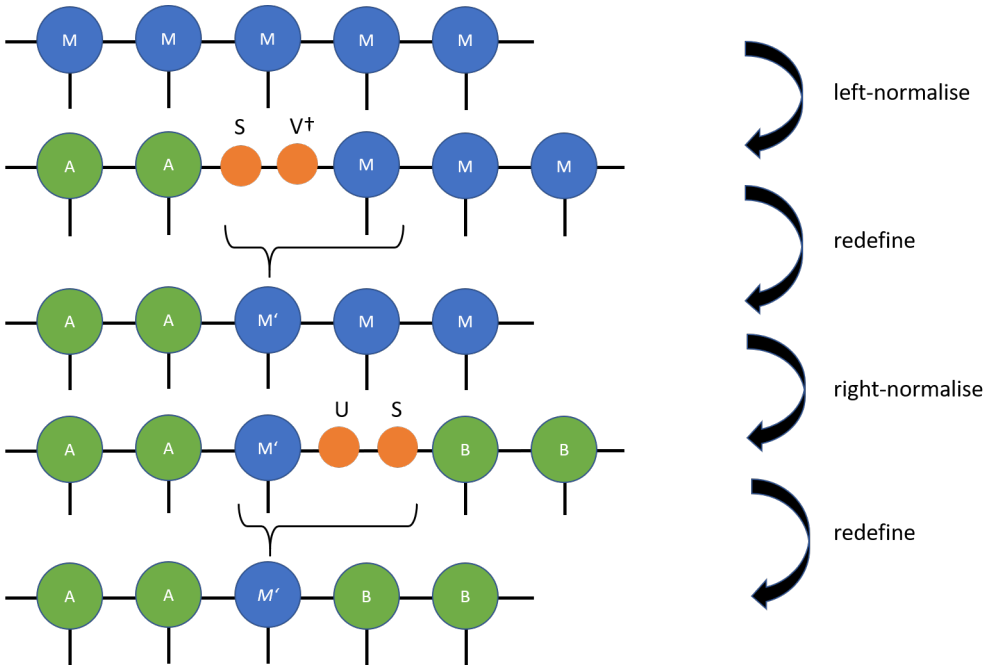

Figure 8: Transformation of a MPS into site-canonical form.

difference being that in this case the B system will have a good orthonormal basis.

Transforming an MPS into **site-canonical** form is one way of solving this problem, by combining the transformations into left- and right-canonical form. Here, we start by choosing a tensor on the chain. Then, we left-normalise the chain on its left, and right-normalise the chain on its right:

$$\begin{aligned} C^{\sigma_1\sigma_2\ldots\sigma_N} &= M^{\sigma_1}_{1\alpha_1}\ldots M^{\sigma_{l-1}}_{\alpha_{l-2}\alpha_{l-1}} M^{\sigma_l}_{\alpha_{l-1}\alpha_l} M^{\sigma_{l+1}}_{\alpha_l\alpha_{l+1}}\ldots M^{\sigma_N}_{\alpha_{N-1}1} \\ &= A^{\sigma_1}_{1\alpha_1}\ldots A^{\sigma_{l-1}}_{\alpha_{l-2}\lambda} \underbrace{S_{\lambda\lambda'}(V^\dagger)_{\lambda'\alpha_{l-1}} M^{\sigma_l}_{\alpha_{l-1}\alpha_l} U_{\alpha_l\kappa} S_{\kappa\kappa'}}_{(M')^{\sigma_l}_{\lambda\kappa'}} B^{\sigma_{l+1}}_{\kappa'\alpha_{l+1}}\ldots B^{\sigma_N}_{\alpha_{N-1}1} \\ &= A^{\sigma_1}_{1\alpha_1}\ldots A^{\sigma_{l-1}}_{\alpha_{l-2}\lambda}(M')^{\sigma_l}_{\lambda\kappa'} B^{\sigma_{l+1}}_{\kappa'\alpha_{l+1}}\ldots B^{\sigma_N}_{\alpha_{N-1}1}. \end{aligned} \tag{5.23}$$

In the last step, the "chosen" tensor has to be contracted with the remnants of the iterated SVDs on the left and right parts of the chain. Possibly, this tensor will have to be SVD'd itself first before this contraction can be performed, in case truncations are desired.

This gives rise to an orthonormal basis in the following way:

$$\begin{aligned}
|\Psi\rangle &= A^{\sigma_1}_{1\alpha_1}...A^{\sigma_{l-1}}_{\alpha_{l-2}\lambda}(M')^{\sigma_l}_{\lambda\kappa'}B^{\sigma_{l+1}}_{\kappa'\alpha_{l+1}}...B^{\sigma_N}_{\alpha_{N-1}1}\,|\sigma_1...\sigma_N\rangle \\
&= \left(A^{\sigma_1}_{1\alpha_1}...A^{\sigma_{l-1}}_{\alpha_{l-2}\lambda}\right)|\sigma_1...\sigma_{l-1}\rangle\,(M')^{\sigma_l}_{\lambda\kappa'}\,|\sigma_l\rangle\left(B^{\sigma_{l+1}}_{\kappa'\alpha_{l+1}}...B^{\sigma_N}_{\alpha_{N-1}1}\right)|\sigma_{l+1}...\sigma_N\rangle \\
&= \underbrace{(A^{\sigma_1}...A^{\sigma_{l-1}})_{1\lambda}\,|\sigma_1...\sigma_{l-1}\rangle}_{|\lambda\rangle_A}(M')^{\sigma_l}_{\lambda\kappa'}\,|\sigma_l\rangle\,\underbrace{(B^{\sigma_{l+1}}...B^{\sigma_N})_{\kappa'1}\,|\sigma_{l+1}...\sigma_N\rangle}_{|\kappa'\rangle_B} \\
&= (M')^{\sigma_l}_{\lambda\kappa'}\,|\sigma_l\rangle\,|\lambda\rangle_A\,|\sigma_l\rangle\,|\kappa'\rangle_B\,.
\end{aligned} \tag{5.24}$$

By the calculations of the previous section, the bases $|\lambda\rangle_A$ and $|\kappa'\rangle_B$ will be orthonormal by construction, and $|\sigma_l\rangle$ is taken to be orthonormal from the outset. Thus we have found an orthonormal basis on which to construct the MPS.

Transforming an MPS into site-canonical form will turn out to be especially useful when we want to calculate the matrix element of an operator between two MPS, as we will show in the next section.

5.3 Basic Matrix Product State Manipulations

Here, we will explain how to perform basic linear-algebraic operations with MPS, namely the inner product and the linear combinations. For the former, we will introduce the important concept of transfer operators, which will be of great use to us in later computations. The latter operation will show that in contrast to what one might intuitively expect, a class of MPS with given bond dimensions is in general not closed under algebraic operations.

5.3.1 Overlaps and Transfer Operators

Aside - Computational Complexity of Tensor Contractions

While the focus of this thesis is the physics of MPS and their algorithms and not a high-performance implementation thereof, it is important to be aware of the fact that the **computational cost** of contracting a tensor network diagram depends on the chosen order of contraction. To make this statement explicit, consider the contraction of the dummy network[a] in fig. 9. Each tensor there has legs of dimension D. The crucial difference is that in the upper line, we first contract the two largest tensors, leading to a cost of $\mathcal{O}(D^5)$ ($\mathcal{O}(D)$ for the contraction of the bond, multiplied by $\mathcal{O}(D^4)$ for the four "dangling" legs of the tensors A and B, for each of which the contraction has to be evaluated). In contrast, choosing a different pair of tensors in the lower line for the first contraction only implies a cost of $\mathcal{O}(D^4)$.

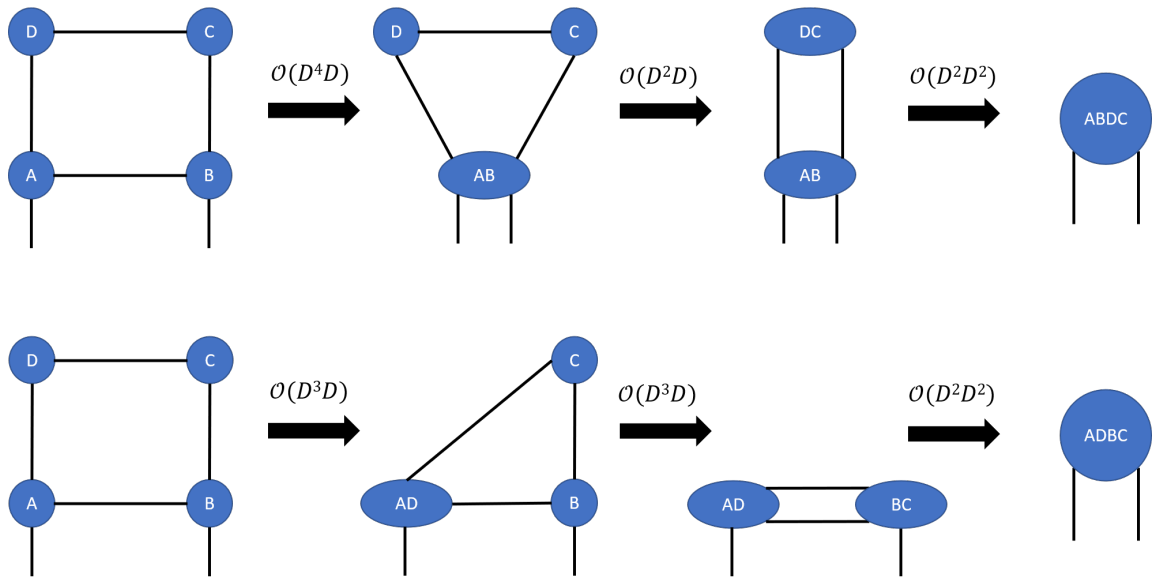

Figure 9: Contraction of a dummy tensor network in two different orders, where each tensor has legs of dimension D. The cost of each step is indicated. Overall, the upper order has a cost of $\mathcal{O}(D^5)$, whereas the lower network has only $\mathcal{O}(D^4)$.

While the second contraction step in the upper network is actually cheaper than in the lower network, it is of course the most expensive contraction that dominates the total cost. When developing and implementing (new) tensor network algorithms, it is important to take such considerations into account.

[a] This example is adapted from von Delft's lectures, ref. [25].

The tensor network representing the overlap of two MPS is shown in fig. 10. In the top line we find the original ket state, and in the bottom line the conjugated bra state. The inner product between two many-body quantum states is given by

$$\begin{aligned}\langle\psi|\phi\rangle &= \sum_{\sigma_1,\sigma_2,\ldots,\sigma_N} \sum_{\sigma_1',\sigma_2',\ldots,\sigma_N'} D^{\sigma_1'\sigma_2'\ldots\sigma_N'} {}^* C^{\sigma_1\sigma_2\ldots\sigma_N} \langle\sigma_1'\sigma_2'\ldots\sigma_N'|\sigma_1\sigma_2\ldots\sigma_N\rangle \\ &= \sum_{\sigma_1,\sigma_2,\ldots,\sigma_N} D^{\sigma_1\sigma_2\ldots\sigma_N} {}^* C^{\sigma_1\sigma_2\ldots\sigma_N},\end{aligned} \tag{5.25}$$

which is of course nothing but a summation over the joint degrees of freedom of both wave functions. Assuming an expansion of the rank-N tensors in matrix product form, such as in fig. 10, this can be written equivalently as

$$\langle\psi|\phi\rangle = \sum_{\sigma_1,\sigma_2,\ldots,\sigma_N} N_{1\alpha_1}^{[1]\sigma_1} {}^* N_{\alpha_1\alpha_2}^{[2]\sigma_2} {}^* N_{\alpha_2\alpha_3}^{[3]\sigma_3} {}^* \ldots N_{\alpha_{N-1}1}^{[N]\sigma_N} {}^* M_{1\beta_1}^{[1]\sigma_1} M_{\beta_1\beta_2}^{[2]\sigma_2} M_{\beta_2\beta_3}^{[3]\sigma_3} \ldots M_{\beta_{N-1}1}^{[N]\sigma_N}. \tag{5.26}$$

In principle, this sum can be performed in any order, and one might try to first sum over all the bond dimensions, before the basis legs are contracted. However, taking into account the computational cost of contracting tensor networks such as in the example illustrated above, the optimal way to perform the contractions proceeds via the definition

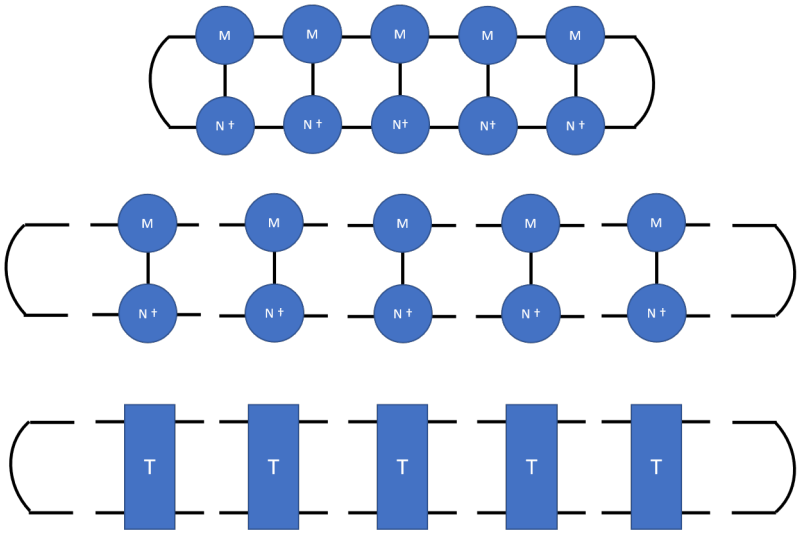

Figure 10: Tensor network representing the contraction of an MPS with a conjugated MPS to find the overlap between the two states. Pairs of tensors can be redefined as transfer operators, which are then successively contracted.

of so-called transfer operators T. They are given by top-bottom pairs of tensors in the overlap-network:

$$\begin{aligned}\langle\psi|\phi\rangle &= \underbrace{\sum_{\sigma_1} N^{[1]\sigma_1 *}_{1\alpha_1} M^{[1]\sigma_1}_{1\beta_1}}_{\equiv T^{[1]}_{\alpha_1\beta_1}} \underbrace{\sum_{\sigma_2} N^{[2]\sigma_2 *}_{\alpha_1\alpha_2} M^{[2]\sigma_2}_{\beta_1\beta_2}}_{\equiv T^{[2]\,\alpha_1\beta_1}_{\alpha_2\beta_2}} \underbrace{\sum_{\sigma_3} N^{[3]\sigma_3 *}_{\alpha_2\alpha_3} M^{[3]\sigma_3}_{\beta_2\beta_3}}_{\equiv T^{[3]\,\alpha_2\beta_2}_{\alpha_3\beta_3}} \dots \underbrace{\sum_{\sigma_N} N^{[N]\sigma_N *}_{\alpha_{N-1}1} M^{[N]\sigma_N}_{\beta_{N-1}1}}_{\equiv T^{[N]\,\alpha_{N-1}\beta_{N-1}}} \\ &= T^{[1]}_{\alpha_1\beta_1} T^{[2]\,\alpha_1\beta_1}_{\alpha_2\beta_2} T^{[3]\,\alpha_2\beta_2}_{\alpha_3\beta_3} \dots T^{[N]\,\alpha_{N-1}\beta_{N-1}}.\end{aligned} \tag{5.27}$$

From an algorithmic perspective, the most straightforward way to calculate the overlap is to build it up iteratively. Defining an initial left-environment $C_{[0]}$ (which is of course nothing else than an identity tensor), we update it by contracting it with the first transfer operator $T_{[1]}$:

$$C^{[0]}_{11} = I, \quad C^{[1]}_{\alpha_1\beta_1} = C^{[0]}_{11} T^{[1]\,11}_{\alpha_1\beta_1} = N^{[1]\sigma_1 *}_{1\alpha_1} C^{[0]}_{11} M^{[1]\sigma_1}_{1\beta_1}. \tag{5.28}$$

The general iteration step is then to take the current C-tensor and to update it with the next transfer operator T in line:

$$C^{[l]}_{\alpha_l\beta_l} = C^{[l-1]}_{\alpha_{l-1}\beta_{l-1}} T^{[l]\,\alpha_{l-1}\beta_{l-1}}_{\alpha_l\beta_l} \tag{5.29}$$

Fig. 11 visualises this construction. At each step, we thus obtain a new rank-2 tensor, with exception of the very last step where no open legs remain - a scalar is the result, which is the sought overlap. Colloquially, this procedure is sometimes referred to as "closing the zipper".

We can repeat this calculation to compute the (squared) norm of an MPS:

$$|| \, |\psi\rangle \, ||^2 = \langle\psi|\psi\rangle \, . \tag{5.30}$$

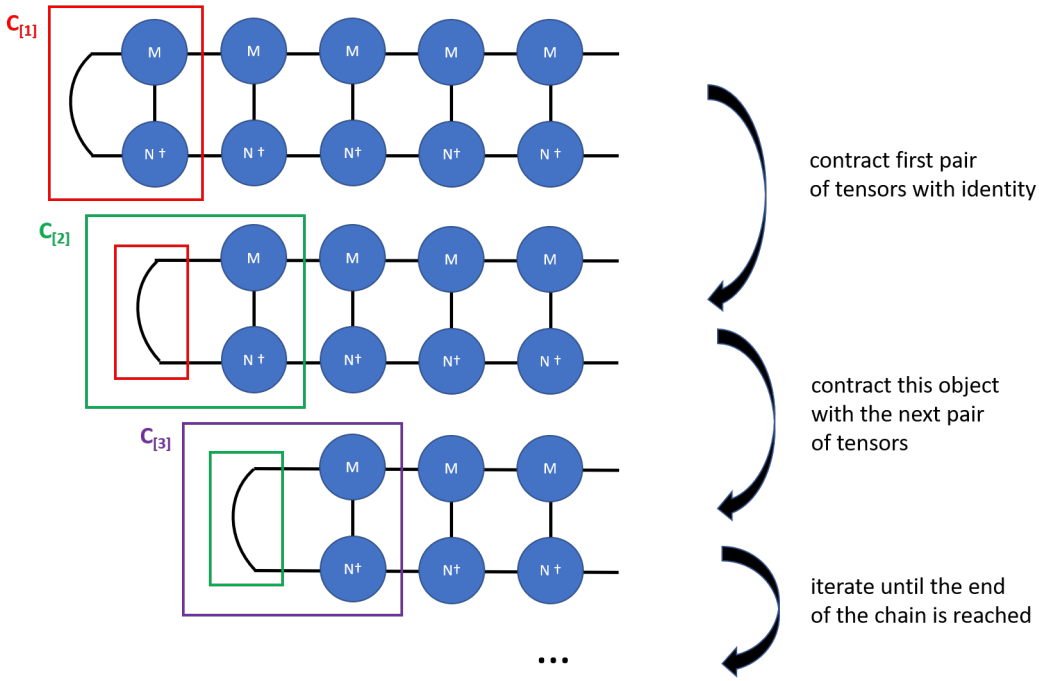

Figure 11: Computation of the overlap of two MPS by successive updates of the left environment C.

Using the results from the previous section, we may assume without loss of generality that the MPS is gauged in left-canonical form. This, however, drastically simplifies our calculation! Consider the first update step:

$$C^{[0]}_{11} = I, \quad C^{[1]}_{\alpha_1\beta_1} = A^{[1]\sigma_1 *}_{1\alpha_1} T^{[0]}_{11} A^{[1]\sigma_1}_{1\beta_1} = A^{[1]\sigma_1 *}_{1\alpha_1} A^{[1]\sigma_1}_{1\beta_1} = I_{\alpha_1\beta_1}, \tag{5.31}$$

which follows immediately from the fact the the A-tensors have been constructed such that $A^\dagger A = I$. Each update step therefore yields a "left zipper" equivalent to the identity matrix. Performing the final contraction is then trivial:

$$I_{11} = 1, \tag{5.32}$$

which proves that the left-gauging is equivalent to a normalisation of an MPS[19]. In a similar fashion, one can iteratively update the environments starting from the right and thus prove that an MPS in right-canonical form is normalised as well.

Replacing conjugate pairs of tensors by transfer operators is however a far more general concept. Any kind of overlap - and later expectation values or correlators - which feature a left-right pseudo-periodicity can be separated into a sequence of transfer operators. Those will of course in general have a more complex structure than the simple contraction of two tensors shown here (e.g. include on-site operators); however the idea of building up the sought contraction iteratively carries over those situations.

[19] In other words, transforming an MPS to a canonical form includes the "division by the square root of the norm" automatically.

5.3.2 Linear Combinations of Matrix Product States

Taking linear combinations of quantum states, such as

$$|\phi\rangle = a\,|\psi_1\rangle + b\,|\psi_2\rangle\,, \tag{5.33}$$

is extremely straightforward when working directly with vector objects. However, there are some caveats when it comes to implementing sums and scalar multiplications with MPS, which we will turn to now.

Starting with the sum of two MPS, let us consider the two states

$$\begin{aligned} |\Psi\rangle &= M^{[1]\,\sigma_1}_{1k_1} M^{[2]\,\sigma_2}_{k_1k_2} \dots M^{[N-1]\,\sigma_{N-1}}_{k_{N-2}k_{N-1}} M^{[N]\,\sigma_N}_{k_{N-1}1}\,|\sigma_1,\sigma_2,\dots,\sigma_{N-1},\sigma_N\rangle\,,\\ |\Phi\rangle &= N^{[1]\,\sigma_1}_{1l_1} N^{[2]\,\sigma_2}_{l_1l_2} \dots N^{[N-1]\,\sigma_{N-1}}_{l_{N-2}l_{N-1}} N^{[N]\,\sigma_N}_{l_{N-1}1}\,|\sigma_1,\sigma_2,\dots,\sigma_{N-1},\sigma_N\rangle\,. \end{aligned} \tag{5.34}$$

Our task is to find the tensors P such that

$$|\Psi\rangle + |\Phi\rangle = P^{[1]\,\sigma_1}_{1p_1} P^{[2]\,\sigma_2}_{p_1p_2} \dots P^{[N-1]\,\sigma_{N-1}}_{p_{N-2}p_{N-1}} P^{[N]\,\sigma_N}_{p_{N-1}1}\,|\sigma_1,\sigma_2,\dots,\sigma_{N-1},\sigma_N\rangle\,, \tag{5.35}$$

is again a valid MPS. Consider the following prescription:

$$\begin{aligned} &\left[M^{[1]\,\sigma_1}_{1k_1}, N^{[1]\,\sigma_1}_{1l_1}\right] \begin{bmatrix} M^{[2]\,\sigma_2}_{k_1k_2} & 0 \\ 0 & N^{[2]\,\sigma_2}_{l_1l_2} \end{bmatrix} \dots \begin{bmatrix} M^{[N-1]\,\sigma_{N-1}}_{k_{N-2}k_{N-1}} & 0 \\ 0 & N^{[N-1]\,\sigma_{N-1}}_{l_{N-2}l_{N-1}} \end{bmatrix} \begin{bmatrix} M^{[N]\,\sigma_N}_{k_{N-1}1} \\ N^{[N]\,\sigma_N}_{l_{N-1}1} \end{bmatrix} |\sigma_1,\sigma_2,\dots,\sigma_{N-1},\sigma_N\rangle \\ &= \left[M^{[1]\,\sigma_1}_{1k_1}, N^{[1]\,\sigma_1}_{1l_1}\right] \begin{bmatrix} M^{[2]\,\sigma_2}_{k_1k_2} \dots M^{[N-1]\,\sigma_{N-1}}_{k_{N-2}k_{N-1}} & 0 \\ 0 & N^{[2]\,\sigma_2}_{l_1l_2} \dots N^{[N-1]\,\sigma_{N-1}}_{l_{N-2}l_{N-1}} \end{bmatrix} \begin{bmatrix} M^{[N]\,\sigma_N}_{k_{N-1}1} \\ N^{[N]\,\sigma_N}_{l_{N-1}1} \end{bmatrix} |\sigma_1,\sigma_2,\dots,\sigma_{N-1},\sigma_N\rangle \\ &= \left(M^{[1]\,\sigma_1}_{1k_1} M^{[2]\,\sigma_2}_{k_1k_2} \dots M^{[N-1]\,\sigma_{N-1}}_{k_{N-2}k_{N-1}} M^{[N]\,\sigma_N}_{k_{N-1}1} + N^{[1]\,\sigma_1}_{1l_1} N^{[2]\,\sigma_2}_{l_1l_2} \dots N^{[N-1]\,\sigma_{N-1}}_{l_{N-2}l_{N-1}} N^{[N]\,\sigma_N}_{l_{N-1}1}\right) |\sigma_1,\sigma_2,\dots,\sigma_{N-1},\sigma_N\rangle\,, \end{aligned} \tag{5.36}$$

which is nothing but the sum of the two MPS. We can thus identify the tensors P as follows:

$$P^{[1]\,\sigma_1}_{1p_1} = \left[M^{[1]\,\sigma_1}_{1k_1}, N^{[1]\,\sigma_1}_{1l_1}\right], \quad P^{[i]\,\sigma_i}_{p_i-1p_i} = \begin{bmatrix} M^{[i]\,\sigma_i}_{k_i-1k_i} & 0 \\ 0 & N^{[i]\,\sigma_i}_{l_i-1l_i} \end{bmatrix}, \quad P^{[N]\,\sigma_N}_{p_{N-1}1} = \begin{bmatrix} M^{[N]\,\sigma_N}_{k_{N-1}1} \\ N^{[N]\,\sigma_N}_{l_{N-1}1} \end{bmatrix}. \tag{5.37}$$

It is important to note, that now each bond index p_i runs in the interval $1 \leq p_i \leq k_i + l_i$ - hence the bond dimension of the resulting MPS has increased. In calculations where multiple sums of MPS are needed, one should therefore take care of compressing the bond dimension after each summation, to avoid a fast growth of the computational resources needed. Furthermore, this implies the somewhat counter-intuitive fact that the set of MPS of fixed bond dimensions is *not* closed under addition.

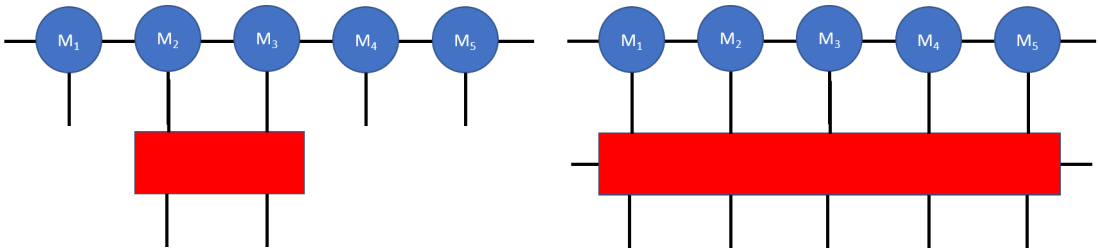

(a) 2-site operator acting on MPS. (b) 5-site operator acting on MPS.

Figure 12: Two examples of generic operators acting on MPS.

Somewhat more straightforward is the scalar multiplication of MPS. Naively, to translate the operation

$$|\Psi\rangle \to a\,|\Psi\rangle\,, \quad a \in \mathbb{C} \tag{5.38}$$

into MPS language, one might assume that it is sufficient to multiply the tensors M in the MPS expansion with a. However, the following reasoning shows that we have to be a little more careful: let us write down the above rescaling explicitly as

$$|\Psi\rangle = \sum_{\sigma_1,\sigma_2,\ldots,\sigma_N} C^{\sigma_1,\sigma_2,\ldots,\sigma_N}\,|\sigma_1,\sigma_2,\ldots,\sigma_N\rangle \to a\,|\Psi\rangle = \sum_{\sigma_1,\sigma_2,\ldots,\sigma_N} a\,C^{\sigma_1,\sigma_2,\ldots,\sigma_N}\,|\sigma_1,\sigma_2,\ldots,\sigma_N\rangle\,. \tag{5.39}$$

We can see that (obviously) each weight of a basis vector has to be multiplied with the factor a. If we now write the state in MPS language as

$$|\Psi\rangle = M^{[1]\,\sigma_1}_{1k_1} M^{[2]\,\sigma_2}_{k_1k_2} \ldots M^{[N]\,\sigma_N}_{k_{N-1}1}\,|\sigma_1,\sigma_2,\ldots,\sigma_N\rangle\,, \tag{5.40}$$

we notice that letting $M \to aM$ leads to an "exponentially boosted" scalar multiplication:

$$'a\,|\Psi\rangle' = \left(aM^{[1]\,\sigma_1}_{1k_1}\right)\left(aM^{[2]\,\sigma_2}_{k_1k_2}\right)\ldots\left(aM^{[N]\,\sigma_N}_{k_{N-1}1}\right)|\sigma_1,\sigma_2,\ldots,\sigma_N\rangle = a^N\,|\Psi\rangle\,. \tag{5.41}$$

The reason for that is course that we *haven't* rescaled the weights of the basis vectors with a, but the M-tensors, which yield the sought weights only *after* performing the matrix multiplication. Therefore, the correct prescription for the scalar multiplication of an MPS is to multiply only *one* of the M-tensors by a, e.g. the first one:

$$M^{[1]\,\sigma_1}_{1k_1} \to a\,M^{[1]\,\sigma_1}_{1k_1}. \tag{5.42}$$

In principle, one can of course also distribute the scalar equally between the tensors on the chain:

$$M^{[l]\,\sigma_l}_{k_{l-1}k_l} \to a^{1/N} M^{[l]\,\sigma_l}_{k_{l-1}k_l}. \tag{5.43}$$

Taking the N^{th}-root might however lead to an additional source of numerical error, hence we will prefer the first prescription.

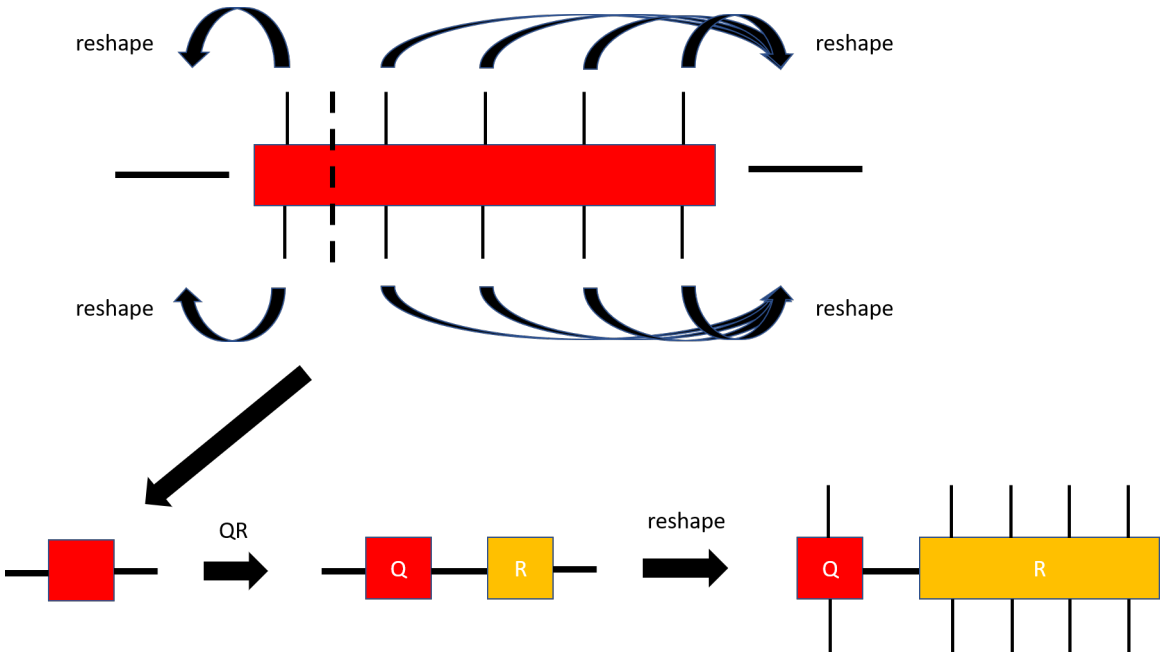

Figure 13: How to turn an arbitrary tensor operator into an MPO by subsequent QR decompositions, first step of the iteration.

5.4 Matrix Product Operators

Matrix product operators (MPO) are the counterpart of MPS, and constitute the second puzzle piece of our translation of standard quantum mechanics into tensor network language. As for MPS, we will start by showing that one may always decompose an arbitrary multi-particle operator into matrix-product language. Then, we will consider the algebra of MPOs and explain how to apply an MPO to an MPS. Most importantly, this will allows us to compute quantities like expectation values and correlators.

The general discussion here follows again ref. [12].

5.4.1 Definition

An arbitrary multiparticle operator O can be constructed as a rank-$2N$ tensor:

$$O \equiv \sum_{\sigma_1',\sigma_2',\ldots,\sigma_N'} \sum_{\sigma_1,\sigma_2,\ldots,\sigma_N} O^{\sigma_1\sigma_2\ldots\sigma_N}_{\sigma_1'\sigma_2'\ldots\sigma_N'} \left|\sigma_1'\sigma_2'\ldots\sigma_N'\right\rangle \left\langle\sigma_1\sigma_2\ldots\sigma_N\right| \tag{5.44}$$

such that when it acts on a wave function C, it yields a again a wave function:

$$(OC)^{\sigma_1\sigma_2\ldots\sigma_N} \equiv \sum_{\sigma_1',\sigma_2',\ldots,\sigma_N'} O^{\sigma_1\sigma_2\ldots\sigma_N}_{\sigma_1'\sigma_2'\ldots\sigma_N'} C^{\sigma_1'\sigma_2'\ldots\sigma_N'} = D^{\sigma_1\sigma_2\ldots\sigma_N} \tag{5.45}$$

Operators which act only non-trivially on a subspace of the product space in which the state lives are correspondingly represented by rank-$2n$ tensors, with $n < N$. Examples

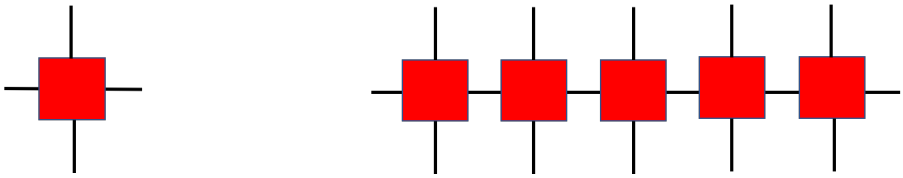

(a) Rank-4 tensor, as building block for an MPO. (b) 5-site matrix product operator

Figure 14: Examples of matrix product operators.

for operators acting on two and five sites, respectively, are shown in fig. 12.

In analogy to how arbitrary wave functions can be represented as MPS, arbitrary operators can be represented as MPOs - i.e. a string of single-site tensors, connected via bonds:

$$O = O^{\sigma_1'\sigma_2'...\sigma_N'}_{\sigma_1\sigma_2...\sigma_N} \left|\sigma_1'\sigma_2'...\sigma_N'\right\rangle \left\langle\sigma_1\sigma_2...\sigma_N\right| = W^{\sigma_1\sigma_1'}_{1\alpha_1} W^{\sigma_2\sigma_2'}_{\alpha_1\alpha_2} ... W^{\sigma_N\sigma_N'}_{\alpha_{N-1}1} \left|\sigma_1'\sigma_2'...\sigma_N'\right\rangle \left\langle\sigma_1\sigma_2...\sigma_N\right| . \tag{5.46}$$

In the second equality, we have reordered the indices on the MPO tensors, such that the physical indices appear in contravariant and the bond indices in covariant notation. Furthermore, dummy indices of dimension one have been added to the boundary tensors. The algorithm which provides a constructive proof that this decomposition is indeed possible is shown in fig. 13. It involves an iterated sequence of QR-decompositions. Note that, similarly as in the representability proof for MPS, the bond dimensions grow exponentially until the middle of the chain in order to account for the exponential number of degrees of freedom in the operator.

For what follows, however, we assume that an MPO with the correct structure is given, as the above decomposition is not a computationally efficient operation. We postpone the discussion how to obtain an exact MPO representation of the operators relevant in the context of quantum many-body physics to the final section of this chapter.

Sometimes it is easier to define boundary vectors v_L and v_R when working with MPOs. Those explicitly project a given rank-4 tensor onto the rank-3 tensor needed as boundary tensor for the MPO. The advantage of this scheme is that one can then define a whole MPO by just keeping a single representative bulk tensor[20], with is repeated a desired number of times. To obtain the boundary tensors, it is then not necessary to save those explicitly, as they can simply be recovered from the bulk tensors by reading out the bond dimension, defining the projectors v_L and v_R and applying them to a bulk tensor. A representation of this idea is shown in fig. 15, where we have intentionally omitted the dummy boundary index in the upper line.

[20] An exception to this is of course the case when the bulk tensors *are* site-dependent. One can still use the scheme with the v_L and v_R projectors, but keeping track of the MPO tensors at each site then becomes a necessity.

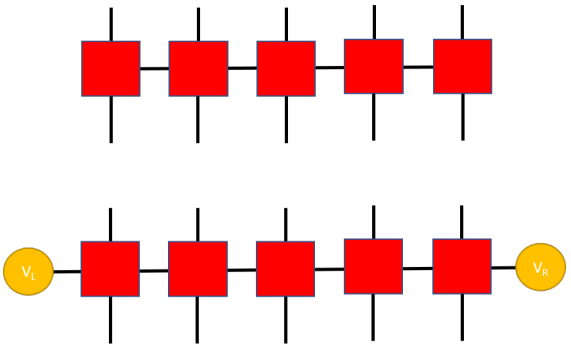

Figure 15: Expressing the boundary tensors of an MPO via the application of projectors v_L and v_R to a representative bulk tensor.

5.4.2 Linear Combinations and Composition of Matrix Product Operators

Just as for MPS, we can take linear combinations of MPOs. In addition, we can also form the composition of two MPOs. We will start with the former operation, which is almost identical to taking linear combinations of MPS.

To add two MPOs, we proceed exactly as for the addition of two MPS. Let

$$\begin{aligned} O &= O^{[1]\,\sigma_1\sigma_1'}_{1\alpha_1} O^{[2]\,\sigma_2\sigma_2'}_{\alpha_1\alpha_2} ... O^{[N]\,\sigma_N\sigma_N'}_{\alpha_{N-1}1} \left|\sigma_1'\sigma_2'...\sigma_N'\right\rangle \left\langle\sigma_1\sigma_2...\sigma_N\right|, \\ P &= P^{[1]\,\sigma_1\sigma_1'}_{1\beta_1} P^{[2]\,\sigma_2\sigma_2'}_{\beta_1\beta_2} ... P^{\sigma_N\sigma_N'}_{[N]\,\beta_{N-1}1} \left|\sigma_1'\sigma_2'...\sigma_N'\right\rangle \left\langle\sigma_1\sigma_2...\sigma_N\right|, \end{aligned} \tag{5.47}$$

then we obtain the MPO tensors representing the operator sum $Q \equiv O + P$ again as a direct sum of the individual MPO tensors:

$$Q = Q^{[1]\,\sigma_1\sigma_1'}_{1\alpha_1} Q^{[2]\,\sigma_2\sigma_2'}_{\alpha_1\alpha_2} ... Q^{[N]\,\sigma_N\sigma_N'}_{\alpha_{N-1}1} \left|\sigma_1'\sigma_2'...\sigma_N'\right\rangle \left\langle\sigma_1\sigma_2...\sigma_N\right| \tag{5.48}$$

with

$$\begin{aligned} Q^{[1]\,\sigma_1,\sigma_1'}_{1q_1} &= \left[O^{[1]\,\sigma_1\sigma_1'}_{1\alpha_1}, P^{[1]\,\sigma_1\sigma_1'}_{1\beta_1}\right], \quad Q^{[i]\,\sigma_i\sigma_i'}_{q_i-1q_i} = \begin{bmatrix} O^{[i]\,\sigma_i\sigma_i'}_{\alpha_i-1\alpha_i} & 0 \\ 0 & P^{[i]\,\sigma_i\sigma_i'}_{\beta_i-1\beta_i} \end{bmatrix}, \\ Q^{[N]\,\sigma_N\sigma_N'}_{q_{N-1}1} &= \begin{bmatrix} O^{[N]\,\sigma_N\sigma_N'}_{\alpha_{N-1}1} \\ P^{\sigma_N\sigma_N'}_{[N]\,\beta_{N-1}1} \end{bmatrix}. \end{aligned} \tag{5.49}$$

We notice again that the bond dimension of the operator sum has increased, with the index q_i running in the interval $1, ..., \alpha_i + \beta_i$.

Unsurprisingly, the scalar multiplication of an MPO, $O \to a\,O$, $a \in \mathbb{C}$, can again be implemented at the level of the individual component tensors by multiplying only *one* of the MPO-tensors:

$$O^{[l]\,\sigma_l\sigma_l'}_{\alpha_{l-1}\alpha_l} \to a\, O^{[l]\,\sigma_l\sigma_l'}_{\alpha_{l-1}\alpha_l} \tag{5.50}$$

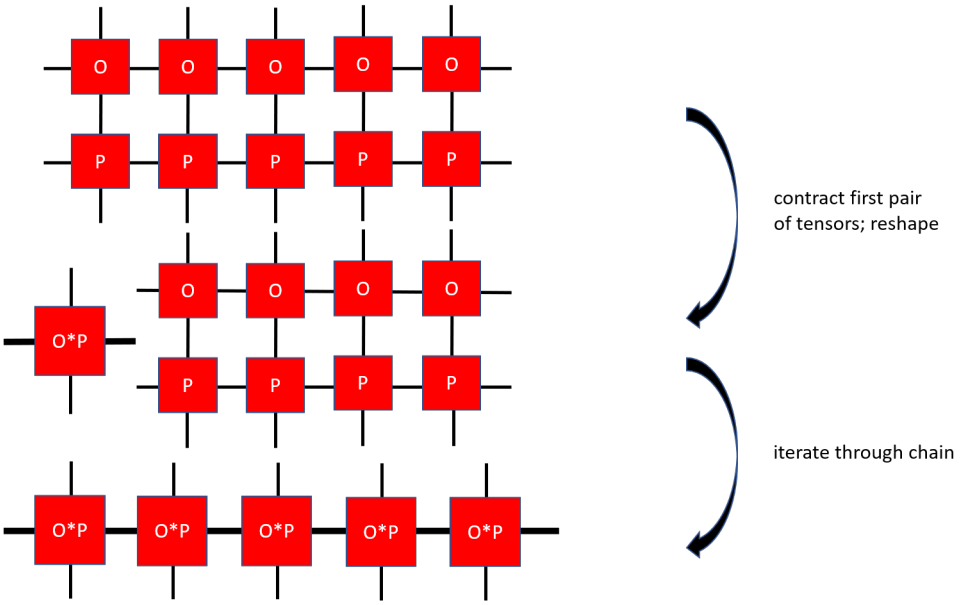

Figure 16: Multiplication of two MPOs. Observe the increasing bond dimensions, represented by the thicker lines.

Compared to addition, the multiplication of two MPOs is more straightforward and doesn't require the construction of direct sums of operators. Consider the composition $Q = OP$ of the two MPOs defined above:

$$
\begin{aligned}
&OP = \\
&= \left(O^{[1]\,\sigma_1\sigma_1'}_{1\alpha_1} O^{[2]\,\sigma_2\sigma_2'}_{\alpha_1\alpha_2} \ldots O^{[N]\,\sigma_N\sigma_N'}_{\alpha_{N-1}1} \left|\sigma_1'\sigma_2'\ldots\sigma_N'\right\rangle \left\langle\sigma_1\sigma_2\ldots\sigma_N\right| \right) \\
&\quad \left(P^{[1]\,\gamma_1\gamma_1'}_{1\beta_1} P^{[2]\,\gamma_2\gamma_2'}_{\beta_1\beta_2} \ldots P^{\gamma_N\gamma_N'}_{[N]\,\beta_{N-1}1} \left|\gamma_1'\gamma_2'\ldots\gamma_N'\right\rangle \left\langle\gamma_1\gamma_2\ldots\gamma_N\right| \right) \\
&= \left(O^{[1]\,\sigma_1\sigma_1'}_{1\alpha_1} P^{[1]\,\sigma_1\gamma_1}_{1\beta_1} \right) \left(O^{[2]\,\sigma_2\sigma_2'}_{\alpha_1\alpha_2} P^{[2]\,\sigma_2\gamma_2}_{\beta_1\beta_2} \right) \ldots \left(O^{[N]\,\sigma_N\sigma_N}_{\alpha_{N-1}1} P^{\sigma_N\gamma_N'}_{[N]\,\beta_{N-1}1} \right) \left|\sigma_1'\sigma_2'\ldots\sigma_N'\right\rangle \left\langle\gamma_1\gamma_2\ldots\gamma_N\right| \\
&= Q^{[1]\,\sigma_1'\gamma_1}_{(1,1)(\alpha_1,\beta_1)} Q^{[2]\,\sigma_2'\gamma_2}_{(\alpha_1,\beta_1)(\alpha_2,\beta_2)} \ldots Q^{[N]\,\sigma_N'\gamma_N}_{(\alpha_{N-1},\beta_{N-1})(1,1)} \left|\sigma_1'\sigma_2'\ldots\sigma_N'\right\rangle \left\langle\gamma_1\gamma_2\ldots\gamma_N\right|
\end{aligned}
\tag{5.51}
$$

with the new MPO tensors

$$
Q^{[i]\,\sigma_i'\gamma_i}_{(\alpha_i-1,\,\beta_i-1)(\alpha_i,\beta_i)} = \sum_{\sigma_i} O^{[i]\,\sigma_i\sigma_i'}_{\alpha_{i-1}\alpha_i} P^{[i]\,\sigma_i\gamma_i}_{\beta_{i-1}\beta_i}. \tag{5.52}
$$

Note that the bond indices of the Q-tensors are now composite indices, running from 1 to $\alpha_i\beta_i$. To implement this multiplication, it is sufficient to sweep through the two MPOs and contract/reshape each pair of tensors separately, as shown in fig. 16.

5.4.3 Matrix Product Operators Acting on Matrix Product States

Letting an MPO act on an MPS is nearly the same operation as the composition of two MPOs, from a computational point of view, and is illustrated in fig. 17. If we take the

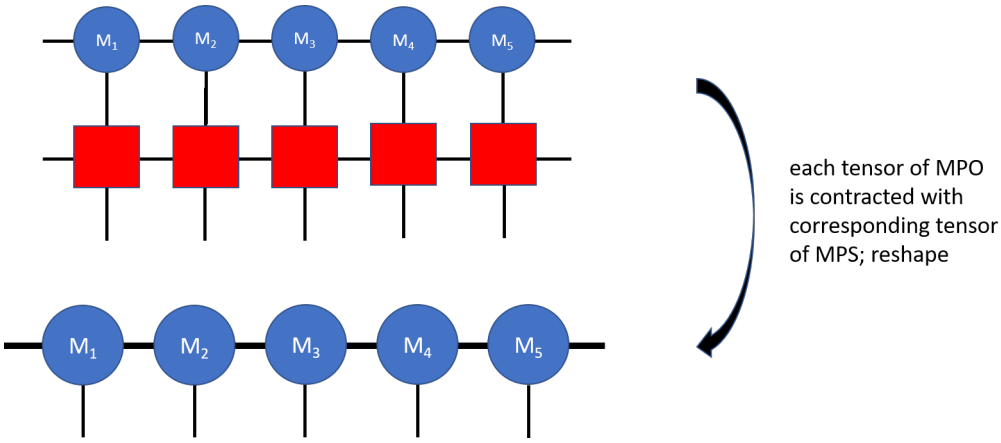

Figure 17: Action of an MPO on an MPS.

MPS

$$|\Psi\rangle = M^{[1]\,\gamma_1}_{1k_1} M^{[2]\,\gamma_2}_{k_1k_2} \dots M^{[N]\,\gamma_N}_{k_{N-1}1} |\gamma_1, \gamma_2, ..., \gamma_N\rangle \tag{5.53}$$

and the MPO

$$O = O^{[1]\,\sigma_1\sigma_1'}_{1\alpha_1} O^{[2]\,\sigma_2\sigma_2'}_{\alpha_1\alpha_2} \dots O^{[N]\,\sigma_N\sigma_N'}_{\alpha_{N-1}1} |\sigma_1'\sigma_2'...\sigma_N'\rangle \langle\sigma_1\sigma_2...\sigma_N| , \tag{5.54}$$

then the operator-vector product $O|\Psi\rangle$ is given by

$$\begin{aligned} O|\Psi\rangle = & \\ &= O^{[1]\,\sigma_1\sigma_1'}_{1\alpha_1} O^{[2]\,\sigma_2\sigma_2'}_{\alpha_1\alpha_2} \dots O^{[N]\,\sigma_N\sigma_N'}_{\alpha_{N-1}1} M^{[1]\,\gamma_1}_{1k_1} M^{[2]\,\gamma_2}_{k_1k_2} \dots M^{[N]\,\gamma_N}_{k_{N-1}1} |\sigma_1'\sigma_2'...\sigma_N'\rangle \langle\sigma_1\sigma_2...\sigma_N|\gamma_1, \gamma_2, ..., \gamma_N\rangle \\ &= \left(O^{[1]\,\gamma_1\sigma_1'}_{1\alpha_1} M^{[1]\,\gamma_1}_{1k_1}\right) \left(O^{[2]\,\gamma_2\sigma_2'}_{\alpha_1\alpha_2} M^{[2]\,\gamma_2}_{k_1k_2}\right) \dots \left(O^{[N]\,\gamma_N\sigma_N'}_{\alpha_{N-1}1} M^{[N]\,\gamma_N}_{k_{N-1}1}\right) |\sigma_1'\sigma_2'...\sigma_N'\rangle \\ &= N^{[1]\,\sigma_1'}_{(1,1)(\alpha_1,k_1)} N^{[2]\,\sigma_2'}_{(\alpha_1,k_1)(\alpha_2,k_2)} \dots N^{[N]\,\sigma_N'}_{(\alpha_{N-1},k_{N-1})(1,1)} |\sigma_1'\sigma_2'...\sigma_N'\rangle , \end{aligned} \tag{5.55}$$

with the new MPS tensors defined as

$$N^{[i]\,\sigma_i'}_{(\alpha_i-1,\,k_i-1)(\alpha_i,k_i)} = \sum_{\gamma_i} O^{[i]\,\gamma_i\sigma_i'}_{\alpha_i-1\,\alpha_i} M^{[i]\,\gamma_i}_{k_i-1\,k_i} . \tag{5.56}$$

This shows that, just as it was the case for the composition of MPOs, the bond dimension of MPO-MPS products increases with each application of an MPO. In general, one thus has to monitor and restrict the bond dimension when many of those products are performed subsequently. In the next chapter, we will discuss an alternative algorithm of applying an MPO to an MPS, which includes a truncation step by directly searching the best approximation of an MPO-MPS product in the space of MPS with a restricted bond dimension.

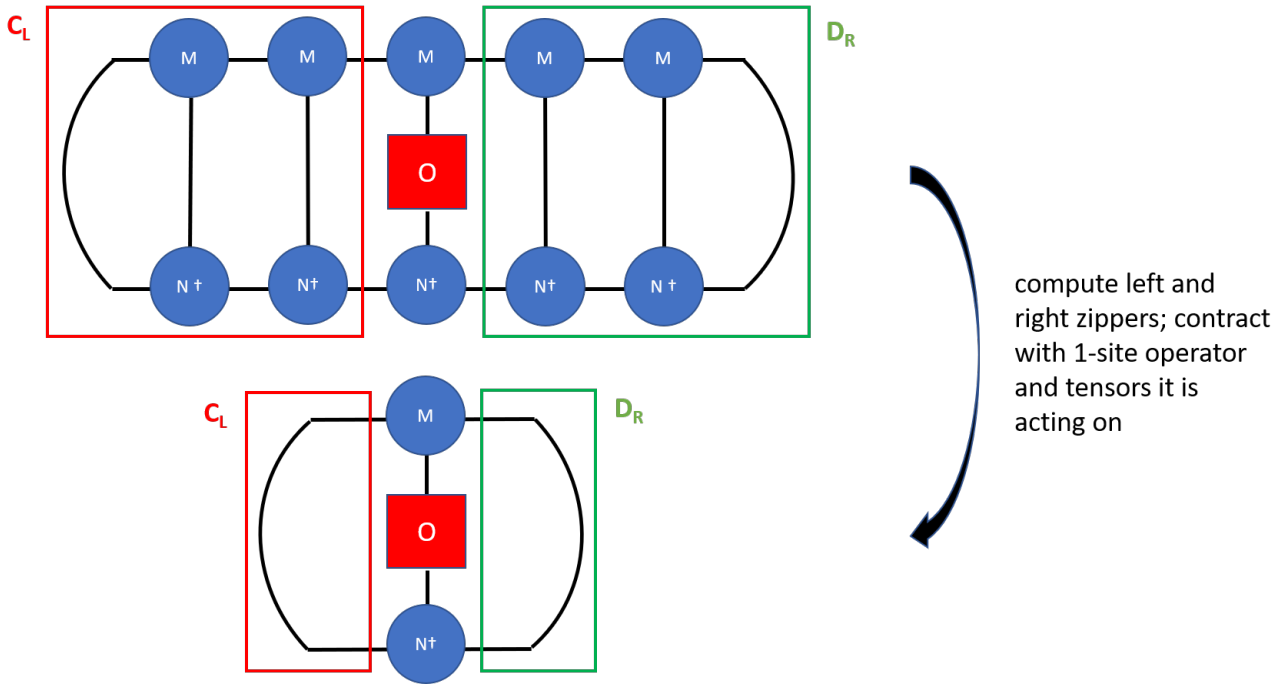

Figure 18: Calculation of the matrix element of a given 1-site operator between two MPS.

5.4.4 Expectation Values of Operators

Another common type of expression one has to deal with are expectation values of operators in a given state, such as

$$\langle\psi|O_{[l]}|\psi\rangle \quad \text{or} \quad \langle\psi|O_{[i]}O_{[j]}|\psi\rangle\,. \tag{5.57}$$

The latter expression corresponds to the correlator between operators at the positions i and j, which we will study in the next subsection.

Evaluating expectation values of single-operators becomes a straightforward task, using the ideas of transfer operators and zippers introduced when discussing the overlap of MPS. In principle, see fig. 18, one can simply calculate the left and right zippers, C and D, and contract the tensor network around the site at which the operator is located:

$$\begin{aligned}\langle\psi|O_{[l]}|\psi\rangle &= \sum_{\substack{\sigma_1,\ldots,\sigma_{l-1}\\ \sigma_{l+1},\ldots,\sigma_N}} \sum_{\gamma_l,\gamma_l'} N^{[1]\sigma_1\,*}_{1\alpha_1} \ldots N^{[l]\gamma_l\,*}_{\alpha_{l-1}\alpha_l} \ldots N^{[N]\sigma_N\,*}_{\alpha_{N-1}1}\, O^{[l]}_{\gamma_l\gamma_l'} N^{[1]\sigma_1}_{1\beta_1} \ldots N^{[l]\gamma_l'}_{\beta_{l-1}\beta_l} \ldots N^{[N]\sigma_N}_{\beta_{N-1}1} \\ &= C^{[L]\,\alpha_{l-1}}_{\beta_{l-1}}\, T^{\alpha_{l-1}\,\alpha_l}_{\beta_{l-1}\beta_l}\, D^{[R]\,\alpha_l}_{\beta_l},\end{aligned} \tag{5.58}$$

with the transfer operator

$$T^{\alpha_{l-1}\,\alpha_l}_{\beta_{l-1}\beta_l} \equiv \sum_{\gamma_l,\gamma_l'} N^{[l]\gamma_l\,*}_{\alpha_{l-1}\alpha_l} O^{[l]}_{\gamma_l\gamma_l'} N^{[l]\gamma_l'}_{\beta_{l-1}\beta_l}. \tag{5.59}$$

While this method is certainly correct, in practice one can achieve a considerable simplification if one transforms the MPS $|\psi\rangle$ into site-canonical form before calculating the

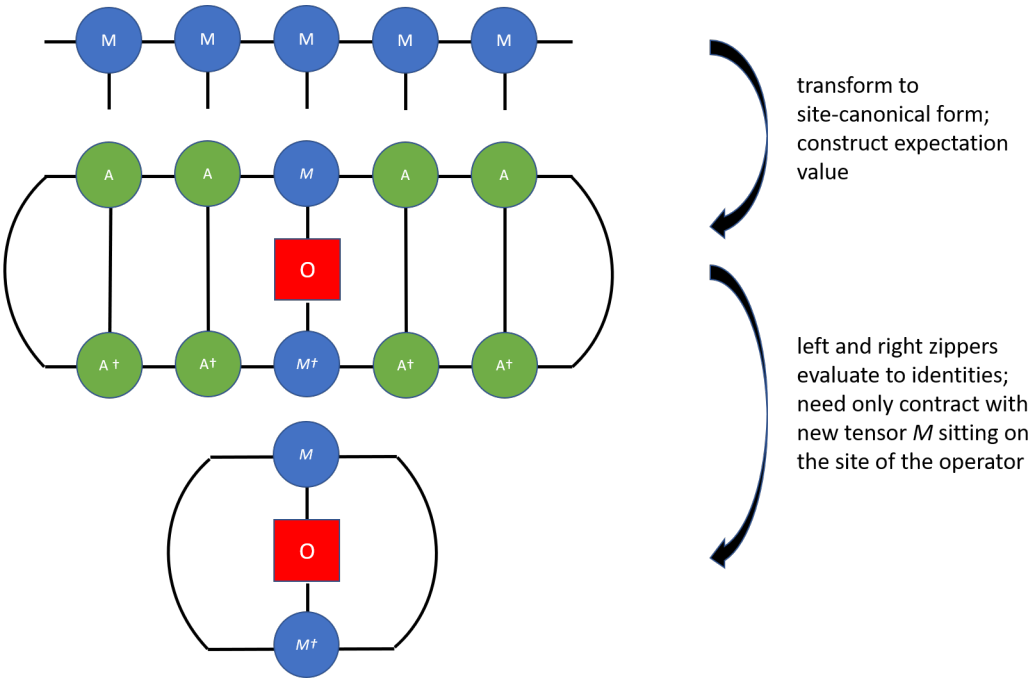

Figure 19: Simplified calculation of the matrix element of a given 1-site operator between, using a prior transformation to the site-canonical form.

expectation value (with respect to the site at which the operator O is located):

$$\begin{aligned}\langle\psi|O_{[l]}|\psi\rangle &= \sum_{\substack{\sigma_1,\dots,\sigma_{l-1}\\ \sigma_{l+1},\dots,\sigma_N}} \sum_{\gamma_l,\gamma_l'} A^{[1]\sigma_1\,*}_{1\alpha_1}\dots M^{[l]\gamma_l\,*}_{\alpha_{l-1}\alpha_l}\dots B^{[N]\sigma_N\,*}_{\alpha_{N-1}1}\, O^{[l]}_{\gamma_l\gamma_l'} A^{[1]\sigma_1}_{1\beta_1}\dots M^{[l]\gamma_l'}_{\beta_{l-1}\beta_l}\dots B^{[N]\sigma_N}_{\beta_{N-1}1} \\ &= \delta^{\alpha_{l-1}}_{\beta_{l-1}}\, T^{\alpha_{l-1}\,\alpha_l}_{\beta_{l-1}\,\beta_l}\, \delta^{\alpha_l}_{\beta_l}.\end{aligned} \tag{5.60}$$

All one has to do is therefore to sum over the outer left and right indices of the transfer matrix T, provided that it has been constructed with the tensor $M_{[l]}$ appearing in the site-canonical form of the MPS.

5.4.5 Correlators

(Two-point) correlators are expressions of the type

$$\langle O_{[i]}O_{[j]}\rangle \equiv \langle\psi|O_{[i]}O_{[j]}|\psi\rangle\,. \tag{5.61}$$

Intuitively, they represent how much the action of a given operator at site i influences its action on site j. For instance, one could use a Pauli Z-gate[21] to read out the spin projection in z-direction at two different sites and compare them. If they tend to be the same up to a certain separation, the state is ordered - correlated - over this correlation length. Studying correlators is of primary importance to probe whether states exhibit a long- or

[21] $S^z = \begin{bmatrix}1 & 0\\ 0 & -1\end{bmatrix}$.

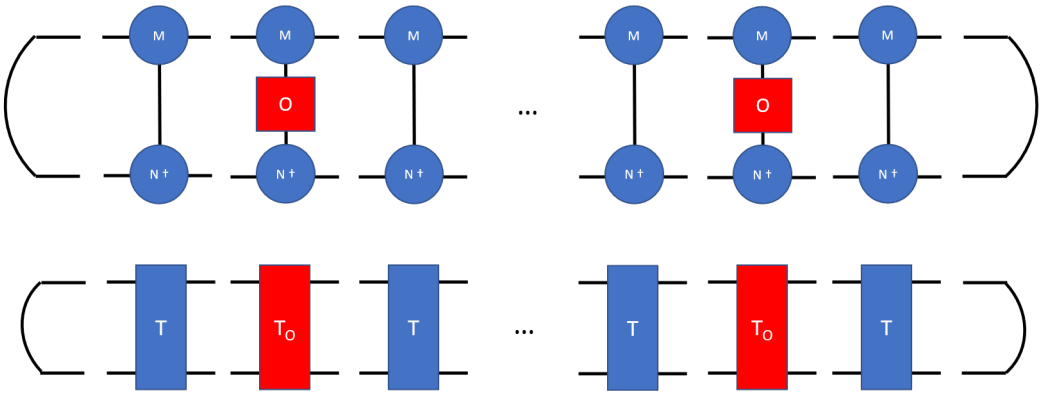

Figure 20: Correlator $\langle\psi|O_{[i]}O_{[j]}|\psi\rangle$ in terms of MPS and equivalent formulation in terms of transfer operators.

short range order.

From a computational perspective, evaluating correlators is no different in comparison to evaluating overlaps or expectation values, and most naturally formulated in the language of transfer matrices. Defining the transfer operators

$$\tilde{T}^{[i]\,\alpha_{i-1}\,\alpha_i}_{\beta_{i-1}\beta_i} \equiv \sum_{\gamma_i,\gamma_i'} N^{[i]\gamma_i\,*}_{\alpha_{i-1}\alpha_i} O^{[i]}_{\gamma_i\gamma_i'} N^{[i]\gamma_i'}_{\beta_{i-1}\beta_i}, \quad \text{and} \quad \tilde{T}^{[j]\,\alpha_{j-1}\,\alpha_j}_{\beta_{j-1}\beta_j} \equiv \sum_{\gamma_j,\gamma_j'} N^{[j]\gamma_j\,*}_{\alpha_{j-1}\alpha_j} O^{[j]}_{\gamma_j\gamma_j'} N^{[j]\gamma_j'}_{\beta_{j-1}\beta_j} \tag{5.62}$$

for the sites containing the operators O, and the "normal" transfer operators T as usual by

$$T^{[l]\,\alpha_{l-1}\,\alpha_l}_{\beta_{l-1}\beta_l} \equiv \sum_{\sigma_l} N^{[l]\sigma_l\,*}_{\alpha_{l-1}\alpha_l} N^{[l]\sigma_l}_{\beta_{l-1}\beta_l}, \tag{5.63}$$

we obtain the correlator as

$$\begin{aligned}\langle O_{[i]}O_{[j]}\rangle = \\ = \sum_{\alpha_1,\ldots,\alpha_{N-1}} \sum_{\beta_1,\ldots,\beta_{N-1}} & T^{[1]\,1\,\alpha_1}_{1\beta_1} \ldots T^{[i-1]\,\alpha_{i-2}\,\alpha_{i-1}}_{\beta_{i-2}\beta_{i-1}} \tilde{T}^{[i]\,\alpha_{i-1}\,\alpha_i}_{\beta_{i-1}\beta_i} T^{[i+1]\,\alpha_i\,\alpha_{i+1}}_{\beta_i\beta_{i+1}} \ldots T^{[j-1]\,\alpha_{j-2}\,\alpha_{j-1}}_{\beta_{j-2}\beta_{j-1}} \tilde{T}^{[j]\,\alpha_{j-1}\,\alpha_j}_{\beta_{j-1}\beta_j} \\ & T^{[j+1]\,\alpha_j\,\alpha_{j+1}}_{\beta_j\beta_{j+1}} \ldots T^{[N]\,\alpha_{N-1}\,1}_{\beta_{N-1}1},\end{aligned} \tag{5.64}$$

which can be computed iteratively.

5.5 Matrix Product States and Entanglement

The purpose of this section is to make the connection between MPS and *physical* quantum states. As we will see shortly, MPS are a generalisation of the state truncation prescription developed in the previous chapter, and thereby yield a direct access to the entanglement entropy contained in a quantum state. We will start by deriving an upper bound

on the entanglement entropy a given MPS can capture, depending on the chosen bond dimension. In order to calculate the entanglement entropy explicitly, this discussion will be followed by introducing the **bond-canonical** form, which is a direct representation of the Schmidt decomposition of a quantum state. Vidal's **Gamma-Lambda** form is then a generalisation of the bond-canonical form, giving immediate access to the Schmidt coefficients across any possible left/right bipartition in an MPS.

For the content presented in this section, we recommend to consult Vidal's original publications [13, 50], where the ideas explained below (and others) have been introduced.

5.5.1 Relationship Between Bond Dimension and Entanglement Entropy

We will begin our analysis of entanglement entropy in the context of MPS by deriving an upper bound on the entanglement entropy an MPS can hold, depending on its bond dimension. For this, no transformation to canonical forms is necessary. Let's start by considering a generic MPS, which is formally split into a left half A and a right half B:

$$\begin{aligned}|\Psi\rangle &= M^{[1]\,\sigma_1}_{1k_1} \dots M^{[l]\,\sigma_l}_{k_{l-1}k_l} M^{[l+1]\,\sigma_{l+1}}_{k_l k_{l+1}} \dots M^{[N]\,\sigma_N}_{k_{N-1}1} |\sigma_1, \dots, \sigma_l, \sigma_{l+1}, \dots, \sigma_N\rangle \\ &= \sum_{k_l} \underbrace{\left(M^{[1]\,\sigma_1} \dots M^{[l]\,\sigma_l}\right)_{1k_l} |\sigma_1, \dots, \sigma_l\rangle}_{\equiv |k_l\rangle_A} \underbrace{\left(M^{[l+1]\,\sigma_{l+1}} \dots M^{[N]\,\sigma_N}\right)_{k_l 1} |\sigma_{l+1}, \dots, \sigma_N\rangle}_{\equiv |k_l\rangle_B} \\ &= \sum_{k_l} |k_l\rangle_A |k_l\rangle_B \,.\end{aligned} \tag{5.65}$$

To find the entropy of entanglement between A and B, we compute the reduced density matrix of, say, the left subsystem. Setting $k_l \equiv k$, the full density matrix is obtained as

$$\rho = |\Psi\rangle\langle\Psi| = \sum_{k,k'} |k\rangle_A |k\rangle_B \langle k'|_A \langle k'|_B \,. \tag{5.66}$$

Then we find the reduced density matrix ρ_A of the system A by tracing over the states spanning the subsystem B:

$$\begin{aligned}\rho_A = \mathrm{Tr}_B(\rho) &= \sum_l \langle l|_B \left[\sum_{k,k'} |k\rangle_A |k\rangle_B \langle k'|_A \langle k'|_B\right] |l\rangle_B \\ &= \sum_{k,k'} |k\rangle_A \left[\sum_l \langle l|k\rangle_B \langle k'|l\rangle_B\right] \langle k'|_A \\ &= \sum_{k,k'} |k\rangle_A \langle k'|k\rangle_B \langle k'|_A \,,\end{aligned} \tag{5.67}$$

where in the second line we have inverted the two scalars in the sum to resolve the identity. We can thus read off the matrix elements of the reduced density matrix as

$$(\rho_A)_{kk'} = \langle k'|k\rangle_B \,. \tag{5.68}$$

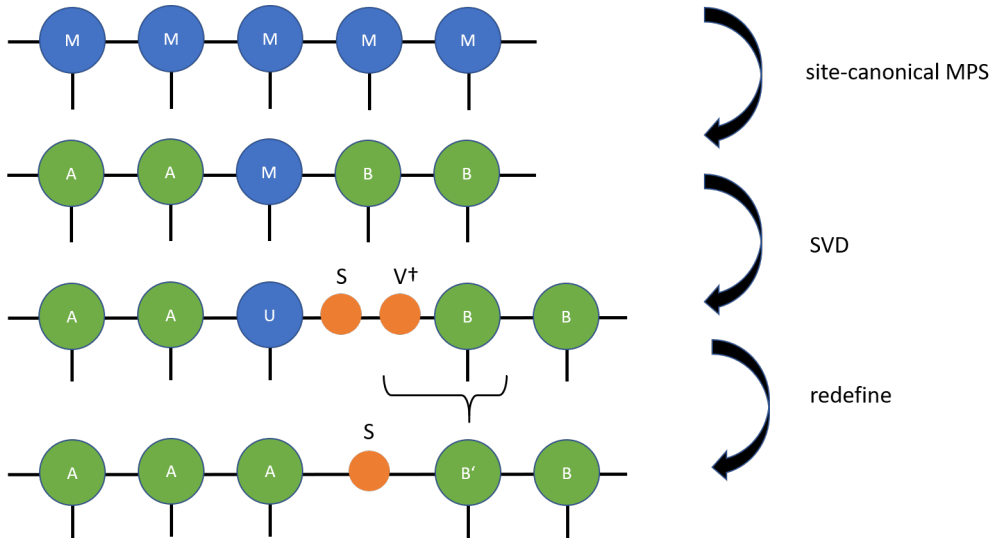

Figure 21: Transformation of an MPS in site-canonical form to bond-canonical form.

By plugging in the definition of the bases in terms of the M-tensors, one can easily derive an exact expression for the matrix elements; however for our discussion it is sufficient to observe that ρ_A is a $D \times D$-matrix, where D is the maximum value of the index k - the bond dimension.

Assuming the reduced density matrix is maximally mixed, we have

$$\rho_A = \text{diag}(\underbrace{\frac{1}{D}, ..., \frac{1}{D}}_{D \text{ times}}). \tag{5.69}$$

Plugging this into the von Neumann entropy immediately yields the inequality

$$S \leq -\sum_{k=1}^{D} \frac{1}{D} \log_2(\frac{1}{D}) = \log_2(D). \tag{5.70}$$

Therefore, an MPS with a bond dimension of D can capture an entanglement entropy up to $\log_2(D)$ for a bipartition at this bond. This implies a straightforward consequence on the physics we want to describe with a given MPS: if we need a certain amount of entanglement entropy in order to accurately model a given effect, the bond dimension has to be chosen as the exponential of that value in order to capture the entanglement!

5.5.2 The Bond-Canonical Form

With the canonical forms we have derived thus far, it is not hard to obtain an exact value for the entanglement entropy at a given bond. In principle, one could of course evaluate the matrix elements of the reduced density matrix ρ_A of a given subsystem, and then calculate the von Neumann entropy by diagonalising this matrix. There is however a much faster and cleaner way to obtain the eigenvalues of the reduced density matrix, building on the site-canonical form of an MPS. The idea is that we want to perform an additional

transformation on the MPS, such that we can rewrite it in a bipartite orthonormal basis. If we achieve this, the Schmidt decomposition and therefore the diagonal elements of the reduced density matrix follow immediately.

Recall the representation of a bipartite quantum system in the Schmidt decomposition:

$$|\psi\rangle = \sum_{i=1}^{r} s_i \, |i\rangle_A \, |i\rangle_B \,, \tag{5.71}$$

where $|i\rangle_A$ and $|i\rangle_B$ are orthonormal bases in both subsystems. Furthermore, we have shown that for a state in site-canonical form,

$$|\Psi\rangle = A^{\sigma_1}_{1\alpha_1} ... A^{\sigma_{l-1}}_{\alpha_{l-2}\lambda} (M')^{\sigma_l}_{\lambda\kappa'} B^{\sigma_{l+1}}_{\kappa'\alpha_{l+1}} ... B^{\sigma_N}_{\alpha_{N-1}1} \, |\sigma_1 ... \sigma_{l-1}\rangle \, |\sigma_l\rangle \, |\sigma_{l+1} ... \sigma_N\rangle \tag{5.72}$$

the bases

$$|\lambda\rangle_A \equiv (A^{\sigma_1} ... A^{\sigma_{l-1}})_{1\lambda} \, |\sigma_1 ... \sigma_{l-1}\rangle \,, \quad |\kappa'\rangle_B \equiv (B^{\sigma_{l+1}} ... B^{\sigma_N})_{\kappa' 1} \, |\sigma_{l+1} ... \sigma_N\rangle \tag{5.73}$$

are both orthonormal bases of the two half-chains, omitting only the local Hilbert space at position l. To generate two orthonormal bases for the "full" half chains, we therefore only have to perform one more SVD on the tensor M on site l, represented graphically in fig. 21:

$$\begin{aligned}
|\Psi\rangle &= A^{\sigma_1}_{1\alpha_1} ... A^{\sigma_{l-1}}_{\alpha_{l-2}\lambda} (M')^{\sigma_l}_{\lambda\kappa'} B^{\sigma_{l+1}}_{\kappa'\alpha_{l+1}} ... B^{\sigma_N}_{\alpha_{N-1}1} \, |\sigma_1 ... \sigma_N\rangle \\
&= A^{\sigma_1}_{1\alpha_1} ... A^{\sigma_{l-1}}_{\alpha_{l-2}\lambda} \underbrace{U^{\sigma_l}_{\lambda\kappa}}_{\equiv \tilde{A}} S_{\kappa\nu} \underbrace{(V^\dagger)_{\nu\kappa'} B^{\sigma_{l+1}}_{\kappa'\alpha_{l+1}}}_{\equiv \tilde{B}} ... B^{\sigma_N}_{\alpha_{N-1}1} \, |\sigma_1 ... \sigma_N\rangle \\
&= A^{\sigma_1}_{1\alpha_1} ... A^{\sigma_{l-1}}_{\alpha_{l-2}\lambda} \tilde{A}^{\sigma_l}_{\lambda\kappa} S_{\kappa\nu} \tilde{B}^{\sigma_{l+1}}_{\nu\alpha_{l+1}} ... B^{\sigma_N}_{\alpha_{N-1}1} \, |\sigma_1 ... \sigma_N\rangle \\
&= \underbrace{\left(A^{\sigma_1} ... \tilde{A}^{\sigma_l}\right)_{1\kappa} |\sigma_1 ... \sigma_l\rangle}_{|\kappa\rangle_A} S_{\kappa\nu} \underbrace{\left(\tilde{B}^{\sigma_{l+1}} ... B^{\sigma_N}\right)_{\nu 1} |\sigma_{l+1} ... \sigma_N\rangle}_{|\nu\rangle_B} \\
&= S_{\kappa\nu} \, |\kappa\rangle_A \, |\nu\rangle_B \,.
\end{aligned} \tag{5.74}$$

This form of the MPS is called the **bond-canonical** form, as we have singled out the Schmidt values on a given bond. Evaluating the entanglement entropy is then a straightforward task; all one has to do is to plug in the squares of the Schmidt values into the definition of the von Neumann entropy.

A priori, it seems that if we wanted to calculate the entanglement entropy for any possible bipartition, we would have to calculate all the different site-canonical and bond-canonical forms separately. There exists however a gauge transformation which gives us access to the Schmidt values for each possible bipartition *immediately*. This will be the subject of the next subsection.

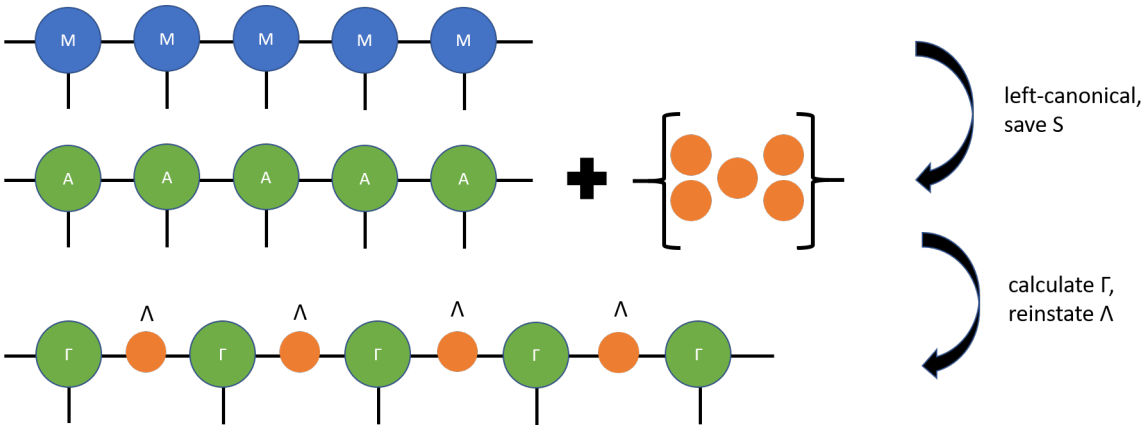

Figure 22: Transformation of an MPS from left-canonical form to Gamma-Lambda form.

5.5.3 Vidal's Gamma-Lambda Form

Our goal thus is to find a gauge transformation of an MPS which always can be separated into a sum over two orthonormal bases, weighted by the respective Schmidt coefficients, regardless of which bond is cut.

To transform a MPS into **Gamma-Lambda form** (cf. ref. [50]) , we start by bringing it into left-canonical form, with one minor difference: in each iteration step, we save the singular value matrix S belonging to a given site on the chain. Once this is done and the MPS brought into left-canonical form, we reinstate the singular value matrices. Renaming

$$\Lambda_{[l]} = S_{[l]}, \tag{5.75}$$

we obtain the Gamma matrices through

$$\Gamma_{[1]} = A_{[1]}, \quad \Lambda_{[l-1]}\Gamma_{[l]} = A_{[l]} \iff \Gamma_{[l]} = \Lambda^{-1}_{[l-1]}A_{[l]}. \tag{5.76}$$

Moreover, the left-normalisation of the A-tensors implies the relations

$$A^\dagger_{[1]}A_{[1]} = \Gamma^\dagger_{[1]}\Gamma_{[1]} = I, \quad A^\dagger_{[l]}A_{[l]} = \Gamma^\dagger_{[l]}\Lambda^\dagger_{[l-1]}\Lambda_{[l-1]}\Gamma_{[l]} = I \quad (l > 1). \tag{5.77}$$

The whole state thus becomes

$$\begin{aligned} |\Psi\rangle &= \Gamma^{\sigma_1}_{[1]}\Lambda_{[1]}\dots\Gamma^{\sigma_{l-1}}_{[l-1]}\Lambda_{[l-1]}\Gamma^{\sigma_l}_{[l]}\Lambda_{[l]}\Gamma^{\sigma_{l+1}}_{[l+1]}\dots\Lambda_{[N-1]}\Gamma^{\sigma_N}_{[N]}\,|\sigma_1\dots\sigma_N\rangle \\ &= \underbrace{\left(\Gamma^{\sigma_1}_{[1]}\Lambda_{[1]}\dots\Gamma^{\sigma_{l-1}}_{[l-1]}\Lambda_{[l-1]}\Gamma^{\sigma_l}_{[l]}\right)_{1\lambda}|\sigma_1\dots\sigma_l\rangle}_{|\lambda\rangle_{A,l}}\,\Lambda^{[l]}_{\lambda\kappa}\,\underbrace{\left(\Gamma^{\sigma_{l+1}}_{[l+1]}\dots\Lambda_{[N-1]}\Gamma^{\sigma_N}_{[N]}\right)_{\kappa 1}|\sigma_{l+1}\dots\sigma_N\rangle}_{|\kappa\rangle_{B,l}} \\ &= \Lambda^{[l]}_{\lambda\kappa}\,|\lambda\rangle_{A,l}\,|\kappa\rangle_{B,l}\,, \end{aligned} \tag{5.78}$$

where the bipartition into two subsystems can now be defined at any site l. To show that this is indeed a Schmidt decomposition, we have to verify that the bases $|\lambda\rangle_{A,l}$ and $|\kappa\rangle_{B,l}$

are orthonormal, respectively:

$$\begin{aligned}
\langle\lambda|\lambda'\rangle_{A,l} &= \left(\Gamma^{\sigma_1}_{[1]}\Lambda_{[1]}...\,\Gamma^{\sigma_{l-1}}_{[l-1]}\Lambda_{[l-1]}\Gamma^{\sigma_l}_{[l]}\right)^*_{1\lambda}\left(\Gamma^{\sigma'_1}_{[1]}\Lambda_{[1]}...\,\Gamma^{\sigma'_{l-1}}_{[l-1]}\Lambda_{[l-1]}\Gamma^{\sigma'_l}_{[l]}\right)_{1\lambda'}\langle\sigma_1,...\,\sigma_l|\sigma'_1,...\,\sigma'_l\rangle \\
&= \left(\Gamma^{\sigma_1}_{[1]}\Lambda_{[1]}...\,\Gamma^{\sigma_{l-1}}_{[l-1]}\Lambda_{[l-1]}\Gamma^{\sigma_l}_{[l]}\right)^\dagger_{\lambda 1}\left(\Gamma^{\sigma_1}_{[1]}\Lambda_{[1]}...\,\Gamma^{\sigma_{l-1}}_{[l-1]}\Lambda_{[l-1]}\Gamma^{\sigma_l}_{[l]}\right)_{1\lambda'} \\
&= \left(\underbrace{\Gamma^{\dagger\,\sigma_l}_{[l]}\Lambda^\dagger_{[l-1]}\Gamma^{\dagger\,\sigma_{l-1}}_{[l-1]}...\,\underbrace{\Gamma^{\dagger\,\sigma_2}_{[2]}\Lambda^\dagger_{[1]}\underbrace{\Gamma^{\dagger\,\sigma_1}_{[1]}\Gamma^{\sigma_1}_{[1]}}_{=I}\Lambda_{[1]}\Gamma^{\sigma_2}_{[2]}}_{=I}...\,\Gamma^{\sigma_{l-1}}_{[l-1]}\Lambda_{[l-1]}\Gamma^{\sigma_l}}_{=I}\right)_{\lambda\lambda'} \\
&= \delta_{\lambda\lambda'}.
\end{aligned} \tag{5.79}$$

Orthonormality is thus guaranteed by a cascade of cancellations, which are themselves due to the properties of the Γ- and Λ-matrices. Verifying orthonormality for the $|\kappa\rangle_{B,l}$-basis is completely analogous to the above calculation. The Λ-matrix on any bond thus indeed holds the Schmidt coefficients, were the state to be cut into two subsystems across that bond.

In the literature, the Gamma-Lambda form is sometimes also referred to as *the* canonical form, due to its useful properties and the fact that the left-canonical form can easily be deduced from it by reabsorbing the Λ-matrices into the Γ-matrices. Equivalently, one could have also chosen the right-canonical form as a starting point for the Gamma-Lambda form. Lastly, note that during the construction of the Γ-tensors, one has to make sure that the matrix inversion of the singular value matrices doesn't become ill-conditioned - as it could potentially be the case for very small singular values. One way of fixing this is to retain only those singular values exceeding a certain threshold, such as 10^{-8}.

5.6 Real Physics in Matrix Product Language

Until now, we have only discussed formal properties of MPOs and MPS. In this final section, we will start to give some simple examples as well as general construction principles of *physically meaningful* MPS and MPOs. The most import take-home message of this section is that there is an explicit way to obtain an MPO representation of short-ranged (and also longer-ranged, but less important for our purposes) Hamiltonians. Those principles apply of course also to operators other than Hamiltonians, which we

will illustrate with further examples.

5.6.1 MPS Representation of Spin States

We commence this section by the comment that in almost all cases, exact representations of quantum states as MPS aren't explicitly needed (since this implies that we already know the state, in which case our job is already done!). It is however instructive to find MPS representations of simple states, in order to match the previous abstract discussions to actual, real physics. One easy example is the **GHZ (Greenberger-Horne-Zeilinger) state** (cf. ref. [51]). It is defined as the following superposition on a 2-state spin chain of length N:

$$|GHZ\rangle = \frac{1}{\sqrt{2}}\left[|0\rangle^{\otimes N} + |1\rangle^{\otimes N}\right]. \tag{5.80}$$

For instance, for a chain of length three we have

$$|GHZ\rangle = \sum_{\sigma_1,\sigma_2,\sigma_3} C^{\sigma_1,\sigma_2,\sigma_3}\,|\sigma_1\sigma_2\sigma_3\rangle = \frac{1}{\sqrt{2}}\left[|000\rangle + |111\rangle\right] = \sum_{\sigma_1,\sigma_2,\sigma_3} A^{\alpha_1}_{\sigma_1} A^{\alpha_1\alpha_2}_{\sigma_2} A^{\alpha_2}_{\sigma_3}\,|\sigma_1\sigma_2\sigma_3\rangle\,. \tag{5.81}$$

From this notation, it becomes immediately clear that we must find matrices A such that, when contracted, they give a rank-3 tensor with exactly two non-zero components: $C^{000} = C^{111} = 1/\sqrt{2}$.

We thus need to find three ingredients: the left boundary tensor, the bulk tensors and the right boundary tensor. Furthermore, we know that the local Hilbert space dimension in each case is two, i.e each site contains two matrices, indexed by $\sigma = 0, 1$. A set of possible matrices to build the GHZ state is the following:

$$A_0 = \begin{bmatrix} 1 & 0 \\ 0 & 0 \end{bmatrix}, \quad A_1 = \begin{bmatrix} 0 & 0 \\ 0 & 1 \end{bmatrix}. \tag{5.82}$$

As boundary tensors, we can then use the vectors

$$A^L_0 = \begin{bmatrix} 1 & 0 \end{bmatrix}, A^L_1 = \begin{bmatrix} 0 & 1 \end{bmatrix}, A^R_0 = \begin{bmatrix} 1 \\ 0 \end{bmatrix}, A^R_1 = \begin{bmatrix} 0 \\ 1 \end{bmatrix}. \tag{5.83}$$

To motivate that those tensors are indeed a good choice, let's calculate some of the wave functions. Take for instance C^{000}:

$$C^{000} = A^L_0 A_0 A^R_0 = \begin{bmatrix} 1 & 0 \end{bmatrix} \begin{bmatrix} 1 & 0 \\ 0 & 0 \end{bmatrix} \begin{bmatrix} 1 \\ 0 \end{bmatrix} = \begin{bmatrix} 1 & 0 \end{bmatrix} \begin{bmatrix} 1 \\ 0 \end{bmatrix} = 1, \tag{5.84}$$

as desired! In contrast, if we replace the inner matrix by A_1, i.e. calculate C^{010}, we obtain:

$$C^{010} = A^L_0 A_1 A^R_0 = \begin{bmatrix} 1 & 0 \end{bmatrix} \begin{bmatrix} 0 & 0 \\ 0 & 1 \end{bmatrix} \begin{bmatrix} 1 \\ 0 \end{bmatrix} = \begin{bmatrix} 1 & 0 \end{bmatrix} \begin{bmatrix} 0 \\ 1 \end{bmatrix} = 0. \tag{5.85}$$

Here, we can see a clear pattern emerging: in order to produce a non-zero coefficient, all the matrices being multiplied must be of the same type, i.e. either all "0-matrices" or all "1-matrices". In other words, only the 000 and 111 strings give non-zero values, which is precisely what we wanted to represent the GHZ state. A similar reasoning holds true for spin chains of an arbitrary length N. Finally, the tensors need to be multiplied with their normalisation factor of $1/\sqrt{2}$, or $2^{-1/2N}$ for normalisations evenly distributed over all tensors.

5.6.2 MPO Representation of Hamiltonians

To represent a Hamiltonian as an MPO, there is a direct factorisation method. We will introduce it via examples - a general construction pattern quickly emerges. Consider, for instance, the Heisenberg XX-Hamiltonian:

$$H = \sum_{l=1}^{N-1} S_l^+ S_{l+1}^- + S_l^- S_{l+1}^+, \quad S^+ = \begin{bmatrix} 0 & 0 \\ 1 & 0 \end{bmatrix}, \quad S^- = \begin{bmatrix} 0 & 1 \\ 0 & 0 \end{bmatrix}, \tag{5.86}$$

where S^+ and S^- are the spin raising and lowering operators. Let's write this out explicitly, e.g. for a spin chain of length three:

$$H = S^+ \otimes S^- \otimes I + S^- \otimes S^+ \otimes I + I \otimes S^+ \otimes S^- + I \otimes S^- \otimes S^+. \tag{5.87}$$

Now see what happens if we define, formally, a matrix of operators:

$$W = \begin{bmatrix} I & 0 & 0 & 0 \\ S^+ & 0 & 0 & 0 \\ S^- & 0 & 0 & 0 \\ 0 & \frac{J}{2} S^- & \frac{J}{2} S^+ & I \end{bmatrix} \tag{5.88}$$

and the corresponding boundary matrices

$$W_L = \begin{bmatrix} 0 & \frac{J}{2} S^- & \frac{J}{2} S^+ & I \end{bmatrix}, \quad W_R = \begin{bmatrix} I \\ S^+ \\ S^- \\ 0 \end{bmatrix}, \tag{5.89}$$

which are read off the last row and first column[22], respectively. This already has a promising structure: we have physical operators - the spin matrices and the identity - which are accessed via physical indices, and we can access them via "more general" matrix indices in the W matrices. So let's suggest that we interpret the position of the physical operators in the W matrices as bond indices. Then we could construct an MPO

[22] This is exactly the effect of the boundary tensors v_L and v_R, introduced previously: they project out the last line and first column, respectively.

Hamiltonian simply by lining up as many W matrices as are needed. Applying the idea to reconstruct the Heisenberg-XX Hamiltonian for the above three-site chain yields:

$$\begin{aligned} W_L W W_R &= \begin{bmatrix} 0 & \frac{J}{2}S^- & \frac{J}{2}S^+ & I \end{bmatrix} \begin{bmatrix} I & 0 & 0 & 0 \\ S^+ & 0 & 0 & 0 \\ S^- & 0 & 0 & 0 \\ 0 & \frac{J}{2}S^- & \frac{J}{2}S^+ & I \end{bmatrix} \begin{bmatrix} I \\ S^+ \\ S^- \\ 0 \end{bmatrix} \\ &= \begin{bmatrix} 0 & \frac{J}{2}S^- & \frac{J}{2}S^+ & I \end{bmatrix} \begin{bmatrix} I \otimes I \\ S^+ \otimes I \\ S^- \otimes I \\ \frac{J}{2}S^- \otimes S^+ + \frac{J}{2}S^+ \otimes S^- \end{bmatrix} \\ &= \frac{J}{2}S^- \otimes S^+ \otimes I + \frac{J}{2}S^+ \otimes S^- \otimes I + \frac{J}{2}I \otimes S^- \otimes S^+ + \frac{J}{2}I \otimes S^+ \otimes S^-, \end{aligned} \tag{5.90}$$

which is exactly the Hamiltonian we wrote down above.

The bulk matrix W can however also be derived systematically, and doesn't need to be plucked out of thin air every time an MPO representation of a Hamiltonian is needed (cf. refs. [52, 53, 54]). For this, we need to consider the different types of terms in the above Hamiltonian and label the different possible transitions between operators in the tensor product. In the case of the XX-Hamiltonian, there are two different types of operator strings:

$$I \overset{4}{\otimes} I \overset{4}{\otimes} \frac{J}{2}S^- \overset{2}{\otimes} S^+ \overset{1}{\otimes} I \overset{1}{\otimes} I, \quad I \overset{4}{\otimes} I \overset{4}{\otimes} \frac{J}{2}S^+ \overset{3}{\otimes} S^- \overset{1}{\otimes} I \overset{1}{\otimes} I. \tag{5.91}$$

This partitioning in four "states" - labelling the operator appended to the immediate left - provides a full classification of *all* possible transitions in the operator strings in the Hamiltonian. Reminiscent of a transition matrix in the context of Markov chains (cf. ref. [55]), this labelling allows us to read off a (4×4) transition matrix for operators. Moving through the operator strings from left to right, the matrix element (i, j) is non-zero if the corresponding transition $(i \to j)$ exists. We therefore obtain the matrix

$$W = \begin{bmatrix} I & 0 & 0 & 0 \\ S^+ & 0 & 0 & 0 \\ S^- & 0 & 0 & 0 \\ 0 & \frac{J}{2}S^- & \frac{J}{2}S^+ & I \end{bmatrix}, \tag{5.92}$$

which is the bulk matrix whose structure we could only justify in retrospect beforehand. This construction principle is of course more general, and can be applied to all operators that admit a counting and labelling of their transitions. Moreover, this also allows us to see how the (operator-) bond dimensions is a direct consequence of the number of transitions in a given operator.

In a very similar fashion, one can obtain more Hamiltonians relevant for the most common spin models. The Ising model with a transverse field,

$$H = -J \sum_{i=1}^{N-1} S_i^z S_{i+1}^z - h \sum_{i=1}^{N} S_i^x, \tag{5.93}$$

can be represented even more compactly, implying a bond dimension of 3:

$$W = \begin{bmatrix} I & 0 & 0 \\ -JS^z & 0 & 0 \\ -hS^z & S^z & I \end{bmatrix}. \tag{5.94}$$

We read off the boundary tensors as

$$W_L = \begin{bmatrix} -hS^z & S^z & I \end{bmatrix}, \quad W_R = \begin{bmatrix} I \\ -JS^z \\ -hS^z \end{bmatrix}. \tag{5.95}$$

Finally, the "complete" Heisenberg Hamiltonian with a transverse field

$$H = \sum_{l=1}^{N-1} \left[J^z S_l^z S_{l+1}^z + \frac{J}{2} S_l^+ S_{l+1}^- + \frac{J}{2} S_l^- S_{l+1}^+ \right] - h \sum_{l=1}^{N} S_l^z \tag{5.96}$$

can be implemented as an MPO via the matrix representation

$$W = \begin{bmatrix} I & 0 & 0 & 0 & 0 \\ S^+ & 0 & 0 & 0 & 0 \\ S^- & 0 & 0 & 0 & 0 \\ S^z & 0 & 0 & 0 & 0 \\ -hS^z & \frac{J}{2}S^- & \frac{J}{2}S^+ & J^z S^z & I \end{bmatrix} \tag{5.97}$$

and corresponding boundary vectors

$$W_L = \begin{bmatrix} -hS^z & \frac{J}{2}S^- & \frac{J}{2}S^+ & J^z S^z & I \end{bmatrix}, \quad W_R = \begin{bmatrix} I \\ S^+ \\ S^- \\ S^z \\ -hS^z \end{bmatrix}. \tag{5.98}$$

5.6.3 Further MPO Representations

Not all relevant operators in quantum mechanics are of course Hamiltonians. We therefore close this section by presenting the MPO representations of other operators needed in the context of this thesis.

The easiest example are on-site operators, i.e. operators of the structure

$$S_i^x \equiv I \otimes ... \otimes \underbrace{I}_{i-1} \otimes \underbrace{S^x}_{i} \otimes \underbrace{I}_{i+1} \otimes ... \otimes I. \tag{5.99}$$

As one can intuitively guess, those can be represented trivially as MPOs by defining the bulk tensors as

$$W_j = \begin{cases} I, & j \neq i \\ S^x, & j = i. \end{cases} \tag{5.100}$$

Since there is no additional structure in the operator space - the bond dimension is zero -, the boundary tensors become $W_L = W_R = 1$.

More interesting to construct are operators which involve sums of terms, as this implies a non-trivial bond dimension. Consider for example the operator of the total spin projection in z-direction:

$$S_{tot}^z = \sum_{i=1}^{N} S_i^z, \tag{5.101}$$

which explicitly (for three sites) is given by

$$S_{tot}^z = S^z \otimes I \otimes I + I \otimes S^z \otimes I + I \otimes I \otimes S^z. \tag{5.102}$$

The MPO representation for the total spin is then

$$W = \begin{bmatrix} I & 0 \\ S^z & I \end{bmatrix} \tag{5.103}$$

with boundary tensors

$$W_L = \begin{bmatrix} S^z & I \end{bmatrix}, \quad W_R = \begin{bmatrix} I \\ S^z \end{bmatrix}. \tag{5.104}$$

Another operator of interest is the spin wave operator:

$$S_k^j = \sqrt{\frac{2}{N+1}} \sum_{i=1}^{N} \sin\left(\frac{ik\pi}{N+1}\right) S_i^j, \tag{5.105}$$

where the index j labels the x, y and z-components of the vector $\vec{S}_k$. As each site is weighted by a prefactor, the bulk tensors become therefore site-dependent, too. Otherwise, the spin wave operator has the same structure as the total magnetisation, and can therefore be expressed as an MPO of bond dimension 2:

$$W_i(k)^j = \begin{bmatrix} I & 0 \\ \sin\left(\frac{ik\pi}{N+1}\right) S^j & I \end{bmatrix}. \tag{5.106}$$

The boundary tensors can again be found (trivially) as the second line and the first column:

$$W_L = \begin{bmatrix} \sin\left(\frac{ik\pi}{N+1}\right) S^j & I \end{bmatrix}, \quad W_R = \begin{bmatrix} I \\ \sin\left(\frac{ik\pi}{N+1}\right) S^j \end{bmatrix}. \tag{5.107}$$

6 Variational Matrix Product State Algorithms

In the previous chapter, we have discussed all the necessary methods to manipulate MPS on a formal level. Furthermore, we have presented a systematic way of implementing relevant quantum mechanical operators as MPOs. However, we still need to explain how to find the states we are interested in, i.e. the eigenstates of the Hamiltonian, and in particular the ground state. While there exist multiple different methods to generate the sought-after states with high precision[23], in this thesis we will focus on variational methods. Their basic principle is that of any variational problem: one wants to extremise a certain quantity, which requires taking a derivative with respect to the degrees of freedom of the problem and then solving the resulting equation. One of the pinnacles of MPS methods, the density matrix renormalisation group (DMRG) (cf. refs. [11, 12, 56, 57, 58, 59]), is built on this principle, and is able to find the ground state of given local Hamiltonians with extraordinary accuracy.

In this chapter, we will discuss variational algorithms - of which DMRG is but one example - in a broader sense. It will be instructive to introduce the class of variational algorithms with a compression scheme for MPS. Building on those principles, it is then straightforward to generalise the algorithm to the case of DMRG and other variational methods, such as the variational application of MPOs to MPS (also shown in ref. [60]). Finally, we will comment on some specific details (and tricks) of the implementation of variational algorithms.

Here, we exclusively deal with DMRG in terms of MPS. The idea of DMRG is however older than that, and the connection to MPS was realised only after several years. For historic details, one may consult the original papers listed above, in particular White's landmark papers [56, 57]. Our presentation is however again modelled after refs. [12, 25].

6.1 Variational Compression

When working with MPS, one usually faces sooner or later the problem of growing bond dimensions, due to the application of an MPO to an MPS or the addition of MPS. A prime example - even though not of immediate relevance in the present project - would be the time evolution of MPS via time evolving block decimation, where layers of neighbouring two-site operators are successively applied to a given MPS[24] (see ref. [13]). To avoid the increasing computational cost associated with the growing bond dimensions, one will need to compress the MPS under construction from time to time, that is, replace it

[23] E.g. a time-evolution in imaginary time, which converges to a projector to the ground state, cf. refs. [12, 13]

[24] A short account of time-evolution is given in the appendix.

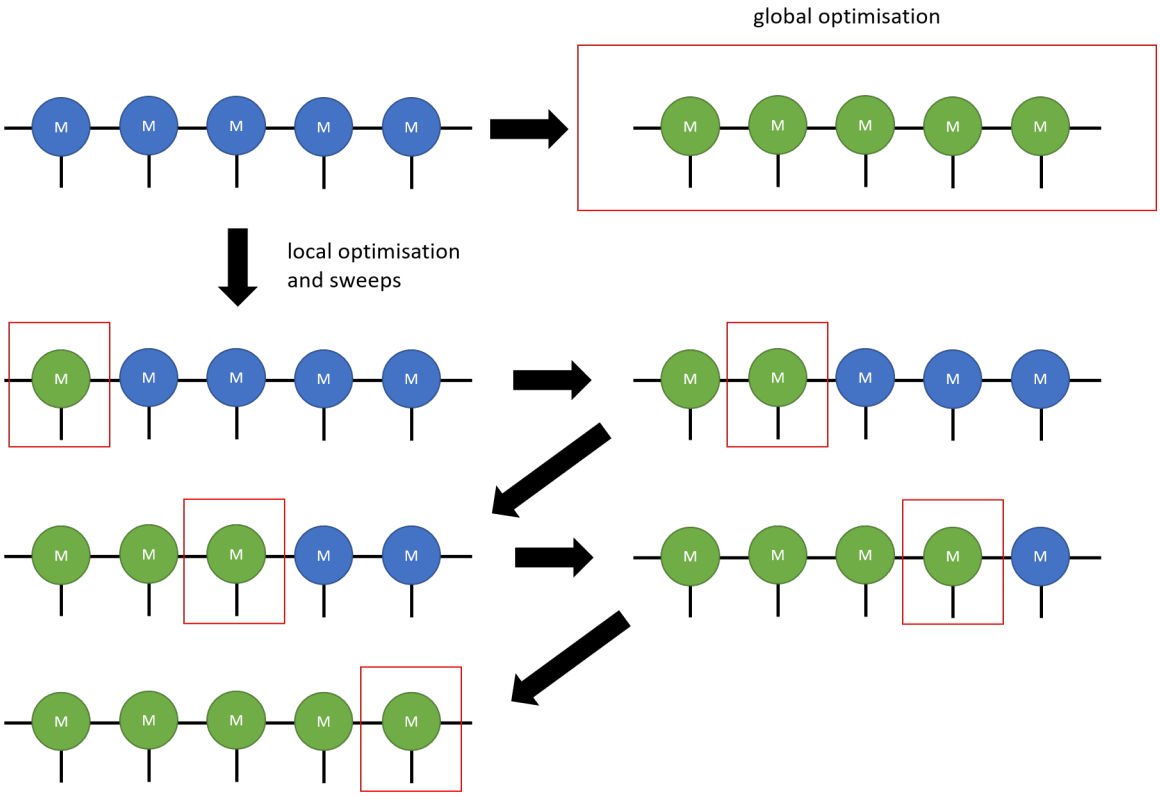

Figure 23: Idea of replacing a single (intractable) optimisation process by sweeps and local updates.

with an MPS with lower bond dimensions. A simple compression scheme would be to perform SVDs - such as in a left-normalisation procedure - after the application of an operator, and only retain a fixed number of singular values. Those **local compression** schemes come essentially for free, however they have the disadvantage of compressing each tensor *independently*. In order to better preserve properties like the long-range order in a given state, **global compression** schemes that take into account the whole state would be a preferable choice. In general, any compressed MPS $|\Psi_{\text{comp}}\rangle$ should approximate the initial MPS $|\Psi_{\text{initial}}\rangle$ optimally in norm, which implies the following equation:

$$\| \, |\Psi_{\text{initial}}\rangle - |\Psi_{\text{comp}}\rangle \, \|^2 < \epsilon \tag{6.1}$$

or

$$\langle \Psi_{\text{initial}} | \Psi_{\text{initial}} \rangle - \langle \Psi_{\text{initial}} | \Psi_{\text{comp}} \rangle - \langle \Psi_{\text{comp}} | \Psi_{\text{initial}} \rangle + \langle \Psi_{\text{comp}} | \Psi_{\text{comp}} \rangle < \epsilon. \tag{6.2}$$

Here, ϵ (typically: $\sim 10^{-8}$, or smaller) is a numerical acceptance threshold the user has to tune to their needs in accuracy.

The basic idea of variational compression - and similarly later of the DMRG algorithm - is the following: instead of varying all degrees of freedom - i.e. the elements of all the tensors - at the same time, we sweep through the MPS chain and take care of each tensor one at a time, thus replacing a large problem with many smaller problems. Fig. 23 illustrates this idea. At each step, we do however take information from the whole

tensor network into account, such that each single tensor is "globally" optimised. Repeating such sweeps multiple times will result in the sought state, usually with high accuracy. The reason why treating those problems tensor by tensor is as attractive as powerful, is that the resulting equations turn out to be simple linear algebra problems, but of manageable dimensions. Standard and well-established numerical solution methods can then be employed to progress further.

Let us now work out what those "on-site" problems to solve will be. Consider a known state $|\Psi_{initial}\rangle$ of given bond dimensions, constructed with tensors generically denoted by M. Desiring an approximation of $|\Psi_{initial}\rangle$ with a smaller bond dimension, we want to find the state $|\Psi_{comp}\rangle$ such that $\| \, |\Psi_{initial}\rangle - |\Psi_{comp}\rangle \, \|^2$ is minimal. Denoting the elements of $|\Psi_{comp}\rangle$ by N, we will perform a minimisation with respect to a given site. In order to find a resulting equation which yields a new, optimised N-tensor, we will have to take the derivative with respect to the conjugated N^*-tensor. The structure of the derivative becomes clearer if we first write down the expression to be minimised in terms of the component tensors:

$$
\begin{aligned}
&\langle \Psi_{\text{initial}} | \Psi_{\text{initial}} \rangle - \big\langle \Psi_{\text{initial}} \big| \Psi_{\text{comp}} \big\rangle - \big\langle \Psi_{\text{comp}} \big| \Psi_{\text{initial}} \big\rangle + \big\langle \Psi_{\text{comp}} \big| \Psi_{\text{comp}} \big\rangle \\
&\quad = \sum_{\sigma_1,\dots\sigma_N} \left(M^{\alpha_1 *} \dots M^{\alpha_{j-2},\alpha_{j-1} *}\right)_{\sigma_1,\dots\sigma_{j-1}} M^{\alpha_{j-1},\alpha_j *}_{\sigma_j} \left(M^{\alpha_j,\alpha_{j+1} *} \dots M^{\alpha_N *}\right)_{\sigma_{j+1},\dots\sigma_N} \\
&\qquad\qquad \left(M^{\alpha_1} \dots M^{\alpha_{j-2},\alpha_{j-1}}\right)_{\sigma_1,\dots\sigma_{j-1}} M^{\alpha_{j-1},\alpha_j}_{\sigma_j} \left(M^{\alpha_j,\alpha_{j+1}} \dots M^{\alpha_N}\right)_{\sigma_{j+1},\dots\sigma_N} \\
&\quad - \sum_{\sigma_1,\dots\sigma_N} \left(M^{\alpha_1 *} \dots M^{\alpha_{j-2},\alpha_{j-1} *}\right)_{\sigma_1,\dots\sigma_{j-1}} M^{\alpha_{j-1},\alpha_j *}_{\sigma_j} \left(M^{\alpha_j,\alpha_{j+1} *} \dots M^{\alpha_N *}\right)_{\sigma_{j+1},\dots\sigma_N} \\
&\qquad\qquad \left(N^{\alpha_1} \dots N^{\alpha_{j-2},\alpha_{j-1}}\right)_{\sigma_1,\dots\sigma_{j-1}} N^{\alpha_{j-1},\alpha_j}_{\sigma_j} \left(N^{\alpha_j,\alpha_{j+1}} \dots N^{\alpha_N}\right)_{\sigma_{j+1},\dots\sigma_N} \\
&\quad - \sum_{\sigma_1,\dots\sigma_N} \left(N^{\alpha_1 *} \dots N^{\alpha_{j-2},\alpha_{j-1} *}\right)_{\sigma_1,\dots\sigma_{j-1}} N^{\alpha_{j-1},\alpha_j *}_{\sigma_j} \left(N^{\alpha_j,\alpha_{j+1} *} \dots N^{\alpha_N *}\right)_{\sigma_{j+1},\dots\sigma_N} \\
&\qquad\qquad \left(M^{\alpha_1} \dots M^{\alpha_{j-2},\alpha_{j-1}}\right)_{\sigma_1,\dots\sigma_{j-1}} M^{\alpha_{j-1},\alpha_j}_{\sigma_j} \left(M^{\alpha_j,\alpha_{j+1}} \dots M^{\alpha_N}\right)_{\sigma_{j+1},\dots\sigma_N} \\
&\quad + \sum_{\sigma_1,\dots\sigma_N} \left(N^{\alpha_1 *} \dots N^{\alpha_{j-2},\alpha_{j-1} *}\right)_{\sigma_1,\dots\sigma_{j-1}} N^{\alpha_{j-1},\alpha_j *}_{\sigma_j} \left(N^{\alpha_j,\alpha_{j+1} *} \dots N^{\alpha_N *}\right)_{\sigma_{j+1},\dots\sigma_N} \\
&\qquad\qquad \left(N^{\alpha_1} \dots N^{\alpha_{j-2},\alpha_{j-1}}\right)_{\sigma_1,\dots\sigma_{j-1}} N^{\alpha_{j-1},\alpha_j}_{\sigma_j} \left(N^{\alpha_j,\alpha_{j+1}} \dots N^{\alpha_N}\right)_{\sigma_{j+1},\dots\sigma_N} \\
&\quad \stackrel{!}{=} \text{minimal.}
\end{aligned}
\tag{6.3}
$$

To execute the minimisation, we differentiate the above expression[25] with respect to $N^{\alpha_{j-1},\alpha_j *}_{\sigma_j}$. One can see immediately that the first two sums will drop out, as they contain

[25] A previous version of this text read "index jungle" instead of "expression", and we continue to deem it the more appropriate choice. Don't let the abundance of indices lead you astray; the above equation is nothing but a sum over different variables.

none of the N^*-tensors. Hence we effectively only need to normalise the second half of the overlap of initial and compressed states:

$$\begin{aligned}
&\frac{\partial}{\partial N_{\sigma_j}^{\alpha_{j-1},\alpha_j *}} \left(\langle \Psi_{\text{initial}} | \Psi_{\text{initial}} \rangle - \langle \Psi_{\text{initial}} | \Psi_{\text{comp}} \rangle - \langle \Psi_{\text{comp}} | \Psi_{\text{initial}} \rangle + \langle \Psi_{\text{comp}} | \Psi_{\text{comp}} \rangle \right) \\
= &\frac{\partial}{\partial N_{\sigma_j}^{\alpha_{j-1},\alpha_j *}} \left(- \langle \Psi_{\text{comp}} | \Psi_{\text{initial}} \rangle + \langle \Psi_{\text{comp}} | \Psi_{\text{comp}} \rangle \right) \\
= &- \sum_{\sigma_1,\ldots\sigma_N} \left(N^{\alpha_1 *}\ldots N^{\alpha_{j-2},\alpha_{j-1} *}\right)_{\sigma_1,\ldots\sigma_{j-1}} \left(N^{\alpha_j,\alpha_{j+1} *}\ldots N^{\alpha_N *}\right)_{\sigma_{j+1},\ldots\sigma_N} \\
&\qquad \left(M^{\alpha_1}\ldots M^{\alpha_{j-2},\alpha_{j-1}}\right)_{\sigma_1,\ldots\sigma_{j-1}} M_{\sigma_j}^{\alpha_{j-1},\alpha_j} \left(M^{\alpha_j,\alpha_{j+1}}\ldots M^{\alpha_N}\right)_{\sigma_{j+1},\ldots\sigma_N} \\
&+ \sum_{\sigma_1,\ldots\sigma_N} \left(N^{\alpha_1 *}\ldots N^{\alpha_{j-2},\alpha_{j-1} *}\right)_{\sigma_1,\ldots\sigma_{j-1}} \left(N^{\alpha_j,\alpha_{j+1} *}\ldots N^{\alpha_N *}\right)_{\sigma_{j+1},\ldots\sigma_N} \\
&\qquad \left(N^{\alpha_1}\ldots N^{\alpha_{j-2},\alpha_{j-1}}\right)_{\sigma_1,\ldots\sigma_{j-1}} N_{\sigma_j}^{\alpha_{j-1},\alpha_j} \left(N^{\alpha_j,\alpha_{j+1}}\ldots N^{\alpha_N}\right)_{\sigma_{j+1},\ldots\sigma_N} \\
&\overset{!}{=} 0
\end{aligned} \tag{6.4}$$

The derivative acting on the sums simply results in the tensor in question being "deleted" from those sums. This furthermore gives us an important pictorial interpretation of derivatives of tensor networks: we simply end up with a network "with a hole", which "occupies" the place of the tensor with respect to which we have taken the derivative. Inspecting the previous equation once more, we can see that the resulting equation contains exactly one copy of the given N-tensor, just as we desired:

$$\begin{aligned}
&\sum_{\sigma_1,\ldots\sigma_N} \left(N^{\alpha_1 *}\ldots N^{\alpha_{j-2},\alpha_{j-1} *}\right)_{\sigma_1,\ldots\sigma_{j-1}} \left(N^{\alpha_j,\alpha_{j+1} *}\ldots N^{\alpha_N *}\right)_{\sigma_{j+1},\ldots\sigma_N} \\
&\qquad \left(M^{\alpha_1}\ldots M^{\alpha_{j-2},\alpha_{j-1}}\right)_{\sigma_1,\ldots\sigma_{j-1}} M_{\sigma_j}^{\alpha_{j-1},\alpha_j} \left(M^{\alpha_j,\alpha_{j+1}}\ldots M^{\alpha_N}\right)_{\sigma_{j+1},\ldots\sigma_N} \\
= &\sum_{\sigma_1,\ldots\sigma_N} \left(N^{\alpha_1 *}\ldots N^{\alpha_{j-2},\alpha_{j-1} *}\right)_{\sigma_1,\ldots\sigma_{j-1}} \left(N^{\alpha_j,\alpha_{j+1} *}\ldots N^{\alpha_N *}\right)_{\sigma_{j+1},\ldots\sigma_N} \\
&\qquad \left(N^{\alpha_1}\ldots N^{\alpha_{j-2},\alpha_{j-1}}\right)_{\sigma_1,\ldots\sigma_{j-1}} N_{\sigma_j}^{\alpha_{j-1},\alpha_j} \left(N^{\alpha_j,\alpha_{j+1}}\ldots N^{\alpha_N}\right)_{\sigma_{j+1},\ldots\sigma_N} .
\end{aligned} \tag{6.5}$$

We thus have derived an equation to solve the compression problem for the given N-tensor, and our task now is to solve this equation for N. As promised in the introduction, all of the other tensors of the state still appear in this equation, which justifies our claim of working globally.

In principle, we could now redefine the parts surrounding the "chosen" N-tensor as well as the left hand side of the equation as matrices. Thus, we could immediately write down a (highly-compressed) matrix-vector equation:

$$A^{\alpha_{j-1},\alpha_j} = B_{\alpha'_{j-1},\alpha'_j}^{\alpha_{j-1},\alpha_j} N_{\sigma_j}^{\alpha'_{j-1},\alpha'_j} \tag{6.6}$$

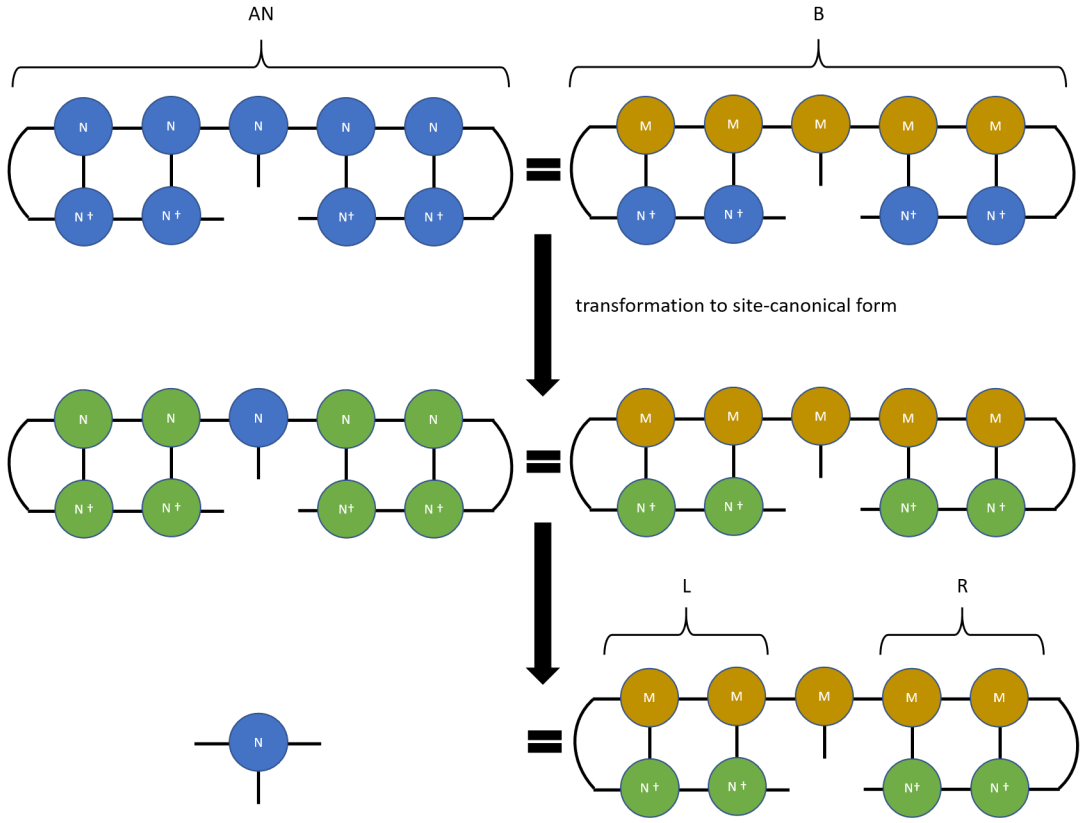

Figure 24: "Tensor network equation" to solve in order to find the optimally compressed tensor N in an MPS iteratively.

with

$$A^{\alpha_{j-1},\alpha_j} \equiv \sum_{\sigma_1,\ldots\sigma_N} \left(N^{\alpha_1 *}\ldots N^{\alpha_{j-2},\alpha_{j-1}*}\right)_{\sigma_1,\ldots\sigma_{j-1}} \left(N^{\alpha_j,\alpha_{j+1}*}\ldots N^{\alpha_N *}\right)_{\sigma_{j+1},\ldots\sigma_N} \left(M^{\alpha_1}\ldots M^{\alpha_{j-2},\alpha_{j-1}}\right)_{\sigma_1,\ldots\sigma_{j-1}} M_{\sigma_j}^{\alpha_{j-1},\alpha_j} \left(M^{\alpha_j,\alpha_{j+1}}\ldots M^{\alpha_N}\right)_{\sigma_{j+1},\ldots\sigma_N} \tag{6.7}$$

and

$$B^{\alpha_{j-1},\alpha_j}_{\alpha'_{j-1},\alpha'_j} \equiv \sum_{\sigma_1,\ldots\sigma_N} \left(N^{\alpha_1 *}\ldots N^{\alpha_{j-2},\alpha_{j-1}*}\right)_{\sigma_1,\ldots\sigma_{j-1}} \left(N^{\alpha_j,\alpha_{j+1}*}\ldots N^{\alpha_N *}\right)_{\sigma_{j+1},\ldots\sigma_N} \left(N^{\alpha_1}\ldots N^{\alpha_{j-2},\alpha_{j-1}}\right)_{\sigma_1,\ldots\sigma_{j-1}} \left(N^{\alpha_j,\alpha_{j+1}}\ldots N^{\alpha_N}\right)_{\sigma_{j+1},\ldots\sigma_N} . \tag{6.8}$$

By combining the respective α_{j-1}, α_j and α'_{j-1}, α'_j indices into a joint index (let's call them β and γ), we can write the above result even more succinctly as:

$$A^{\beta} = B^{\beta}_{\gamma} N^{\gamma}, \tag{6.9}$$

where we have suppressed the explicit σ_j index on the N tensor. This final form should convince you that we really are dealing with a "simple" matrix-vector problem, if the previous index jungle hasn't. A brute-force, but inefficient, way to find the sought-after optimal N is therefore to calculate the objects A and B, and to invert the matrix B. Sweeping through the whole chain of tensors and solving this equation at each site

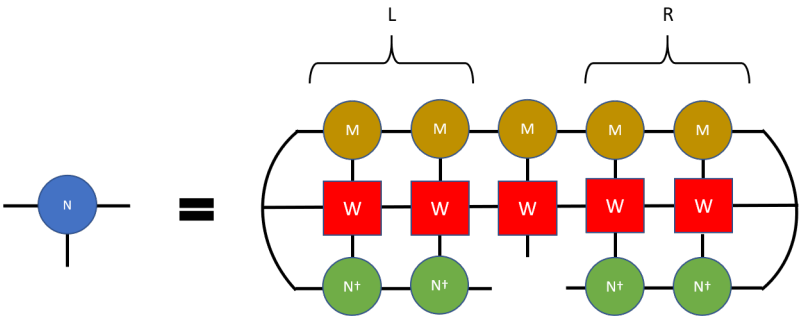

Figure 25: Iteration step in the variational application of an MPO to an MPS, reminiscent of the "direct" variational compression.

would then result in the optimally compressed state.

The efficiency and numerical stability of this algorithm can however largely be increased by making use of the site-canonical form of $|\Psi_{\text{comp}}\rangle$. Fig. 24 shows the idea: in the initial version of the algorithm, the sought tensor N (in blue) is surrounded by left and right environments, which are summarised in the matrix A. If, however, we ensure that at each minimisation step, the state $|\Psi_{\text{comp}}\rangle$ is in site-canonical form with respect to N, the left and right environments simply collapse to identities. As shown in the bottom line of fig. 24, we therefore don't have to solve *any* equation (or invert potentially large matrices) - we obtain the optimal tensor N immediately by contracting the network on the right.

Further comments on a stable implementation of the variational compression algorithm will be deferred to the last section in this chapter.

6.1.1 Variational Application of Matrix Product Operators

We can employ a slight variation of the variational compression algorithm to evaluate the application of an MPO O to an MPS $|\Psi\rangle$. Recall that applying an MPO to an MPS leads to an increase of the bond dimension of the latter, which in practice requires a subsequent compression. Applying the MPO variationally combines its application and the compression into a single step.

Analogously to the above case, we are searching the state $|\Psi_{\text{comp}}\rangle$ (with a given, smaller bond dimension), such that the norm difference

$$\| |\Psi_{\text{comp}}\rangle - O|\Psi\rangle \|^2 \tag{6.10}$$

is minimised. We can go through the same calculations as before, taking a derivative with respect to the conjugate N-tensors building up the compressed state $|\Psi_{\text{comp}}\rangle$, which

yields

$$\frac{\partial}{\partial N_{\sigma_j}^{\alpha_{j-1},\alpha_j *}} \left\langle \Psi_{\text{comp}} \middle| \Psi_{\text{comp}} \right\rangle \stackrel{!}{=} \frac{\partial}{\partial N_{\sigma_j}^{\alpha_{j-1},\alpha_j *}} \left\langle \Psi_{\text{comp}} \middle| O\Psi \right\rangle . \tag{6.11}$$

Incidentally, this is the exact same kind of equation encountered in the previous section, with the only difference that the tensor network corresponding to the right hand side has an additional layer due to the presence of the MPO. Translating the crucial iteration step into a tensor network (including a site-canonical form of the compressed state that is built up) leads to the contraction pattern shown in fig. 25. In complete analogy to the "pure" variational compression just discussed, we obtain the optimal tensor for a single site in the compressed state immediately by evaluating the tensor network on the right hand side, without the need to solve any equation.

6.2 The Density Matrix Renormalisation Group

As mentioned in the introduction to this chapter, the density matrix renormalisation group is one of the great achievements of numerical many-body physics in the last decades, and still a topic of active research. We will derive below the DMRG algorithm in one of its simpler forms, with details about its implementation deferred to the next section. Several possible extensions will be mentioned in the penultimate chapter of this thesis, discussing future projects and algorithmic improvements.

The goal of the DMRG algorithm is to find the ground state $|\psi_0\rangle$ of a given Hamiltonian H. As the ground state of a system is the state which minimises the energy expectation value

$$\frac{\langle \psi_0 | H | \psi_0 \rangle}{\langle \psi_0 | \psi_0 \rangle} \stackrel{!}{=} \text{minimal}, \tag{6.12}$$

we obtain again an equation in terms of MPO and MPS that we can minimise tensor by tensor. In practice, one uses the above equation in a slightly different - but equivalent - form, by enforcing the normalisation of the state $|\psi_0\rangle$ explicitly with a Lagrange multiplier λ:

$$\langle \psi_0 | H | \psi_0 \rangle - \lambda \langle \psi_0 | \psi_0 \rangle \stackrel{!}{=} \text{minimal}. \tag{6.13}$$

For what follows, we will proceed exactly as in the previous case of variational compression.

Starting to rewrite the expression to be minimised explicitly in terms of the tensors in-

volved, we obtain the contraction

$$
\begin{aligned}
&\langle\psi|H|\psi\rangle - \lambda\,\langle\psi|\psi\rangle = \\
&\quad \sum_{\sigma_1,\ldots,\sigma_N,\sigma'_1,\ldots\sigma'_N} (M^{\alpha_1 *}\ldots M^{\alpha_{j-2},\alpha_{j-1}*})_{\sigma_1,\ldots\sigma_{j-1}}\, M^{\alpha_{j-1},\alpha_j *}_{\sigma_j}\, (M^{\alpha_j,\alpha_{j+1}*}\ldots M^{\alpha_N *})_{\sigma_{j+1},\ldots\sigma_N} \\
&\qquad\qquad (W^{\alpha_1}\ldots W^{\alpha_{j-2},\alpha_{j-1}})^{\sigma'_1,\ldots\sigma'_{j-1}}_{\sigma_1,\ldots\sigma_{j-1}}\, W^{\alpha_{j-1},\alpha_j}_{\sigma_j}\, (W^{\alpha_j,\alpha_{j+1}}\ldots W^{\alpha_N})^{\sigma'_{j+1},\ldots\sigma'_N}_{\sigma_{j+1},\ldots\sigma_N} \\
&\qquad\qquad (M^{\alpha_1}\ldots M^{\alpha_{j-2},\alpha_{j-1}})_{\sigma'_1,\ldots\sigma'_{j-1}}\, M^{\alpha_{j-1},\alpha_j}_{\sigma'_j}\, (M^{\alpha_j,\alpha_{j+1}}\ldots M^{\alpha_N})_{\sigma'_{j+1},\ldots\sigma'_N} \\
&\quad -\lambda \sum_{\sigma_1,\ldots,\sigma_N} (M^{\alpha_1 *}\ldots M^{\alpha_{j-2},\alpha_{j-1}*})_{\sigma_1,\ldots\sigma_{j-1}}\, M^{\alpha_{j-1},\alpha_j *}_{\sigma_j}\, (M^{\alpha_j,\alpha_{j+1}*}\ldots M^{\alpha_N *})_{\sigma_{j+1},\ldots\sigma_N} \\
&\qquad\qquad (M^{\alpha_1}\ldots M^{\alpha_{j-2},\alpha_{j-1}})_{\sigma_1,\ldots\sigma_{j-1}}\, M^{\alpha_{j-1},\alpha_j}_{\sigma_j}\, (M^{\alpha_j,\alpha_{j+1}}\ldots M^{\alpha_N})_{\sigma_{j+1},\ldots\sigma_N} \\
&\quad \stackrel{!}{=} \text{minimal.}
\end{aligned}
\tag{6.14}
$$

The main difference in this expression is of course the appearance of the W-tensors as elements of the MPO Hamiltonian, in comparison to the contraction defining the variational compression. As the degrees of freedom we would now like to determine are the elements of the M-tensors, we take the derivative with respect to the corresponding M^*-tensor:

$$
\begin{aligned}
&\frac{\partial}{\partial M^{\alpha_{l-1}\alpha_l *}_{\sigma_l}} \left[\langle\psi|H|\psi\rangle - \lambda\,\langle\psi|\psi\rangle\right] \\
&= \sum_{\substack{\sigma_1,\ldots,\sigma_{j-1},\sigma_{j+1},\ldots,\sigma_N \\ \sigma'_1,\ldots\sigma'_N}} (M^{\alpha_1 *}\ldots M^{\alpha_{j-2},\alpha_{j-1}*})_{\sigma_1,\ldots\sigma_{j-1}}\, (M^{\alpha_j,\alpha_{j+1}*}\ldots M^{\alpha_N *})_{\sigma_{j+1},\ldots\sigma_N} \\
&\qquad\qquad (W^{\gamma_1}\ldots W^{\gamma_{j-2},\gamma_{j-1}})^{\sigma'_1,\ldots\sigma'_{j-1}}_{\sigma_1,\ldots\sigma_{j-1}}\, W^{\gamma_{j-1},\gamma_j}_{\sigma_j,\sigma'_j}\, \left(W^{\gamma_j,\gamma j+1}\ldots W^{\gamma_N}\right)^{\sigma'_{j+1},\ldots\sigma'_N}_{\sigma_{j+1},\ldots\sigma_N} \\
&\qquad\qquad \left(M^{\beta_1}\ldots M^{\beta_{j-2},\beta_{j-1}}\right)_{\sigma'_1,\ldots\sigma'_{j-1}}\, M^{\beta_{j-1},\beta_j}_{\sigma'_j}\, \left(M^{\beta_j,\beta_{j+1}}\ldots M^{\beta_N}\right)_{\sigma'_{j+1},\ldots\sigma'_N} \\
&\quad -\lambda \sum_{\sigma_1,\ldots,\sigma_{j-1},\sigma_{j+1},\ldots,\sigma_N} (M^{\alpha_1 *}\ldots M^{\alpha_{j-2},\alpha_{j-1}*})_{\sigma_1,\ldots\sigma_{j-1}}\, (M^{\alpha_j,\alpha_{j+1}*}\ldots M^{\alpha_N *})_{\sigma_{j+1},\ldots\sigma_N} \\
&\qquad\qquad \left(M^{\beta_1}\ldots M^{\beta_{j-2},\beta_{j-1}}\right)_{\sigma_1,\ldots\sigma_{j-1}}\, M^{\beta_{j-1},\beta_j}_{\sigma_j}\, \left(M^{\beta,\alpha_{j+1}}\ldots M^{\beta_N}\right)_{\sigma_{j+1},\ldots\sigma_N} \stackrel{!}{=} 0.
\end{aligned}
\tag{6.15}
$$

The reason why DMRG is slightly harder in comparison to variational compression is that the tensor M of interest is now contained *twice* in the above expression. However, it is straightforward to show that this is in fact equal to a generalised eigenvalue problem.

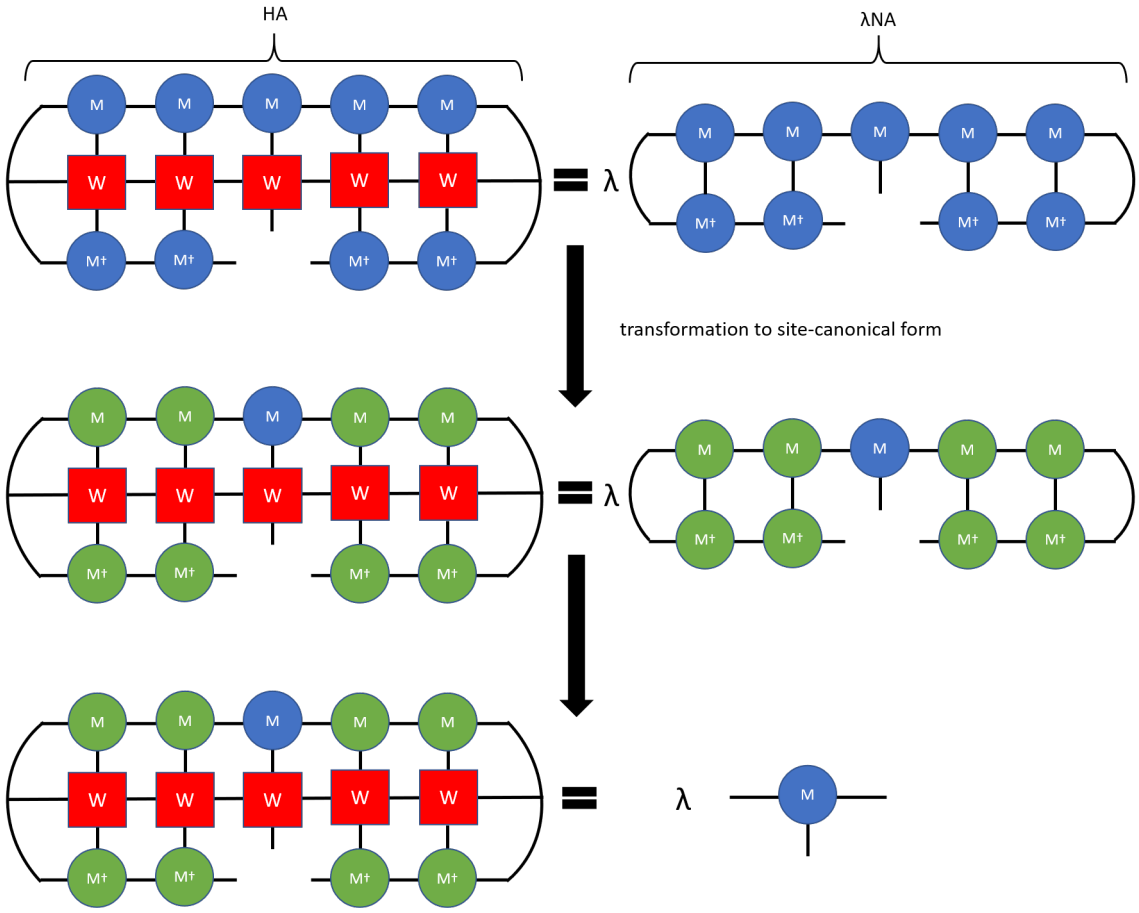

Figure 26: Generalised eigenvalue equation at the heart of DMRG represented as a tensor network. From the top to the middle panel, the MPS to be optimised is transformed into site-canonical form, which results in the simplified tensor network shown in the lowest panel.

Define the following operators:

$$H^{\alpha_{j-1},\alpha_j,\sigma_j}_{\beta_{j-1},\beta_j,\sigma'_j} = \sum_{\substack{\sigma_1,\ldots,\sigma_{j-1},\sigma_{j+1},\ldots,\sigma_N \\ \sigma'_1,\ldots,\sigma'_{j-1},\sigma'_{j+1},\ldots,\sigma'_N}} \left(M^{\alpha_1 *}\ldots M^{\alpha_{j-2},\alpha_{j-1}*}\right)_{\sigma_1,\ldots\sigma_{j-1}} \left(M^{\alpha_j,\alpha_{j+1}*}\ldots M^{\alpha_N *}\right)_{\sigma_{j+1},\ldots\sigma_N}$$
$$\left(W^{\gamma_1}\ldots W^{\gamma_{j-2},\gamma_{j-1}}\right)^{\sigma'_1,\ldots\sigma'_{j-1}}_{\sigma_1,\ldots\sigma_{j-1}} W^{\gamma_{j-1},\gamma_j}_{\sigma_j,\sigma'_j} \left(W^{\gamma_j,\gamma_{j+1}}\ldots W^{\gamma_N}\right)^{\sigma'_{j+1},\ldots\sigma'_N}_{\sigma_{j+1},\ldots\sigma_N}$$
$$\left(M^{\beta_1}\ldots M^{\beta_{j-2},\beta_{j-1}}\right)_{\sigma'_1,\ldots\sigma'_{j-1}} \left(M^{\beta_j,\beta_{j+1}}\ldots M^{\beta_N}\right)_{\sigma'_{j+1},\ldots\sigma'_N} \tag{6.16}$$

and

$$N^{\alpha_{j-1},\alpha_j}_{\beta_{j-1},\beta_j} = \sum_{\sigma_1,\ldots,\sigma_{j-1},\sigma_{j+1},\ldots,\sigma_N} \left(M^{\alpha_1 *}\ldots M^{\alpha_{j-2},\alpha_{j-1}*}\right)_{\sigma_1,\ldots\sigma_{j-1}} \left(M^{\alpha_j,\alpha_{j+1}*}\ldots M^{\alpha_N *}\right)_{\sigma_{j+1},\ldots\sigma_N}$$
$$\left(M^{\beta_1}\ldots M^{\beta_{j-2},\beta_{j-1}}\right)_{\sigma_1,\ldots\sigma_{j-1}} \left(M^{\beta,\alpha_{j+1}}\ldots M^{\beta_N}\right)_{\sigma_{j+1},\ldots\sigma_N}. \tag{6.17}$$

Then we can rewrite the equation for M as

$$H^{\alpha_{j-1},\alpha_j,\sigma_j}_{\beta_{j-1},\beta_j,\sigma'_j} M^{\alpha_{j-1},\alpha_j}_{\sigma_j} = \lambda N^{\alpha_{j-1},\alpha_j}_{\beta_{j-1},\beta_j} M^{\alpha_{j-1},\alpha_j}_{\sigma_j}, \tag{6.18}$$

which has the structure

$$HM = \lambda NM. \tag{6.19}$$

Again, as it was the case for the variational compression, this is a type of equation that one could solve using standard numerical linear algebra methods. However, we can again drastically simplify the calculation by ensuring that the MPS to be found is always in site-canonical form with respect to the site we are solving for, as shown in the lower panel of fig. 26. This, in turn, implies that the matrix N is trivial:

$$H^{\alpha_{j-1},\alpha_j,\sigma_j}_{\beta_{j-1},\beta_j,\sigma'_j} M^{\alpha_{j-1},\alpha_j}_{\sigma_j} = \lambda M^{\beta_{j-1},\beta_j}_{\sigma'_j}. \tag{6.20}$$

Redefining the primed and unprimed indices as a multi-indices $a \equiv \{\alpha_{j-1}, \alpha_j, \sigma_j\}$ and $b \equiv \{\beta_{j-1}, \beta_j, \sigma'_j\}$, we therefore obtain an ordinary eigenvector equation:

$$H^a_b M^a = \lambda M^b. \tag{6.21}$$

Sweeping through the chain and solving this equation for its lowest eigenvalue at each site thus yields successively better approximations for the tensors making up the true ground state. The corresponding eigenvalues, once they have converged after multiple sweeps, then give the estimate for the ground state energy.

6.2.1 Using DMRG to Find Excited States

Once one has found the ground state $|\psi_0\rangle$ of a given system, one can use a DMRG-based algorithm to find excited states. The key point is again to set up an equation that is optimised variationally, with the only difference of enforcing an additional orthogonality to the space of all the lowest-lying states found so far. For instance, the first excited state would be given by imposing orthogonality to the ground state:

$$\langle\psi_1|H|\psi_1\rangle - \lambda_1 \langle\psi_1|\psi_1\rangle - \lambda_2 \langle\psi_1|\psi_0\rangle \stackrel{!}{=} \text{minimal}. \tag{6.22}$$

Those types of equations can again be solved by similar procedures as the ones we have discussed. They result in a more general eigenvalue problem of the structure

$$HA = \lambda_1 A + \lambda_2 G, \tag{6.23}$$

where A and G are a shorthand notation for the tensors in the first excited and the ground state. To solve this equation, one needs to introduce additional projectors onto the orthogonal complement of G.

6.3 Implementing Variational Algorithms

To finish this section, we will give some details about the actual implementation of the variational algorithms discussed above, and in particular of the DMRG algorithm. While

the algorithm as it was explained earlier is in principle functional, it is not yet necessarily robust, nor is it efficient. We will focus on the following aspects: first, we present convergence measures for variational algorithms. In particular, we discuss the variance of the Hamiltonian as the most suitable convergence measure for DMRG. Second, in order to achieve a more robust convergence to the ground state, one can enlarge the variational space taken into account at each step by optimising multiple sites at once. In the same vein, better (and faster) convergence can also be achieved through a savvy choice of the initial state. Afterwards, we will briefly discuss the Lanczos algorithm, which is a numerical method to find the extremal eigenvalues of a linear operator - using this will save us from doing a full (and expensive) spectral decomposition. The most important improvement, however, is to build the site-canonical state and the corresponding environments dynamically on the fly which avoids a re-gauging of the MPS at every iteration step.

All of the above aspects have been considered in the numerical part of the present thesis. The explicit inclusion of symmetries, as well as working with periodic boundary conditions, are further possible upgrades and will be briefly discussed in the final part. To summarise this discussion and to give the reader a concrete idea of a working DMRG implementation, we provide a simple DMRG pseudocode at the end of this chapter.

6.3.1 Monitoring Convergence

A very important aspect of a working implementation of variational algorithms is to assess whether sufficient convergence to the sought state has been reached after a given number of sweeps. In general, one can compare the MPS obtained after a full sweep to the MPS before the sweep, and check if their (normalised) overlap is sufficiently close to one:

$$\frac{\langle\psi|\psi'\rangle}{\langle\psi|\psi\rangle\,\langle\psi'|\psi'\rangle} \stackrel{?}{=} 1 \Rightarrow \left|1 - \frac{\langle\psi|\psi'\rangle}{\langle\psi|\psi\rangle\,\langle\psi'|\psi'\rangle}\right| \to 0. \tag{6.24}$$

This is the convergence check we will employ to ensure that an MPO is correctly applied to an MPS in the corresponding variational algorithm.

In the DMRG algorithm, we can (and should) use the fact that we are searching for eigenvalues and eigenstates as additional information, to make sure that the sweeps have converged. One simple metric could be to read out the sequence of energies found in subsequent optimisation steps, and to halt the routine once they have "sufficiently stabilised", e.g. by checking that their variance has fallen below a certain threshold.

In practice, however, while one can often observe a fast convergence to the ground state *energy*, this doesn't necessarily imply that the *state* under construction is the sought ground state without any "impurities". For instance, if a system has a very small energy

gap between the ground state and the first excited state, it is possible that the ground state approximation still contains a non-negligible weight of the first excited state, even though the energy has a priori converged. A better metric is therefore to study the variance of the Hamiltonian in the (approximated) ground state $\left|\tilde{0}\right\rangle$, given by

$$\Delta H \equiv \left\langle \tilde{0}\middle| H^2 |\tilde{0}\right\rangle - \left\langle \tilde{0}\middle| H |\tilde{0}\right\rangle^2 . \tag{6.25}$$

Let $\left|\tilde{0}\right\rangle$ be a superposition of the true ground state $|0\rangle$ and a small perturbation $|\epsilon\rangle$, living in the complement of span$\{|0\rangle\}$ (the latter being therefore not an eigenstate of H):

$$\left|\tilde{0}\right\rangle \equiv |0\rangle + \alpha |\epsilon\rangle , \quad \alpha \ll 1. \tag{6.26}$$

Then we can calculate ΔH as

$$\begin{aligned} \Delta H &= \left\langle 0\middle| H^2 |0\right\rangle + \alpha \left\langle \epsilon\middle| H^2 |0\right\rangle + \alpha \left\langle 0\middle| H^2 |\epsilon\right\rangle + \alpha^2 \left\langle \epsilon\middle| H^2 |\epsilon\right\rangle \\ &\quad - \left[\langle 0|H|0\rangle + \alpha \langle \epsilon|H|0\rangle + \alpha \langle 0|H|\epsilon\rangle + \alpha^2 \langle \epsilon|H|\epsilon\rangle\right]^2 \\ &= E_0^2 + \alpha^2 \left\langle \epsilon\middle| H^2 |\epsilon\right\rangle - \left[E_0^2 + 2E_0 \alpha^2 \langle \epsilon|H|\epsilon\rangle + \mathcal{O}(\alpha^4)\right] \\ &= \alpha^2 \left[\left\langle \epsilon\middle| H^2 |\epsilon\right\rangle - 2E_0 \langle \epsilon|H|\epsilon\rangle\right] + \mathcal{O}(\alpha^4). \end{aligned} \tag{6.27}$$

Evidently, by construction we have $\Delta H = 0$ if the algorithm has converged to the true ground state $|0\rangle$. Otherwise, as shown by the above reasoning, measuring a variance of $\Delta H = \alpha$ indicates a perturbation to the ground state of the order of $\sqrt{\alpha}$. If one solely aims to determine the ground state energy of a given system, small perturbations to the true ground state can be neglected given that the energy has converged. However, if precision calculations with the thus determined ground state are required, it is important to suppress any perturbations caused by excited states as much as possible.

6.3.2 Two-Site Updates

One caveat one has to be aware of when using DMRG is hidden in the very foundations of the algorithm: as DMRG is a minimisation procedure, there is at least in principle a possibility of converging to a *local* minimum, instead of the sought *global* minimum - the ground state. Ultimately, this is due to the fact that at each step, we are only optimising a restricted set of degrees of freedom of the full quantum states. Were we to vary all the parameters at the same time, we could ensure convergence to the global minimum without doubt - but this is exactly the problem we are trying to break down into pieces, by using algorithms such as DMRG.

It is however possible to improve the robustness of the convergence to a global minimum by locally enlarging the variational space. The easiest way of doing this - and which is a common way to implement DMRG professionally - uses two-site updates instead of

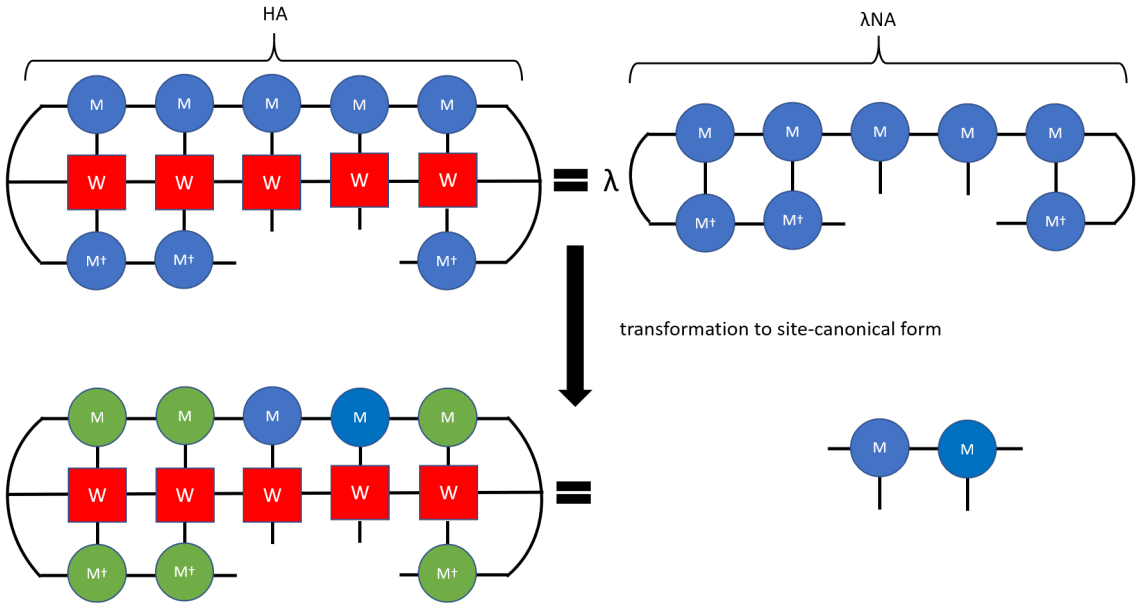

Figure 27: Generalised eigenvalue equation of DMRG in a two-site update scheme. Again, a transformation to site-canonical form yields an ordinary eigenvalue equation.

one-site updates. Instead of sweeping through the tensors one-by-one, one performs the minimisation with respect to two tensors at once. The resulting eigenvector thus found is then split in two new, optimised tensors, before the sweep through the chain of tensor continues.

6.3.3 Choice of the Initial State

One further possibility to ensure a more robust convergence to the ground state is by using an initial state which already has a high overlap with the ground state. While, usually, starting the algorithm with a random initial state leads to satisfying results, using a "better" initial state can provide an additional performance-boost in the convergence to the true ground state.

A good way to obtain such an initial state is employing an infinite version of the DMRG algorithm - iDMRG - to successively grow a chain until it reaches the length of the finite-size system one wants to investigate using DMRG. More details and a short introduction to iDMRG are provided in the appendix.

6.3.4 Finding Extremal Eigenvalues with the Lanczos scheme

In principle, at each optimisation step one has to solve an eigenvalue problem. We are, however, usually only interested in the lowest[26] eigenvalue pertaining to each local eigenvalue problem. Doing a full spectral decomposition would therefore be not only numerically expensive, but also yield an important number of results which are effectively discarded.

A much better way to obtain the lowest local eigenvalue is therefore to use eigensolver algorithms that specifically target the extremal eigenvalues (and the corresponding eigenvectors). One of the most common such algorithms is the **Lanczos algorithm**, which is outlined below.

Aside - Lanczos Algorithm

In the Lanczos scheme (cf. refs. [61, 62]), we project the Hamiltonian onto a subspace of the full Hilbert space, such that it admits a tridiagonal structure. The reason for this is that tridiagonal matrices are easily numerically diagonalisable. A suitable choice for such a subspace is the **Krylov space** of order l:

$$K_l\left(H, |v_0\rangle\right) \equiv \text{span}\{|v_0\rangle, H|v_0\rangle, ..., H^{l-1}|v_0\rangle\}, \tag{6.28}$$

where $|v_0\rangle$ is an arbitrary initial vector. Instead of evaluating the matrix elements of H directly in this basis, one then constructs iteratively the orthonormal **Krylov basis** $\{|v_i\rangle\}$ of K_l. The main iteration step is given by

$$|v_{i+1}\rangle = \frac{1}{\langle v_i|H|v_{i-1}\rangle}\left[H|v_i\rangle - \sum_{j=0}^{i}|v_j\rangle\langle v_j|H|v_i\rangle\right]. \tag{6.29}$$

One can then show that the final series actually only contains contributions from $|v_i\rangle$ and $|v_{i-1}\rangle$. This immediately implies that the representation H_{K_l} of H in the Krylov basis is indeed tridiagonal, as desired. Evaluating the minimal/maximal eigenvalues of H_{K_l} gives then an approximation of the minimal/maximal eigenvalues of H. Often, it is sufficient to construct only few Krylov vectors in order to obtain a good estimate of the true ground state.

6.3.5 Dynamic Gauging and Construction of Environments

As we have explained when introducing the DMRG, the algorithm becomes most effective when dealing with an MPS in site-canonical form, with respect to the site being optimised in each iteration step. Naively, one could therefore apply a transformation

[26] Or the highest, in case one wants to calculate the upper end of the spectrum. This will be relevant in the next section, when the maximal energy is needed for a rescaling of the Hamiltonian.

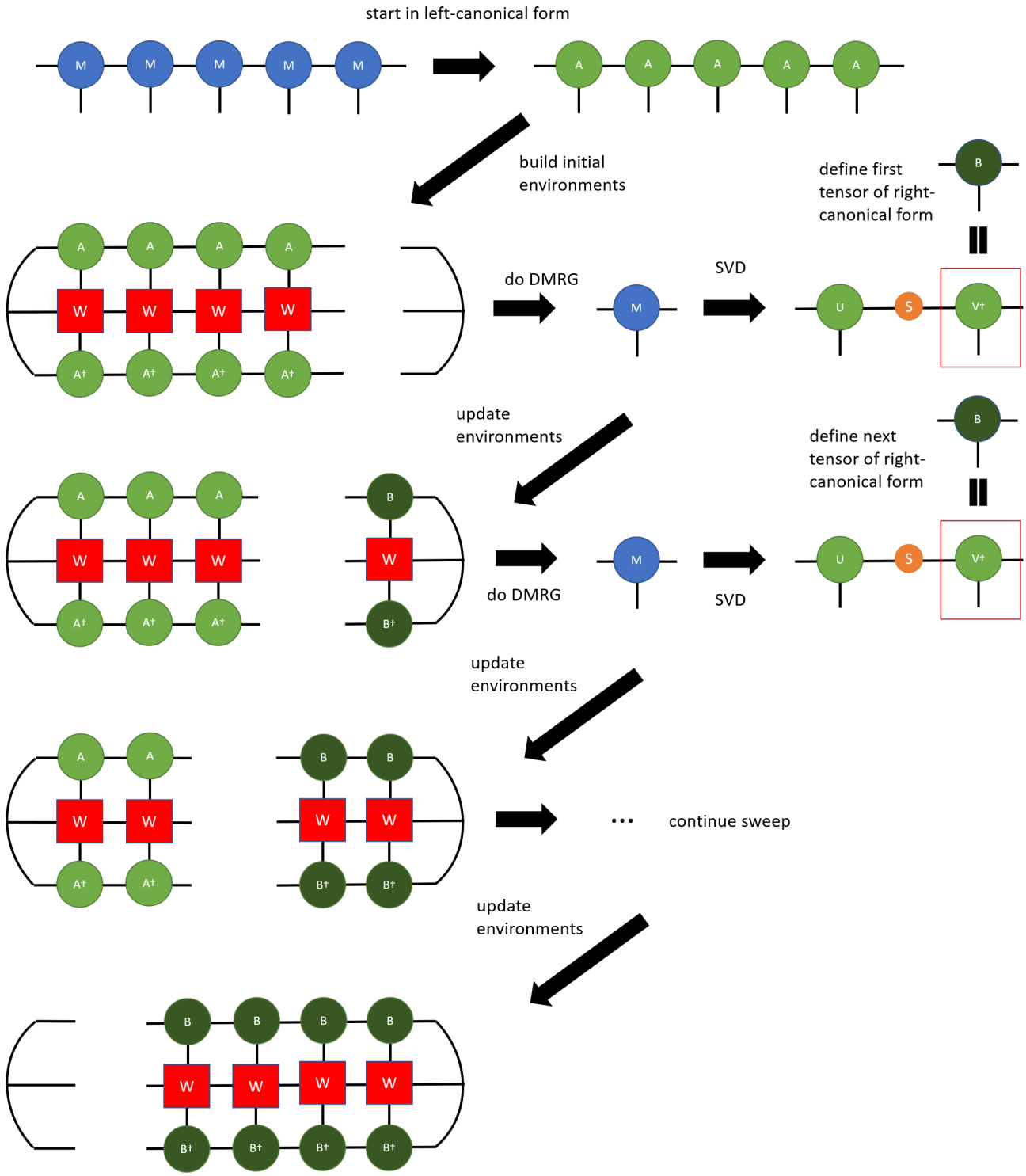

Figure 28: Dynamic construction of the left and right environments used to build the effective Hamiltonian in DMRG, shown for a one-site optimisation scheme.

into the site-canonical form each time before the local eigenvalue problem is tackled. While this would work in principle, this would lead to a great number of redundant calculations. Consider a site-canonical MPS, with a tensor M_1 somewhere in the bulk, left-normalised tensors A to its left and right-normalised tensors B to its right:

$$|\psi\rangle = AA \dots AAM_1BB \dots BB. \tag{6.30}$$

If this is the MPS which is optimised with DMRG, one would next need the site-canonical form of this state with respect to, say, the tensor M_2 to the left of M_1:

$$|\psi\rangle = AA...AM_2BBB...BB. \tag{6.31}$$

Writing it out in this symbolic fashion makes explicit that, effectively, only three tensors are changed during a site-canonisation, if the transformation is with respect to a tensor M_2 directly on the left (or on the right of) the "chosen" tensor M_1. All the other A- and B-tensors are unaffected by this re-gauging. Therefore, the transformation to the-site canonical form would be optimally implemented[27] by manipulating only the three tensors of interest at each optimisation step, and simply keeping the others. A graphical representation of this dynamic update is shown in fig. 28. There, we start by initialising a left and a right environment, and prepare to sweep from right to left. Doing the first DMRG optimisation, we recover the tensor M. Performing an SVD on M, we can update the environments by adding a layer to the right environment, and deleting the rightmost layer of the left environment. This procedure continues until a full right-left sweep is completed. Changing the sweep direction then works in the exact same way, with the left environment being built up and the right environment shrunk.

[27] In the context of DMRG, not in general.

Algorithms-DMRG

Input: MPO representation of Hamiltonian H (with environments vL, vR), number N of sites, maximal number Nsweep of sweeps, tolerance eps, bond dimension D.

Output: Ground state G, ground state energy E0.

```
G = randomMPS(N, D);
Llist = [vL], Rlist = [vR] ;
for i in range(N-1) do
    L = contract(L, G[i], H[i], conj(G[i])) ;
    Llist.append(L) ;
end
for i in range(N-1, 0, -1) do
    Rlist.append(0) ;
end
for sweep in range(Nsweeps) do
    for j in range(N-1, 0, -1) do
        H = contract(Llist[j], H[j], Rlist[N-1-j]) ;
        E0, v0 = eigensolver(H, which="smallest eigenvalue") ;
        U, S, VHerm = svd(v0) ;
        G[j] = VHerm ;
        G[j-1] = contract(G[j-1], contract(U, S)) ;
        R = contract(G[j], H[j], conj(G[j]), Rlist[N-1-j]) ;
        Rlist[N-j] = R ;
    end
    for j in range(N-1) do
        H = contract(Llist[j], H[j], Rlist[-1-j]) ;
        E0, v0 = eigensolver(H, which="smallest eigenvalue") ;
        U, S, VHerm = svd(v0) ;
        G[j] = U ;
        G[j+1] = contract(contract(S, V), M[j+1]) ;
        L = contract(Llist[j], G[j], H[j], conj(G[j])) ;
        Llist[j+1] = L ;
    end
    var = varianceMPO(H, G) ;
    if var < eps then
        break ;
    end
end
return G, E0 ;
```

7 Spectral Functions and the Kernel Polynomial Method

Having introduced MPS as the tools to work with many-body quantum mechanics in a numerically efficient way, and DMRG as a state-of-the-art tool to find the ground state of a quantum system, we would like to study the full spectrum of a given Hamiltonian. The quantity which gives us access to that information is the spectral function, which we will introduce below. While there exist different possibilities to calculate the spectral function, we will employ the kernel polynomial method (see ref. [14]) for this task, which has crucial advantages over other, more direct calculation schemes. In particular, we will motivate why obtaining the spectral function through a Fourier transform of a time-evolved MPS is much slower, computationally speaking, and more prone to errors. After explaining the general framework of the method - an expansion in terms of Chebyshev polynomials - we will use it to derive approximation schemes for the spectral density of a Hamiltonian, as well as for the spectral function. For the latter, we will expose how the central steps of the calculation can be performed in the MPS framework established in this thesis. As in the previous chapter, a pseudocode implementation of the kernel polynomial method can be found on the final page, which closes the presentation of the necessary theoretical background.

This chapter is mainly based on refs. [14, 27], which provide detailed derivations and explanations, going much beyond the topics discussed below, in a very accessible way. Here, we are merely summarising this information as self-contained as possible. We have however rearranged certain parts as to insert them suitably into this thesis, and made the necessary calculations more explicit, where needed. In order to facilitate a comparison between this chapter and the references, we employ their notation as widely as possible and encourage the reader to consult the original publications and the references therein.

7.1 Spectral Functions

The goal of this chapter is to present a way to study the energy excitations of a system, that is, to get access to its spectrum. Even though knowledge of the ground state as obtained through DMRG methods is a good starting point to investigate the zero-temperature physics of a system, only being able to locate the energy excitations will give us access to the "full picture". For simplicity, in this thesis we will only consider the spectral function at zero temperature. Extending the calculations to finite temperature is however possible with relatively little effort, and will be described to some detail in the penultimate chapter dealing with possible future projects. Furthermore, we will restrict ourselves to introducing the spectral function of interest on a heuristic level, as a full discussion is beyond the scope of this thesis.

In general, the objects we are interested in are of the form

$$A^{BC}(\omega) = \langle 0|B\,\delta(\omega - H + E_0)\,C|0\rangle\,, \tag{7.1}$$

where $|0\rangle$ is the ground state of the Hamiltonian H, and A and B are operators acting in the corresponding Hilbert space. This expression holds the same information as the time-dependent correlator

$$G^{BC}(t) = \langle 0|B(t)\,C(0)|0\rangle\,, \tag{7.2}$$

of which $A^{BC}(\omega)$ is the Fourier transform in frequency space:

$$\begin{aligned} A^{BC}(\omega) &= \frac{1}{2\pi}\int dt\, e^{i\omega t} G^{BC}(t) = \frac{1}{2\pi}\int dt\, e^{i\omega t}\,\langle 0|B(t)\,C(0)|0\rangle \\ &= \frac{1}{2\pi}\int dt\, e^{i\omega t}\,\big\langle 0\big|e^{iHt}B(0)\,e^{-iHt}\,C(0)|0\big\rangle = \langle 0|\,B(0)\,\frac{1}{2\pi}\int dt\, e^{i(\omega - H + E_0)t}\,C(0)\,|0\rangle \\ &= \langle 0|B\,\delta(\omega - H + E_0)\,C|0\rangle\,. \end{aligned} \tag{7.3}$$

More precisely, the objects we want to compute are based on correlations between the same type of operators, i.e.

$$A^{B^\dagger B}(\omega) = \big\langle 0\big|B^\dagger\,\delta(\omega - H + E_0)\,B|0\big\rangle\,. \tag{7.4}$$

We can then understand the above spectral function on an intuitive level as follows: the frequency ω runs through the excitation energies of the system above the ground state, and therefore starts at $\omega = 0$. Every state $B\,|0\rangle$ which is an *eigenstate* of the Hamiltonian will then lead to a peak of the delta-function at its corresponding eigenenergy ω. Therefore, evaluating the object $A^{B^\dagger B}(\omega)$ with respect to a complete set of observables will allow us to obtain a precise localisation in frequency space of the eigenstates of the Hamiltonian.

Several types of operators are especially useful to study the elementary excitations of a model. It is obvious that, while all different choices for B do lead to precise locations of the eigenstates, different B's give different perspectives. In this thesis, we will mostly employ the dynamical correlator studying the on-site orientation of spins:

$$A^{{S_i^z}^\dagger S_i^z}(\omega) = A^{S_i^z S_i^z}(\omega) = \langle 0|S_i^z\,\delta(\omega - H + E_0)\,S_i^z|0\rangle\,. \tag{7.5}$$

This quantity therefore describes the real space localisation of the energy eigenstates. Another possibility would be to study the eigenstates in momentum space directly, by working with the spin wave operators

$$S_k^j = \sqrt{\frac{2}{N+1}}\sum_{i=1}^{N}\sin\left(\frac{ik\pi}{N+1}\right)S_i^j, \tag{7.6}$$

for $j = x, y, z$. In this case, scanning through the different wavevectors k would yield the localisation of the energy eigenstates in momentum space, i.e. the dispersion relation of the spin wave excitations. Note, however, that this model is only sensitive to low-energy excitations which can be cast in spin-wave form - higher-lying excitations wouldn't be eigenstates of the "naive" spin-wave operator.

7.2 Direct Calculation via Time-Evolution of MPS

To understand the usefulness of the kernel polynomial method, it is best to first consider the direct calculation of the spectral function. One possibility[28] to achieve this builds on evaluating the time-dependent correlator $G^{BC}(t)$ first, and performing a subsequent Fourier transformation to obtain the spectral function. Rewriting the operator $B(t)$ explicitly in the Heisenberg picture, $G^{BC}(t)$ becomes

$$G^{BC}(t) = \left\langle 0 \middle| e^{iHt} B(0)\, e^{-iHt} C(0) |0\right\rangle = e^{iE_0 t} \left\langle 0 \middle| B(0)\, e^{-iHt} C(0) |0\right\rangle \equiv e^{iE_0 t} \left\langle 0|B|C'\right\rangle_t , \quad (7.7)$$

with

$$|C'\rangle_t = e^{-iHt} C(0)\, |0\rangle . \quad (7.8)$$

The state $|C'\rangle_t$ can then be computed using standard time-evolution methods for MPS (see refs. [13, 64, 65, 60]), the simplest of which is described in the appendix. In order to calculate the spectral function $A^{BC}(\omega)$, one would then need to sample a sufficient number of times and time-evolved states[29], and evaluate the corresponding Fourier integral

$$A^{BC}(\omega) = \frac{1}{2\pi} \int dt\, e^{i\omega t} G^{BC}(t). \quad (7.9)$$

numerically.

There are several drawbacks to this procedure. One major disadvantage is that the time evolution of MPS is prone to errors - the "Trotter error", and a truncation error -, which would therefore be propagated throughout the calculation. Even though this can at least be partially mitigated by employing more precise time evolution schemes, there remains a second drawback. Incidentally, to sample the full spectral function $A(\omega)$ one would have to define a discrete frequency space prior to the sampling, and then do the Fourier integral for each value of ω separately. As we will prove in the next section, the kernel polynomial method avoids this additional step, as the spectral function is evaluated *directly* in the frequency space, with ω entering the calculation as a simple parameter in the final step.

[28] Another possibility is the so-called **correction vector method**, see for instance ref. [63] and further references in [27].

[29] One can reduce the numerical costs of doing so by employing a **linear prediction method**, see ref. [66] and further references in [27].

7.3 The Kernel Polynomial Method

A superior way to calculate the spectral function[30] $A^{BC}(\omega)$ is provided by the kernel polynomial method (cf. ref. [14]). The main idea is to expand the delta function in the spectral function as a (truncated) series in a basis of orthogonal polynomials, which avoids the explicit Fourier transformation. Furthermore, the final series to be evaluated will contain coefficients which can be obtained using standard MPS algebra, and can therefore be implemented with relatively little additional programming.

Especially suited for a series expansion in this context is the basis of Chebyshev polynomials, which we will introduce on a general level in the first subsection. To improve the convergence behaviour of the truncated Chebyshev expansion, we will furthermore employ a damping kernel alongside the expansion coefficients. As the Chebyshev polynomials are only defined in the interval $[-1, 1]$, we will have to take care of mapping the support of any operator used in a Chebyshev expansion into this interval. This is explained in the second subsection. Afterwards, we explicitly derive series expansions for two examples, the spectral density and the spectral function, in order to illustrate the method. In the final subsection, we then explain how to perform those calculations using MPS.

7.3.1 General Construction

Given a complete system of orthogonal functions $\{h_i(x)\}$ over a real interval $[a, b]$ and a scalar product[31] in the corresponding function space

$$\langle f, g\rangle = \int_{[a,b]} dx\, w(x) f(x) g(x), \tag{7.10}$$

we may always express a function $f(x)$ as an infinite series in this basis:

$$f(x) = \sum_{i=0}^{\infty} c_i h_i(x). \tag{7.11}$$

The expansion coefficients are then as usual defined as the projection of the function $f(x)$ to be expanded onto the basis functions:

$$c_i \equiv \frac{\langle h_i, f\rangle}{\langle h_i, h_i\rangle}. \tag{7.12}$$

Furthermore, we require the basis functions $h(x)$ to be orthogonal, where the appropriate notion of orthogonality is given through the inner product, such that

$$\langle h_i, h_j\rangle = \langle h_i, h_i\rangle \delta_{ij} \tag{7.13}$$

[30] The method is even more general than this. Roughly speaking, it can be used to approximate quantities based on the eigenvalue spectrum of a given operator (cf. ref. [14]).

[31] In general, the scalar product may be defined with a weight function $w(x)$, defined in the same interval.

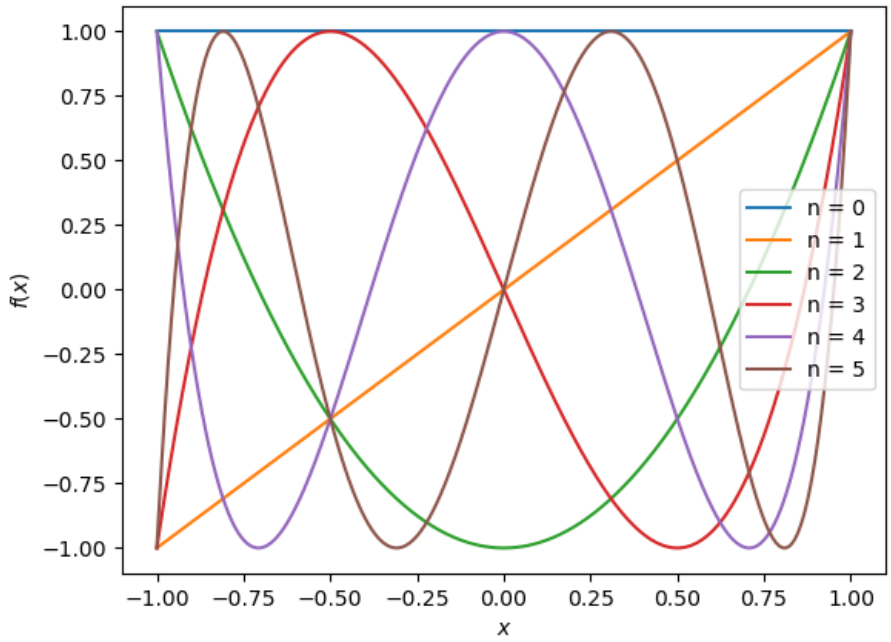

Figure 29: First six Chebyshev polynomials, plotted in their domain $[-1, 1]$. One can clearly discern that they are bounded from above and below, due to their being expressed in terms of a cosine.

holds.

One specific choice of such an orthogonal set of basis function, the **Chebyshev polynomials**[32] $T_n(x)$ (see ref. [67]), is defined by considering the interval $[-1, 1]$ and the weight function

$$w(x) = \frac{1}{\pi\sqrt{1-x^2}}. \tag{7.14}$$

They can be shown to obey the following recursion relation:

$$T_{n+1}(x) = 2x\,T_n(x) - T_{n-1}(x), \tag{7.15}$$

with the two base cases

$$T_0(x) = 1, \quad T_1(x) = x. \tag{7.16}$$

It is then an easy task to calculate the first few polynomials thus defined:

$$\begin{aligned} T_2(x) &= 2x^2 - 1 \\ T_3(x) &= 4x^3 - 3x \\ T_4(x) &= 8x^4 - 8x^2 + 1 \end{aligned} \tag{7.17}$$

[32] Here, we consider only the Chebyshev polynomials of the **first kind**. There also exist the **Chebyshev polynomials of the second kind**, which are defined through the weight function $w(x) = \pi\sqrt{1-x^2}$.

For illustration purposes, we show the first six Chebyshev polynomials in fig. 29. It is however not necessary to calculate every Chebyshev polynomial by hand, as it is possible to derive a closed-form expression for $T_n(x)$ from the Chebyshev recursion relation:

$$T_n(x) = \cos(n \arccos(x)). \tag{7.18}$$

This shows explicitly that the Chebyshev polynomials map the interval $[-1, 1]$ to itself; they are thus bounded from above and below. Evaluating the defining scalar product, one finds that the Chebyshev polynomials of the first kind obey the orthogonality relation

$$\langle T_n, T_m \rangle = \int_I dx \, \frac{1}{\pi\sqrt{1-x^2}} \, T_n(x) \, T_m(x) = \begin{cases} 0, & n \neq m \\ 1, & n = m = 0 \\ \frac{1}{2}, & n = m \neq 0. \end{cases} \tag{7.19}$$

A general expansion of a function $f(x)$ in terms of the Chebyshev polynomials is then given through the following infinite series:

$$f(x) = \sum_{i=0}^{\infty} \frac{\langle f, T_i \rangle}{\langle T_i, T_i \rangle} T_i(x) = c_0 + 2 \sum_{i=1}^{\infty} c_i T_i(x). \tag{7.20}$$

Equivalently, one can use the weight factor explicitly in the series expansion:

$$f(x) = \frac{1}{\pi\sqrt{1-x^2}} \left[\mu_0 + 2 \sum_{i=1}^{\infty} \mu_i T_i(x) \right], \tag{7.21}$$

which defines the **Chebyshev moments** μ_i. Those replace the general expansion coefficients c_i, and are given by the simpler integral

$$\mu_i = \int_I dx \, f(x) \, T_i(x), \tag{7.22}$$

which frees us from integrating over the inverse square root factor. It is therefore this latter expansion in terms of Chebyshev moments which we will employ in the remainder of this text.

Truncating the Chebyshev expansion of the function $f(x)$ after a finite number of terms is not yet the best possible approximation for a given number of terms, as the summation will in general lead to so-called **Gibbs oscillations**. The convergence behaviour can however be improved[33] by introducing additional **damping factors** g_n alongside the Chebyshev moments μ_n. Redefining the series expansion, the damped approximation of $f(x)$ to order N is then

$$\tilde{f}_N(x) = \frac{1}{\pi\sqrt{1-x^2}} \left[g_0\mu_0 + 2 \sum_{n=1}^{N-1} g_n \mu_n T_n(x) \right]. \tag{7.23}$$

[33] A much more detailed description of Gibbs oscillations and damping kernel can again be found in ref. [14].

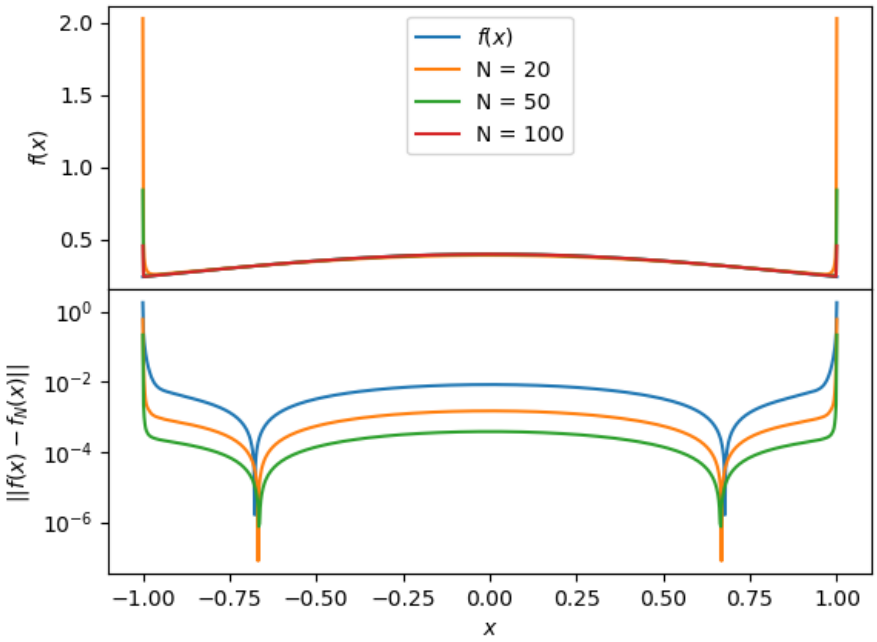

Figure 30: Approximation of a Gaussian, using a truncated series of Chebyshev polynomials, with different orders of expansion. The lower panel shows the absolute error. Here, no damping factor has been used.

Mathematically speaking, one therefore seeks the set of coefficients $\{g_n \,|\, 0 \leq n \leq N-1\}$, such that the absolute difference of the approximated functions in norm converges to 0 in the "most suitable" (i.e. fastest with increasing N) manner:

$$||f_N(x) - \tilde{f}_N(x)|| \xrightarrow[N\to\infty]{} 0. \tag{7.24}$$

As this convergence also depends on the function to be approximated, there doesn't exist one set of damping coefficients which is the most appropriate for every case. One standard choice[34] for the coefficients g_n is the so-called **Jackson damping** (cf. ref. [68]):

$$g_n = \frac{(N-n+1)\cos\left(\frac{n\pi}{N+1}\right) + \sin\left(\frac{n\pi}{N+1}\right)\cot\left(\frac{\pi}{N+1}\right)}{N+1}, \tag{7.25}$$

which we will employ in the remainder of this work. Without further proof, let us finally remark that the approximation error upon employing the Jackson damping scales approximately as $\mathcal{O}(1/N_{\text{Cheby}})$, where N_{Cheby} is the number of terms kept in the series expansion (cf. ref. [27]).

To illustrate those general ideas, we have expanded a standard Gaussian function

$$f(x) = \frac{1}{\sqrt{2\pi}} e^{-x^2/2} \tag{7.26}$$

[34]Other possible kernels are for instance the **Lorentz** or the **Féjer** kernel.

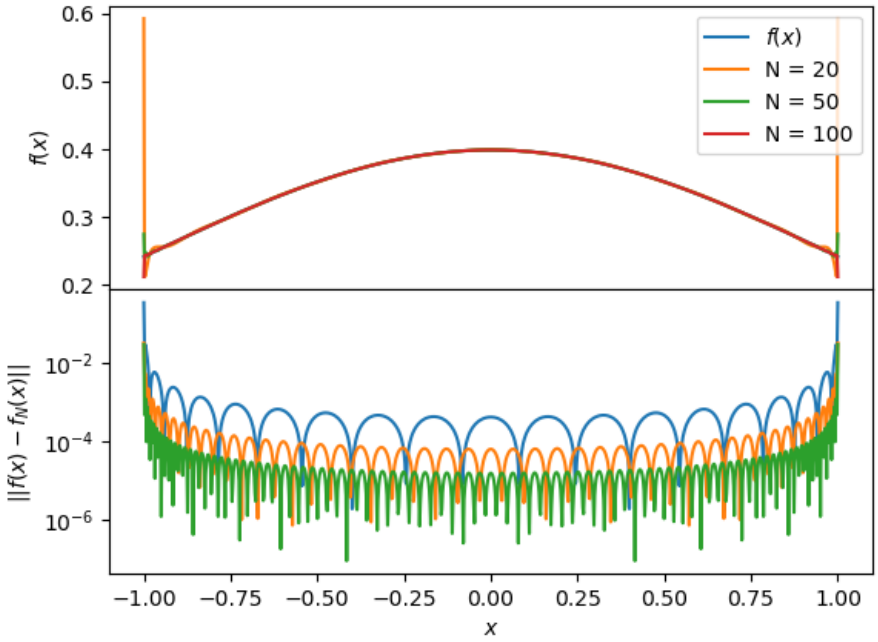

Figure 31: Approximation of a Gaussian, using a truncated series of Chebyshev polynomials, with different orders of expansion. The lower panel shows the absolute error. Here, we have included Jackson damping.

in the interval $[-1, 1]$ as a truncated series of Chebyshev polynomials. Fig. 30 shows the straightforward expansion without damping, whereas in fig. 31 we have employed the Jackson damping. In both cases, we have compared series with 20, 50, and 100 terms, respectively. While both approximation methods yield good results "in the bulk" - with slightly lower overall errors in the damped case, the difference becomes most obvious at the boundaries, where the divergence is well-regulated in the damped case. One important consequence, which this example nicely illustrates, is that working close to the boundaries of the interval $[-1, 1]$ may lead to convergence issues, and potentially requires an artificial restriction of the domain of the Chebyshev polynomials. We will address this issue further in the next subsection.

7.3.2 Rescaling of the Operators

An approximation of a function in terms of Chebyshev polynomials is only defined on the interval $[-1, 1]$. However, we want to employ the method to deal with a Hamiltonian H, whose spectrum $\text{spec}(H) \equiv \{E_i\}$ is in general *not* contained in $[-1, 1]$. We will therefore need to rescale the Hamiltonian, such that its bandwidth $E_{\text{max}} - E_0$ is (strictly) contained in the support of the Chebyshev polynomials. As motivated in the example presented in the previous section, working close to the boundaries of $[-1, 1]$ may cause convergence issues. It is thus preferable to instead rescale the Hamiltonian to the interval

$$[-W', W'], \quad \text{with} \quad W' \equiv 1 - \epsilon, \tag{7.27}$$

where ϵ is a small "safeguard". The proposed (linear) rescaling in ref. [27] is then given by

$$H^{\text{res}} \equiv \frac{H - E_0}{a} - W', \quad \omega^{\text{res}} \equiv \frac{\omega}{a} - W', \tag{7.28}$$

with the constant a defined through the many-body bandwidth W_*:

$$a \equiv \frac{W_*}{2W'}, \quad W_* \equiv E_{\text{max}} - E_0. \tag{7.29}$$

We note here that Holzner et al. propose to improve the convergence of the Chebyshev expansion by choosing the parameter W_* *smaller* than the full many-body bandwidth (in order to explicitly aim at the low-energy regions with the highest spectral weight) (cf. ref. [27]). This idea hasn't been pursued further in our approach, and will be presented in slightly more detail in the final part of this work, when we discuss possible extensions.

As a sanity check, let's verify that the spectrum of the rescaled Hamiltonian is indeed contained in the interval $[-W', W']$:

$$\begin{aligned} H^{\text{res}} |0\rangle &= \left(\frac{H - E_0}{a} - W' \right) |0\rangle = \left(\frac{E_0 - E_0}{a} - W' \right) |0\rangle = -W' |0\rangle \\ H^{\text{res}} |E_{\text{max}}\rangle &= \left(\frac{E_{\text{max}} - E_0}{a} - W' \right) |E_{\text{max}}\rangle = \left(\frac{W_*}{a} - W' \right) |E_{\text{max}}\rangle \\ &= (2W' - W') |E_{\text{max}}\rangle = W' |E_{\text{max}}\rangle , \end{aligned} \tag{7.30}$$

as desired.

7.3.3 Example 1: The Spectral Density

As an introductory example for the above-presented methods, we will calculate an approximation to the **spectral density** of a given operator, e.g. an Hamiltonian H with energy eigenvalues $\{E_i\}$. For simplicity, let H be finite and represented by an $N \times N$-matrix. Then we can define the spectral density as a sum over delta-functions, placed at the (by construction real) eigenvalues of the operator:

$$\rho(E) = \frac{1}{N} \sum_{i=0}^{N} \delta(E - E_i). \tag{7.31}$$

Intuitively speaking, this describes a function which "lights up" whenever we hit an eigenvalue E_i of H. Obviously, $\rho(E)$ has support on the interval spanned by the smallest and largest algebraic eigenvalues, $[E_{\text{min}}, E_{\text{max}}]$. We seek an approximation for $\rho(E)$ in terms of Chebyshev polynomials.

First, we need to rescale the support of $\rho(E)$ to the interval $[-W', W']$ in order to be able to perform the expansion. Defining, as above,

$$H^{\text{res}} \equiv \frac{H - E_0}{a} - W', \quad E^{\text{res}} \equiv \frac{E}{a} - W' \tag{7.32}$$

we observe that the delta-function now becomes

$$\delta(E^{\text{res}} - E_i^{\text{res}}) = \delta\left(\frac{E - E_i}{a}\right) = |a|\,\delta(E - E_i). \tag{7.33}$$

Therefore, we can express the spectral density through its rescaled version as

$$\rho(E) = \frac{1}{N}\sum_{i=0}^{N}\delta(E - E_i) = \frac{1}{N}\sum_{i=0}^{N}\frac{1}{|a|}\delta(E^{\text{res}} - E_i^{\text{res}}) = \frac{1}{|a|}\rho^{\text{res}}(E^{\text{res}}). \tag{7.34}$$

Now we can set up the expansion of the rescaled spectral density in terms of Chebyshev polynomials (calling the integration variable E, for simplicity), by calculating the Chebyshev moments:

$$\begin{aligned}\mu_n &= \int_{[-1,1]} dE\,\rho^{\text{res}}(E)T_n(E) = \frac{1}{N}\sum_{i=0}^{N}\int_{[-1,1]} dE\,\delta(E - E_i^{\text{res}})\,T_n(E) \\ &= \frac{1}{N}\sum_{i=0}^{N} T_n(E_i^{\text{res}}) = \frac{1}{N}\sum_{i=0}^{N}\langle i|T_n(H^{\text{res}})|i\rangle = \frac{1}{N}\,\text{Tr}(T_n(H^{\text{res}})).\end{aligned} \tag{7.35}$$

Note that in the final term, all we need to do is evaluate the trace of a polynomial of a finite matrix, which we may always do[35]. The rescaled (and damped) spectral density, approximated to order M, follows then as

$$\tilde{\rho}_M^{\text{res}}(E^{\text{res}}) = \frac{1}{\pi\sqrt{1 - (E^{\text{res}})^2}}\left[g_0\mu_0 + 2\sum_{n=1}^{M-1} g_n\mu_n T_n(E^{\text{res}})\right], \tag{7.36}$$

which is easily scaled back to the initial expression, as shown above. This simple example further illustrates that the Chebyshev approach is very well suited for the approximation of quantities built from delta-functions, as the integral in the evaluation of the Chebyshev moments is killed by construction.

7.3.4 Example 2: The Spectral Function

Now, finally, we show how we can exploit the kernel polynomial method to approximate the zero-temperature spectral function, as defined in the first section of this chapter:

$$A^{BC}(\omega) = \langle 0|B\,\delta(\omega - H + E_0)\,C|0\rangle\,. \tag{7.37}$$

[35]Unfortunately, this isn't necessarily as straightforward as the above calculation suggests. Ref. [14] discusses the **stochastic evaluation** of these traces.

Again, we begin by defining the rescaled versions of the Hamiltonian and its eigenvalues:

$$H^{\text{res}} \equiv \frac{H - E_0}{a} - W', \quad \omega^{\text{res}} \equiv \frac{\omega}{a} - W'. \tag{7.38}$$

As this leads to a linear rescaling of the argument of the delta-function in a as in the previous example, we find immediately

$$A^{BC}(\omega) = \frac{1}{|a|} \langle 0|B\, \delta(\omega^{\text{res}} - H^{\text{res}})\, C|0\rangle\,, \tag{7.39}$$

where the rescaled expectation value is in the correct form to be approximated by a Chebyshev series, with $\omega^{\text{res}} \in [-W', W']$.

Finding the Chebyshev moments is now even more straightforward than in the previous example, as we only have to integrate over a delta-function (*without* the additional sum implying a trace):

$$\mu_n = \int_{[-1,1]} d\omega\, \delta(\omega - H^{\text{res}}) T_n(H^{\text{res}}). \tag{7.40}$$

The (damped) approximation of the delta-function to order N is therefore given by

$$\delta_N(\omega^{\text{res}} - H^{\text{res}}) = \frac{1}{\pi\sqrt{1-(\omega^{\text{res}})^2}} \left[g_0\mu_0 + 2\sum_{i=1}^{N-1} g_i T_i(H^{\text{res}})\, T_i(\omega^{\text{res}}) \right]. \tag{7.41}$$

This expression can then be used to recover the approximated spectral function:

$$\begin{aligned} A^{BC}(\omega) &= \frac{1}{|a|}\frac{1}{\pi\sqrt{1-(\omega^{\text{res}})^2}} \langle 0|\, B \left[g_0\mu_0 + 2\sum_{i=1}^{N-1} g_i T_i(H^{\text{res}})\, T_i(\omega^{\text{res}}) \right] C\,|0\rangle \\ &= \frac{1}{|a|}\frac{1}{\pi\sqrt{1-(\omega^{\text{res}})^2}} \left[g_0 \underbrace{\mu_0\, \langle 0|B\, C|0\rangle}_{\equiv\mu_0} + 2\sum_{i=1}^{N-1} g_i \underbrace{\langle 0|B\, T_i(H^{\text{res}})\, C|0\rangle}_{\equiv\mu_i}\, T_i(\omega^{\text{res}}) \right] \\ &= \frac{1}{|a|}\frac{1}{\pi\sqrt{1-(\omega^{\text{res}})^2}} \left[g_0\mu_0 + 2\sum_{i=1}^{N-1} g_i\mu_i\, T_i(\omega^{\text{res}}) \right], \end{aligned} \tag{7.42}$$

where in the final step we have recovered the usual Chebyshev expansion by defining new Chebyshev moments through the corresponding expectation values:

$$\begin{aligned} \mu_0 &\equiv \mu_0\, \langle 0|B\, C|0\rangle = \langle 0|B\, C|0\rangle \quad (\mu_0 = 1, \text{ initially}) \\ \mu_n &\equiv \langle 0|B\, T_n(H^{\text{res}})\, C|0\rangle\,. \end{aligned} \tag{7.43}$$

The only "hard" calculations that have to be done, therefore, are the evaluations of the Chebyshev moments through the given expectation values. Once we have found the Chebyshev moments for a given pair A, B of operators, evaluating the remaining sum approximating the spectral function $A^{BC}(\omega)$ is of negligible computational cost, as it merely involves the addition and multiplication of scalar quantities. Moreover, this allows us to justify the claim stated in the beginning of this chapter: due to our direct

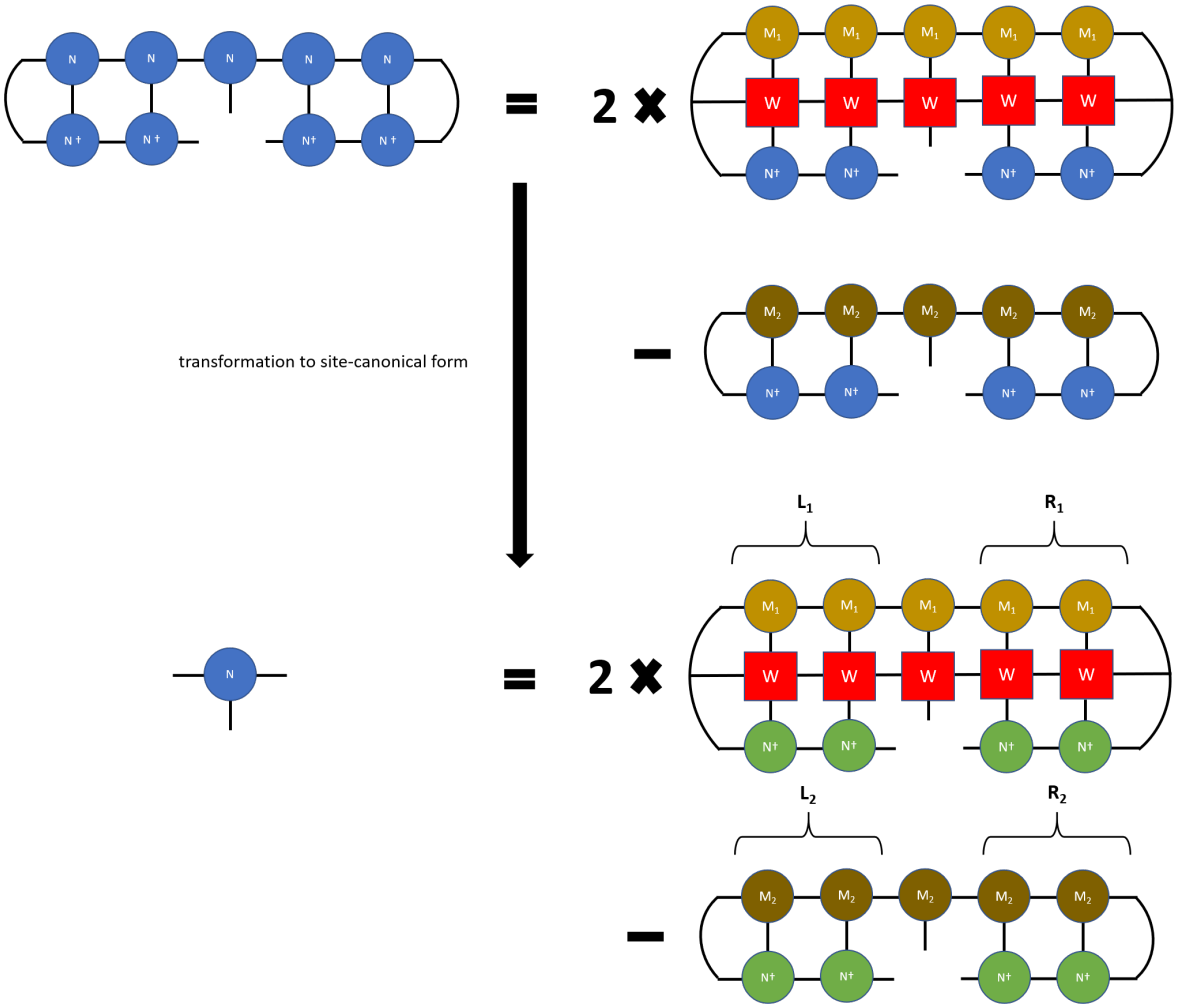

Figure 32: Main iteration step in a variational calculation of the MPS sum $|t_n\rangle = 2H|t_{n-1}\rangle - |t_{n-2}\rangle$. This operation combines the application of an MPO to an MPS, the sum of two MPS and the subsequent compression to a lower bond dimension by finding the best approximation variationally without any intermediate steps.

evaluation of the spectral function in frequency space, the computation has essentially become independent of the frequencies ω. In other words, an arbitrarily high number of increments in frequency space can now be used without any additional computational cost (compared to the cost of evaluating the Chebyshev moments). At the level of the implementation, it is therefore best to generate the Chebyshev moments in a separate data file, such that final sum to evaluate the spectral function can be calculated completely independently, and the Chebyshev moments be re-used at will.

7.3.5 Expansion in Terms of MPS Language

The above presentation is in principle general, and allows for a calculation of the spectral function in *any* framework capable of representing operator and vector quantities. In the results section, we will therefore compare implementations of the kernel polynomial

method based both on exact diagonalisation and on MPS. To calculate the Chebyshev moments using the latter, we start by defining the **Chebyshev vectors** $|t_n\rangle$ as

$$\mu_n = \langle 0|B|t_n\rangle\,, \quad \text{with} \quad |t_n\rangle \equiv T_n(H^{\text{res}})\,C\,|0\rangle\,. \tag{7.44}$$

Using the defining recursion relation of the Chebyshev polynomials, we can rewrite the daunting n^{th}-order polynomial of the Hamiltonian as

$$\begin{aligned} |t_n\rangle &= T_n(H^{\text{res}})\,C\,|0\rangle = \left[2H^{\text{res}}\,T_{n-1}(H^{\text{res}}) - T_{n-2}(H^{\text{res}})\right]\,C\,|0\rangle \\ &\equiv 2H^{\text{res}}\,|t_{n-1}\rangle - |t_{n-2}\rangle\,. \end{aligned} \tag{7.45}$$

In the same fashion, we obtain the two starting vectors from the two base cases of the Chebyshev recursion relation:

$$|t_0\rangle = C\,|0\rangle\,, \quad |t_1\rangle = H^{\text{res}}\,|t_0\rangle\,. \tag{7.46}$$

Assuming that we have knowledge of the ground state $|0\rangle$ - found by DMRG - we can therefore calculate *all* the Chebyshev vectors $|t_n\rangle$ by applying the rescaled MPO-Hamiltonian H^{res} and by forming linear combinations of the MPS. Note, however, as applying MPOs to MPS and taking sums of MPS increases the bond dimension, a truncation procedure in each iteration step will be required. In the present work, we calculate each Chebyshev vector in a single step by evaluating the Chebyshev recursion variationally, as illustrated by the tensor network in fig. 32. This results immediately in a compressed state, representing the Chebyshev vector to the desired accuracy.

Finally, in order to rescale the Hamiltonian to the correct energy range, we also need to determine the upper end of its spectrum. This could be achieved with the same DMRG setup, e.g. by letting

$$H_{\text{MPO}} \to -H_{\text{MPO}}. \tag{7.47}$$

Alternatively - which is the method employed in this work -, we can adapt the DMRG code such that in each local eigenvalue equation, the maximum eigenvalue is approximated instead of the minimum eigenvalue, thus implying that the algorithm converges to the maximum energy state. When using a library implementation of the Lanczos algorithm such as `eigsh` from `scipy.sparse`, this can be achieved by changing a single parameter. The rescaled Hamiltonian is then a linear combination of the initial Hamiltonian and the identity operator, and therefore has an MPO bond dimension increased by one.

Algorithms-Kernel Polynomial Method

Input: MPO representations of Hamiltonian H and of operator B, number N of sites, number NCheby of Chebyshev terms, energy half-bandwidth W.

Output: Matrix of Chebyshev moments.

```
G, E0 = DMRG(H, energy=minimum);
Emax = DMRG(H, energy=maximum);
Hres = rescaleHamiltonian(H, E0, Emax, W) ;
Chebys = zeros(NCheby, N) ;
for i in range(N) do
    GB = G.applyMPO(B);
    t0 = G.applyMPO(B);
    t1 = t0.applyMPO(Hres);
    mu0 = overlap(GB,t0) mu1 = overlap(GB,t1) ChebVectors = [t0, t1];
    ChebMoments = [mu0, mu1];
    for j in range(2, NCheby) do
        tn = ChebVariational(Hres, ChebVectors[j-1], ChebVectors[j-2]);
        ChebVectors.append(tn);
        mu = overlap(GB, ChebVectors[j]);
        ChebMoments.append(mu);
        ChebVectors[j-2] = 0 ;
    end
    Chebys[:, i] = ChebMoments
end
return Chebys ;
```

Part III

Case Studies and Results

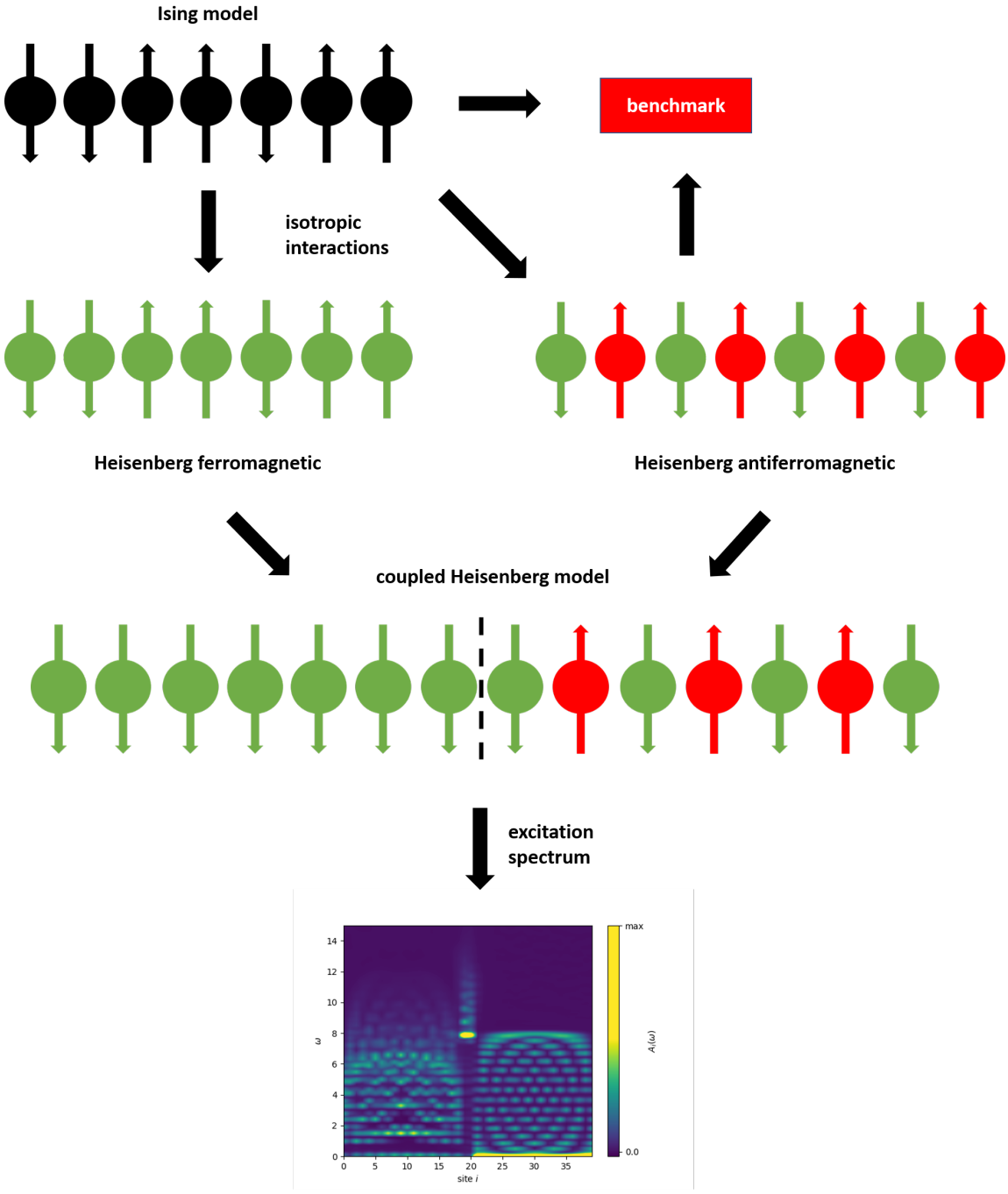

8 Benchmarking of the MPS Algorithms

Before we analyse the model of an interface between a ferromagnetic and an antiferromagnetic Heisenberg chain, we will present several benchmark results to assess the correct working of our algorithms. For this, we will employ two different methods: first, we study small systems (of the order of ten to twenty sites) for which results may be obtained through exact diagonalisation methods, with modest computational effort. The primary purpose of those results is merely to ensure the correct working of the substantially more involved MPS algorithms by comparing the respective results. Second, we will analyse larger versions (up to 200 sites) of the same systems, for which we have presented analytical solutions in the thermodynamic limit. This will serve on the one hand as a check that our algorithms scale appropriately to larger system sizes; on the other hand it will permit us to study the impact of the finite system size (and when a system can be considered large enough to faithfully approximate the thermodynamic limit).

The following benchmark discussion is based on the two spin chain models discussed in this thesis, the (transverse field) Ising model and the (anti-)ferromagnetic Heisenberg model. For both systems, we will calculate the ground state energy and thus confirm the analytical prediction. In addition, we will study the magnetisation of the Ising model as a function of the transverse field and find the critical point in the associated parameter space. Furthermore, we will calculate the entanglement entropy of the ground state of the Ising model. To finish this benchmarking section, we confirm the correct implementation of the kernel polynomial method by calculating the dynamical correlators of the Heisenberg model.

On a more technical level, we will perform various ground state calculations with different bond dimensions and different system sizes, and monitor the converge properties of the states thus found. In the same vein, we will evaluate the dynamical correlator for different numbers of Chebyshev polynomials kept in the expansion. This allows us to find a range of parameters suitable for the calculations in the next chapter.

8.1 Summary of Analytical Properties

For the ease of reading, we will summarise the relevant analytical results below. Extensive versions of those calculations have been discussed in the first part of this thesis.

8.1.1 Transverse Field Ising Model

For convenience, we reproduce the definition of the transverse field Ising model in one dimension here:

$$H = J \sum_i S_i^z S_{i+1}^z - h \sum_i S_i^x. \tag{8.1}$$

At zero temperature, this Hamiltonian depends on the ratio J/h in the associated parameter space. Assuming the thermodynamic limit and periodic boundary conditions, the ground state energy per spin site is then given by

$$E_0 = \frac{J}{2\pi} \int_{-\pi}^{\pi} dx \, \sqrt{1 + h^2 - 2h\cos(x)}. \tag{8.2}$$

Furthermore, the magnetisation in z-direction follows as

$$\langle M^z \rangle = \frac{1}{\pi} \int_0^{\pi} dk \, \frac{1 - \frac{J}{h}\cos(k)}{\sqrt{1 - \frac{2J}{h}\cos(k) + \left(\frac{J}{h}\right)^2}}. \tag{8.3}$$

Finally, note the remarkable scaling of the entanglement entropy at criticality, upon considering a subsystem of length L:

$$S(L) \propto \frac{c}{3} \log(L), \tag{8.4}$$

where c is the central charge of the associated conformal field theory. In the thermodynamic limit, c is known to be $1/2$.

8.1.2 Heisenberg Model

Analytical solutions for the Heisenberg model

$$H = J \sum_i \vec{S}_i \cdot \vec{S}_{i+1} = J \sum_i \left[\frac{1}{2} \left(S_i^+ S_{i+1}^- + S_i^- S_{i+1}^+ \right) + S_i^z S_{i+1}^z \right] \tag{8.5}$$

can only be found in one dimension, e.g. via the Bethe ansatz. In the ferromagnetic case ($J < 0$), the ground state energy per site is easily determined to be

$$E_0^{FM} = -\frac{|J|}{4}, \tag{8.6}$$

as the ground state is built from a configuration in which all spins are parallel. The antiferromagnetic case ($J > 0$), however, is much more complicated. Its ground state energy per site can be determined to be

$$E_0^{AFM} = -J\ln(2) + \frac{J}{4}, \tag{8.7}$$

which contains an additional $-J\ln(2)$ term in comparison to the ferromagnetic ground state energy. This complication is due to the fact that the ground state of the antiferromagnetic Heisenberg model is *not* the Néel state[36], but arises through a superposition of

[36] Which, recall, is built from alternating spins.

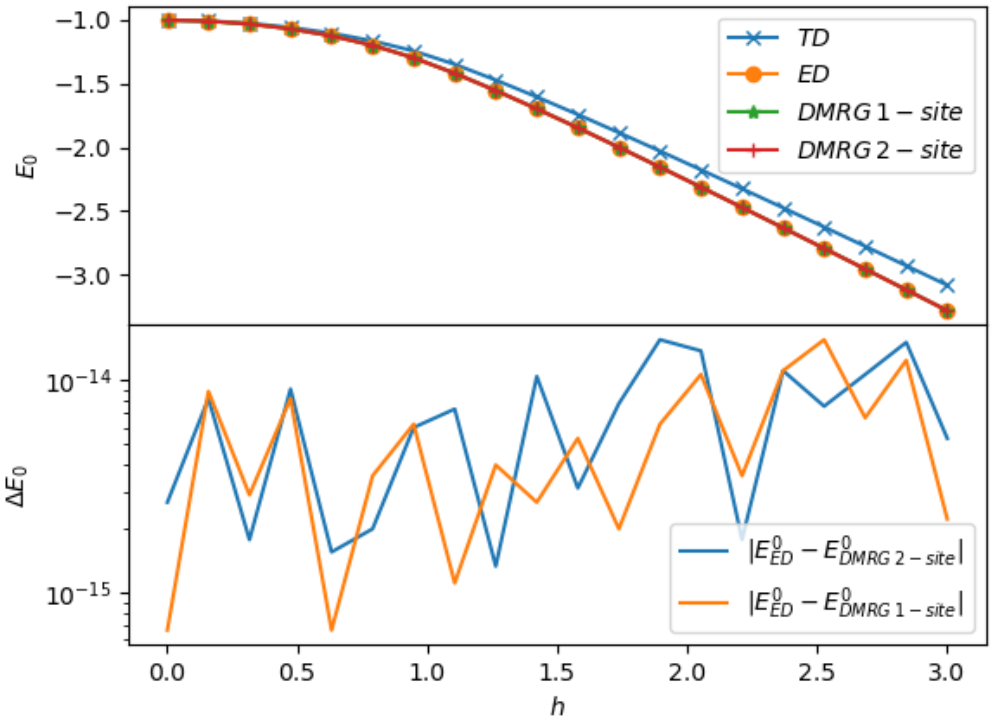

Figure 33: Ground state energy per site for the transverse field Ising model with 16 sites, as a function of the magnetic field h. Shown is a comparison of single-site and two-site DMRG algorithms, as well as a comparison to exact diagonalisation. In the lower panel, the absolute error of the DMRG results compared to the exact results is given.

states with $N/2$ spin flips, with respect to the ferromagnetic ground state. On a microscopic level, the spin flip terms S^+S^- and S^-S^+ are at the origin of this behaviour, as they map the Néel state to a state with a different spin configuration, thus preventing it from being an exact eigenstate[37].

8.2 Results for the Transverse Field Ising Model

First, we present benchmark results for the transverse field Ising model. To summarise our main findings, we will show an excellent agreement between MPS results and equivalent calculations performed with exact diagonalisation techniques. Especially properties like the ground state energy and the magnetisation could be determined with very small deviations from the thermodynamic limit. However, we found that the entanglement entropy is very sensible to the finite system size, and/or the open boundary conditions employed in the large-scale MPS calculations.

[37] It is, however, an exact eigenstate of the Ising model (without transverse field), as in this case the spin flips are by construction "switched off".

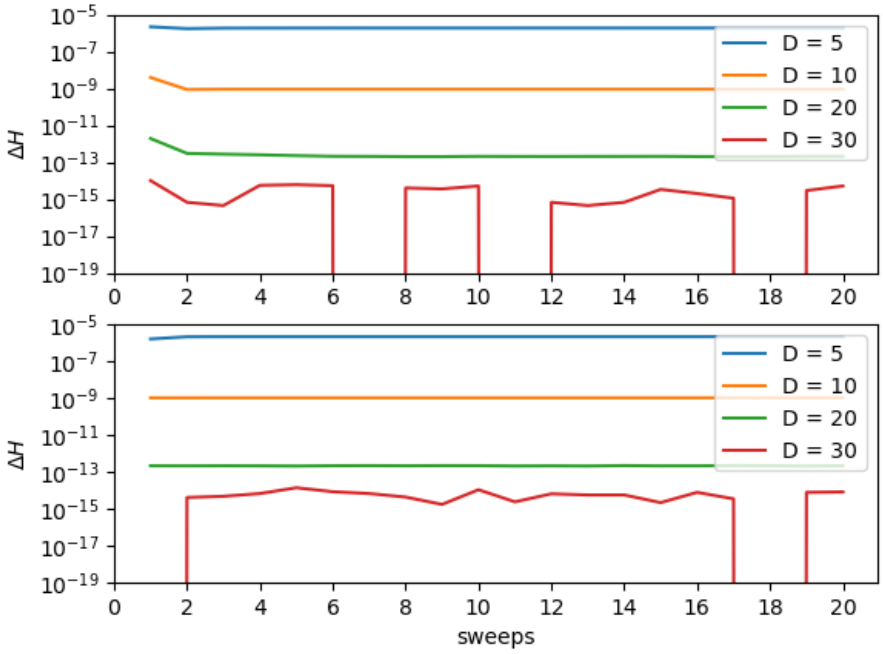

Figure 34: Variance of the Hamiltonian ΔH when calculating the ground state energy of the transverse field Ising model at criticality, as a function of the number of sweeps. A comparison for different bond dimensions is shown. Upper panel: one-site DMRG; lower panel: two-site DMRG.

8.2.1 Ground State Energy and Convergence Properties

We begin our analysis with the ground state energy of a small Ising model. Studying a spin chain with 16 sites and open boundary conditions, we find the results shown in fig. 33. There, we compare the ground state energies found through exact diagonalisation with the corresponding DMRG result, for both a single-site and a two-site DMRG algorithm. For both DMRG algorithms we have employed a bond dimension of 20.

Firstly, we can conclude that both DMRG implementations determine the ground state energy exceptionally well in as few as 2-3 sweeps, as the direct comparison with the exact diagonalisation results shows. Regardless of whether the one- or the two-site algorithm has been used, the errors are of the order of $\mathcal{O}(10^{-14}\text{-}10^{-15})$ and therefore well below any numerically relevant threshold. For the present purpose, it therefore doesn't make any difference if we use the one-site or the (computationally more expensive) two-site algorithm. Unless otherwise stated, we will employ the one-site DMRG-algorithm in what follows.
Second, there is a clear discrepancy between the ground state energy in the thermodynamic limit - included in fig. 33 for comparison - and the ground state energies for the finite system with 16 sites. Even though the ground state energy in the thermodynamic limit clearly shows the same overall behaviour, the absolute difference to the finite-size

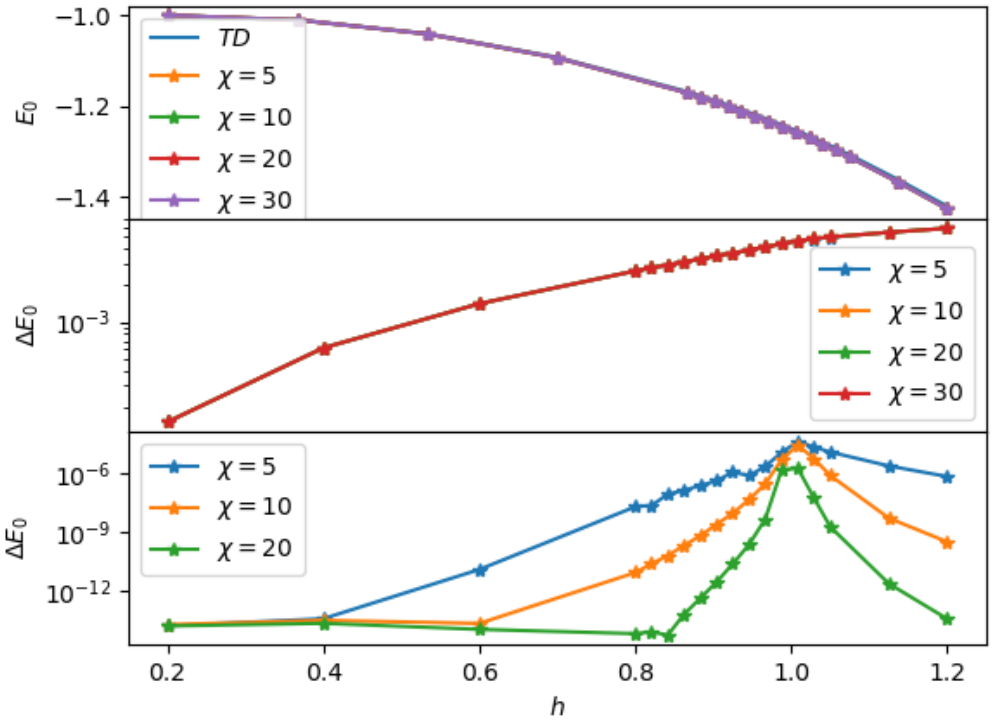

Figure 35: Ground state energy of the transverse field Ising model with 200 sites, found by DMRG. In the upper panel we compare the per-site energies found for different bond dimensions and the thermodynamic limit, whereas the middle panel shows the absolute error between the DMRG results and the thermodynamic limit. Lowest panel: absolute difference between ground state energies found with bond dimensions 5, 10 and 20 and the ground state energy found with bond dimension 30.

results grows monotonically with increasing h, up to roughly 0.1 for the largest values of h considered. This is due to our using of a finite-size model with open boundary conditions, as those are better suited for MPS- and DMRG-calculations. A more reliable approximation of the thermodynamic limit using only small, finite systems can be achieved for instance by exactly diagonalising a periodic chain. For our present discussion, however, we won't pursue this idea further.

While choosing a bond dimension of 20 was justified in retrospect by the comparison with the exact diagonalisation result, this merely proves that the ground state energy has converged suitably. In order to assess convergence to the ground state itself - and thus the suppression of contributions due to low-lying excited states - we have computed the variance ΔH of the Hamiltonian for various bond dimensions in a system with 40 sites, as visualised in fig. 34. To directly address the "worst case", those calculations have been performed approximately[38] at criticality ($h = 1$), and we study the convergence of ΔH

[38]Strictly speaking, there is no critical point for a finite system.

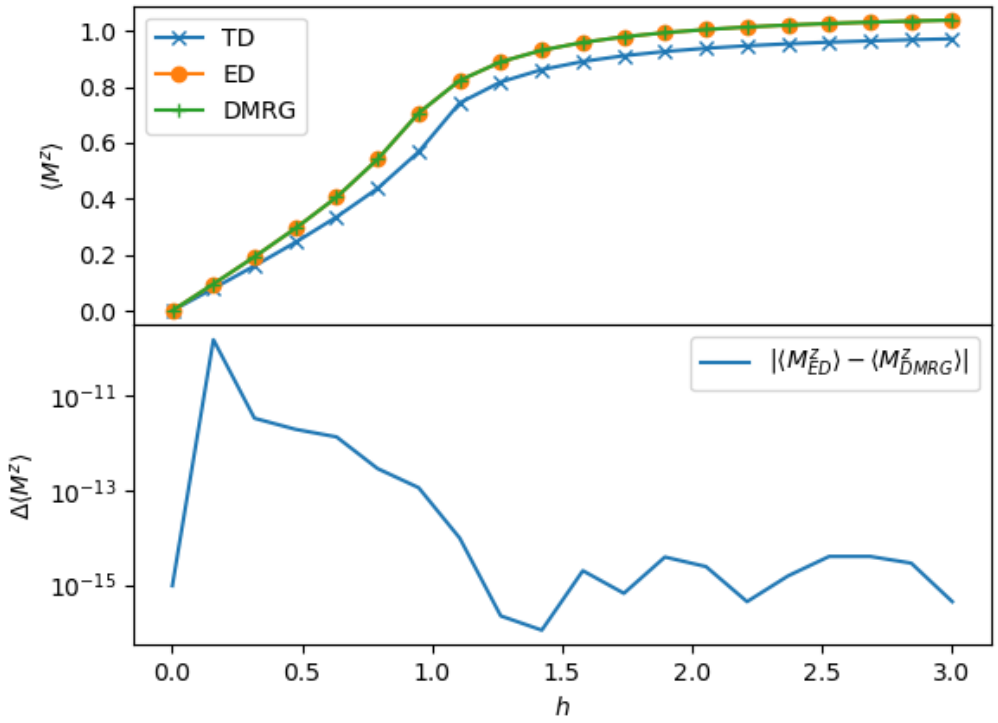

Figure 36: Total magnetisation of the ground state per site for the transverse field Ising model with 16 sites, as a function of the magnetic field. Shown is a comparison of two-site DMRG, the result obtained by exact diagonalisation, and the result in the thermodynamic limit. In the lower panel, the absolute error of the DMRG results compared to the exact results is given.

depending on the number of DMRG sweeps. Furthermore, we compare again a one-site and a two-site DMRG algorithms to investigate whether the increased variational space is needed to obtain a better approximation of the true Ising ground state.

Most importantly, one can see a clear improvement in the convergence with increasing bond dimension. For bond dimensions of 5, 10 and 20 (the first being included mostly for purposes of demonstration), we find variances of the Hamiltonian of the orders of roughly 10^{-6}, 10^{-9} and 10^{-13}, respectively. While especially the former two indicate a residual presence of low-energy excited states in the numerically determined ground state, using a bond dimension of 20 will in general yield a very good approximation of the sought state. If even better results are desired, a bond dimension of 30 can be employed, which effectively works at the threshold of numerical accuracy for the system considered. Furthermore, we observe effectively no monotonous convergence depending on the number of sweeps, in contrast to what one might have intuitively expected. Rather, for too low bond dimensions the algorithm quickly gets stuck in a local minimum, whereas for the "big enough" bond dimension fluctuations at the order of the numerical precision occur. We lastly observe that the differences between the one- and

two-site DMRG schemes are, again, minor, and only seem to have an impact on the speed of convergence on the very first sweeps. The main parameter which limits the precision that can be reached in the present system is therefore the bond dimension, irrespective of the chosen update scheme.

To understand the finite-size effects better, we have recalculated the ground state energy per site for a large model with 200 sites, shown in fig. 35, this time omitting the comparison to exact diagonalisation. It strikes us immediately that the thermodynamic limit is now *much* better approximated, as illustrated in the middle panel of fig. 35. The absolute difference between the ground state energies found through DMRG and the exact results grows monotonically with h, but culminates at a sub-per cent level for $h = 1.2$, irrespective of the chosen bond dimension. Comparing the different ground state energy estimates among each other in the lowest panel of fig. 35 allows us to get a better understanding of the errors due to the different bond dimensions. As a reference, we take the "best" estimate with the highest bond dimension of 30 and compute the absolute difference with the other estimates. In general, we can see that the absolute difference peaks for values of h around the critical value of $h = 1.0$, confirming that this point in parameter space requires a higher bond dimension in order to capture the physics to a suitable accuracy. Furthermore, we can clearly observe that with increasing bond dimension, the deviation from the "best" estimates decreases, and becomes increasingly centred around the critical value of the transverse field. All in all, we can however assert for the time being that an Ising model with 200 sites is at least a good approximation to the thermodynamic limit, and well reachable within the computational limits of DMRG.

8.2.2 Magnetisation

As a further check of our MPS methods, we compute the ground state magnetisation in z-direction of the transverse field Ising model as a function of the external magnetic field h. Again, we start with a comparison of the magnetisation calculated with MPS and with exact diagonalisation for a small model with 16 sites, shown in fig. 36. For completeness, we also show the magnetisation curve in the thermodynamic limit.

Similar to the previous calculation of the ground state energy of a small system, the agreement between both results is excellent, as proven by the absolute errors in the lower panel of fig. 36. For small magnetic fields, the magnetisation in z-direction (in which the transverse field is applied) is small, and then rises with increasing values of h. While this model is too small to accurately approximate the effects of a quantum phase transition, we can still distinguish areas of a "non-saturated" magnetisation (for $h < 1$) and of a "saturated" magnetisation (for $h > 1$). In the former, the interaction in x-direction outweighs the interaction in z-direction, implying only a small magnetisation,

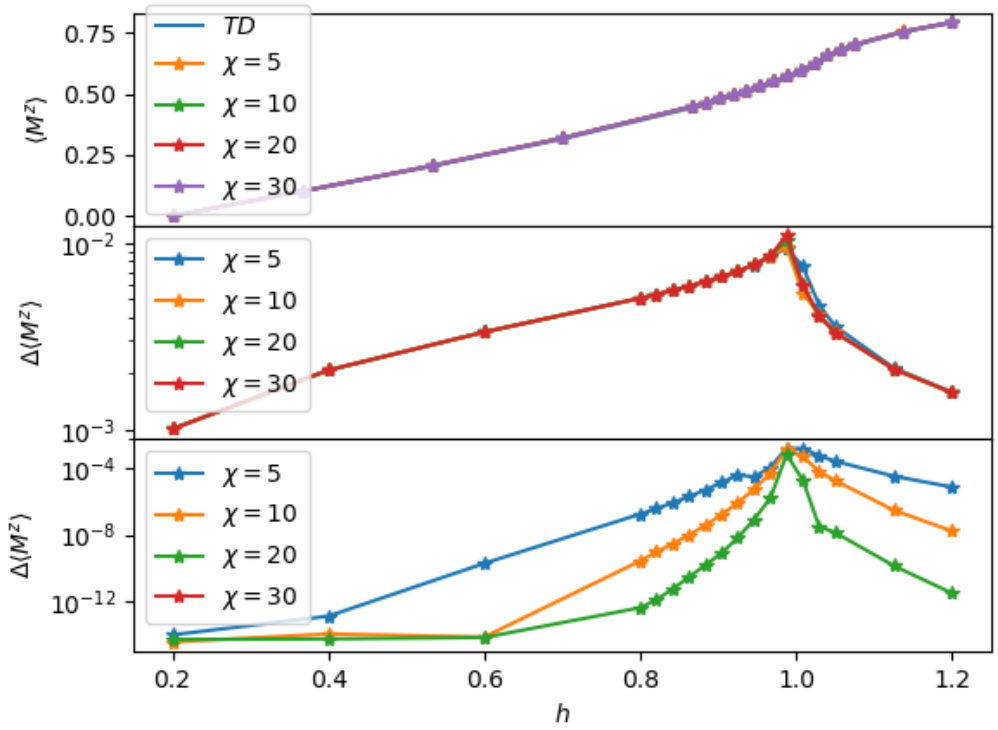

Figure 37: Absolute value of the magnetisation per site for the transverse field Ising model, as a function of the magnetic field h. Shown is a comparison of different system sizes with the analytical result in the thermodynamic limit. The two lower panels display the absolute deviation of the results from the TD limit, and the absolute deviation from the result with the highest bond dimension of 30.

whereas in the latter regime it is energetically favourable for the spins to be aligned with the magnetic field, leading to the "full" on-site magnetisation. A comparison with the thermodynamic limit illustrates, as in the case of the ground state energy, that the overall scaling is well reproduced already on a small system. In the thermodynamic limit, however, the magnetisation tends to be roughly 0.1 lower than in the system studied, with the largest absolute deviations again around the critical parameter $h = 1$.

Using the same large system with 200 sites as in the previous subsection, we study the finite-size approximation of the thermodynamic limit in fig. 37. As before, the upper panel shows the total magnetisation for different bond dimensions, as well as a plot of the analytical prediction in the thermodynamic limit. The agreement between the numerical results and the analytical prediction is again good, as confirmed by the absolute errors in the middle panel of fig. 37. As can be expected, the errors are largest at the critical value of h, with the errors slightly exceeding the per cent level. Otherwise, the dependence of the errors on the bond dimension is again best seen by comparing the "best" estimate with a bond dimension of 30 to the others in the lowest panel of fig. 37.

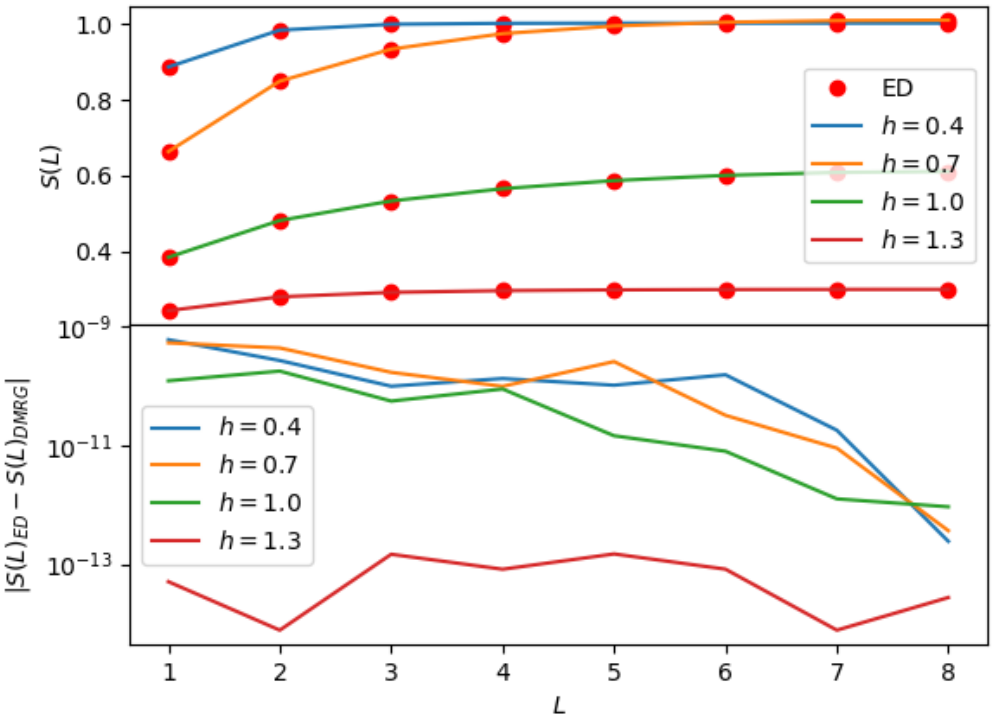

Figure 38: Entanglement entropy for the transverse field Ising model with 16 sites, depending on the length L of subsystem considered. Shown are the entanglement entropies for different values of the transverse field, and a comparison between the results using exact diagonalisation and MPS. In the lower panel, the absolute error of the DMRG results compared to the exact results is given.

Just as it was the case for the ground state energy, the absolute errors decrease significantly with increasing bond dimension, being the largest at the critical magnetic field.

8.2.3 Entanglement Entropy

Having characterised the convergence to the thermodynamic limit through the ground state energy and the magnetisation, we will now shift our attention to studying the entanglement entropy in the Ising model. The benchmark presented below serves as check to investigate how the bipartite entanglement entropy depends on the length of the subsystem studied. This prepares the calculation in the subsequent chapter inasmuch that for a model with a predefined interface, we expect to see a different entanglement entropy depending on whether the division into subsystems includes the interface or not. In complete analogy to the two previous subsections, we will start by computing the entanglement entropy of the ground state of the transverse field Ising model for a small system, and compare the results of DMRG and exact diagonalisation. Then, we will study the scaling of the entanglement entropy for a large system with 200 sites, and see

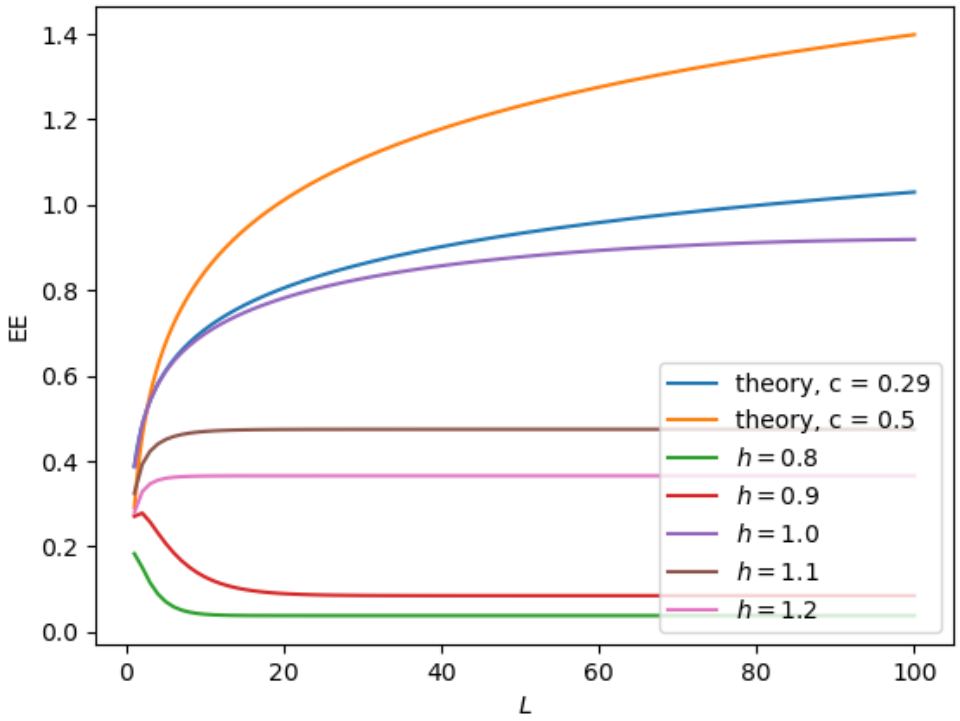

Figure 39: Entanglement entropy for the transverse field Ising model with 200 sites, depending on the length of subsystem considered. Shown are the entanglement entropies for different values of the transverse field, with the entanglement entropy corresponding to a critical transverse field $h = 1$ exhibiting the characteristic logarithmic scaling. Two theory fits illustrate the derived central charge c, and the central charge expected in the thermodynamic limit.

how well this approximates the scaling in the thermodynamic limit.

Fig. 38 shows the scaling of the entanglement entropy for a small Ising model with 16 sites, depending on the length of the (left) subsystem. In addition, we have computed the scalings for different values of the transverse magnetic field, as indicated in the legend. In general, the agreement of MPS-based methods and exact diagonalisation is again excellent, with total errors being of the order of 10^{-9} or lower. For small ($h = 0.4$) and big ($h = 1.3$) values of the transverse field, the entanglement entropy quickly saturates to a constant value. In contrast, for $h = 0.7$ and $h = 1.0$, the characteristic log-dependence is starting to appear, albeit feebly due to the finite system size. This agrees with the fact that for finite system sizes, the "critical value" is less than the critical value in the thermodynamic limit. Finally, we can observe a notably smaller error between DMRG and exact diagonalisation in the ordered phase for $h = 1.3$ (the red curve), which furthermore exhibits the lowest entanglement entropy of the phases studied here.

Analysing the entanglement entropy in a large system with 200 sites and a bond di-

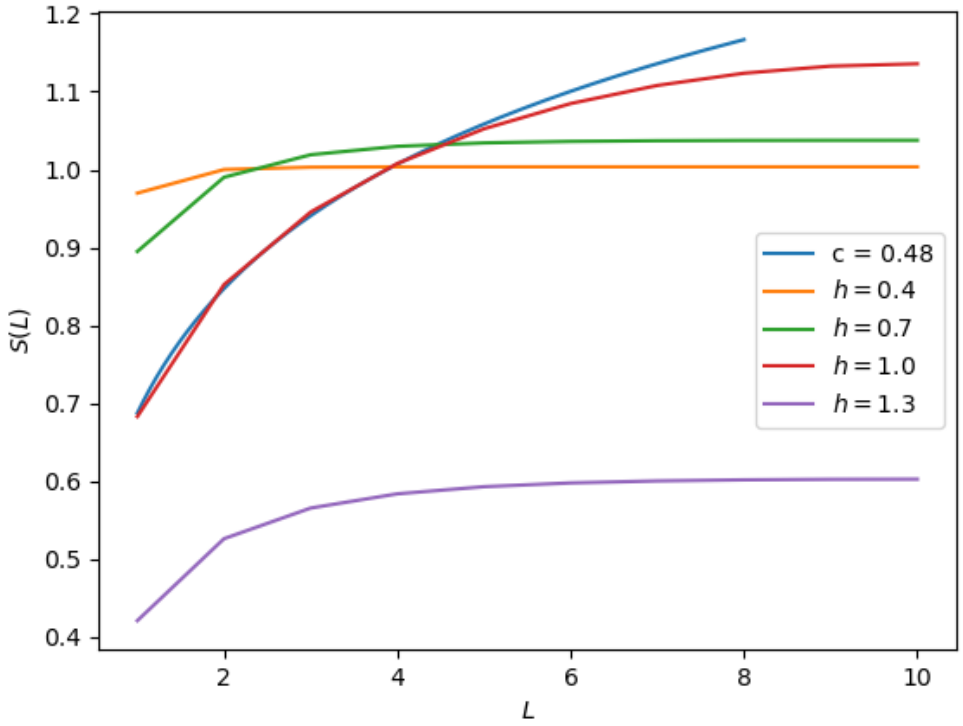

Figure 40: Entanglement entropy for the transverse field Ising model with 20 sites, depending on the length of subsystem considered. Results are obtained with exact diagonalisation for periodic boundary conditions, as opposed to the open boundary conditions used in the remainder of this work.

mension of 30 in fig. 39 confirms the distinguished log-scaling of the entanglement entropy for the critical value $h = 1$. Despite the large system size, however, we cannot yet approximate the entanglement entropy in the thermodynamic limit in a convincing fashion. Fig. 39 shows, in addition to the numerical results, two theory fits for the entanglement entropy. In the "blue" case, we have fitted the theoretical prediction to our data, obtaining a central charge of $c = 0.29$. In contrast, the "orange" case shows a fit with fixed central charge of $c = 0.5$, and therefore showcases how the entanglement entropy in the true thermodynamic limit should scale. Apart from this study at criticality, we can furthermore numerically confirm that the entanglement off-criticality quickly saturates to a constant value. Curiously, a behaviour that wasn't yet hinted at in the previous study of the small system, for values of the transverse field *below* the critical value, the entanglement entropy approaches a constant value from above. While not violating the fact that the entanglement entropy scales asymptotically like a constant, it remains to be assessed whether this behaviour is due to the finite system size, the open boundary conditions or an artefact of our implementation.

Let us finally remark that this scaling of the entanglement entropy seems to depend cru-

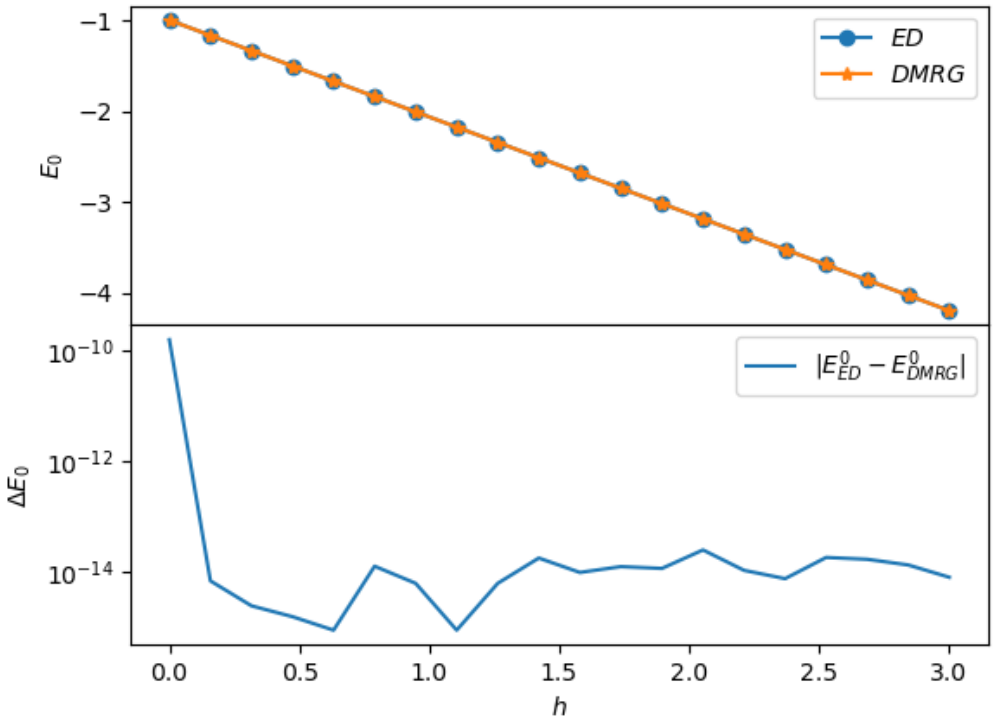

Figure 41: Ground state energy per site for the ferromagnetic transverse field Heisenberg model with 16 sites, as a function of the magnetic field. Shown is a comparison of DMRG results and exact diagonalisation. In the lower panel, the absolute error of the DMRG results compared to the exact results is given.

cially on the boundary conditions being periodic or open. For completeness, in fig. 40 we have re-calculated the entanglement entropy for an Ising model with 20 sites but with periodic boundary conditions, using exact diagonalisation. Fitting the theoretical curve to the critical result, we obtain the much better approximation $c = 0.48$ of the central charge $c_{TD} = 1/2$ in the thermodynamic limit.

8.3 Results for the Heisenberg Spin Chain

Having discussed the transverse field Ising model as a first toy model, we now propose to graduate to the Heisenberg model, which will provide the stepping stone towards the non-trivial interface of Heisenberg models, to be studied in the next chapter. We begin our analysis in a similar fashion as in the previous subsection by comparing the ground state energies of small ferro- and antiferromagnetic Heisenberg models obtained through exact diagonalisation and MPS methods. Hereafter, we study large antiferromagnetic Heisenberg models up to 200 sites to investigate the impact of the finite system size on the convergence to the ground state energy in the thermodynamic limit. Finally, we will provide some benchmarks of the kernel polynomial method, and thereby study

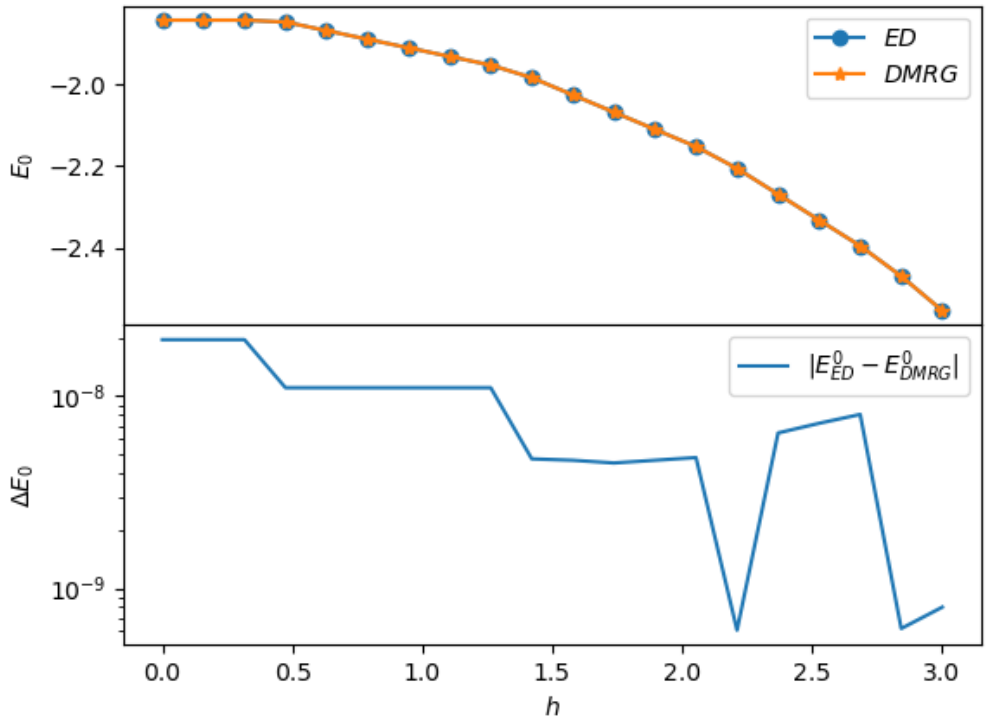

Figure 42: Ground state energy per site for the ferromagnetic transverse field Heisenberg model with 16 sites, as a function of the magnetic field. Shown is a comparison of DMRG results and exact diagonalisation. In the lower panel, the absolute error of the DMRG results compared to the exact results is given.

the localisation of the elementary excitations of the Heisenberg model in real space.

8.3.1 Ground State Energy and Convergence Properties

A computation of the ground state energy of the ferromagnetic Heisenberg model is shown in fig. 41, where we again compare the DMRG results with a bond dimension of 20 to the exact results for a small system of 16 sites. We have computed the ground state energy for different values of a transverse magnetic field in z-direction, and the lower panel of fig. 41 shows again the absolute difference between the two numerical results. As for the Ising model, the agreement is excellent over nearly the entire parameter range with errors of the order of 10^{-14} , only admitting a comparatively "large" error of about 10^{-10} for small values of the transverse field.

Somewhat more interesting is the ground state energy of the antiferromagnetic Heisenberg model, which we have computed with the same settings in fig. 42. While the agreement between both numerical results is still very good (and good enough for all intents and purposes), we do observe absolute errors higher by several orders of mag-

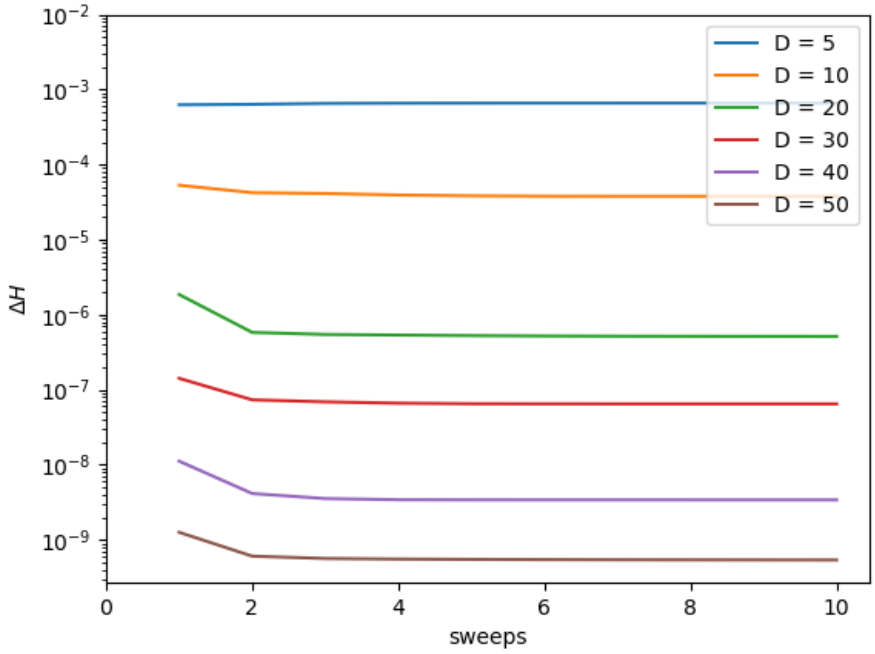

Figure 43: Variance of the Hamiltonian ΔH when calculating the ground state energy of the antiferromagnetic Heisenberg model (with 40 sites), as a function of the number of sweeps. A comparison for different bond dimensions is shown.

nitude than for the ferromagnetic case. This fact supposedly originates in the much more complicated structure of the antiferromagnetic ground state.

In contrast to the Ising model (unless at criticality), where we could achieve low variances of the Hamiltonian with relatively small bond dimensions, the choice of the bond dimension has a huge impact on the convergence to the true ground state of the antiferromagnetic Heisenberg model[39], which is shown in fig. 43. Analysing a model with 40 sites, we can see that for increasing bond dimensions, the convergence to the ground state improves but doesn't reach the level of precision we have reached with the Ising model. The saturated levels seem to be separated into two regimes: one for the very low bond dimensions 5 and 10, whose variances converge to values around 10^{-3} and 10^{-4}, and a second regime for the bond dimensions bigger than 20. Here, we get a variance of 10^{-6} or better, culminating at slightly below 10^{-9} for a bond dimension of 50, the highest studied in this case. In order to obtain sensible results, we therefore propose to use a bond dimension of *at least* 20, but preferably more if the availability of computational resources permits it.

To analyse the effect of the finite system size of the Heisenberg model, we have re-

[39] As the ground state of the ferromagnetic Heisenberg model is a product state, there is no point in studying the effect of the bond dimension.

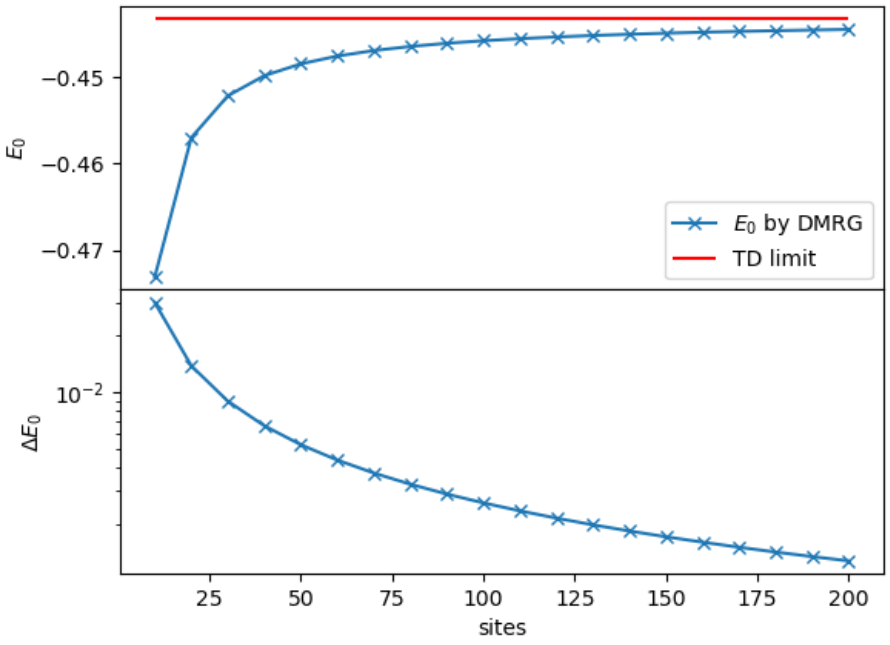

Figure 44: Ground state energy per site for the antiferromagnetic Heisenberg model found by DMRG, as a function of the system size. Shown is a comparison of DMRG results and the analytical result in the thermodynamic limit. In the lower panel, the absolute error of the DMRG results compared to the analytical results is given.

calculated the antiferromagnetic ground state energy for system sizes between 10 and 200 sites, in order to assess the speed of convergence towards the analytic result in the thermodynamic limit. This calculation, done for a model with no transverse field, is shown in fig. 44. In the upper panel, it is clearly visible that the ground state energy converges (from below) to the analytic value, as expected for an increasing system size. The lower panel shows again the absolute error which decreases correspondingly, dropping below a per cent level at roughly 25 sites. It is noteworthy that the convergence considerably slows down for models with more than about 100 sites.

8.3.2 Real Space Spectral Function

As our final benchmark task, we compute the dynamical correlator in real space for the ferromagnetic and antiferromagnetic Heisenberg models, and compare them to the same calculation with exact diagonalisation methods. We start by studying a small system with six sites, and choose to truncate the Chebyshev expansion after 300 terms. Fig. 45 shows the dynamical correlator for an antiferromagnetic coupling, whereas fig. 46 visualises the ferromagnetic coupling. In each case, the upper panel displays the excitations as obtained by the MPS-based kernel polynomial method, and the lower panel corresponds to the same calculation done with exact diagonalisation. For our purposes,

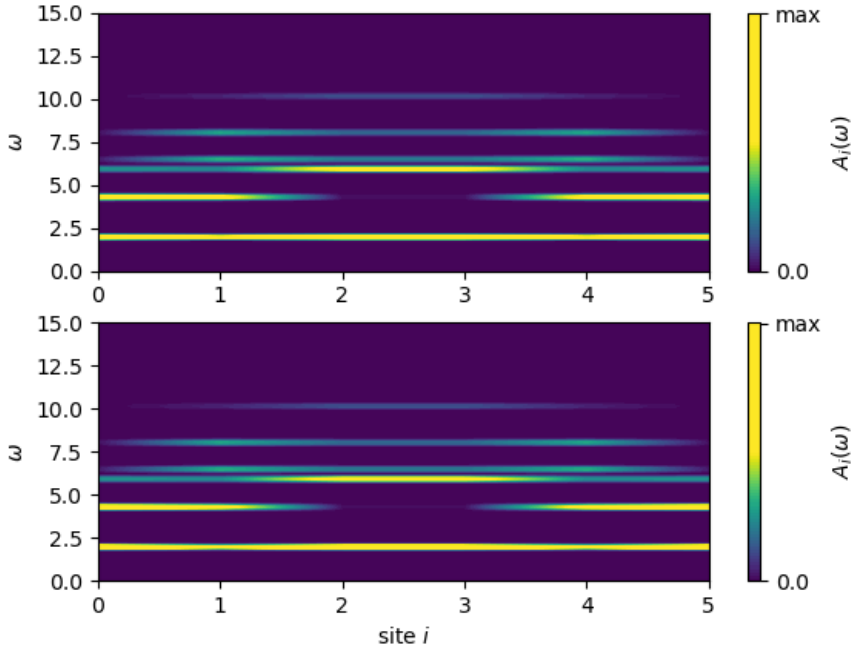

Figure 45: Dynamical correlator for the antiferromagnetic Heisenberg model with six sites and a bond dimension of 20. Upper panel: results obtained through exact diagonalisation. Lower panel: results obtained through DMRG/MPS methods.

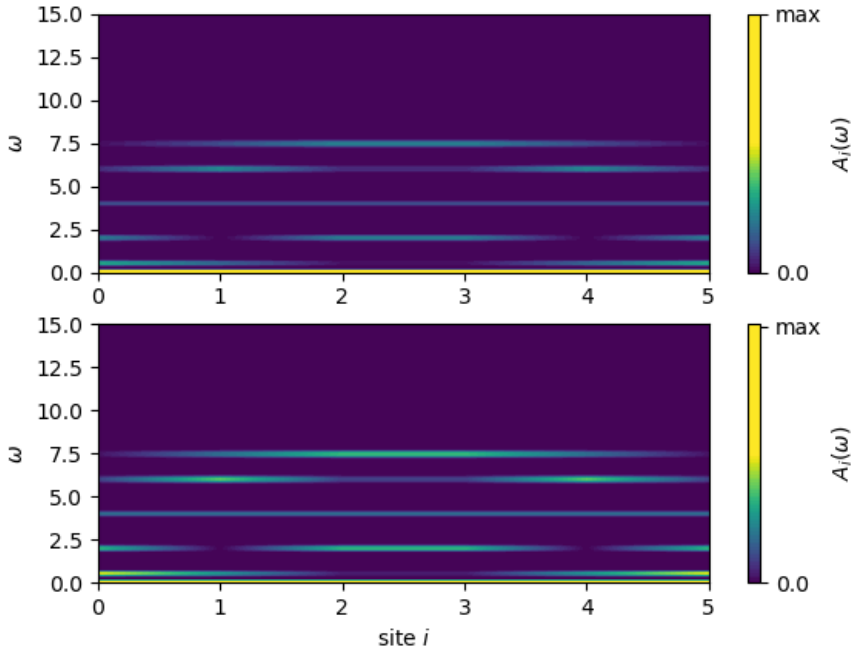

Figure 46: Dynamical correlator for the ferromagnetic Heisenberg model with six sites and a bond dimension of 20. Upper panel: results obtained through exact diagonalisation. Lower panel: results obtained through DMRG/MPS methods.

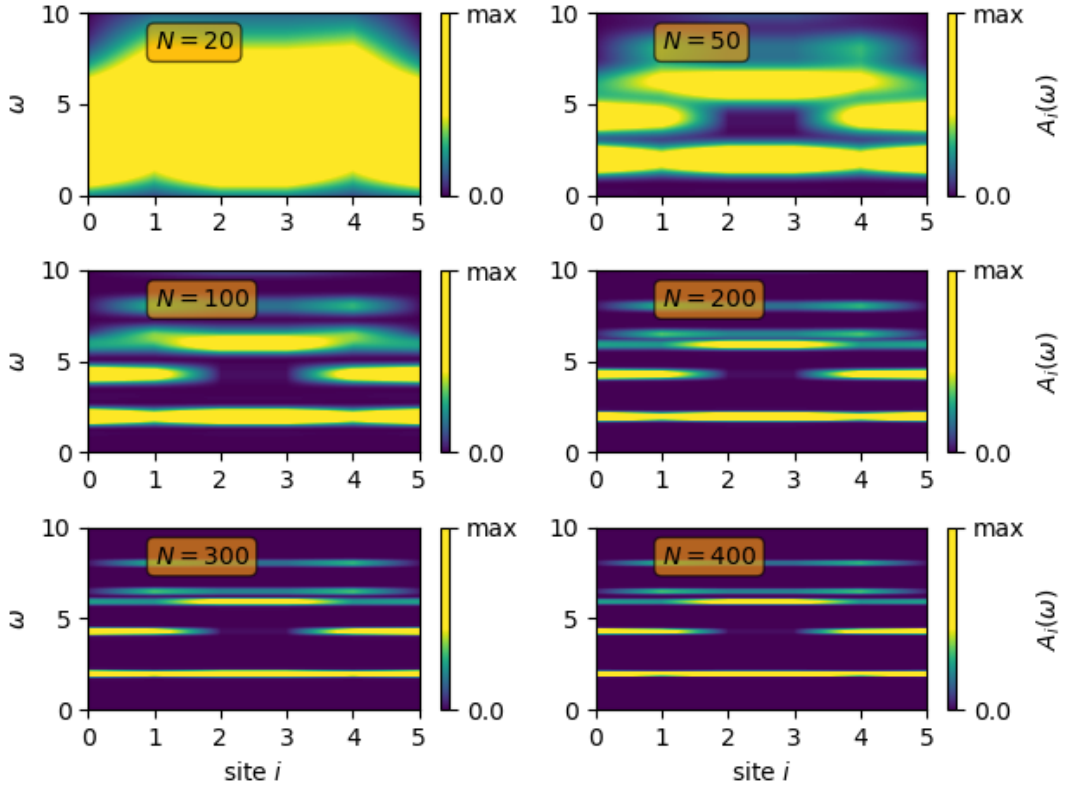

Figure 47: Dynamical correlator for the antiferromagnetic Heisenberg model with six sites, evaluated for different numbers of Chebyshev polynomials kept in the Chebyshev expansion. From left to right, upper, to lower: spectral function evaluated with 20, 50, 100, 200, 300 and 400 terms.

the results obtained through the two methods can be considered as equal.

The resolution - or the quality of approximation - of the results obtained with a Chebyshev expansion depends on the number of Chebyshev polynomials kept in the expansion. To illustrate how the results change qualitatively, we have re-calculated the dynamical correlator for the antiferromagnetic Heisenberg model with 20, 50, 100, 200, 300 and 400 terms, respectively. Those results are shown in fig. 47. Following the progression of an increasing number of Chebyshev polynomials, it is clear that for less than 100 terms (for 6 system sites), one cannot speak of a representative result. It is only for 200 or more terms in the expansion that we can discern a clear (and converged) pattern. We therefore propose as a rule of thumb that the number of Chebyshev polynomials to keep in a truncated series should - at least - be of the order of roughly 40 times the system size.

We note that in few cases, the values found for the spectral function were slightly below zero, despite the former being non-negative by construction. Recalling that convergence to the true ground state in the antiferromagnetic Heisenberg model was very sensitive to a large enough bond dimension, we have re-calculated the real space spectral function with different bond dimensions and studied how the ratio $|\min A_i(\omega)/\max A_i(\omega)|$ varies.

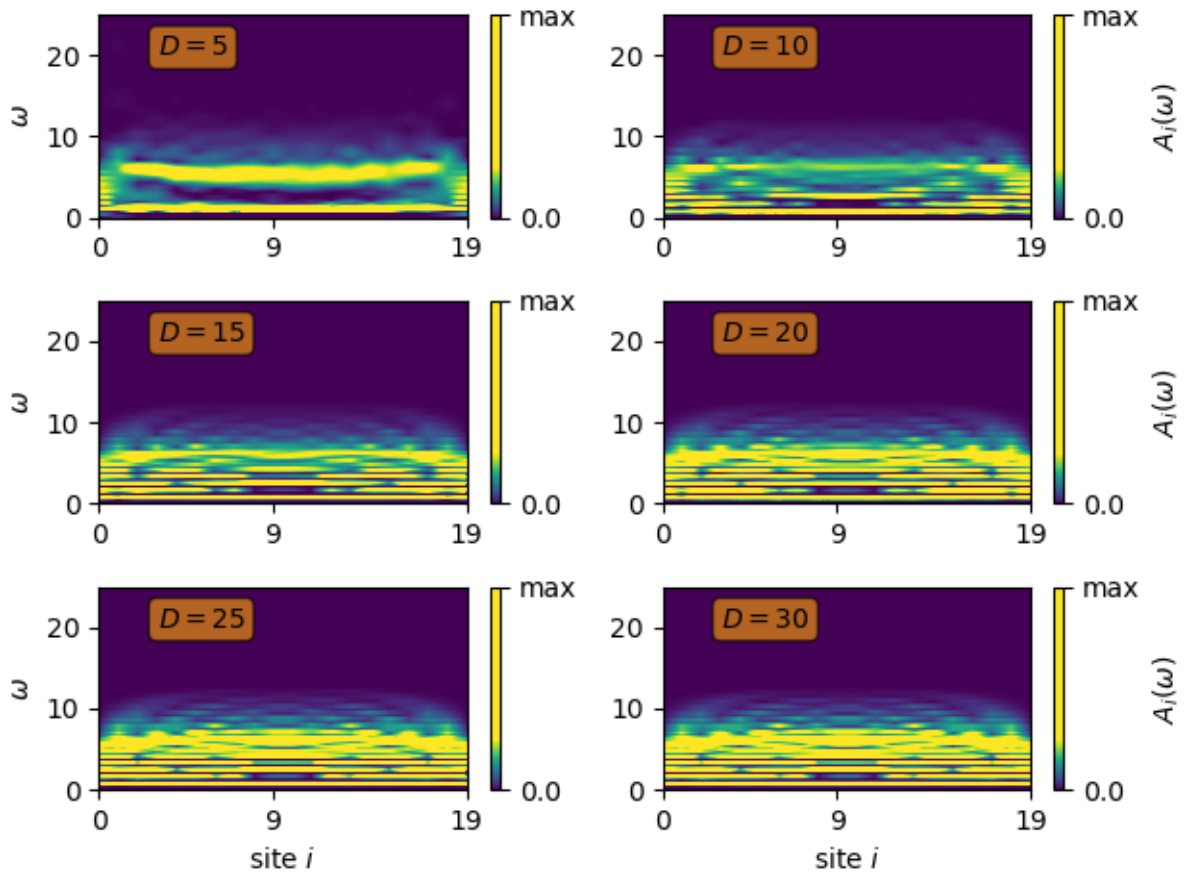

Figure 48: Real space spectral function for the antiferromagnetic Heisenberg model, evaluated with a local magnetic field h of different strengths on the rightmost system site.

In order to be able to compare this estimate better with the results presented in the next section, we employ the same system size of 20 sites as the antiferromagnetic half-chain of the interface model discussed below. In agreement with our just established rule of thumb, we therefore keep 800 terms in the series expansion. Tab. 1 and fig. 48 summarise our findings, and confirm that increasing the bond dimension leads to a reduced error in the spectral function. This suggests that the few negative values found are not an artefact of our implementation of the kernel polynomial method, but due to non-negligible weights of excited states in the approximated ground state, which a too small bond dimension cannot sufficiently suppress. Fig. 48 confirms however that a suitable convergence of the spectral function, permitting us to localise the spinon excitations in real space, is reached for bond dimensions of roughly 20 or higher. We will therefore continue to employ this bond dimension in the remainder of this work.

Lastly, we have observed divergence issues in the calculation of the Chebyshev moments for "too small" safeguards ϵ in the rescaling of the Hamiltonian bandwidth into the interval $[-1+\epsilon, 1-\epsilon]$. While in the literature (cf. ref. [27]) a value of 0.025 has been proposed (and successfully used), in our work it was necessary to increase this safe-

guard to $\epsilon = 0.25$ in order to ensure convergence. It remains to investigate why this was the case.

D	5	10	15	20	25	30
$\lvert\frac{\min A_i(\omega)}{\max A_i(\omega)}\rvert$	0.35739	0.15595	0.11410	0.08504	0.03383	0.01355

Table 1: Ratio of the smallest algebraic value of the real-space spectral function to the largest value, as a function of the bond dimension. The error becomes smaller with increasing bond dimension.

8.4 Conclusion

Globally, and most importantly, we can conclude that the algorithms employed in this thesis work as intended. The agreement between the results due to exact diagonalisation and MPS methods is excellent for all the representative systems studied in this chapter, and often at the level of machine precision. Furthermore, using a higher number of system sites of the order of $100 - 200$ enables us to reproduce known analytical results in the thermodynamic limit with a sub-per cent error. For smaller system sizes, the presence of finite-size effects has to be taken into account.

The DMRG algorithms show a good convergence behaviour for both one- and two-site schemes, with negligible differences between the two for the cases studied. We will therefore employ the computationally cheaper one-site algorithm. While convergence to the ground state energy depends relatively little on the chosen bond dimension, the convergence to the "true" ground state does. Contributions from other states appear to be sufficiently suppressed for bond dimensions of 20 or higher (benchmarking on a model with 40 sites). This value however strongly depends on the system being at (or close to) criticality, as confirmed by the study of the critical Ising model. As expected, in those cases we need to increase the bond dimension to a value of about 30 (or higher) in order to accurately capture those ground states. However, as we are mainly interested in non-critical systems for the remainder of this work, this won't be a major concern to us. Suffice it to say that for high-precision results at criticality, one either has to increase the bond dimension sufficiently in order to capture the full scaling of the entanglement entropy, or use different tensor network methods to begin with. The multiscale entanglement renormalisation ansatz (MERA) (cf. ref. [69]) is especially suited for this task.

The most important finite-size effects appeared in the calculation of the bipartite entanglement entropy. While we did find the characteristic logarithmic scaling at criticality, even as much as 200 sites were not sufficient to reproduce the exact scaling law expected in the thermodynamic limit. In contrast, studying a small, but periodic system *did*

Parameter	Description	Value employed
N	System size.	$16 - 200$
N_{Cheby}	Number of terms to keep in Chebyshev expansion.	$40N - 50N$
N_{sweeps}	Number of DMRG sweeps.	up to 10
D	Bond dimension.	$20 - 30$
ϵ	Safeguard for rescaling of Hamiltonian.	0.25

Table 2: Overview over the parameters used in the present work, which were found to lead to satisfying results.

model the expected behaviour very well. We therefore conclude that the scaling of the entanglement entropy crucially depends on working with either very large or periodic systems.

Finally, we have tested the kernel polynomial method by comparing the Chebyshev moments calculated with MPS methods and with exact diagonalisation. Again, we have found an excellent agreement between the two. The resolution of the spectral function calculated through the kernel polynomial method depends on the number of terms kept in the series expansion, which itself depends on the system size. We have obtained a good resolution by truncating the series after $40N$ to $50N$ terms, for a system of size N. Resolutions lower than this significantly alter the quality of the results in frequency space, and in extreme cases may not even have converged to at least an approximation of the desired result. A slight numerical error of the spectral function has been observed, but shown to be due to the bond dimension being too small for high-precision results. This however doesn't affect the quality of our results, showing the real-space localisation of the elementary excitations. Choosing the safeguard ϵ large enough furthermore ensures the suppression of possible divergencies in the Chebyshev expansion, which might arise if one is working too close to the boundaries of the interval $[-1, 1]$.

Our findings - the parameter values of interest for the present computation - are summarised in table 2.

9 Interface of FM and AFM Heisenberg Spin Chains

As an application of our MPS algorithms beyond simple benchmark results, we will now commence our analysis of a heterostructure of a ferromagnetic and an antiferromagnetic Heisenberg spin-$\frac{1}{2}$ chain with open boundary conditions. Both halves of the chain are built from a standard isotropic Heisenberg nearest-neighbour interaction, with an additional coupling parameter J_{int} to model the interface between the chains:

$$H = \underbrace{J_{\text{AFM}} \sum_{i=1}^{N/2} \vec{S}_i \cdot \vec{S}_{i+1}}_{\text{antiferromagnetic}} \underbrace{- |J_{\text{FM}}| \sum_{i=N/2+1}^{N} \vec{S}_i \cdot \vec{S}_{i+1}}_{\text{ferromagnetic}} + \underbrace{J_{\text{int}}\, \vec{S}_{N/2} \cdot \vec{S}_{N/2+1}}_{\text{interface}} \underbrace{- h \sum_{i=1}^{N} S_i^z}_{\text{tranverse field}} . \tag{9.1}$$

If desired, one can apply an isotropic transverse field of strength h to the model, as implemented in the final term of the expression.

The left part of the chain is considered to be the antiferromagnetic part, exhibiting $S = 1/2$ spinon excitations, whereas the right part will be taken to be the ferromagnet with $S = 1$ magnon excitations. Both chains interact via an interface, whose coupling strength may vary from the rest of the spin couplings, which are taken to be equal in magnitude (and conventionally set to unity).

In the context of this thesis, we will mainly be interested in the ground state of the joint system and its properties, as well as the elementary excitations above the ground state. It will be particularly interesting to see how those depend on the coupling strength of the two chains, and to what extend they resemble the elementary excitations of the disjoint Heisenberg chains.

9.1 Setup of the Computation

Before we present the results of our computation, we will give some important information about the implementation. In particular, we will present the MPO representation and several aspects concerning the setup.

9.1.1 MPO Representation

Recalling the MPO representation of the antiferromagnetic Heisenberg Hamiltonian

$$H = \sum_{i=1}^{N} \vec{S}_i \cdot \vec{S}_{i+1} - h \sum_{i=1}^{N} S_i^z = J \sum_{i=1}^{N} \left[\frac{1}{2} \left(S_i^+ S_{i+1}^- + S_i^- S_{i+1}^+ \right) + S_i^z S_{i+1}^z \right] - h \sum_{i=1}^{N} S_i^z \tag{9.2}$$

through the operators

$$W(J) = \begin{bmatrix} I & 0 & 0 & 0 & 0 \\ S^+ & 0 & 0 & 0 & 0 \\ S^- & 0 & 0 & 0 & 0 \\ S^z & 0 & 0 & 0 & 0 \\ -hS^z & \frac{J}{2}S^- & \frac{J}{2}S^+ & J^zS^z & I \end{bmatrix} \tag{9.3}$$

and the boundary vectors

$$W_L(J) = \begin{bmatrix} -hS^z & \frac{J}{2}S^- & \frac{J}{2}S^+ & J^zS^z & I \end{bmatrix}, \quad W_R(J) = \begin{bmatrix} I \\ S^+ \\ S^- \\ S^z \\ -hS^z \end{bmatrix}, \tag{9.4}$$

it is straightforward to write down an MPO representation of our model. Let the left part of the chain be antiferromagnetic and the right part ferromagnetic, then we obtain the corresponding Hamiltonian as the MPO

$$H = \underbrace{W_L(J)^{[1]}\, W(J)^{[2]} \ldots W(J)^{[N/2-2]}}_{\text{antiferromagnetic}} \overbrace{W(J_{\text{int}})^{[N/2-1]}}^{\text{interface}} \underbrace{W(-J)^{[N/2]} \ldots W(-J)^{[N-1]}\, W_R(-J)^{[N]}}_{\text{ferromagnetic}}. \tag{9.5}$$

Note here the placement of the interface term with the coupling J_{int} as the last term of the antiferromagnetic chain. This is due to the fact that the coupling J_{int} appears in the bottom line of the matrix W, and will therefore be shifted "one place to the right" in the tensor product strings upon matrix multiplication. Verifying this by explicit multiplication is straightforward.

9.1.2 Overview of the Computation

Based on the results gathered in the preceding benchmark calculations, we have chosen to set up our computation as follows: we will start by analysing the ground state energy and the convergence to the true ground state. For the latter, we investigate different bond dimensions in the range between 10 and 50, to find one that yields acceptable accuracy for the lowest computational overhead. Afterwards we will study the ground state energy. To analyse finite-size effects, we will determine the ground state energy for systems up to 200 sites, such that we can interpolate to the ground state energy in the thermodynamic limit. Analysing different coupling strengths, primarily in the interval $[0.0, 5.0]$, will reveal to us a possible dependence of the ground state energy on the interface between the systems.

Parameter	Description	Value Employed, Remarks
N	System size to study finite size effects.	10 - 200
N_{fin}	Smaller system size to calculate entanglement entropy, structure of the ground state and energy excitations.	40, with 20 sites describing the antiferromagnetic model on the left and 20 sites describing the ferromagnetic model on the right.
N_{Cheby}	Number of terms to keep in Chebyshev expansion.	1600 - 2000 for 40 sites
ΔH	Desired maximal variance of Hamiltonian in the ground state.	10^{-6} or less
N_{sweeps}	Number of DMRG sweeps.	Depending on ΔH, roughly 10.
D	Bond dimension.	Depending on ΔH, roughly 20 - 30.
ϵ	Safeguard for rescaling of Hamiltonian.	0.25
h	Transverse magnetic field in z-direction.	$0.0, 0.1 ... 5.0$ (weak field desired for symmetry breaking).
J_{int}	Coupling strength between the antiferromagnetic and the ferromagnetic Heisenberg models.	$0.1 ... 5.0$

Table 3: Overview of the parameters and settings used to obtain the results in this work.

Next, we will analyse the structure of the ground state in more detail. Our main tool will be the bipartite entanglement entropy, which can easily be calculated from the output of the DMRG algorithm. Here, we will work with a smaller system of 40 sites in order to create more data points in the corresponding parameter space. We will be especially interested in studying how the entanglement entropy varies upon crossing the boundary, and what impact the coupling strength has on the entanglement between the two subsystems. To complete the study of the ground state, we will attempt to visualise the ground state structure by calculating the on-site magnetisation in z-direction. For all of those calculations, we will employ different values of the transverse magnetic field, however in order to break the spin symmetry inherent to the Heisenberg model we will employ a transverse field of at least $h = 0.1$.

Finally, we will study the excitations of the coupled systems by calculating the real space spectral function with the kernel polynomial method. For this, it will be instructive to start with the spectral function of a weakly coupled system and see how tuning the coupling strength leads to new effects.

A summary of the parameters and settings employed for this study is provided in table

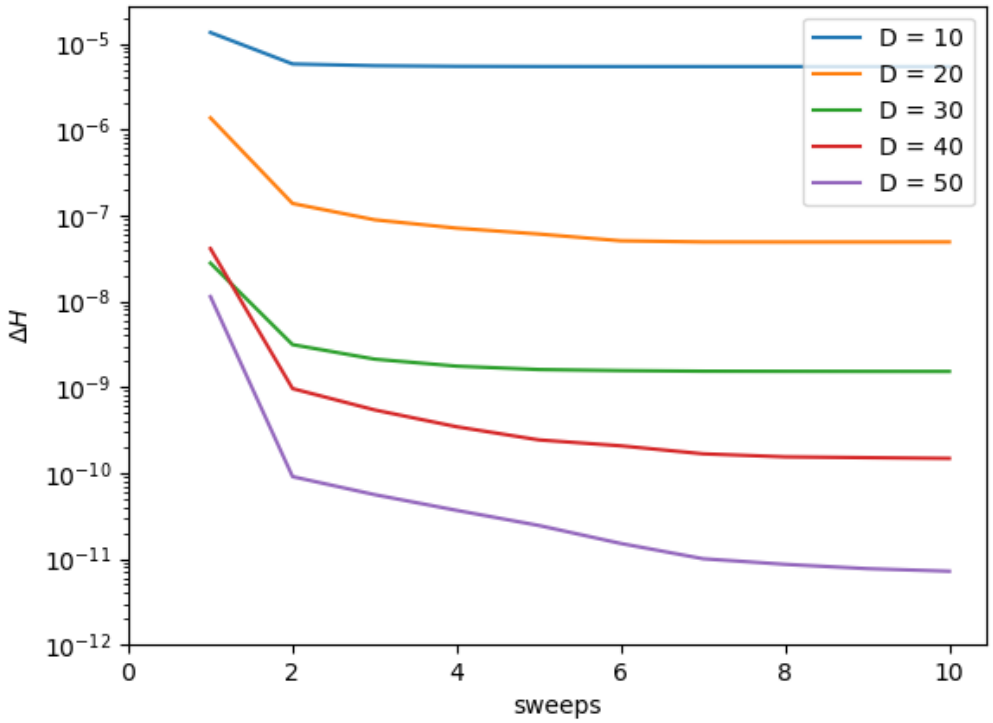

Figure 49: Variance of the Hamiltonian ΔH when calculating the ground state energy of the coupled Heisenberg model (with 40 sites), as a function of the number of sweeps. A comparison for different bond dimensions is shown.

3.

9.2 Results

In the following we present the results we have obtained by studying the interface of an antiferromagnetic and a ferromagnetic Heisenberg model. Our first focus will be to determine the ground state, the ground state energy and the entanglement entropy in the ground state. Afterwards, we will study the elementary excitations above the ground state by computing the spectral function in position space.

9.2.1 Ground State Energy and Convergence Properties

Before we calculate the ground state energy of the coupled Heisenberg chain, we analyse the variance of the Hamiltonian during the ground state search for various different values of the bond dimension, to ensure that we choose a bond dimension capable of approximating the true ground state for the following calculations. Fig. 49 shows, similarly to the previous chapter, how the variance of the Hamiltonian depends on the number of DMRG sweeps. Several facts strike our attention, in comparison to the similar analysis

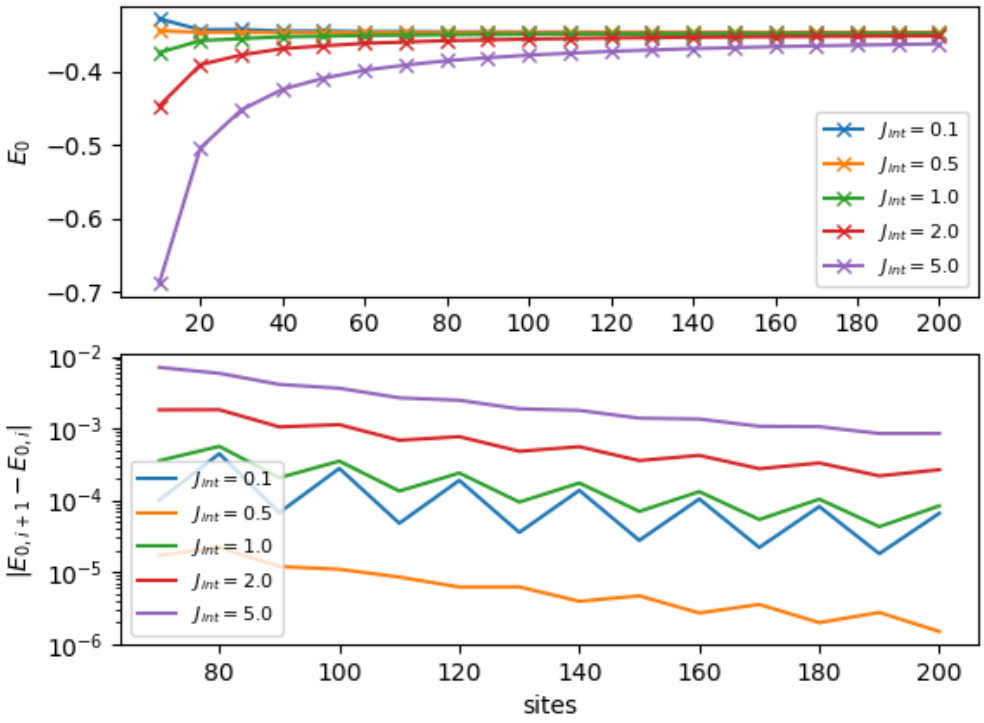

Figure 50: Ground state energy per site for the coupled Heisenberg model found by DMRG, as a function of the system size. Different coupling strengths are compared. Lower panel: difference between subsequent values for the ground state energy, starting at site 70.

in fig. 43: despite the fact that the coupled Heisenberg chain contains the antiferromagnetic chain, the variance here is lower than in the previous case for a comparable bond dimension. Looking e.g. at ΔH for a bond dimension of 20, we now obtain a variance of the order of 10^{-7}, whereas for the antiferromagnetic Heisenberg model we could only achieve a variance of 10^{-6}. Moreover, the convergence of the DMRG sweeps is slowed down in comparison to the uncoupled spin chains. While before a good convergence could be reached in as few as two or three sweeps, we now have to go as high as six to nine sweeps, depending on the bond dimension, to reach a roughly steady state. This behaviour is more pronounced for the larger bond dimensions, as can be expected due to their higher number of parameters to be optimised. All in all, for most of what follows we will work with a bond dimension of 20, as this strikes a good balance between accuracy and performance. Finally, we remark that the "crossing" in the first sweep between the variances ΔH for bond dimensions of 30 and 40 is likely due to the random initial conditions.

Building on the above findings, we now proceed to calculate the ground state energy. To obtain an estimate of the ground state energy of the system in the thermodynamic limit, we perform DMRG on systems with sizes between 10 and 200 sites. The results

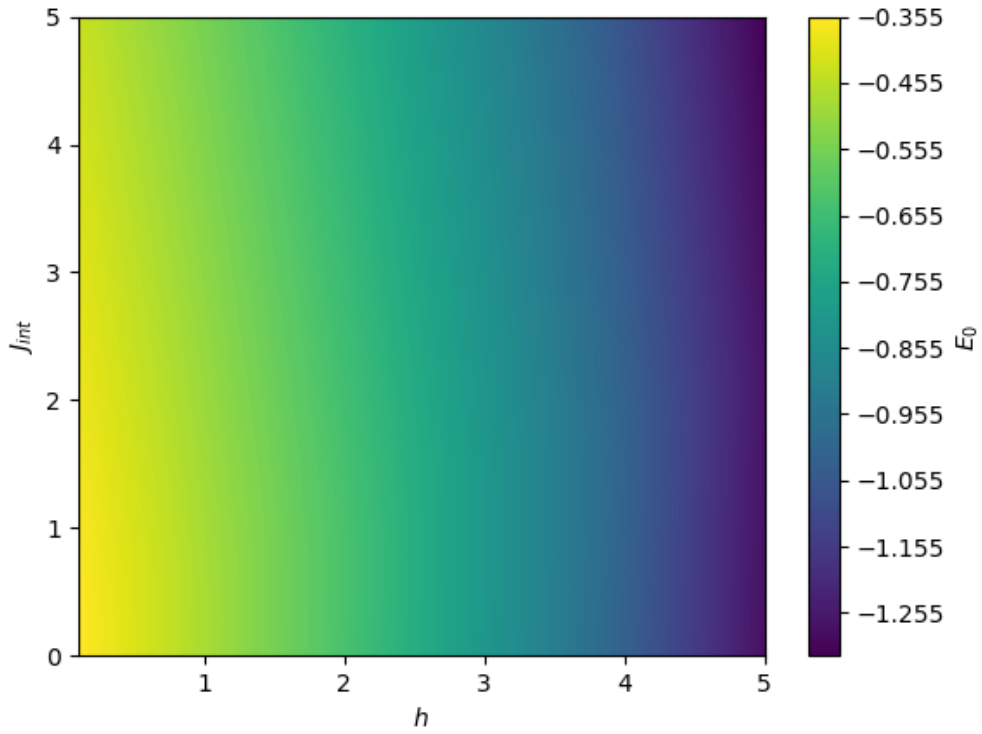

Figure 51: Ground state energy per site for the coupled Heisenberg model, shown as a function of the h-J_{int} parameter space. Results are obtained with DMRG for 40 sites.

are shown in fig. 50, where we have plotted the convergence of the ground state energy for the values $\{0.1, 0.5, 1.0, 2.0, 5.0\}$ of the couplings between the two half-chains. In the lower panel of fig. 50, we have calculated the difference between two subsequent values of the ground state energy, starting at 70 sites in order for the results not to be disturbed by the initial "divergencies". Firstly, we can observe that the ground state energy depends only very weakly on the value of the coupling J_{int}. Secondly, we can assert that, in general, higher values of the coupling strength lead to a slower convergence. Nevertheless, we observe a mostly "Cauchy sequence"-like behaviour, indicating that we are indeed approximating a convergence to the true ground state energy in the thermodynamic limit. The values for the ground state energy, calculated with 200 sites, are summarised below in table 4.

To study the dependence of the ground state energy on the external magnetic field, we have re-calculated the ground state energy in the whole relevant h-J_{int}-parameter space, for a system with 40 sites. The result in shown in fig. 51. This confirms our previous finding with the ground state energy scaling only very weakly with the coupling strength. In contrast, we do observe the Heisenberg-Ising-like dependency of the ground state energy on the external transverse field, with stronger fields leading to a lower ground state energy.

J_{int}	Ground State Energy E_0
0.1	-0.34613
0.5	-0.34653
1.0	-0.34771
2.0	-0.35091
5.0	-0.36178

Table 4: Summary of the ground state energy E_0 per site, calculated for 200 sites in the system.

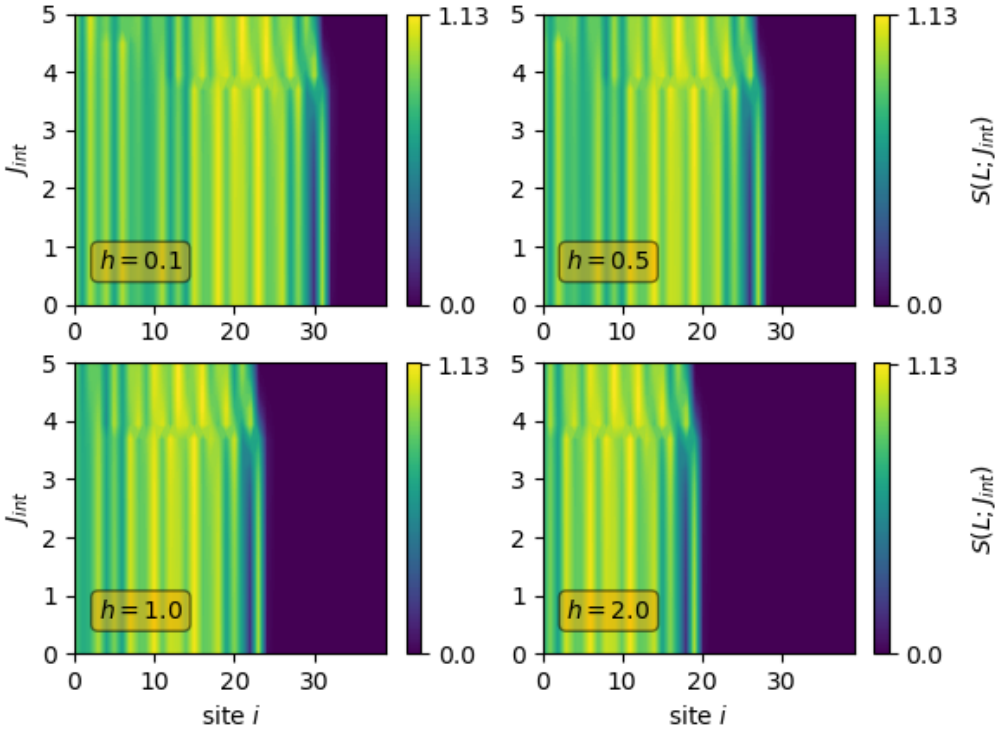

Figure 52: Bipartite entanglement entropy evaluated at each site of the coupled Heisenberg model. Shown is a comparison between different transverse magnetic fields and coupling strengths.

9.2.2 Entanglement Entropy in the Ground State

Having found the ground state energy as a function of the coupling strength J_{int} and the magnetic field h, it will be instructive to analyse the structure of the ground state further. For this, we will calculate the bipartite entanglement entropy between a left and a right subsystem of the ground state, as a function of the chosen subsystem length. Furthermore, we will vary the coupling strength J_{int} between 0.0 and 5.0 and calculate the results for several different values of the magnetic field h.

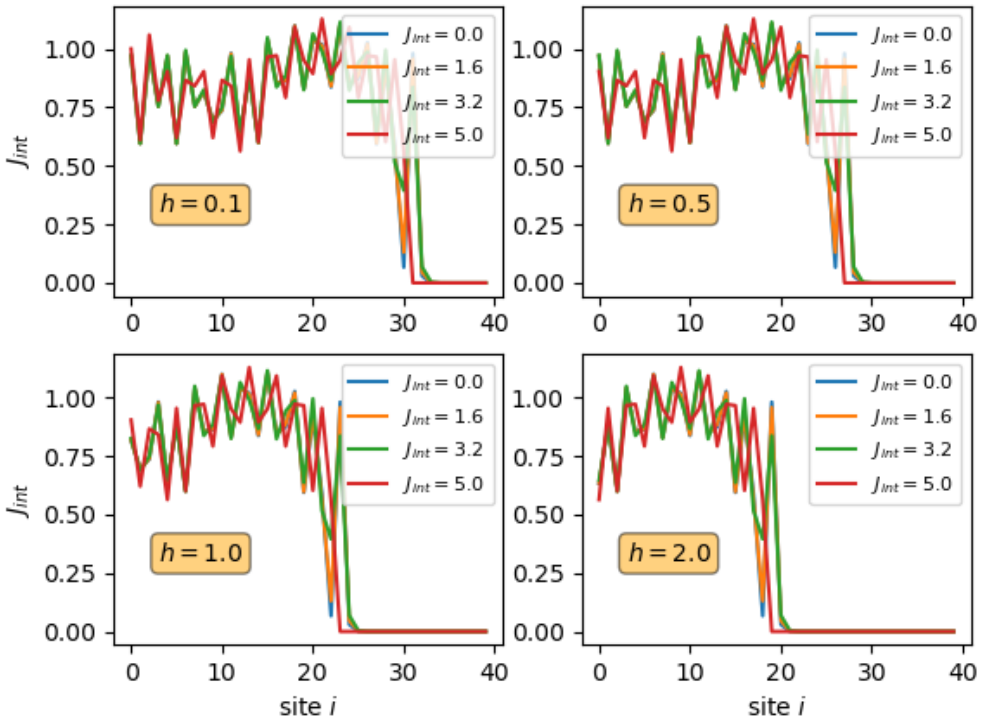

Figure 53: Bipartite entanglement entropy evaluated at each site of the coupled Heisenberg model. Shown is a comparison between different transverse magnetic fields and coupling strengths.

Fig. 52 shows the bipartite entanglement entropy computed for each given site - therefore each division into a left and right subsystem with respect to that site - as a function of the coupling strength. Furthermore, we have performed the calculation for four different values of the transverse field, with $h \in \{0.1, 0.5, 1.0, 2.0\}$. Similar to what we found when analysing the ground state energy in the whole parameter space, the entanglement entropy varies mainly due to the strength of the external magnetic field. In all four cases displayed in fig. 52, we can discern a clear separation into a left region, dominated by the antiferromagnetic interactions, and a right region, dominated by the ferromagnetic interactions. In the left part, the entanglement entropy fluctuates weakly around the value $S(L) = 1$, whereas in the right part there is a sudden drop to zero. Just before the boundary (coming from left), there is a "valley" of low entanglement entropy, which is separated from the ferromagnetic region by a final "hill". This reveals to us that the ground state of the coupled Heisenberg model tends to keep its structure, with an antiferromagnetic ground state on the left and a ferromagnetic ground state on the right (which is a product state, and therefore has an entanglement entropy of zero). Crucially, for a weak magnetic field the entanglement entropy of the antiferromagnetic model reaches further into the ferromagnetic region than one might have expected, with

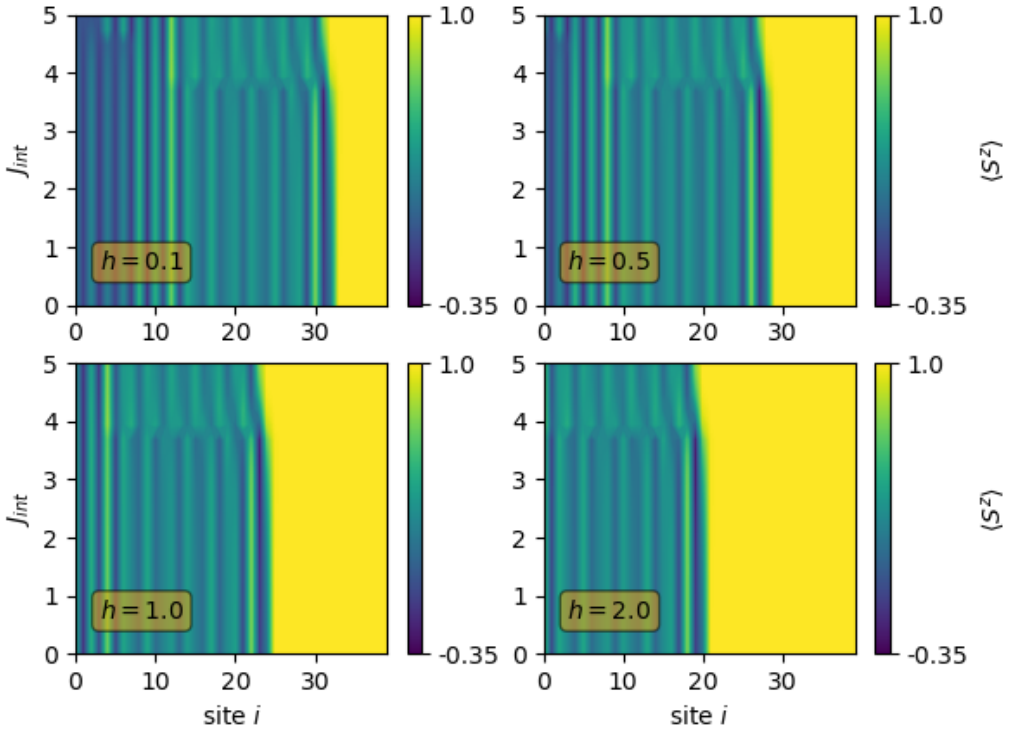

Figure 54: Magnetisation in z-direction per site of the ground state of the coupled Heisenberg model. Shown is a comparison between different transverse magnetic fields and coupling strengths.

the "entanglement boundary" being located around site 30. Only upon increasing the transverse field do we shift the entanglement boundary back to the middle of the system at site 20, where the physical interface is located.

To investigate the dependence of the entanglement entropy on the interaction strength more precisely, we show the entanglement entropy for several selected coupling strengths and the same external magnetic fields in fig. 53. This illustrates again that the dependence of the entanglement entropy on the exact value of the coupling strength is rather weak. For the smaller magnetic fields considered, the highest (relative) values of the entanglement entropy are reached on the sites just before the "entanglement boundary". An exception to this is the lower right subplot with the highest magnetic field (which therefore "forces" the entanglement entropy to match the structure given by the physical left-right separation of the model). There, the maximum is reached in the middle of the antiferromagnetic left part.

The structure of the entanglement entropy in the ground state is mimicked by the on-site magnetisation in z-direction, $\langle S_i^z \rangle$, for each site i, which we have calculated in fig. 54. It shows the same clear separation between a fully magnetised area on the right,

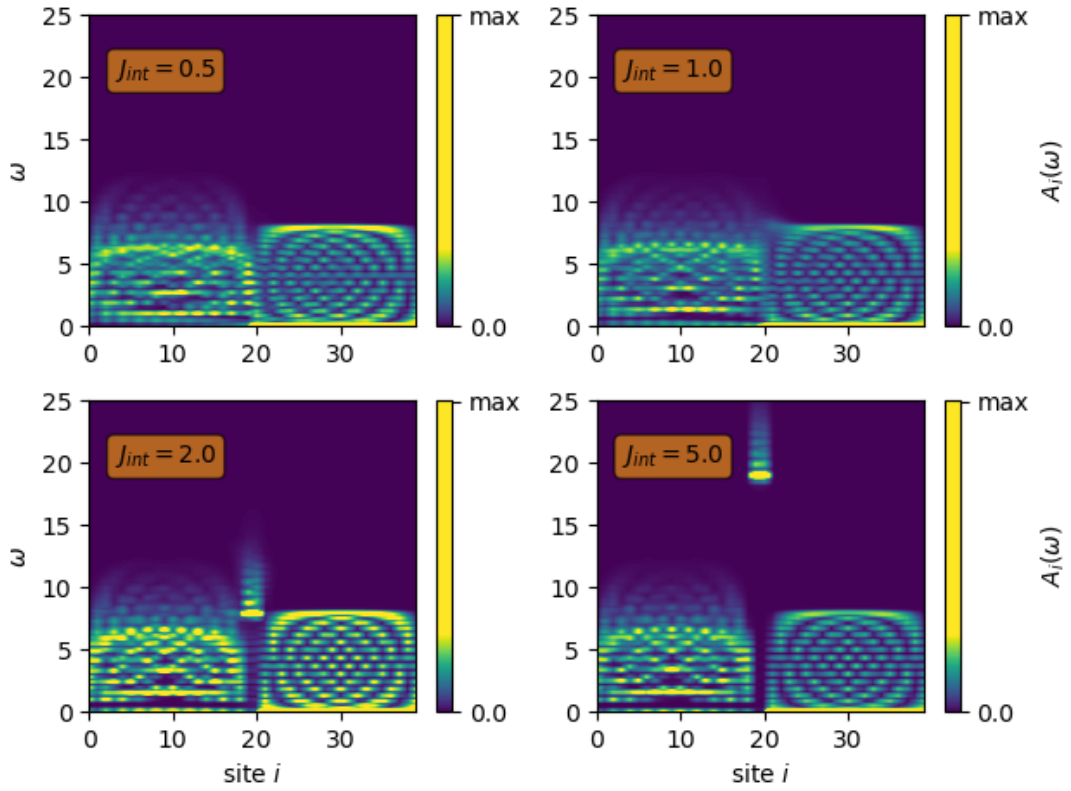

Figure 55: Real space spectral function for the coupled Heisenberg model, evaluated for no transverse magnetic field and different values of the coupling.

corresponding to the ferromagnetic ground state, and an area with the magnetisation fluctuating around 0, as we would expect for the antiferromagnetic ground state.

9.2.3 Real-Space Spectral Function

Finally, we calculate the real-space spectral function of the system to see how the energy excitations are distributed with respect to the boundary in the system. As in the previous cases, we will study several different values for the coupling strength at the interface, for two different values of the transverse field.

Fig. 55 shows the result for no transverse field. The different nature of the two coupled spin chains is clearly visible. Increasing the coupling strength between the two systems affects the real space excitations for both half-chains relatively feebly; however a small energy gap seems to open in the antiferromagnetic half for increasing couplings. Furthermore, a boundary mode emerges at the physical interface, with an eigenenergy proportional to the coupling strength.

When the transverse magnetic field is turned on, we obtain fig. 56 for $h = 1.0$. Clearly, no magnon excitations can occur in the ferromagnetic half of the system, as all the spins

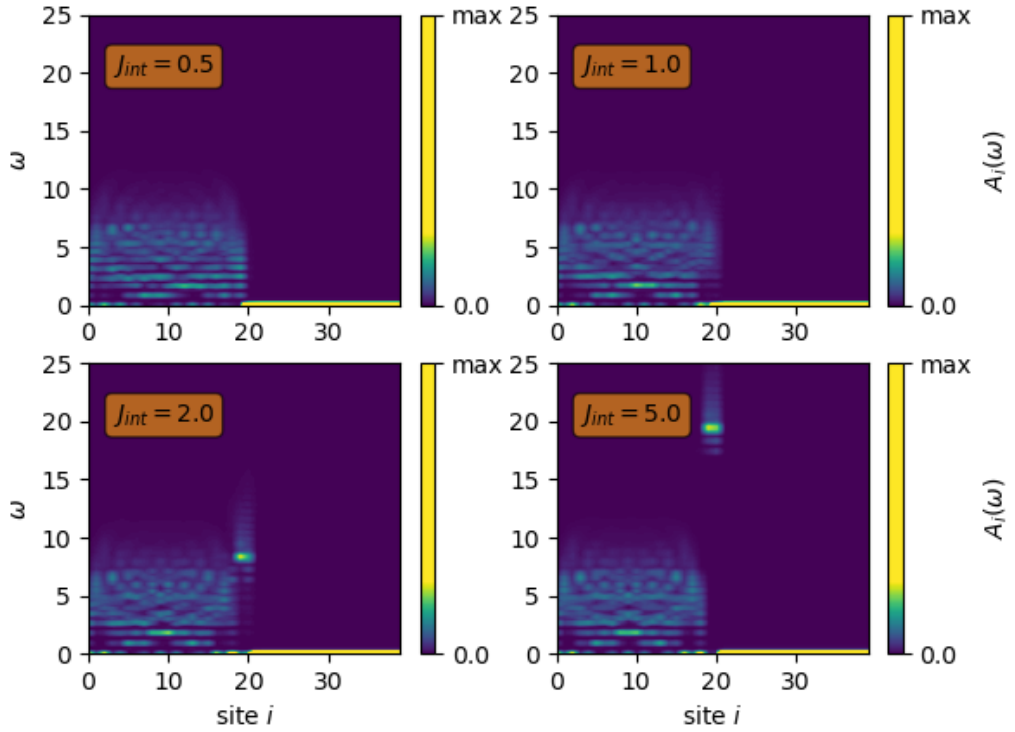

Figure 56: Real space spectral function for the coupled Heisenberg model, evaluated for a transverse magnetic field with $h = 1.0$ and different values of the coupling.

have aligned with the transverse field. In the antiferromagnetic subsystem, elementary eigenstates do exist, but with a much smaller weight than in the case with no transverse field. One does however find the same boundary mode at the physical interface, as in the case of no transverse field.

To probe the above-described boundary effects more precisely, we can compare them to the antiferromagnetic half chain with a localised Zeeman field on the rightmost system site, as shown in fig. 57. In order to recreate the left half of the coupled system as precisely as possible, we have employed a system with 20 sites, and correspondingly truncate the Chebyshev series after 800 terms in the expansion. As field strengths, we employ the same values as for the coupling constant of the two chains. It is striking that the localised field perturbs the symmetry of the excitations in real space much more distinctly than the different couplings before. While an edge mode analogous to the previously found boundary mode emerges, it is considerably weaker in comparison. This suggests that the boundary mode investigated above is an effect genuinely due to the coupling of the two spin chains.

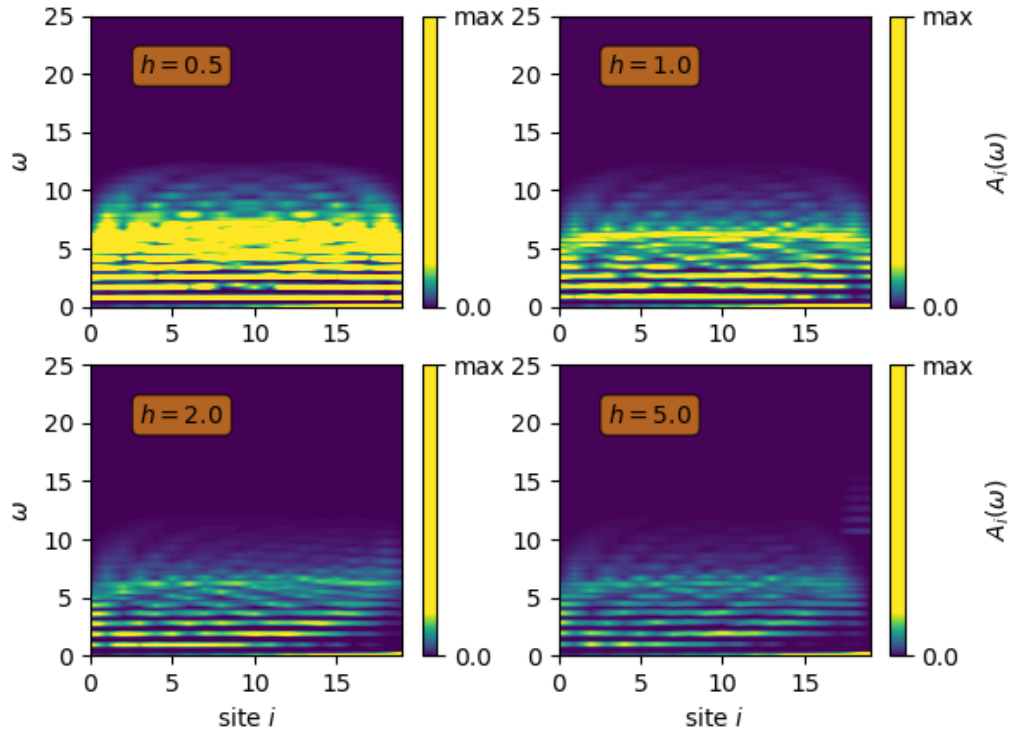

Figure 57: Real space spectral function for the antiferromagnetic Heisenberg model, evaluated with a local magnetic field h of different strengths on the rightmost system site.

Part IV

Outlook and Conclusion

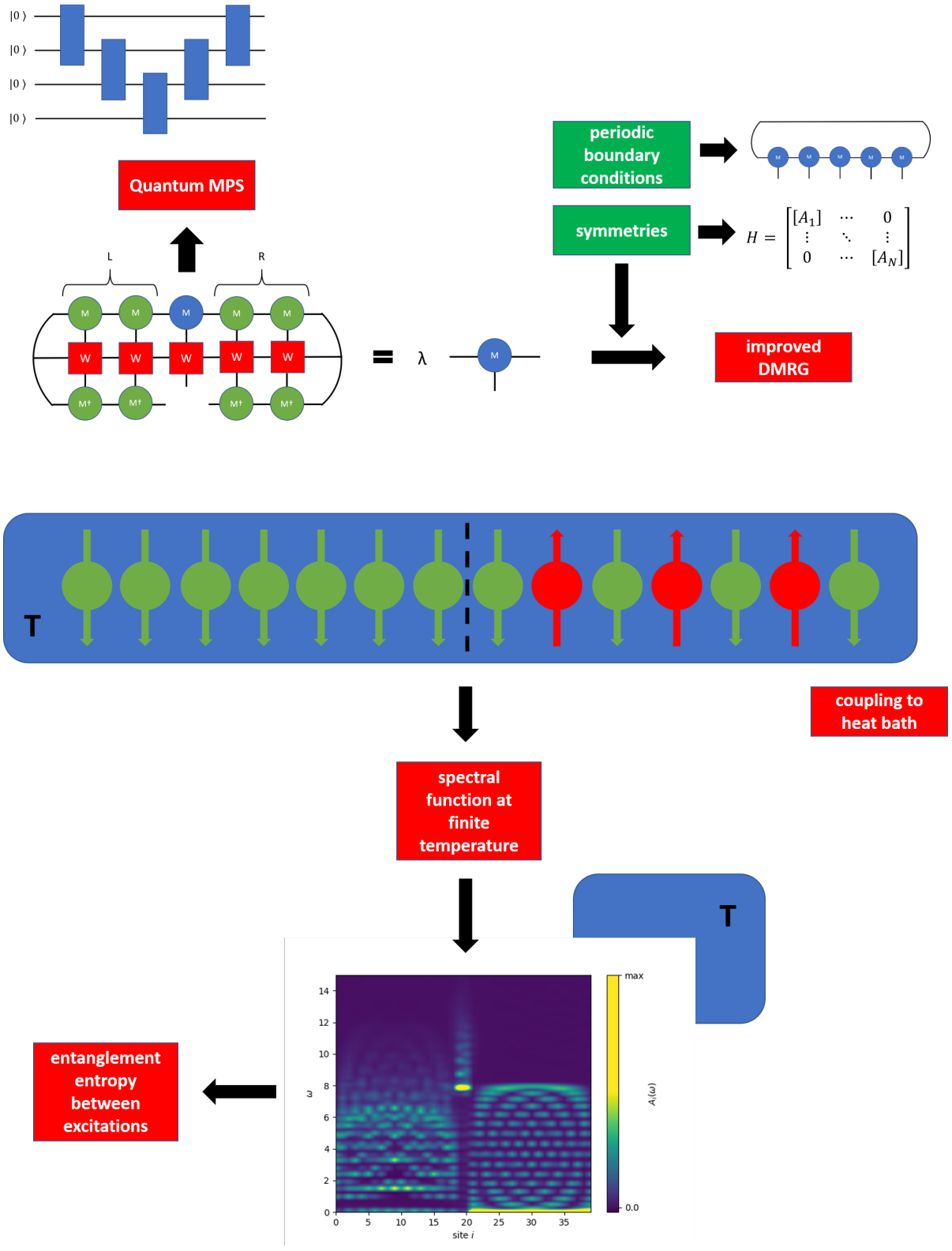

10 Outlook

We will commence this final part by discussing possible extensions of the work done in this thesis. There are two main areas we will focus on: first, we discuss how we could improve the numerical methods employed to obtain our results. Hereafter - and more importantly - we will present variations of the model investigated, and further physics aspects one could study. In particular, we derive in some detail the calculation of the finite-temperature spectral function with the kernel polynomial method, which provides an important generalisation of the zero-temperature spectral function considered until now. Furthermore, we would like to motivate more involved studies of the entanglement between the two half-chains, especially focusing on different measures of entanglement and the entanglement between elementary excitations. Lastly, we mention a possible connection to quantum computation.

10.1 Computational and Algorithmic Improvements

The first and most obvious improvement to get more (and more precise) results, would naturally be to employ more computational resources. For the present project, our intention was to write an MPS software package that is able to perform the calculation on a home PC, without any access to high-performance computers. While we had to accept certain boundaries in terms of system sizes, precision etc., we have nevertheless attempted to provide results which allow objective conclusions about the system studied. One could therefore easily improve the existing results by studying a coupled system with a greater number of sites, such as 100, say. Correspondingly, it would be desirable to increase the bond dimension to at least 30 or more, as we have here chosen the smallest acceptable bond dimension in terms of the variance of the Hamiltonian in the ground state. Naturally, one then also needs to increase the number of Chebyshev moments that are needed to calculate the spectral function, in order to keep the same resolution. With our prescription for the number of Chebyshev moments yielding a good resolution, one would thus need to calculate (at least) 4000-5000 moments per site. However, reaching an even higher number of Chebyshev moments would of course be desirable.

Apart from working with more powerful computational resources, there are also several possible improvements of algorithmic aspects, of which we name but a few.

10.1.1 Exploiting Symmetries and Periodic Boundary Conditions in DMRG

Firstly, it would be desirable to adapt the DMRG code used for this thesis in order to exploit symmetries in the Hamiltonian. Recall that a symmetry A implies a block-diagonal

structure of the Hamiltonian:

$$H = \begin{bmatrix} \begin{bmatrix} A_1 \end{bmatrix} & & & 0 \\ & \begin{bmatrix} A_2 \end{bmatrix} & & \\ & & \ddots & \\ 0 & & & \begin{bmatrix} A_n \end{bmatrix} \end{bmatrix}, \tag{10.1}$$

where the A_i's symbolically represent the orthogonal subspaces associated with the different quantum numbers of the operator A. A powerful DMRG implementation should be able to make use of these additional structures, as one could search for the extremal eigenvalues in the corresponding subspaces, thus leading to a greatly reduced numerical cost. Introductory accounts of working with symmetries - especially non-Abelian symmetries - in DMRG can be found for instance in refs. [70, 71].

While this is a valid and useful prospect for ground state studies of further spin models, it is however of minor importance for the results obtained with the kernel polynomial method. There, as DMRG is only used in the very first step of the algorithm, we have found a potential speed-up in the ground state search negligible compared to the numerical cost of evaluating the Chebyshev moments.

Furthermore, we have seen that the use of open boundary conditions (which are natural in the MPS formalism) implies considerable finite-size effects, in particular in studying the scaling of the entanglement entropy in the ground state. Conversely, using periodic boundary conditions in combination with exact diagonalisation gave a much better estimate for significantly smaller systems. In order to be able to study the entanglement entropy in large systems with MPS, it would be worthwhile to upgrade our DMRG implementation as to incorporate periodic boundary conditions. While for several years, DMRG implementations with periodic boundary conditions performed much worse than their counterparts, recent results suggest that it is possible to handle periodic MPS efficiently, too (cf. refs. [72, 73, 74]).

10.1.2 Improved Resolution of the Spectral Function

Ref. [27] furthermore suggests to reduce the bandwidth of the Hamiltonian being rescaled into the interval $[-1, 1]$, as this leads to a better resolution of the spectral function (or, equivalently, the same resolution with fewer terms kept in the expansion, and therefore a reduced computational overhead related to the calculation of the Chebyshev moments). Working with that smaller bandwidth entails an additional step in the algorithm, where one needs to ensure that the Chebyshev vectors are indeed projected into the corresponding low-energy subspace. Otherwise, divergencies in the Chebyshev moments may occur, if such high-energy contributions remain "accidentally" present in the state.

The main idea behind the algorithmic implementation of this truncation scheme is to iterate through the current Chebyshev vector and to construct a local Krylov basis at each site. This then allows us to locally project onto the low-energy degrees of freedom. For more details, we refer the reader to the above-mentioned publication.

10.1.3 Development of an MPS Library

For future research projects, it would furthermore be desirable to develop a full, general MPS library. While we have implemented a variety of different MPS algorithms during the course of this work, we would like to extend our library with a powerful time-evolution algorithm, such as the **time-dependent variational principle** (TDVP)[40] (cf. ref. [60, 75]). This would allow us to explicitly perform real and imaginary time-evolutions, and provide an important interface and benchmark for the comparison with other numerical simulation methods.

On a structural level, we would like to pursue an object-oriented approach for future studies. The Python code used in this thesis manipulates as central objects lists of arrays, representing the MPS and MPOs. In order to work with MPS algorithms in a high-level approach, a next step will be to initialise single MPS and MPOs as instances of the corresponding classes `MPS` and `MPO`, whose methods should contain the standard MPS/MPO algebra, compressions etc. By defining overloaded operators for linear-algebraic operations, the implementation of algorithms such as the kernel polynomial method will be greatly simplified.

10.2 Temperature-Dependent Spectral Functions

The most direct generalisation of the methods presented in this thesis is to consider the **spectral function for finite temperatures**. In fact, this calculation is a straightforward extension of the zero-temperature spectral function obtained with the kernel polynomial method, with only minor additional complications. In the spirit of giving a concrete starting point for future works building on the ideas developed in this thesis, we will present the derivation of the finite-temperature spectral function in enough detail, such that the reader would be able to start implementing it themselves.

The principle resource for the calculations below is again ref. [27].

[40] Often also referred to as "tangent space projection" or "tangent space method".

10.2.1 Chebyshev Expansion of Functions of Two Variables

In order to calculate the spectral function at finite temperature, we will need the **multivariate version of the Chebyshev expansion** developed in the previous part. Full details can again be found in ref. [14], for simplicity here we will focus directly on the expansion in terms of two variables. The weighted scalar product generalises immediately to

$$\langle f|g\rangle = \int_{-1}^{1} dxdy \, \frac{1}{\pi^2\sqrt{1-x^2}\sqrt{1-y^2}} f(x,y)\, g(x,y), \tag{10.2}$$

such that the Chebyshev expansion of the function $f(x,y)$ is given by

$$f(x,y) = \sum_{i,j=0}^{\infty} \frac{\langle f|T_iT_j\rangle}{\langle T_iT_j|T_iT_j\rangle} T_i(x)\, T_j(y). \tag{10.3}$$

Including the explicit normalisation of the Chebyshev polynomials $T_i(x)$, we may rewrite this as

$$f(x,y) = \frac{1}{\pi^2\sqrt{1-x^2}\sqrt{1-y^2}} \sum_{i,j=0}^{\infty} \mu_{ij} \frac{2}{1+\delta_{i,0}} \frac{2}{1+\delta_{j,0}} T_i(x)\, T_j(y), \tag{10.4}$$

where we have defined the **multivariate Chebyshev moments** as

$$\mu_{ij} = \int_{-1}^{1} dxdy \, f(x,y)\, T_i(x)\, T_j(y). \tag{10.5}$$

10.2.2 Chebyshev Expansion of the Temperature-Dependent Spectral Function

Just as the zero-temperature spectral function is defined as the Fourier transform of the time-dependent correlator in frequency space,

$$A^{BC}(\omega) = \frac{1}{2\pi} \int dt\, e^{i\omega t} G^{BC}(t), \quad G^{BC}(t) = \langle 0|B(t)C(0)|0\rangle\,, \tag{10.6}$$

the spectral function at finite temperature may be obtained as the Fourier transform of the corresponding finite-temperature correlator:

$$A_T^{BC}(\omega) = \frac{1}{2\pi} \int dt\, e^{i\omega t} G_T^{BC}(t), \quad G_T^{BC}(t) = \mathrm{Tr}\left[\rho_T B(t)C(0)\right], \tag{10.7}$$

with the standard definition

$$\rho_T = \frac{e^{-\beta H}}{Z}, \quad Z = \mathrm{Tr}\left[e^{-\beta H}\right] \tag{10.8}$$

for the thermal state at inverse temperature β. As the Chebyshev expansion is particularly suited for quantities built from delta-function of the spectrum of the corresponding Hamiltonian, we will now motivate a suitable way of rewriting the finite-temperature spectral function.

Starting with the easier case of the partition function, it is straightforward to reformulate it as an integral over the density of states $\rho(\omega)$. The latter can be defined as

$$\rho(\omega) = \mathrm{Tr}\left[\delta(\omega - H)\right], \tag{10.9}$$

such that the partition function becomes

$$\begin{aligned} Z &= \int d\omega\, e^{-\beta\omega}\rho(\omega) \\ &= \int d\omega\, e^{-\beta\omega}\,\mathrm{Tr}\left[\delta(\omega - H)\right] = \int d\omega\, e^{-\beta\omega}\sum_{k=1}^{D}\langle k|\,\delta(\omega - H)\,|k\rangle \\ &= \sum_{k=1}^{D}\langle k|\int d\omega\, e^{-\beta\omega}\delta(\omega - E_k)\,|k\rangle = \sum_{k=1}^{D}\langle k|\,e^{-\beta E_k}\,|k\rangle \\ &= \sum_{k=1}^{D}\langle k|\,e^{-\beta H}\,|k\rangle = \mathrm{Tr}\left[e^{-\beta H}\right], \end{aligned} \tag{10.10}$$

where we have evaluated the trace in the energy eigenbasis $\{|k\rangle\}$. It is therefore the density of states that we seek to approximate in terms of Chebyshev polynomials. The corresponding Chebyshev moments are then given by

$$\begin{aligned} \mu_i^{\rho} &= \int_{-1}^{1} d\omega\,\rho(\omega)\,T_i(\omega) = \int_{-1}^{1} d\omega\;\mathrm{Tr}\left[\delta(\omega - H)\right]\,T_i(\omega) \\ &= \sum_{k=1}^{D}\langle k|\int d\omega\,\delta(\omega - H)\,|k\rangle\,T_i(\omega) = \sum_{k=1}^{D}\langle k|\int d\omega\,\delta(\omega - E_k)T_i(\omega)\,|k\rangle \\ &= \sum_{k=1}^{D}\langle k|\,T_i(E_k)\,|k\rangle = \mathrm{Tr}\left[T_i(H)\right]. \end{aligned} \tag{10.11}$$

Rewriting the Fourier transform defining the spectral function is slightly more involved, and requires the following definition, in analogy to the above-defined density of states:

$$\rho^{BC}(\omega', \omega) \equiv \mathrm{Tr}\left[\delta(\omega' - H)\,B\,\delta(\omega - H)\,C\right]. \tag{10.12}$$

It is then possible to express the finite-temperature spectral function as an integral over

this density:

$$
\begin{aligned}
A_T^{BC}(\omega) &= \frac{1}{Z}\int d\omega'\, e^{-\beta\omega'}\rho^{BC}(\omega', \omega+\omega') \\
&= \frac{1}{Z}\int d\omega'\, e^{-\beta\omega'}\sum_{k=0}^{D}\langle k|\,\delta(\omega'-H)\,B\,\delta(\omega+\omega'-H)\,C\,|k\rangle \\
&= \frac{1}{Z}\sum_{k=0}^{D}\langle k|\int d\omega'\, e^{-\beta\omega'}\delta(\omega'-E_k)\,B\,\delta(\omega+\omega'-H)\,C\,|k\rangle \\
&= \frac{1}{Z}\sum_{k=0}^{D}\langle k|\, e^{-\beta E_k}\,B\,\delta(\omega-H+E_k)\,C\,|k\rangle \\
&= \frac{1}{Z}\sum_{k=0}^{D}\langle k|\, e^{-\beta E_k}\,B\int\frac{dt}{2\pi}\, e^{i(\omega-H+E_k)t}\,C\,|k\rangle \\
&= \frac{1}{Z}\int\frac{dt}{2\pi}e^{i\omega t}\sum_{k=0}^{D}\langle k|\, e^{-\beta E_k}\, e^{iE_k t}B\, e^{-iHt}\,C\,|k\rangle \\
&= \frac{1}{Z}\int\frac{dt}{2\pi}e^{i\omega t}\sum_{k=0}^{D}\langle k|\, e^{-\beta H}\, e^{iHt}B\, e^{-iHt}\,C\,|k\rangle \\
&= \int\frac{dt}{2\pi}e^{i\omega t}\sum_{k=0}^{D}\langle k|\,\rho_T\,B(t)\,C\,|k\rangle = \int\frac{dt}{2\pi}e^{i\omega t}\,\mathrm{Tr}\left[\rho_T B(t)C(0)\right] \\
&= \int\frac{dt}{2\pi}\, e^{i\omega t}G_T^{BC}(t).
\end{aligned}
\tag{10.13}
$$

Calculating the multivariate Chebyshev moments is then again straightforward:

$$
\begin{aligned}
\mu_{ij}^{BC} &= \int_{-1}^{1} dxdy\,\rho^{BC}(x,y)\,T_i(x)\,T_j(y) = \int_{-1}^{1} dxdy\;\mathrm{Tr}\left[\delta(x-H)\,B\,\delta(y-H)\,C\,\right]\,T_i(x)\,T_j(y) \\
&= \int_{-1}^{1} dxdy\,\sum_{k=1}^{D}\langle k|\,\delta(x-H)\,B\,\delta(y-H)\,C\,|k\rangle\,T_i(x)\,T_j(y) \\
&= \sum_{k=1}^{D}\langle k|\int_{-1}^{1} dxdy\,T_i(x)\,\delta(x-H)\,B\,T_j(y)\,\delta(y-H)\,C\,|k\rangle \\
&= \mathrm{Tr}\left[T_i(H)\,B\,T_j(H)\,C\right].
\end{aligned}
\tag{10.14}
$$

Evaluating the full finite-temperature spectral function then "merely" requires the evaluation of N_{Cheby} Chebyshev moments μ_i^{ρ} and μ_{ij}^{BC}, where N_{Cheby} is the number of terms to be kept in the series expansion. Finally, in order to obtain a closed expression for the

spectral function, one therefore has to (numerically) evaluate the integrals

$$\begin{aligned} A_T^{BC}(\omega) = &\frac{\mu_{00}^{BC}}{Z} \int d\omega' \frac{e^{-\beta\omega'}}{\pi^2\sqrt{1-\omega'^2}\sqrt{1-\omega^2}} \\ &+ \frac{2}{Z} \int d\omega' \frac{e^{-\beta\omega'}}{\pi^2\sqrt{1-\omega'^2}\sqrt{1-\omega^2}} \left(\mu_{01}^{BC}\, T_1(\omega+\omega') + \mu_{10}^{BC}\, T_1(\omega')\right) \\ &+ \frac{4}{Z} \sum_{i,j=1}^{N_{Cheby}} \mu_{ij}^{BC} \int d\omega' \frac{e^{-\beta\omega'}}{\pi^2\sqrt{1-\omega'^2}\sqrt{1-\omega^2}}\, T_i(\omega')\, T_j(\omega+\omega') \end{aligned} \tag{10.15}$$

and

$$Z = \mu_0^\rho \int d\omega \frac{e^{-\beta\omega}}{\pi^2\sqrt{1-\omega^2}} + 2 \sum_{i=1}^{N_{Cheby}} \mu_i^\rho \int d\omega \frac{e^{-\beta\omega}}{\pi^2\sqrt{1-\omega^2}} T_i(\omega). \tag{10.16}$$

For reasons of brevity, we have omitted the use of damping factors as well as an explicit rescaling of the Hamiltonian, but they should both be understood as featuring implicitly in the two final integrals.

In complete analogy to the zero-temperature case, the biggest advantage of this scheme is that the temperature only enters the equations at the very end, and can be considered an ordinary parameter. We would therefore expect a greatly reduced error in comparison to schemes where the finite-temperature state is constructed explicitly, by an evolution in imaginary time. This construction can be achieved in a very similar manner as the "standard" time-evolution of states, and is briefly described in the appendix. In this sense, the kernel polynomial method allows us to circumvent time-evolution-induced errors *doubly*, by directly working in the frequency *and* temperature space.

10.3 Further Ideas for Future Studies

There is a multitude of other possibilities to continue and extend the present project, and we will content ourselves with merely naming them. A detailed discussion is beyond the scope of this thesis, and we refer the reader to the literature indicated below and the references therein for in-depth information.

Building on our study of the entanglement entropy in the ground state, it would be interesting to investigate how long-ranged the entanglement at the boundary is. One way of determining this in more detail would be to consider not the entanglement between a left and a right subsystem, but the entanglement between a "window" of several spins and the rest of the chain. A pictorial representation of this setup is shown in fig. 58. By sweeping "windows" of variable lengths across the boundary, one could precisely determine how entangled the region around the boundary is, and how far the entanglement stretches across the chain. In the current framework, this could be implemented by

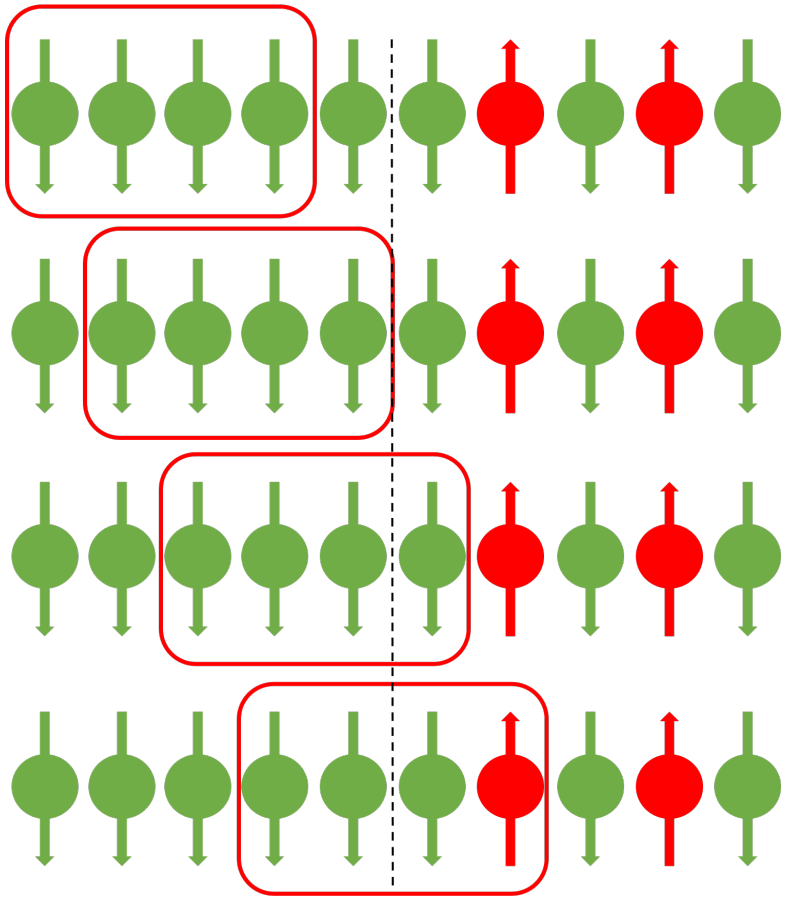

Figure 58: Sweeping a "window-like" subsystem through the spin chain and across the boundary, to determine the entanglement entropy between the window and the rest of the chain.

simply calculating the reduced density matrix of the window explicitly, and evaluating the von Neumann entropy by a spectral decomposition of the latter. This is however not an optimal prescription, as the size of the reduced density matrix again scales exponentially with the length of the window. It would therefore be desirable to define a canonical form of the MPS, which is equivalent to the Schmidt decomposition of the window and the rest of the chain, and thus allows us to read off the corresponding singular values directly.

In the same vein, one can conduct different information-theoretic analyses across the boundary. One especially suitable quantity to consider would be the **quantum mutual information** (cf. ref. [7]), defined by

$$\begin{aligned} S(A:B) &= S(A) + S(B) - S(A,B) \\ &= -\operatorname{Tr}\left(\rho^A \ln\left(\rho^A\right)\right) - \operatorname{Tr}\left(\rho^B \ln\left(\rho^B\right)\right) + \operatorname{Tr}\left(\rho^{AB} \ln\left(\rho^{AB}\right)\right) \end{aligned} \tag{10.17}$$

for subsystems A and B and the corresponding reduced density matrices ρ^A and ρ^B (ρ^{AB} being the density matrix of the joint system). Defining the two subsystems as the left and the right half-chain, one could therefore study how much information one obtains by measuring only one of the subsystems, as a function of the parameters determining

the interface between the two systems.

A somewhat larger, more ambitious future project would be to study the entanglement between elementary excitations in both half-chains. This would require a modelling of spinons and magnons as MPS. MPS representations of quasiparticles have been studied in the literature (see for instance refs. [76, 77, 78] and references therein), but require substantially more work than we could have done in the scope of this project. Nevertheless, this provides an exciting continuation.

Finally, we mention the implementation of the tensor network formalism in terms of quantum circuits (cf. e.g. refs. [79, 80, 81]). While tensor networks and MPS undeniably are one of the best tools available in the numerical analysis of quantum systems, they remain classical methods and as such are subject to the laws of classical computation. Near-term quantum computing devices are a promising candidate for first, reliable quantum simulations of condensed matter systems, and are hoped to provide an alternative to state-of-the art classical simulations in the near future. Using quantum circuit representations of MPS to simulate quantum dynamics is therefore an interesting hybrid approach, and it would be a fascinating comparison to work out the results discussed in this thesis with a true quantum implementation.

11 Conclusion

Numerous topics have been discussed in the present thesis. In doing so, we have had two main objectives: first, we presented matrix product state methods as a state-of-the-art numerical method, allowing us to efficiently study quantum systems out of the reach of exact diagonalisation techniques, due to the exponential scaling of the associated Hilbert space. Second, we have applied those techniques to a simple yet non-trivial system, built from the interface of a ferromagnetic and an antiferromagnetic Heisenberg spin chain.

As for the first objective, our main goal was to present a pedagogical account of matrix product states, and, more generally, tensor network techniques, suitable for newcomers in the field. We have introduced the necessary background in quantum mechanics and quantum information and shown why matrix product states are a particularly useful parametrisation of many-body quantum states, due to the fact that they allow us to steer the amount of entanglement entropy contained in a quantum state. By discussing two toy models of condensed matter physics - the Heisenberg and Ising models - we have motivated the fact that the ground states of those models have an exceptionally low entanglement entropy. It is this property, which is generalised for locally interacting Hamiltonians in higher dimensions by the famous "area laws", which provides the link to a physically meaningful description of those ground states in terms of tensor networks.

Hereafter, we have developed the most important matrix product state manipulations and algorithms from scratch, emphasising that those merely translate known notions from standard quantum mechanics into a (slightly) different language. In particular, we have focused on variational algorithms and the density matrix renormalisation group, to date one of the most successful methods to determine the ground states of one dimensional quantum systems. A prime example of a recent application of matrix product state techniques is the kernel polynomial method, which allows us to calculate spectral functions directly in frequency space, thereby circumventing the prior sampling of time increments and the numerical Fourier transformation associated with a naive time-domain approach. We have explained this method in detail and shown how one can implement it, using only basic matrix product states manipulations.

Having conducted an extensive benchmark of the algorithms used in this thesis, we have fulfilled our second objective by studying the interface of an antiferromagnetic and ferromagnetic Heisenberg spin chain. In particular, we have determined the ground state energy, the entanglement entropy and the location of the elementary eigenmodes in real- and frequency-space. Varying the parameters of the model - the coupling strength and the transverse field - has led to the conclusion that the physical properties of the

model seem to depend feebly on the coupling, and vary most significantly with the transverse field. However, tuning the coupling strength has created a boundary mode at the physical interface, whose eigenenergy is proportional to the coupling. A comparison with an antiferromagnetic Heisenberg half-chain with a localised edge-field furthermore suggests that this boundary mode is a true interaction effect. Further properties of the boundary mode will be the object of future projects.

Finally, in order to give a flavour of how one could continue the present work, we have discussed several prospective improvements. While we have obtained at least approximations of the thermodynamic limit in the cases studied, one may of course always study larger systems and/or use higher bond dimensions, or equivalently, employ more powerful computational resources. Nevertheless, the improvements we deem more interesting rather concern the physics of the model. To begin with, having calculated the spectral function at zero temperature, it is only natural to conduct finite-temperature studies of the same setup. We have given precise instructions how such a finite-temperature approach follows from the calculations in this thesis. Furthermore, it is worth investigating how long-ranged the entanglement around the interface is, by considering the entanglement between a "window" of spins and the rest of the chain. In a similar spirit, one could calculate how the entanglement entropy scales across the boundary if low-lying excitations are present in the system. This, on the other hand, involves a modelling of those excitations/quasiparticles in terms of matrix product states, which is an area of active research. Finally, we mentioned an interesting connection to quantum simulations with the implementation of matrix product states in terms of quantum circuits.

While many aspects have been discussed in this work, we have of course barely scratched the surface of the application of matrix product states to problems in condensed matter physics. Mainly, our hope is that this thesis might serve as a gateway to tensor network techniques and motivate how a quantum information-based point of view gives rise to a particularly useful way of tackling cutting-edge problems in quantum physics numerically. If this thesis serves an interested reader in setting up their own matrix product state and tensor network algorithms, we know that this hope has been fulfilled.

Part V

Appendix and References

A Infinite MPS and Infinite DMRG

In this thesis, we have exclusively worked with finite MPS. It is however easily possible to set up an MPS formalism in the thermodynamic limit. One of the workhorses for those cases is the infinite density matrix renormalisation group (iDMRG), relatively close in spirit to White's initial proposal of the DMRG algorithm (cf. refs. [56, 57]) which did not yet make use of the MPS structure. The main reason for including a short discussion of infinite MPS and iDMRG is that it gives a possibility to improve the convergence of the DMRG algorithm, which we have used in the present work. This section barely scratches the surface of infinite-MPS calculations, and should be considered a short, informal addendum, rather than an in-depth derivation. Its sole purpose is to get to iDMRG as fast as possible, and motivate how it gives rise to a state that can be used as an initial state for DMRG.

Much more detailed accounts of iDMRG and infinite MPS can be found in refs. [12, 82, 83].

A.1 Infinite MPS

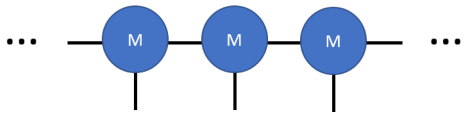

Figure 59: An MPS structure, repeated throughout real space.

In contrast to what one might intuitively think, infinite, or more accurately, translationally invariant, MPS are actually a simplification compared to finite MPS. The idea is to consider a unit cell, typically constructed from one or two tensors, which is then simply taken to be repeated throughout space. In other words, one has to calculate only the tensors in the unit cell, which automatically guarantees full knowledge of the entire state.

As a general rule of thumb, such a unit cell is obtained by working with a small number of tensors, which are then successively refined in a given algorithm. Once a certain threshold of convergence has been reached - probed for instance by monitoring the change of quantities derived from the unit cell in subsequent update steps -, those tensors are considered to be appropriate representatives of the state in the thermodynamic limit.

A.2 Infinite DMRG

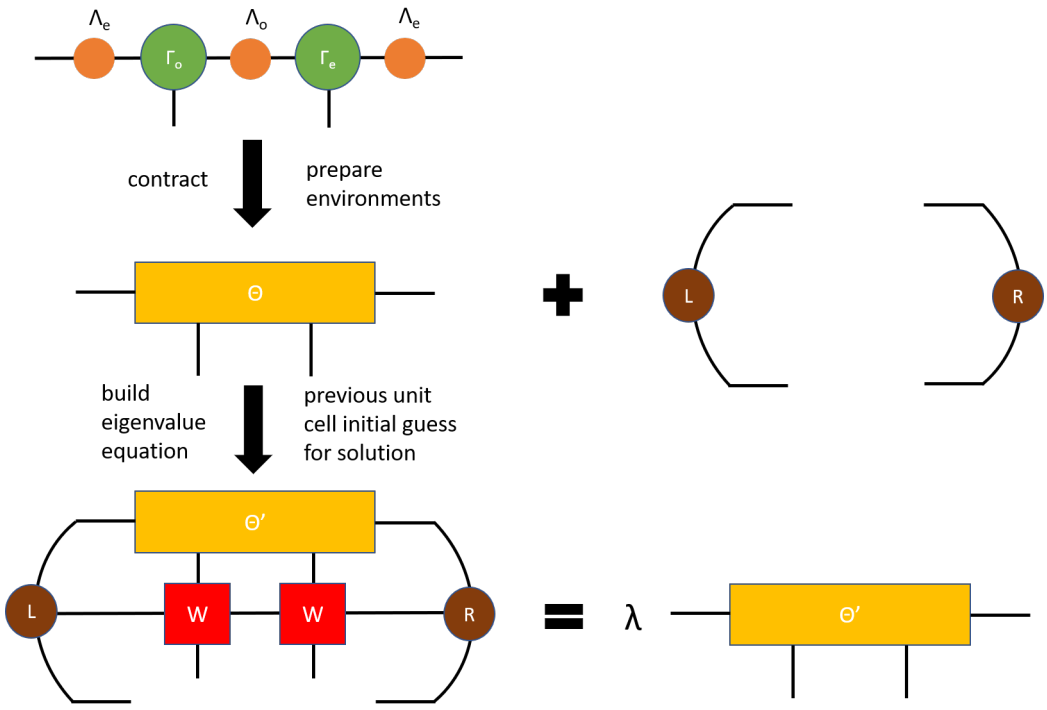

Figure 60: Setting up the environments and the eigenvalue equation for iDMRG.

We will present here the two-site version of iDMRG. The main difference to the classical DMRG algorithm is that we are not sweeping through a chain of tensors, but successively updating left and right environments, until they accurately model the physics contained in the "virtual" semi-infinite half-chain.

In the case of iDMRG, it is most convenient to work with a unit cell in Gamma-Lambda form. Without re-deriving the details, the heart of the algorithm is again an eigenvalue equation, as represented in fig. 60. To perform the contraction, one has to define the left and right environments L and R, which in the initial step of the algorithm are taken to be identity tensors. A reshaping of the unit cell and solving of the eigenvalue equation for the lowest eigenvalue then yields the updated tensor Θ'. As shown in fig. 61, one then has to recover the Gamma-Lambda structure of the unit cell. This leaves us with two optimised tensors, that can be absorbed in the left and right environments, thus updating the latter. This is also a further justification for the choice of a two-site unit cell. If we had chosen a one-site unit cell, we would only get one optimised tensor in each step, which means that we could only update the environments in alternating order.

The steps of solving the eigenvalue equation and updating the environments are repeated until a suitable convergence is observed, in which case we consider the unit cell to be a "true" representation of the thermodynamic limit.

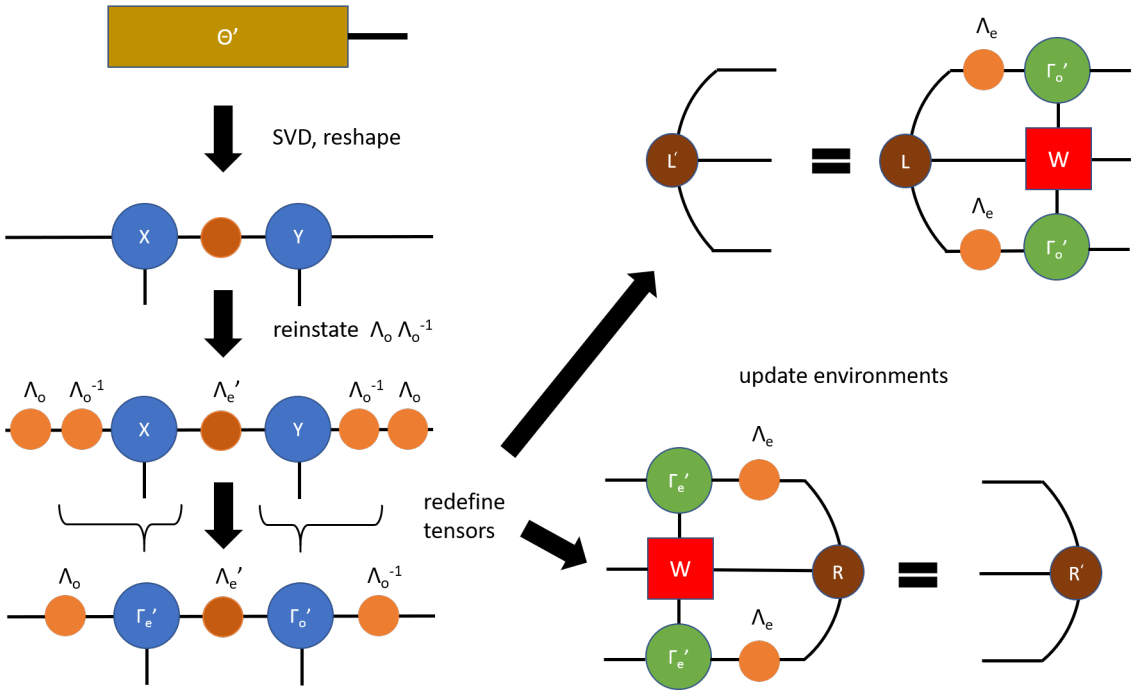

Figure 61: Updating the unit cell and the environments in iDMRG.

In order to use this procedure to get an initial state estimate for a finite DMRG algorithm, we simply set up a separate container to which the new, optimised unit cells obtained in each step are appended. Note however that this MPS effectively grows "from the middle to the left and to the right"; hence one needs to care of saving the tensors in each step in the appropriate location in the container. Depending on the length of the MPS considered in the corresponding DMRG procedure, this estimate will most likely not yet have converged to the true ground state, but nevertheless provides a better estimate for the initial state than a random MPS.

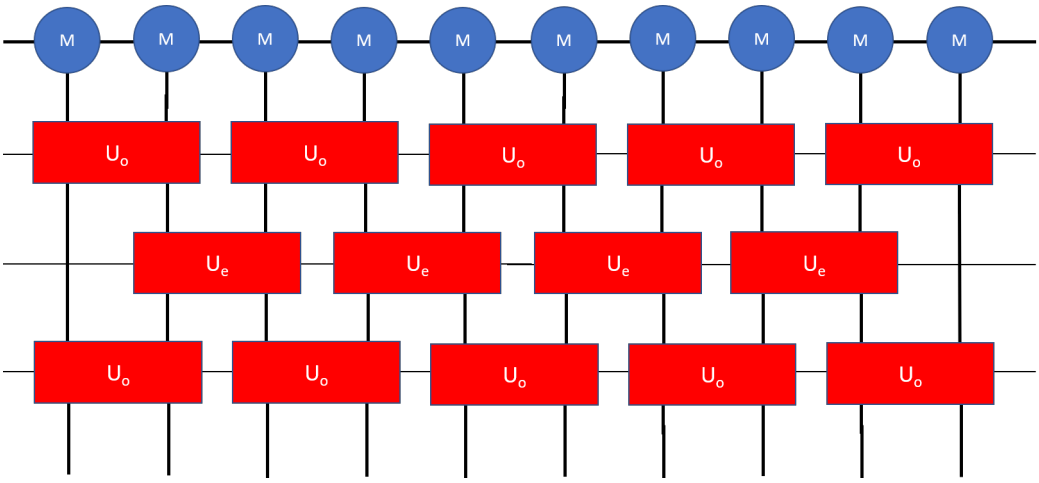

Figure 62: General idea of TEBD: the Hamiltonian is decomposed into (mutually commuting) even and odd gates, which are applied in successive layers.

B Time-Evolution of Matrix Product States

While the time-evolution of MPS isn't explicitly used for the work done in this thesis, it represents a central class of quantum mechanics operations and deserves to be exposed in a general overview of MPS algorithms. However, the time-evolution of an MPS has been used implicitly when we discussed why the kernel polynomial method should be the preferred method to calculate the spectral function. Mainly, we argued that a time-evolution of MPS was prone to errors. Justifying this claim is the objective of this short section. In addition, time-evolution also constitutes the basis of calculations with thermal states, which will be presented in the next chapter of the appendix.

Incidentally, there exist different ways of implementing a time-evolution of states in MPS language[41]. We will present below the most basic such algorithm - Vidal's **time-evolving block decimation**, or TEBD, for short (cf. refs. [12, 13, 60]). It has the crucial advantage over other time-evolution algorithms that it can be derived in a very clean fashion from basic quantum mechanics and admits a crystal-clear representation in terms of tensor networks.

The main idea of TEBD is to take the time-evolution operator

$$U(t) = e^{-iHt} \Rightarrow |\psi(t)\rangle = U(t)\,|\psi(0)\rangle \tag{B.1}$$

literally, and to represent it as a tensor operator, to be multiplied with an MPS. To achieve this, the matrix exponential itself will be decomposed into small, two-site contributions, which can easily be calculated exactly. Applying a large network of those "small" time-evolution operators to an MPS, such as illustrated in fig. 62, will yield a "sufficiently

[41] For a supremely complete overview of time-evolution algorithms, including a review of MPS algebra, consult ref. [60].

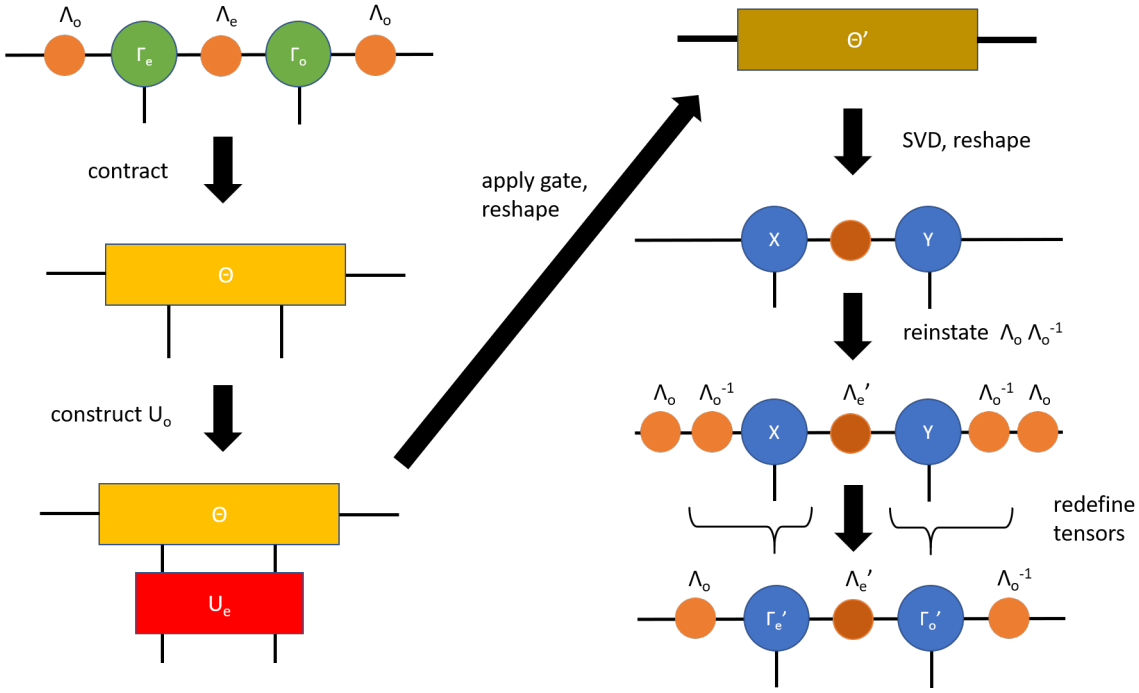

Figure 63: Even update step of the TEBD algorithm: a two-site gate is applied to a sequence of tensors in Gamma-Lambda form, such that the initial structure can recovered easily.

good" approximation to the true time-evolved state, $|\psi(t)\rangle$ (to be detailed below).

B.1 Trotter Decomposition of the Hamiltonian

In order to obtain an expression of the matrix exponential $\exp(-iHt)$ in terms of smaller tensors, we have to start by setting up a decomposition of the Hamiltonian. Here, we will make the important assumption that each term in the Hamiltonian only connects a site and its neighbouring site[42]:

$$H = \sum_l \underbrace{h_l}_{\text{connects l, l+1}} = \sum_{1,3,5,..} h_l + \sum_{2,4,6,...} h_l \equiv H_o + H_e, \tag{B.2}$$

allowing us to formally define a decomposition into an "even" and an "odd" Hamiltonian. Crucially, we observe that two *different* odd (or two different even) h_l's *must* commute, as we defined every h_l to connect only sites l and $l+1$. Next, we divide the time interval in question into N slices: $t \equiv N\tau$. Then the time-evolution operator becomes:

$$\exp(-iHt) = (\exp(-iH\tau))^N = (\exp(-i(H_o + H_e)\tau))^N. \tag{B.3}$$

Applying the Baker-Campbell-Haussdorff formula now yields the so-called **first order Suzuki-Trotter approximation** (cf. refs. [84, 85]):

$$\exp(-iHt) = (\exp(-iH_o\tau)\exp(-iH_e\tau) + \mathcal{O}(\tau^2))^N. \tag{B.4}$$

[42]Thus, all nearest-neighbour interactions are good to go from our point of view.

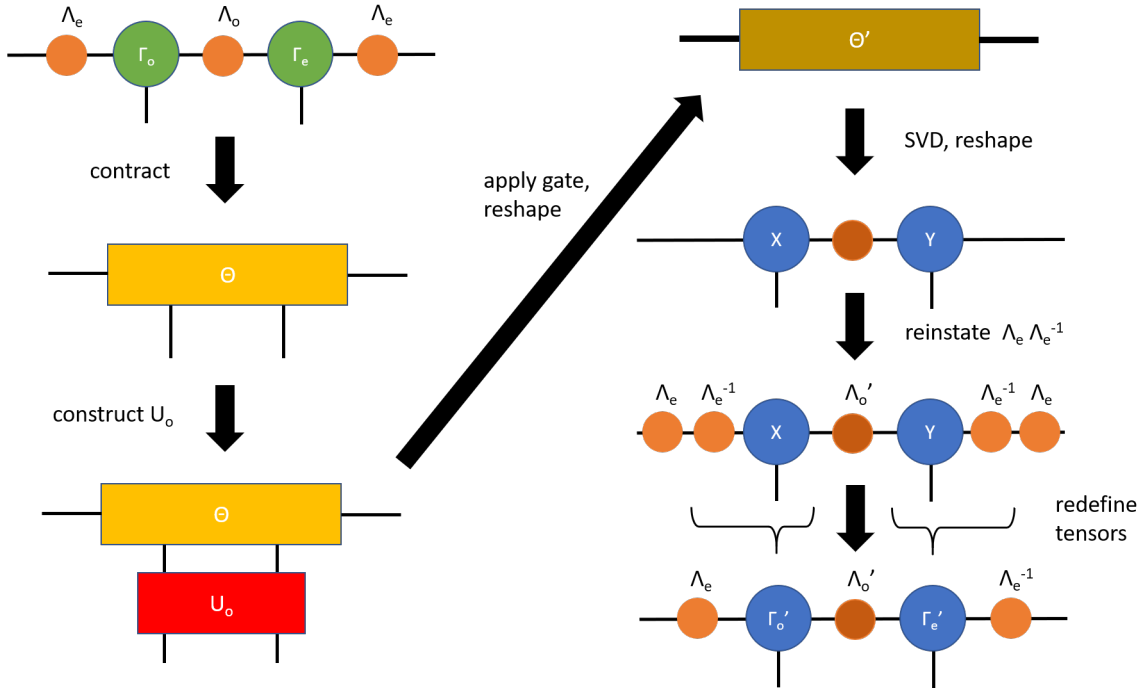

Figure 64: Odd update step of the TEBD algorithm: a two-site gate is applied to a sequence of tensors in Gamma-Lambda form, such that the initial structure can recovered easily.

Therefore, for large values of N (or, equivalently, small values of τ), we can approximate the time-evolution operator by a successive application of two exponentials, to be repeated N times.

Since both H_o and H_e are sums of mutually commuting terms, we can expand the matrix exponentials further, this time without any need for an approximation:

$$\exp(-iH_o\tau) = \exp(-ih_1\tau)\exp(-ih_3\tau)...\exp(-ih_{N-1}\tau) = U_{[1]}U_{[3]}...U_{[N-1]} \tag{B.5}$$

and

$$\exp(-iH_e\tau) = \exp(-ih_2\tau)\exp(-ih_4\tau)...\exp(-ih_N\tau) = U_{[2]}U_{[4]}...U_{[N]}. \tag{B.6}$$

The bottom line of all this is that we have now found an explicit decomposition of the time-evolution operator into smaller operators connecting only two sites, each. Each string of these "two-site gates" is applied N times, such that the time-evolution operator in the first-order Trotter scheme becomes:

$$\exp(-iHt) = (U_{[1]}U_{[3]}...U_{[N-1]}U_{[2]}U_{[4]}...U_{[N]})^N. \tag{B.7}$$

Translating this into a tensor network is the basic idea of the TEBD algorithm.

One of the main sources of error of the TEBD scheme is therefore inherent to the Suzuki-Trotter decomposition of the matrix exponential $\exp(-iHt)$. Vidal shows that (cf. ref. [13]) in a first order decomposition, the error ϵ scales as

$$\epsilon \propto \tau^2 t^2. \tag{B.8}$$

The error could therefore be reduced by increasing the number of increments, thus decreasing the value of τ, however one cannot escape the error due to large simulation times t ("running into a wall"). Another strategy to obtain smaller errors is to employ higher-order Suzuki-Trotter decomposition, such as up to second order:

$$\exp(-iHt) = (\exp(-iH_o\tau/2)\exp(-iH_e\tau)\exp(-iH_o\tau/2) + \mathcal{O}(\tau^3))^N. \tag{B.9}$$

In general, for an n^{th} order Suzuki-Trotter decomposition, the error is given by (cf. ref. [13])

$$\epsilon \propto \tau^{2n}t^2. \tag{B.10}$$

While this allows to extend the range of reachable times, it is unavoidable that the simulation will eventually break down.

Furthermore, note that an additional source of errors follows from the truncation that has to be applied to the MPS after each application of a "time-evolution layer". It is however the above-described Trotter error which *fundamentally* limits the algorithm.

B.2 Time-Evolving Block Decimation

While the tensor network in fig. 62 summarises the gist of the algorithm, a stable version of the time-evolution algorithm is best implemented by transforming the MPS to (and keeping it in) Gamma-Lambda form. One can then sweep through the chain and successively apply the even and odd gates, as specified by the Trotter scheme in use. The even and odd update steps in the algorithm are explained in figs. 63 and 64. Note that this induces a further possible source of error, as the inverse of the (diagonal) singular value matrix Λ has to be taken during the update. For small singular values, this might lead to additional numerical instabilities. For further details, we refer the reader to refs. [12, 13, 50].

C Thermal States and Purifications

In the main part of the thesis, we have discussed temperature-dependent spectral functions as a possible extension of the present work, highlighting how the kernel polynomial method allows their efficient calculation. Here, we will present in somewhat more detail how a temperature-dependent MPS is obtained from its zero-temperature analogue directly. In essence, this can be achieved with an imaginary time-evolution in a spirit very similar to the real-time evolution of quantum states. The main difference is that a temperature-dependent quantum state needs to be defined as a density matrix, i.e. is by construction a mixed state. Implementing an imaginary time evolution therefore requires a direct translation between pure and mixed states, which is achieved by an additional piece of formalism: the **purification** of quantum states (see ref. [7]).

More information about finite-temperature calculations with MPS and DMRG can be found in refs. [86, 87, 88] and in Schollwöck's review, ref. [12].

C.1 Thermal States

Imagine a given Hamiltonian has been diagonalised, and its eigenstates and spectrum are defined as $H|\Psi_i\rangle = E_i|\Psi_i\rangle$. Assume furthermore that the system is connected to a reservoir at temperature T, which means that we can describe its physics in the canonical ensemble. Each state of the system thus occurs with a weight given by its Boltzmann factor, $\exp(-E_i/k_BT)$. Normalising the Boltzmann factors by introducing the partition function defines the probabilities for each state:

$$p_i = \frac{1}{Z}\exp(-E_i/k_BT), \quad \text{with} \quad Z = \sum_i \exp(-E_i/k_BT). \tag{C.1}$$

Knowing the (classical) probabilities with which different (pure) states occur, we can construct the density matrix corresponding to this state as

$$\rho_T = \frac{1}{Z}\sum_i \exp(-E_i/k_BT)\,|\Psi_i\rangle\langle\Psi_i|\,. \tag{C.2}$$

This is the **thermal density matrix**. In general, if we are not working in the eigenbasis of the Hamiltonian, we can thus write it down as

$$\rho_T = \frac{1}{Z}\sum_i \exp(-H/k_BT)\,|\psi_i\rangle\langle\psi_i| = \frac{1}{Z}\sum_i \exp(-\beta H)\,|\psi_i\rangle\langle\psi_i|\,, \tag{C.3}$$

where in the final step we have employed the common definition $\beta = 1/k_BT$.

C.2 Purifications

The need for purifications arises through the fact that MPS are - by definition - pure, whereas many states of interest - such as thermal states - are by construction mixed. To bridge this gap, we need a mapping from a mixed to a pure state. This becomes possible if we augment the corresponding Hilbert space with an additional, auxiliary Hilbert space, as we will now show.

In general, we can write a physical state (pure or mixed) as follows, using the density operator formalism:

$$\rho = \sum_{\sigma_1,\sigma_2} \rho_{\sigma_1,\sigma_2} \left|\sigma_1\right\rangle_P \left\langle\sigma_2\right|_P , \tag{C.4}$$

where the subscript P makes explicit that we are decomposing the density operator in the physical space. The idea behind the purification is then the following:

- We want the state to be pure. As this can't in general be the case for the physical Hilbert space, we have to augment the Hilbert space until we obtain a pure state by construction.
- To reconnect this purified state to the initial state, we demand that if we trace out the augmented part of the Hilbert space, we get back the initial state.

Let's prove that the following construction does the job:

$$\left|\Psi\right\rangle_{\text{pure}} = \sum_{\sigma} \sqrt{\rho_\sigma} \left|\sigma\right\rangle_A \left|\sigma\right\rangle_P . \tag{C.5}$$

Here, the original Hilbert space has simply been "doubled" by introducing a copy of the basis vectors (A - auxiliary), such that $\left|\Psi\right\rangle_{\text{pure}}$ lives in $\mathcal{H}_A \otimes \mathcal{H}_P$. ρ_σ denotes the eigenvalues of the initial density matrix. This is a "single" state, therefore by construction pure.

To verify that this construction also fulfils our second condition, we trace out the auxiliary state:

$$\begin{aligned}
\text{Tr}_A \left(\left|\Psi\right\rangle_{\text{pure}} \left\langle\Psi\right| \right) &= \sum_{\sigma'} \left\langle \sigma' \right|_A \left[\sum_{\sigma_1,\sigma_2} \sqrt{\rho_{\sigma_1}\rho_{\sigma_2}} \left|\sigma_1\right\rangle_A \left|\sigma_1\right\rangle_P \left\langle\sigma_2\right|_P \left\langle\sigma_2\right|_A \right] \left| \sigma' \right\rangle_A \\
&= \sum_{\sigma',\sigma_1,\sigma_2} \sqrt{\rho_{\sigma_1}\rho_{\sigma_2}} \delta_{\sigma'\sigma_1} \delta_{\sigma'\sigma_2} \left|\sigma_2\right\rangle_P \left\langle\sigma_2\right|_P \\
&= \sum_{\sigma'} \rho_{\sigma'} \left| \sigma' \right\rangle_P \left\langle \sigma' \right|_P ,
\end{aligned} \tag{C.6}$$

which is nothing but the density matrix of the initial, physical state.

C.3 Thermal Matrix Product States

Let's now construct the purified version of the thermal many-body state in the canonical ensemble. As shown above, in thermal equilibrium (and in the energy eigenbasis), the physical density operator is given by

$$\rho_P = \sum_\sigma e^{-\beta E_\sigma} \left|\sigma\right\rangle_P \left\langle\sigma\right|_P , \tag{C.7}$$

which is already in diagonal form. According to the prescription just introduced, constructing the purified state then merely involves taking the square root of those eigenvalues:

$$\left|\Psi\right\rangle_\beta = \sum_\sigma e^{-\beta E_\sigma/2} \left|\sigma\right\rangle_A \left|\sigma\right\rangle_P . \tag{C.8}$$

Note the subscript indicating the temperature-dependence of the purified state. We can once more cast this into a somewhat more general form, by introducing a physical Hamiltonian H_P, which only acts on the physical space:

$$\left|\Psi\right\rangle_\beta = e^{-\beta H_P/2} \sum_\sigma \left|\sigma\right\rangle_A \left|\sigma\right\rangle_P \equiv e^{-\beta H_P/2} \left|\Psi\right\rangle_0 . \tag{C.9}$$

The purified state at any temperature can therefore be obtained by applying a matrix exponential built from the Hamiltonian to the corresponding zero-temperature state. Algorithmically speaking, this is no different than applying a time-evolution operator to a state, which can be achieved with methods such as described in the previous chapter of the appendix.

D Exact Solution of the Transverse Field Ising Model

We will now present the analytic solution of the transverse field Ising model in one dimension in more detail, complementing the calculation in the main part of this thesis. The most important component is the Jordan-Wigner transformation, which allows us to understand the spin operators in terms of fermionic excitations. Therefore, we will introduce it in detail and derive the important transformation rules. In the end, we will be able to write down a quadratic Hamiltonian in terms of Jordan-Wigner fermions, which can be diagonalised by a passage to momentum space and a subsequent canonical transformation. For convenience, recall the form of the transverse field Ising Hamiltonian:

$$H = -J \sum_{i=1}^{N} S_i^x S_{i+1}^x - h \sum_{i=1}^{N} S_i^z. \tag{D.1}$$

Using periodic boundary conditions, we can separate out the final term:

$$H = -J \sum_{i=1}^{N-1} S_i^x S_{i+1}^x - h \sum_{i=1}^{N} S_i^z - J S_N^x S_1^x. \tag{D.2}$$

D.1 Jordan-Wigner Transformation

As shown in theory part of this thesis, it is desirable to understand a given quantum system in terms of quasiparticles, with the latter offering a straightforward way to construct the spectrum of the system. The Jordan-Wigner transformation provides a way of mapping spin operators to free fermions, and yields furthermore a particularly appealing rewriting of the interaction terms in the Ising model. We will therefore start by defining the transformation, and then show how the different spin-terms in the Ising model may be rewritten in terms of fermions.

Aside - (Anti-)Commutators of Tensor Products

There exists an exact formula to evaluate the (anti-)commutator of operators which are tensor products, it is however not terribly enlightening. Here we will merely quote the simplest cases which are relevant to us. (cf. ref. [89, 90]) For bipartite tensor products, we have

$$[A_1 \otimes A_2, B_1 \otimes B_2] = \frac{1}{2}([A_1, B_1] \otimes \{A_2, B_2\} + \{A_1, B_1\} \otimes [A_2, B_2]) \tag{D.3}$$

and

$$\{A_1 \otimes A_2, B_1 \otimes B_2\} = \frac{1}{2}([A_1, B_1] \otimes [A_2, B_2] + \{A_1, B_1\} \otimes \{A_2, B_2\}), \tag{D.4}$$

and for tripartite tensor products we obtain

$$\begin{aligned}[A_1 \otimes A_2 \otimes A_3, B_1 \otimes B_2 \otimes B_3] = \frac{1}{4}([A_1, B_1] \otimes \{A_2, B_2\} \otimes \{A_3, B_3\} \\ + \{A_1, B_1\} \otimes [A_2, B_2] \otimes \{A_3, B_3\} \\ + \{A_1, B_1\} \otimes \{A_2, B_2\} \otimes [A_3, B_3] \\ + [A_1, B_1] \otimes [A_2, B_2] \otimes [A_3, B_3])\end{aligned} \tag{D.5}$$

and

$$\begin{aligned}\{A_1 \otimes A_2 \otimes A_3, B_1 \otimes B_2 \otimes B_3\} = \frac{1}{4}([A_1, B_1] \otimes [A_2, B_2] \otimes \{A_3, B_3\} \\ + [A_1, B_1] \otimes \{A_2, B_2\} \otimes [A_3, B_3] \\ + \{A_1, B_1\} \otimes [A_2, B_2] \otimes [A_3, B_3] \\ + \{A_1, B_1\} \otimes \{A_2, B_2\} \otimes \{A_3, B_3\}).\end{aligned} \tag{D.6}$$

The spin operators on a given site are S_i^x, S_i^y and S_i^z, or equivalently S_i^+, S_i^- and S_i^z. In the following, we want to define fermionic operators $c_i(S^+, S^-, S^z)$ and $c_i^\dagger(S^+, S^-, S^z)$ such that

$$\{c_i, c_j^\dagger\} = \delta_{ij}, \quad \{c_i, c_j\} = 0 \quad \text{(valid fermions)} \tag{D.7}$$

holds. One simple guess could be to just define the spin raising and lowering operators as the fermionic creation and annihilation operators, by defining empty and occupied fermion states as $|\text{down}\rangle = |0\rangle$ and $|\text{up}\rangle = |1\rangle$:

$$S^+ = c^\dagger, \quad S^- = c \quad \Rightarrow c^\dagger |0\rangle = |1\rangle, \quad c|1\rangle = |0\rangle. \tag{D.8}$$

This idea is further corroborated by the fact that S^+ and S^- anticommute on the same site. However, this is not true if we consider the action of S^+ and S^- on different sites:

$$\begin{aligned}[S_i^-, S_j^+] =& E \otimes ... \otimes E \otimes S_i^- \otimes E \otimes ... \otimes E \otimes S_j^+ \otimes E \otimes ... \otimes E \\ & - E \otimes ... \otimes E \otimes S_i^- \otimes E \otimes ... \otimes E \otimes S_j^+ \otimes E \otimes ... \otimes E \\ =& 0,\end{aligned} \tag{D.9}$$

which is a direct consequence of the multiparticle operators being tensor products. So how do we turn the commutator into an anticommutator?

The idea is that we need to include some extra information from the rest of the spin chain into the fermionic operators under construction, such that we recover the correct anticommutation relations. There are multiple equivalent ways of doing this, one is the

following:

$$c_j = \left(\bigotimes_{l<j} S_l^z\right) \otimes S_j^+, \quad c_j^\dagger = \left(\bigotimes_{l<j} S_l^z\right) \otimes S_j^-. \tag{D.10}$$

Now let's check that our claim is indeed correct by computing the corresponding anti-commutators!

For $j \neq k$ (and $j < k$), we have

$$\begin{aligned}
\{c_j, c_k^\dagger\} &= \left\{ \left(\bigotimes_{l<j} S_l^z\right) \otimes S_j^+ \otimes \underbrace{\left(\bigotimes_{i=j+1}^{k} E_i\right)}_{=E}, \left(\bigotimes_{m<j} S_m^z\right) \otimes S_j^z \otimes \underbrace{\left(\bigotimes_{n=j+1}^{k-1} S_n^z\right) \otimes S_k^-}_{=B} \right\} \\
&= \frac{1}{4}\Bigg(\underbrace{\left[\left(\bigotimes_{l<j} S_l^z\right), \left(\bigotimes_{m<j} S_m^z\right) \right]}_{=0} \otimes \left[S_j^+, S_j^z\right] \otimes \{E, B\} \\
&\quad + \left[\left(\bigotimes_{l<j} S_l^z\right), \left(\bigotimes_{m<j} S_m^z\right) \right] \otimes \}S_j^+, S_j^z\} \otimes \underbrace{[E, B]}_{=0} \\
&\quad + \left\{ \left(\bigotimes_{l<j} S_l^z\right), \left(\bigotimes_{m<j} S_m^z\right) \right\} \otimes \left[S_j^+, S_j^z\right] \otimes \underbrace{[E, B]}_{=0} \\
&\quad + \left\{ \left(\bigotimes_{l<j} S_l^z\right), \left(\bigotimes_{m<j} S_m^z\right) \right\} \otimes \underbrace{\left\{S_j^+, S_j^z\right\}}_{=0} \otimes \{E, B\} \Bigg) = 0,
\end{aligned} \tag{D.11}$$

where we only needed to evaluate elementary commutators. The first three lines yield zero immediately, and the relation $\left\{S_j^+, S_j^z\right\} = 0$ can be easily checked to hold true. In a very similar fashion, we can check what happens when we consider the fermionic operators at the same site:

$$\begin{aligned}
\{c_j, c_j^\dagger\} &= \left\{ \left(\bigotimes_{l<j} S_l^z\right) \otimes S_j^+, \left(\bigotimes_{m<j} S_m^z\right) \otimes S_j^- \right\} \\
&= \frac{1}{2}\Bigg(\underbrace{\left[\left(\bigotimes_{l<j} S_l^z\right), \left(\bigotimes_{m<j} S_m^z\right) \right]}_{=0} \otimes \left[S_j^+, S_j^-\right] + \underbrace{\left\{ \left(\bigotimes_{l<j} S_l^z\right), \left(\bigotimes_{m<j} S_m^z\right) \right\}}_{=2\bigotimes(S^zS^z)=2\bigotimes E} \otimes \underbrace{\left\{S_j^+, S_j^-\right\}}_{=E} \Bigg) \\
&= \frac{1}{2}\, 2 \left(\bigotimes_{l<j} E_l\right) \otimes E_j \equiv E,
\end{aligned} \tag{D.12}$$

which is nothing but the identity matrix for the whole system. We have thus defined a

valid set of fermionic operators!

To make the connection to spin systems, we would like to express typical spin-spin interactions in terms of of the newly defined fermionic operators. Instead of considering the anticommutator, let's see what the commutator of two fermionic operators on the same site gives:

$$\begin{aligned}\left[c_j, c_j^\dagger\right] &= \left[\left(\bigotimes_{l<j} S_l^z\right) \otimes S_j^+, \left(\bigotimes_{m<j} S_m^z\right) \otimes S_j^-\right] \\ &= \frac{1}{2}\Bigg(\underbrace{\left[\left(\bigotimes_{l<j} S_l^z\right), \left(\bigotimes_{m<j} S_m^z\right)\right]}_{=0} \otimes \left\{S_j^+, S_j^-\right\} + \underbrace{\left\{\left(\bigotimes_{l<j} S_l^z\right), \left(\bigotimes_{m<j} S_m^z\right)\right\}}_{=2\bigotimes(S^zS^z)=2\bigotimes E} \otimes \underbrace{\left[S_j^+, S_j^-\right]}_{=S_j^z}\Bigg) \\ &= \left(\bigotimes_{l<j} E_l\right) \otimes S_j^z \equiv S_j^z.\end{aligned} \tag{D.13}$$

This reveals us that we can express the Pauli spin operator in z-direction as

$$S_j^z = c_j c_j^\dagger - c_j^\dagger c_j = 1 - 2c_j^\dagger c_j, \tag{D.14}$$

where we have used the usual anticommutator in the last equality. To get an expression for S_j^x, consider:

$$\begin{aligned}\left(\bigotimes_{l<j} S_l^z\right)(c_j + c_j^\dagger) &= \left(\bigotimes_{l<j} S_l^z\right)\left(\left(\bigotimes_{l<j} S_l^z\right) \otimes S_j^+ + \left(\bigotimes_{l<j} S_l^z\right) \otimes S_j^-\right) \\ &= \underbrace{\left(\bigotimes_{l<j} S_l^z S_l^z\right)}_{=\bigotimes E} \underbrace{\left(S_j^+ S_j^-\right)}_{=S_j^x} \equiv S_j^x.\end{aligned} \tag{D.15}$$

This expression is of limited use on its own, however it does lead to a closed expression for a corresponding interaction term:

$$\begin{aligned}S_j^x S_{j+1}^x &= \left(\left(\bigotimes_{l<j} S_l^z\right) \otimes (c_j + c_j^\dagger) \otimes E_{j+1}\right)\left(\left(\bigotimes_{l<j} S_l^z\right) \otimes S_j^z \otimes (c_{j+1} + c_{j+1}^\dagger)\right) \\ &= \left(\bigotimes_{l<j} E_l\right) \otimes \underbrace{\left(c_j S_j^z + c_j^\dagger S_j^z\right)}_{-c_j + c_j^\dagger} \otimes \left(c_{j+1} + c_{j+1}^\dagger\right) \\ &\equiv \left(c_j^\dagger - c_j\right)\left(c_{j+1} + c_{j+1}^\dagger\right),\end{aligned} \tag{D.16}$$

where the expressions $c_j S_j^z = -c_j$ and $c_j^\dagger S_j^z = c_j^\dagger$ can be verified in exactly the same way as all of the other expressions considered in this section.

To summarise, the Jordan-Wigner transformation maps the spin operators in a spin chain to fermionic excitations, and in particular yields the relationships

$$S_j^z = c_j c_j^\dagger - c_j^\dagger c_j, \quad S_j^x S_{j+1}^x = \left(c_j^\dagger - c_j\right)\left(c_{j+1} + c_{j+1}^\dagger\right). \tag{D.17}$$

D.1.1 The Ising Hamiltonian in Terms of Jordan-Wigner Fermions

The relations derived above are (conveniently) in a plug-and-play form, and as such ready to be inserted into the Ising Hamiltonian:

$$\begin{aligned} H =& -J\sum_{i=1}^{N}(c_i^\dagger c_{i+1} + c_i^\dagger c_{i+1}^\dagger - c_i c_{i+1} - c_i c_{i+1}^\dagger) - h\sum_{i=1}^{N}(c_i c_i^\dagger - c_i^\dagger c_i) \\ & - J(c_N^\dagger c_1 + c_N^\dagger c_1^\dagger - c_N c_1 - c_N c_1^\dagger). \end{aligned} \tag{D.18}$$

The last term in this expression is typically dropped, invoking the thermodynamic limit $N \to \infty$. This leaves us with the quadratic Hamiltonian

$$\begin{aligned} H &= -J\sum_{i=1}^{N-1}(c_i^\dagger c_{i+1} + c_i^\dagger c_{i+1}^\dagger - c_i c_{i+1} - c_i c_{i+1}^\dagger) - h\sum_{i=1}^{N}\underbrace{(c_i c_i^\dagger - c_i^\dagger c_i)}_{=1-2c_i^\dagger c_i} \\ &= -J\sum_{i=1}^{N-1}(c_i^\dagger c_{i+1} + c_i^\dagger c_{i+1}^\dagger - c_i c_{i+1} - c_i c_{i+1}^\dagger) + 2h\sum_{i=1}^{N} c_i^\dagger c_i, \end{aligned} \tag{D.19}$$

where we have dropped a constant term. Diagonalising this Hamiltonian is therefore all that is left to do.

D.2 Diagonalisation and Bogoliubov Transformation

Recall how we have shown how a simple, general quadratic Hamiltonian in terms of fermions

$$H = \sum_{i,j} \epsilon_{ij} c_i^\dagger c_j \tag{D.20}$$

may be diagonalised by a canonical transformation to the "true" quasiparticle operators, representing the elementary excitations of the system. Well, now we have to deal with a slightly more complicated quadratic expression, which will require a more involved transformation technique, known as the **Bogoliubov transformation**. First, however, we will transform the above Hamiltonian to momentum space by introducing the Fourier transform

$$d_k = \frac{1}{\sqrt{N}}\sum_l c_l e^{-ikl}, \quad d_k^\dagger = \frac{1}{\sqrt{N}}\sum_l c_l^\dagger e^{ikl}, \tag{D.21}$$

where the wavevector k takes N discrete values in the first Brillouin zone, $k \in [-\pi, \pi]$. Note that this is by construction a unitary transformation of the real space fermionic operators, thus defining a new, equally valid set of fermionic quasiparticle excitations. We can of course then express the real space operators through the momentum space fermions:

$$c_j = \frac{1}{\sqrt{N}} \sum_k d_k e^{ikl}, \quad c_j^\dagger = \frac{1}{\sqrt{N}} \sum_k d_k^\dagger e^{-ikl}. \tag{D.22}$$

Inserting those into our Hamiltonian, we obtain

$$\begin{aligned} H =& \frac{-J}{N} \sum_j \sum_{k,k'} \left[d_k^\dagger d_{k'} e^{-i(k-k')j} e^{ik'} + d_k^\dagger d_{k'}^\dagger e^{-i(k+k')j} e^{-ik'} - d_k d_{k'} e^{i(k+k')j} e^{ik'} - d_k d_{k'}^\dagger e^{i(k-k')j} e^{-ik'} \right] \\ &+ \frac{2h}{N} \sum_j \sum_{k,k'} d_k^\dagger d_{k'} e^{-i(k-k')j}. \end{aligned} \tag{D.23}$$

This can be solved in the usual manner by evaluating the representation of the Kronecker delta $\delta_{kk'} = \frac{1}{N} \sum_j e^{i(k-k')j}$:

$$\begin{aligned} H &= -J \sum_k \left[d_k^\dagger d_k e^{ik} + d_k^\dagger d_{-k}^\dagger e^{ik} - d_k d_{-k} e^{-ik} - \underbrace{d_k d_k^\dagger}_{=1-d_k^\dagger d_k} e^{-ik} \right] + 2h \sum_k d_k^\dagger d_k \\ &= \sum_k \left[-J(e^{ik} + e^{-ik}) + 2h \right] d_k^\dagger d_k + J \sum_k e^{-ik} - J \sum_k \left[d_k^\dagger d_{-k}^\dagger e^{ik} - d_k d_{-k} e^{-ik} \right] \\ &= \sum_k \left[-2J \cos(k) + 2h \right] d_k^\dagger d_k + J \sum_k e^{-ik} \\ &\quad - J \sum_k \left[d_k^\dagger d_{-k}^\dagger (\cos(k) + i \sin(k)) - d_k d_{-k} (\cos(k) - i \sin(k)) \right] \\ &= \sum_k \left[-2J \cos(k) + 2h \right] d_k^\dagger d_k + J \sum_k e^{-ik} - iJ \sum_k \left[d_k^\dagger d_{-k}^\dagger \sin(k) + d_k d_{-k} \sin(k) \right] \\ &= -\sum_k \left[(2J \cos(k) - 2h) d_k^\dagger d_k + iJ \sin(k) (d_k^\dagger d_{-k}^\dagger + d_k d_{-k}) \right], \end{aligned} \tag{D.24}$$

where we have again dropped a constant contribution in the last line. Furthermore, note how in the third- to second-last equation, the even cosine contributions vanish. This is guaranteed through the fermionic anticommutation relations.

This is as far as the Fourier transform will get us. We have managed to get rid of some of the quadratic fermionic terms, but the Hamiltonian is still not in diagonal form. Moreover, we have now picked up some bilinear terms involving negative k's - how do we deal with that? The answer is the introduction of yet another transformation to new quasiparticles, the so-called **Bogoliubov transformation**. This is most easily obtained

by defining vectors of creation and annihilation operators and writing our Hamiltonian as a (formal) matrix-vector product:

$$H = -\sum_k \begin{bmatrix} d_k^\dagger & d_{-k} \end{bmatrix} M(k) \begin{bmatrix} d_k \\ d_{-k}^\dagger \end{bmatrix}, \tag{D.25}$$

with

$$M(k) = \begin{bmatrix} J\cos(k) - h & iJ\sin(k) \\ -iJ\sin(k) & -(J\cos(k) - h) \end{bmatrix} \equiv \begin{bmatrix} a(k) & ib(k) \\ -ib(k) & -a(k) \end{bmatrix}. \tag{D.26}$$

Note how the two diagonal elements account for the prefactor of 2 in the Hamiltonian, as the sum runs over the positive and negative k's. In order to understand the Ising model in terms of fermionic modes, we need to diagonalise the matrix $M(k)$ unitarily. This is a straightforward calculation, and yields the diagonal matrix

$$D(k) \equiv U^\dagger(k) M(k) U(k) = \begin{bmatrix} -\epsilon(k) & 0 \\ 0 & \epsilon(k) \end{bmatrix}, \quad \epsilon^2(k) = a^2(k) + b^2(k). \tag{D.27}$$

The unitary similarity transforms $U(k)$ are found by (ortho-)normalising the eigenvectors of $M(k)$; the latter are given by

$$v_1 = \begin{bmatrix} \frac{i}{b(k)}\left(a(k) - \epsilon(k)\right) \\ 1 \end{bmatrix}, \quad v_2 = \begin{bmatrix} \frac{i}{b(k)}\left(a(k) + \epsilon(k)\right) \\ 1 \end{bmatrix}. \tag{D.28}$$

We then can immediately read off $U(k)$, and obtain $U^\dagger(k)$ by taking the hermitian conjugate of the former:

$$U(k) = \begin{bmatrix} \frac{i\sqrt{a(k)-\epsilon(k)}}{\sqrt{2\epsilon(k)}} & \frac{i\sqrt{a(k)+\epsilon(k)}}{\sqrt{2\epsilon(k)}} \\ \frac{b(k)}{\sqrt{2\epsilon(k)(\epsilon(k)-a(k))}} & \frac{b(k)}{\sqrt{2\epsilon(k)(\epsilon(k)+a(k))}} \end{bmatrix}, \quad U^\dagger(k) = \begin{bmatrix} -\frac{i\sqrt{a(k)-\epsilon(k)}}{\sqrt{2\epsilon(k)}} & \frac{b(k)}{\sqrt{2\epsilon(k)(\epsilon(k)-a(k))}} \\ -\frac{i\sqrt{a(k)+\epsilon(k)}}{\sqrt{2\epsilon(k)}} & \frac{b(k)}{\sqrt{2\epsilon(k)(\epsilon(k)+a(k))}} \end{bmatrix}. \tag{D.29}$$

Finally, this allows us to rewrite the Hamiltonian as

$$H = -\sum_k \begin{bmatrix} d_k^\dagger & d_{-k} \end{bmatrix} U(k) D(k) U^\dagger(k) \begin{bmatrix} d_k \\ d_{-k}^\dagger \end{bmatrix}. \tag{D.30}$$

If we now redefine the new fermionic operators f as

$$U^\dagger(k) \begin{bmatrix} d_k \\ d_{-k}^\dagger \end{bmatrix} \equiv \begin{bmatrix} f_k \\ f_{-k}^\dagger \end{bmatrix} \iff \begin{bmatrix} f_k \\ f_{-k}^\dagger \end{bmatrix} = U(k) \begin{bmatrix} d_k \\ d_{-k}^\dagger \end{bmatrix}, \tag{D.31}$$

we will automatically recover a Hamiltonian in the correct, diagonal form:

$$\begin{aligned} H &= -\sum_k \begin{bmatrix} f_k^\dagger & f_{-k} \end{bmatrix} D(k) \begin{bmatrix} f_k \\ f_{-k}^\dagger \end{bmatrix} \\ &= -\sum_k \left[-\epsilon(k) f_k^\dagger f_k + \epsilon(k) f_{-k} f_{-k}^\dagger \right] = -\sum_k \left[-\epsilon(k) f_k^\dagger f_k + \epsilon(-k)(1 - f_k^\dagger f_k) \right] \\ &= \sum_k \left[2\epsilon(k) f_k^\dagger f_k \right] - \sum_k \epsilon(k). \end{aligned} \tag{D.32}$$

Here, we have used the fact that the dispersion relation $\epsilon(k)$ is symmetric in k. Furthermore, in order to obtain the correct Hamiltonian of a free fermion gas, we had to exploit the fermionic anticommutator in the second line. From this diagonal form, we can easily read off all the eigenenergies of the fermionic excitations. Recall that the wavevector k can take N discrete values in the first Brillouin zone - well, for each of those k's, we know what energy we must pay to create the corresponding excitation. Hence if we know the occupation of each orbital, we can calculate the total energy in our Ising model as

$$E = 2\sum_k n_k \sqrt{J^2 - 2Jh\cos(k) + h^2}, \quad n_k \in \{0, 1\}. \tag{D.33}$$

As each k-orbital can be either occupied by a fermion or empty, we recover 2^N distinct energy configurations, as we should.

By the same token, we can read off and evaluate the ground state energy as

$$E_0 = -\sum_k \epsilon(k), \tag{D.34}$$

or, converting the discrete sum to an integral in the first Brillouin zone in the thermodynamic limit:

$$E_0 = -\frac{1}{2\pi}\int_{-\pi}^{\pi} dk\, \sqrt{J^2 - 2Jh\cos(k) + h^2}. \tag{D.35}$$

Unfortunately, this doesn't admit an exact solution, but can of course be evaluated numerically. As the ground state energy effectively only depends on the ratio J/h of the two parameters, one often considers a unit coupling of $J = 1$ and studies how the ground state energy varies with the transverse magnetic field h:

$$E_0 = -\frac{1}{2\pi}\int_{-\pi}^{\pi} dk\, \sqrt{1 + h^2 - 2h\cos(k)}. \tag{D.36}$$

E Magnetisation of the Transverse Field Ising Model

Knowledge of the relationship between spin operators and the quasiparticle operators describing the true excitations of the Ising model ($S_i \rightarrow$ Jordan-Wigner $\rightarrow$ Fourier $\rightarrow$ Bogoliubov $\rightarrow f_k$) allows us to calculate ground state expectation values. The simplest example is the magnetisation in z-direction, which we will evaluate now.

It is defined by the vacuum expectation value

$$\langle M^z \rangle = \sum_l \langle 0|S_l^z|0\rangle \,. \tag{E.1}$$

First, we rewrite $\langle M^z \rangle$ in terms of the "Jordan-Wigner-fermions" c_i and $c_i^\dagger$:

$$\langle M^z \rangle = \sum_l \Big[\langle 0|c_l c_l^\dagger|0\rangle - \langle 0|c_l^\dagger c_l|0\rangle \Big] \,. \tag{E.2}$$

Expressing the fermionic operators c_i and $c_i^\dagger$ through their momentum-space counterparts yields

$$\begin{aligned} \langle M^z \rangle &= \frac{1}{N} \sum_l \sum_{k,k'} \Big[\langle 0|e^{i(k-k')l} d_k d_{k'}^\dagger|0\rangle - \langle 0|e^{-i(k'-k)l} d_k^\dagger d_{k'}|0\rangle \Big] \\ &= \sum_k \Big[\langle 0|d_k d_k^\dagger|0\rangle - \langle 0|d_k^\dagger d_k|0\rangle \Big] = \sum_k \Big[1 - 2\langle 0|d_k^\dagger d_k|0\rangle \Big] \,. \end{aligned} \tag{E.3}$$

Now we can exploit the fact that we know the decomposition of the momentum space fermions d_k and $d_k^\dagger$ in terms of the fundamental excitations of the Ising model:

$$d_k = -\frac{i\sqrt{a(k)-\epsilon(k)}}{\sqrt{2\epsilon(k)}} f_k + \frac{b(k)}{\sqrt{2\epsilon(k)(\epsilon(k)-a(k))}} f_{-k}^\dagger \equiv -iu(k) f_k + v(k) f_{-k}^\dagger. \tag{E.4}$$

Plugging this in the ground state expectation value $\langle 0|d_k^\dagger d_k|0\rangle$ gives

$$\begin{aligned} \langle 0|d_k^\dagger d_k|0\rangle &= \langle 0| \Big[iu(k) f_k^\dagger + v(k) f_{-k} \Big] \Big[-iu(k) f_k + v(k) f_{-k}^\dagger \Big] |0\rangle \\ &= u^2(k) \langle 0|f_k^\dagger f_k|0\rangle + iu(k)v(k) \Big(\langle 0|f_k^\dagger f_{-k}^\dagger|0\rangle - \langle 0|f_{-k} f_k|0\rangle \Big) + v^2(k) \langle 0|f_{-k} f_{-k}^\dagger|0\rangle \\ &= v^2(k) \langle 0|f_{-k} f_{-k}^\dagger|0\rangle \,, \end{aligned} \tag{E.5}$$

as the three other vacuum expectation values immediately evaluate to zero. This allows us to find the magnetisation as

$$\langle M^z \rangle = \sum_k \left[1 - 2\frac{b^2(k)}{2\epsilon(k)(\epsilon(k)-a(k))} \right] = -\sum_k \frac{a(k)}{\epsilon(k)} = \sum_k \frac{h - J\cos(k)}{\sqrt{J^2 - 2Jh\cos(k) + h^2}}. \tag{E.6}$$

In order to be able to evaluate the sum over k, we transform it to an integral in the thermodynamic limit:

$$\langle M^z \rangle = \frac{1}{2\pi} \int_{-\pi}^{\pi} dk \, \frac{h - J\cos(k)}{\sqrt{J^2 - 2Jh\cos(k) + h^2}} = \frac{1}{\pi} \int_0^{\pi} dk \, \frac{1 - \frac{J}{h}\cos(k)}{\sqrt{1 - \frac{2J}{h}\cos(k) + \left(\frac{J}{h}\right)^2}}. \tag{E.7}$$

This integral can be calculated numerically, in exact analogy to the ground state energy.

F Programming with Matrix Product States

In this chapter of the appendix, we will provide some details about the coding practices employed in this work, to help the reader in setting up their own tensor network algorithms. As the manipulation of tensor networks, and in particular MPS, builds on (multi-)linear-algebraic operations with matrices and tensors, in principle any programming language with an interface to linear algebra-libraries will be a suitable pick. Common choices include MATLAB, Python, Julia and C++. For our work, we have decided to employ Python, as one can achieve reasonably fast performances due to vectorised operations in the `numpy` and `scipy` libraries, while retaining a high-level user interface. Furthermore, due to a plethora of other existing modules, it is easy to incorporate other functionalities in our code.

The fundamental objects of our work are of course MPS and MPOs. Both are initialised as lists of tensors of the required dimensions, which are `numpy`-arrays. An easy way to build a "dummy" MPS is to initialise some random tensors of dimensions (D, d, D) and to save them in a corresponding list:

```
import numpy as np
M = [np.random.rand(D,d,D) for i in range(N)]
```

Here, D is the bond dimension, d the physical dimension and N the number of desired tensors. It is easy to adapt the above for-loop to take care of the boundary tensors, which can carry a dummy index. While is seems straightforward in the above example, one common source of mistakes is a mismatch between the "tensor leg" one desires to perform an operation with, and its position within the numerical multi-dimensional array. It is therefore customary to indicate the intended leg order in one's code:

```
# index ordering and contraction pattern

#  1 - --- M - --- 3    .............           -1 --- M --- -5
#          |                                        |
#          |                                        |
#          2                                        |
#                                                1  |
#          4                                        |
#          |                                        |
#          |                                        |
#  1 - --- O - --- 3    .............          -2  --- O --- -4
#          |                                        |
#          |                                        |
#          2                                       -3
```

The above snippet represents the contraction of an MPO-tensor O with an MPS-tensor M. On the left, we have indicated the order in which the different legs are initialised: we start on the left and then proceed counter-clockwise. This is however not the only convention in use; hence it is crucial to be aware of it. The right half pictures the contracted

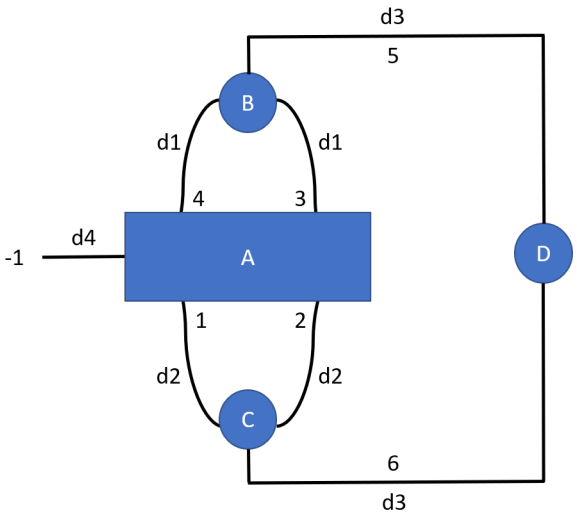

Figure 65: Tensor network with four different tensors. Shows how to set up the contraction of a given tensor network numerically: the d's are the dimensions of each leg/bond, the numbers implement the contraction pattern.

network. Using negative indices is related to the function performing the contraction, and further explained below.

Central operation with tensors in MPS are SVDs and contractions. To perform SVDs, one often needs to reshape the given tensor in order to bring it in matrix form:

```
T = np.random.rand(D,d,D)
T = T.reshape(D, D*d)
```

In the above case, one can picture the reshaping as "flipping the basis leg to the right bond". Then, we can perform an SVD:

```
from numpy import linalg as LA
U, S, V_herm = LA.svd(T, full_matrices=False)
```

Truncating the matrices is then a simple exercise in correct indexing:

```
U = U[:, :n]
S = S[:n]
V_herm = V_herm[:n, :]
```

where n is some number which defines how many singular values one desires to keep (which should be less than or equal to the number of diagonal elements of S, of course). To find the lowest eigenvalues of a given matrix, we use the Lanczos algorithm as it is implemented in `scipy.sparse.linalg.eigsh`:

```
from scipy.sparse.linalg import eigsh
E, v = eigsh(H, k=1, which="SA", v0=v0)
```

In this code snippet, we assume that a linear operator H and an initial guess for the eigenvector v_0 are given. The function then returns (an approximation of) the eigenvector

belonging to the smallest algebraic ("SA") eigenvalue, and the corresponding list of eigenvalues (which is here of course of length one).

Finally, in order to contract any number of tensors, we employ the `ncon` (cf. ref. [91]) function, which has been specifically designed for this task. As inputs for `ncon`, we have to supply a list of tensors and the contraction pattern we want to apply. This is best understood with an explicit example, such as the network shown in fig. 65. We explicitly initialise the tensors with different leg dimensions, to highlight the importance of the fact that only legs of the same dimension can be contracted. The `ncon` function the takes the list of tensors as first input, and a list of the contraction patterns as second input:

```
# define local dimensions and tensors
d1 = 2
d2 = 3
d3 = 4
d4 = 5
A = np.random.rand(d2,d2,d1,d1,d4)
B = np.random.rand(d1,d3,d1)
C = np.random.rand(d2,d3,d2)
D = np.random.rand(d3,d3)

# contract network
TN_con = ncon([A,B,C,D], [[1,2,3,4,-1], [4,5,3], [1,6,2], [5,6]])
#              tensors     A-sequence   B-seq.   C-seq.   D-seq.
```

Positive indices are contracted, and therefore appear exactly twice in the second argument, and negative indices remain open (and thus appear once). Consider for instance the first index of tensor A, which is connected to the first index of tensor C: both have been initialised with a dimension of d_2, and therefore represent a valid contraction.

All of the algorithms developed in this thesis use the few basic principles presented above, albeit embedded in more complex loop structures.

G Exact Diagonalisation Methods

In the context of this thesis, we have used exact diagonalisation methods in various places, most notably to benchmark our MPS-algorithms. The goal of this section is to summarise several facts about exact diagonalisation, in the hope that the reader can profit from it to quickly produce their own algorithms. Many more details can be found in ref. [92].

G.1 Building a Hamiltonian Matrix

Central to an exact diagonalisation is of course a construction of a matrix representation of the operator to be diagonalised. Below, we show how such a construction can be easily achieved, using the ubiquitous example of the transverse field Ising model. As a reminder, the Ising chain of length N is defined through

$$H = J\sum_{i=1}^{N} S_i^x S_{i+1}^x - h\sum_{i=1}^{N} S_i^z, \quad S_{N+1}^x \equiv S_1^x. \tag{G.1}$$

Here, we have used periodic boundary conditions which effectively creates an "Ising ring". In principle, it would be straightforward to implement the matrix representation of this Hamiltonian by separately evaluating the tensor products (which the above notation has efficiently swept under rug). For a chain of length $N = 4$, we have for instance

$$\begin{aligned} H = &- J[S_1^x \otimes S_2^x \otimes E_3 \otimes E_4 + E_1 \otimes S_2^x \otimes S_3^x \otimes E_4 + E_1 \otimes E_2 \otimes S_3^x \otimes S_4^x \\ &+ S_1^x \otimes E_2 \otimes E_3 \otimes S_4^x] \\ &- h[S_1^z \otimes E_2 \otimes E_3 \otimes E_4 + E_1 \otimes S_2^z \otimes E_3 \otimes E_4 + E_1 \otimes E_2 \otimes S_3^z \otimes E_4 \\ &+ E_1 \otimes E_2 \otimes E_3 \otimes S_4^z] \end{aligned} \tag{G.2}$$

The key to implementing this matrix efficiently (and for any more general case) is to realise that we only need to deal with operator strings of the type

$$S_j^i \equiv E_1 \otimes ... \otimes E_{j-1} \otimes S^i \otimes E_{j+1} \otimes ... \otimes E_N, \tag{G.3}$$

This expression is ready-made for single-site couplings to external fields. However, it also allows us to easily obtain spin-spin couplings, by observing that multiplications of tensor product operators are evaluated separately in every constituent space, e.g.

$$\begin{aligned} S_j^i S_{j+1}^i &= \big(E_1 \otimes ... \otimes E_{j-1} \otimes S^i \otimes E_{j+1} \otimes E_{j+2} \otimes ... \otimes E_N\big) \\ &\quad \big(E_1 \otimes ... \otimes E_{j-1} \otimes E_j \otimes S_{j+1}^i \otimes E_{j+2} \otimes ... \otimes E_N\big) \\ &= E_1 \otimes ... \otimes E_{j-1} \otimes S_j^i \otimes S_{j+1}^i \otimes E_{j+2} \otimes ... \otimes E_N \end{aligned} \tag{G.4}$$

It is easy to generate operator strings such as $E_1 \otimes ... \otimes E_{j-1} \otimes S^i \otimes E_{j+1} \otimes ... \otimes E_N$ with a for loop; all that is then left to do to obtain the matrix representation of the Hamiltonian is to multiply, weigh and add those operator strings accordingly. Needless to say, this method is of course not restricted to Hamiltonians, but can be used to generate any operator based on the tensor product of spin operators.

A slightly more efficient way of dealing with large matrices - especially if they contain many zero-entries - is provided by **sparse matrices**, whose properties are summarised below. All calculations in this thesis based on exact diagonalisation have been performed using sparse matrices.

Aside - Sparse matrices

If a matrix contains many zero entries, it becomes numerically inefficient to save every entry of the corresponding array. Instead, one can use so-called **sparse matrices**, such as provided by the `scipy.sparse.csr_matrix` class. The idea of sparse matrices is that instead of all elements, the computer only saves the non-zero or non-trivial elements. For instance, the sparse matrix representation of the Pauli z-gate would be

$$\sigma_z = \begin{bmatrix} 1 & 0 \\ 0 & -1 \end{bmatrix} \iff (0,0) : 1,\ (1,1) : -1. \tag{G.5}$$

This example is of course merely illustrates the principle. If however one builds large Hamiltonian matrices, the sparse matrix structure will lead to a significant performance gain.

G.2 Working with Exact Diagonalisation

Once we have implemented the Hamiltonian, it is easy to diagonalise it using standard linear algebra tools. While a full diagonalisation is of course possible, it is often not necessary (nor practical in terms of run time). Especially for ground state searches, it is far more efficient to target the lowest energy state(s) explicitly, by using an algorithm such as the Lanczos scheme. The ground state and ground state energy for a Hamiltonian H can then be found simply as

```
from scipy.sparse.linalg import eigsh
E0, v0 = eigsh(H, k=1, which='SA')
```

Computations with these states then become a straightforward application of the manipulation of `numpy` arrays. A standard ground state expectation value $\langle 0|A|0\rangle$ of the operator A can be simply expressed as

```
import numpy as np
a = np.vdot(v0, A.dot(v0))
```

Pay special attention to using the complex scalar product in `numpy`, as this is indispensable for the correct physical results.

It is equally straightforward to set up the kernel polynomial method based on exact diagonalisation instead of MPS, as the central recursion relations defining the Chebyshev moments are general vector equations whose validity doesn't depend on the representation of the vectors. All that is left to do - after the ground state of a Hamiltonian H has been found, and the Hamiltonian properly rescaled - is to translate the recursion relations

$$|t_n\rangle = 2H^{\text{res}} |t_{n-1}\rangle - |t_{n-2}\rangle , \quad |t_0\rangle = C |0\rangle , \quad |t_1\rangle = H^{\text{res}} |t_0\rangle . \tag{G.6}$$

into the appropriate language of arrays, e.g. as

```
t0 = C_op.dot(G)
t1 = H.dot(t0)
Cheb_vectors = [t1, t0]
for i in range(2, Ncheby):
    Cheb_vectors.append(2*H.dot(Cheb_vectors[i-1]) - Cheb_vectors[i-2])
```

Then the Chebyshev moments

$$\mu_n = \langle 0|B|t_n\rangle \tag{G.7}$$

can easily be determined as

```
G_B = B_op.dot(G)
Cheb = np.zeros(Ncheby)
for i in range(Ncheby):
    Cheb[i] = np.vdot(G_B, Cheb_vectors[i])
```

Once those calculations have run, the spectral function is determined with the same code regardless of whether exact diagonalisation or MPS-methods have been used, as it only requires the Chebyshev moments as input.

Finally, let us mention how to find the reduced density matrix of, say, the first L spins of a spin-$1/2$ chain of length N. Denoting those L spins as the subsystem A, and the rest of the chain as subsystem B, an arbitrary quantum state is given by

$$|\psi\rangle \equiv \sum_{i\in A}\sum_{i'\in B} c_{ii'} |i\rangle |i'\rangle \iff \rho = \sum_{i,j\in A}\sum_{i',j'\in B} c_{ii'}c^*_{jj'} |i\rangle |i'\rangle \langle j| \langle j'| . \tag{G.8}$$

The reduced density matrix follows as

$$\begin{aligned} \rho^L = \text{Tr}_B(\rho) &= \sum_{k\in B} \langle k| \left[\sum_{i,j\in A}\sum_{i',j'\in B} c_{ii'}c^*_{jj'} |i\rangle |i'\rangle \langle j| \langle j'|\right] |k\rangle \\ &= \sum_{i,j\in A}\left[\sum_{k\in B} c_{ii'}c^*_{jj'}\delta_{ki'}\delta_{kj'}\right] |i\rangle \langle j| = \sum_{i,j\in A}\left[\sum_{k\in B} c_{ik}\left(c^\dagger\right)_{kj}\right] |i\rangle \langle j| . \end{aligned} \tag{G.9}$$

We therefore recognise the matrix elements of the reduced density matrix as a matrix multiplication of the expansion coefficients of $|\psi\rangle$. This can therefore be implemented by

simply reshaping the wave function into a matrix, and doing the corresponding multiplication:

```
psi = np.reshape(psi, (2**L, 2**(N-L)))
rho_L = psi@np.conj(psi.T)
```

Finding the spectrum of the reduced density matrix, and therefore the entanglement entropy, is then a straightforward application of a standard eigensolver:

```
from numpy.linalg import eig
u, v = eig(rho_L)
S_vN = np.sum(-u[u > 0]*np.log2(u[u > 0]))
```

Despite the density matrix being a positive matrix, requiring $u > 0$ protects against numerical errors related to evaluating the logarithm for a very small (or zero) number.

List of Figures

List of Tables

References

[1] A. Mourachkine. *Room-Temperature Superconductivity*. 2006. arXiv: cond-mat/0606187v1 [cond-mat].

[2] Masatoshi Sato and Yoichi Ando. "Topological superconductors: a review". In: *Reports on Progress in Physics* 80.7 (2017), p. 076501. DOI: 10.1088/1361-6633/aa6ac7.

[3] Xiao-Liang Qi and Shou-Cheng Zhang. "Topological insulators and superconductors". In: *Rev. Mod. Phys.* 83 (4 2011), pp. 1057–1110. DOI: 10.1103/RevModPhys.83.1057.

[4] A Yu Kitaev. "Unpaired Majorana fermions in quantum wires". In: *Physics-Uspekhi* 44.10S (2001), pp. 131–136. DOI: 10.1070/1063-7869/44/10s/s29.

[5] Roman M. Lutchyn, Jay D. Sau and S. Das Sarma. "Majorana Fermions and a Topological Phase Transition in Semiconductor-Superconductor Heterostructures". In: *Phys. Rev. Lett.* 105 (7 2010), p. 077001. DOI: 10.1103/PhysRevLett.105.077001.

[6] Yuval Oreg, Gil Refael and Felix von Oppen. "Helical Liquids and Majorana Bound States in Quantum Wires". In: *Phys. Rev. Lett.* 105 (17 2010), p. 177002. DOI: 10.1103/PhysRevLett.105.177002.

[7] Michael A. Nielsen and Isaac L. Chuang. *Quantum Computation and Quantum Information: 10th Anniversary Edition*. Cambridge University Press, 2010. DOI: 10.1017/CBO9780511976667.

[8] Bei Zeng et al. *Quantum Information Meets Quantum Matter*. Springer-Verlag, 2019. DOI: 10.1007/978-1-4939-9084-9.

[9] M. Hastings. "An Area Law for One Dimensional Quantum Systems". In: *Journal of Statistical Mechanics Theory and Experiment* 2007 (May 2007). DOI: 10.1088/1742-5468/2007/08/P08024.

[10] M. Fannes, B. Nachtergaele and R. F. Werner. "Finitely correlated states on quantum spin chains". In: *Communications in Mathematical Physics* 144.3 (1992), pp. 443 –490. DOI: 10.1007/BF02099178.

[11] Stellan Östlund and Stefan Rommer. "Thermodynamic Limit of Density Matrix Renormalization". In: *Phys. Rev. Lett.* 75 (19 1995), pp. 3537–3540. DOI: 10.1103/PhysRevLett.75.3537.

[12] Ulrich Schollwöck. "The density-matrix renormalization group in the age of matrix product states". In: *Annals of Physics* 326.1 (2011). January 2011 Special Issue, pp. 96–192. ISSN: 0003-4916. DOI: https://doi.org/10.1016/j.aop.2010.09.012.

[13] Guifré Vidal. "Efficient Simulation of One-Dimensional Quantum Many-Body Systems". In: *Phys. Rev. Lett.* 93 (4 2004), p. 040502. DOI: 10.1103/PhysRevLett.93.040502.

[14] Alexander Weiße et al. "The kernel polynomial method". In: *Rev. Mod. Phys.* 78 (1 2006), pp. 275–306. DOI: 10.1103/RevModPhys.78.275.

[15] J. Lado and M. Sigrist. "Solitonic in-gap modes in a superconductor-quantum antiferromagnet interface". In: *Physical Review Research* 2 (June 2020). DOI: 10.1103/PhysRevResearch.2.023347.

[16] John B. Parkinson and Damian J. J. Farnell. *An Introduction to Quantum Spin Systems*. Springer-Verlag Berlin Heidelberg, 2010. DOI: 10.1007/978-3-642-13290-2.

[17] "Two soluble models of an antiferromagnetic chain". In: *Annals of Physics* 16.3 (1961), pp. 407–466. ISSN: 0003-4916. DOI: https://doi.org/10.1016/0003-4916(61)90115-4.

[18] "The one-dimensional Ising model with a transverse field". In: *Annals of Physics* 57.1 (1970), pp. 79–90. ISSN: 0003-4916. DOI: https://doi.org/10.1016/0003-4916(70)90270-8.

[19] Michael Karabach et al. "Introduction to the Bethe Ansatz I". In: *Computers in Physics* 11.1 (1997), pp. 36–43. DOI: 10.1063/1.4822511.

[20] Michael Karbach, Kun Hu and Gerhard Müller. "Introduction to the Bethe Ansatz II". In: *Computers in Physics* 12.6 (1998), pp. 565–573. DOI: 10.1063/1.168740.

[21] M. Karbach, Kun Hu and G. Muller. *Introduction to the Bethe Ansatz III*. 2000. arXiv: cond-mat/0008018v1 [cond-mat].

[22] José Latorre, Enrique Rico Ortega and Gustavo Vidal. "Ground state entanglement in quantum spin chains". In: *Quantum Information and Computation* 4 (May 2003). DOI: 10.26421/QIC4.1-4.

[23] G. Vidal et al. "Entanglement in Quantum Critical Phenomena". In: *Phys. Rev. Lett.* 90 (22 2003), p. 227902. DOI: 10.1103/PhysRevLett.90.227902.

[24] Román Orús. "A practical introduction to tensor networks: Matrix product states and projected entangled pair states". In: *Annals of Physics* 349 (2014), pp. 117–158. ISSN: 0003-4916. DOI: https://doi.org/10.1016/j.aop.2014.06.013.

[25] Jan von Delft. *Lectures on Tensor Networks, 2020*. URL: https://www.theorie.physik.uni-muenchen.de/lsvondelft/teaching/index.html. (accessed: 20.07.2021).

[26] Guifre Vidal. *Explorations in Condensed Matter, PSI 2015/16*. URL: https://pirsa.org/C15058. (accessed: 20.07.2021).

[27] Andreas Holzner et al. “Chebyshev matrix product state approach for spectral functions”. In: *Phys. Rev. B* 83 (19 2011), p. 195115. DOI: 10.1103/PhysRevB.83.195115.

[28] M. Nielsen. “The Fermionic canonical commutation relations and the Jordan-Wigner transform”. In: 2005. URL: https://www.semanticscholar.org/paper/The-Fermionic-canonical-commutation-relations-and-Nielsen/18341dd1f056fdcad2ebf4ea2df59db522e041f6.

[29] A. Rényi. “On measures of entropy and information”. In: *Proceedings of the 4th Berkeley symposium on mathematics, statistics and probability* (1960), pp. 547–561. URL: https://projecteuclid.org/proceedings/berkeley-symposium-on-mathematical-statistics-and-probability/proceedings-of-the-fourth-berkeley-symposium-on-mathematical-statistics-and/Chapter/On-Measures-of-Entropy-and-Information/bsmsp/1200512181.

[30] Stephen Blundell. *Magnetism in condensed matter*. Oxford master series in condensed matter physics. Oxford: Oxford University Press, 2001. ISBN: 0198505914. URL: https://global.oup.com/academic/product/magnetism-in-condensed-matter-9780198505914?cc=fi&lang=en&.

[31] W. Heisenberg. “Zur Theorie des Ferromagnetismus”. In: *Z. Phys.* 49.9-10 (1928), pp. 619–636. DOI: 10.1007/BF01328601.

[32] Eytan Barouch, Barry M. McCoy and Max Dresden. “Statistical Mechanics of the XY Model. I”. In: *Phys. Rev. A* 2 (3 1970), pp. 1075–1092. DOI: 10.1103/PhysRevA.2.1075.

[33] Eytan Barouch and Barry M. McCoy. “Statistical Mechanics of the XY Model. II. Spin-Correlation Functions”. In: *Phys. Rev. A* 3 (2 1971), pp. 786–804. DOI: 10.1103/PhysRevA.3.786.

[34] Eytan Barouch and Barry M. McCoy. “Statistical Mechanics of the XY Model. III”. In: *Phys. Rev. A* 3 (6 1971), pp. 2137–2140. DOI: 10.1103/PhysRevA.3.2137.

[35] Barry M. McCoy, Eytan Barouch and Douglas B. Abraham. “Statistical Mechanics of the XY Model. IV. Time-Dependent Spin-Correlation Functions”. In: *Phys. Rev. A* 4 (6 1971), pp. 2331–2341. DOI: 10.1103/PhysRevA.4.2331.

[36] Ernst Ising. “Beitrag zur Theorie des Ferromagnetismus”. In: *Zeitschrift fur Physik* 31.1 (Feb. 1925), pp. 253–258. DOI: 10.1007/BF02980577.

[37] J. Hubbard. “Electron Correlations in Narrow Energy Bands”. In: *Proceedings of the Royal Society of London Series A* 276.1365 (Nov. 1963), pp. 238–257. DOI: 10.1098/rspa.1963.0204.

[38] Charles L. Cleveland and Rodrigo Medina A. "Obtaining a Heisenberg Hamiltonian from the Hubbard model". In: *American Journal of Physics* 44.1 (1976), pp. 44–46. DOI: 10.1119/1.10537.

[39] H. Bethe. "Zur Theorie der Metalle". In: *Zeitschrift fur Physik* 71.3-4 (Mar. 1931), pp. 205–226. DOI: 10.1007/BF01341708.

[40] Subir Sachdev. *Quantum Phase Transitions*. 2nd ed. Cambridge University Press, 2011. DOI: 10.1017/CBO9780511973765.

[41] Pascual Jordan and Eugene P. Wigner. "About the Pauli exclusion principle". In: *Z. Phys.* 47 (1928), pp. 631–651. DOI: 10.1007/BF01331938.

[42] J. G. Valatin. "Comments on the theory of superconductivity". In: *Nuovo Cim.* 7 (1958), pp. 843–857. DOI: 10.1007/BF02745589.

[43] N. N. Bogolyubov, V. V. Tolmachev and D. V. Shirkov. "A New method in the theory of superconductivity". In: *Fortsch. Phys.* 6 (1958), pp. 605–682. DOI: 10.1002/prop.19580061102.

[44] Xu-Dong Liu and Yan He. "The Entanglement Entropy of Transverse Field Ising Model". In: *International Journal of Modern Physics and Application* 4.4 (2017), pp. 19–23. ISSN: 2375-3870. URL: http://www.aascit.org/journal/archive2?journalId=909&paperId=4922.

[45] Ettore Majorana. "Teoria simmetrica dell'elettrone e del positrone". In: *Nuovo Cim.* 14 (1937), pp. 171–184. DOI: 10.1007/BF02961314.

[46] G. C. Wick. "The Evaluation of the Collision Matrix". In: *Phys. Rev.* 80 (2 1950), pp. 268–272. DOI: 10.1103/PhysRev.80.268.

[47] Mark Srednicki. "Entropy and area". In: *Phys. Rev. Lett.* 71 (5 1993), pp. 666–669. DOI: 10.1103/PhysRevLett.71.666.

[48] Jens Eisert, Marcus Cramer and M. Plenio. "Colloquium: Area laws for the entanglement entropy". In: *Reviews of Modern Physics* 82 (Aug. 2008). DOI: 10.1103/RevModPhys.82.277.

[49] R. J. Baxter. "Dimers on a Rectangular Lattice". In: *Journal of Mathematical Physics* 9.4 (1968), pp. 650–654. DOI: 10.1063/1.1664623.

[50] Guifré Vidal. "Efficient Classical Simulation of Slightly Entangled Quantum Computations". In: *Phys. Rev. Lett.* 91 (14 2003), p. 147902. DOI: 10.1103/PhysRevLett.91.147902.

[51] Daniel M. Greenberger, Michael A. Horne and Anton Zeilinger. *Going Beyond Bell's Theorem*. 2007. arXiv: 0712.0921 [quant-ph].

[52] Gregory M. Crosswhite and Dave Bacon. "Finite automata for caching in matrix product algorithms". In: *Phys. Rev. A* 78 (1 2008), p. 012356. DOI: 10.1103/PhysRevA.78.012356.

[53] C. Hubig, I. P. McCulloch and U. Schollwöck. "Generic construction of efficient matrix product operators". In: *Phys. Rev. B* 95 (3 2017), p. 035129. DOI: 10.1103/PhysRevB.95.035129.

[54] B Pirvu et al. "Matrix product operator representations". In: *New Journal of Physics* 12.2 (2010), p. 025012. DOI: 10.1088/1367-2630/12/2/025012.

[55] Paul Gagniuc. *Markov Chains: From Theory to Implementation and Experimentation*. May 2017. ISBN: 978-1-119-38755-8. DOI: 10.1002/9781119387596.

[56] Steven R. White. "Density matrix formulation for quantum renormalization groups". In: *Phys. Rev. Lett.* 69 (19 1992), pp. 2863–2866. DOI: 10.1103/PhysRevLett.69.2863.

[57] Steven R. White. "Density-matrix algorithms for quantum renormalization groups". In: *Phys. Rev. B* 48 (14 1993), pp. 10345–10356. DOI: 10.1103/PhysRevB.48.10345.

[58] U. Schollwöck. "The density-matrix renormalization group". In: *Rev. Mod. Phys.* 77 (1 2005), pp. 259–315. DOI: 10.1103/RevModPhys.77.259.

[59] J Dukelsky et al. "Equivalence of the variational matrix product method and the density matrix renormalization group applied to spin chains". In: 43.4 (1998), pp. 457–462. DOI: 10.1209/epl/i1998-00381-x.

[60] Sebastian Paeckel et al. "Time-evolution methods for matrix-product states". In: *Annals of Physics* 411 (2019), p. 167998. ISSN: 0003-4916. DOI: https://doi.org/10.1016/j.aop.2019.167998.

[61] Cornelius Lanczos. "An iteration method for the solution of the eigenvalue problem of linear differential and integral operators". In: *J. Res. Natl. Bur. Stand. B* 45 (1950), pp. 255–282. DOI: 10.6028/jres.045.026.

[62] Joshua Izaac and Jingbo Wang. *Computational Quantum Mechanics*. Springer International Publishing, 2018. DOI: 10.1007/978-3-319-99930-2.

[63] S. Ramasesha et al. "Low-lying electronic excitations and nonlinear optic properties of polymers via symmetrized density matrix renormalization group method". In: *Synthetic Metals* 85.1 (1997), pp. 1019–1022. ISSN: 0379-6779. DOI: https://doi.org/10.1016/S0379-6779(97)80136-1.

[64] Steven R. White and Adrian E. Feiguin. "Real-Time Evolution Using the Density Matrix Renormalization Group". In: *Phys. Rev. Lett.* 93 (7 2004), p. 076401. DOI: 10.1103/PhysRevLett.93.076401.

[65] AJ Daley et al. "Time-dependent density-matrix renormalization-group using adaptive effective Hilbert spaces". In: *Journal of Statistical Mechanics: Theory and Experiment* 2004 (Apr. 2004). DOI: 10.1088/1742-5468/2004/04/P04005.

[66] William H. Press et al. *Numerical Recipes 3rd Edition: The Art of Scientific Computing*. USA: Cambridge University Press, 2007. ISBN: 0521880688. URL: https://www.cambridge.org/fi/academic/subjects/mathematics/numerical-recipes/numerical-recipes-art-scientific-computing-3rd-edition?format=HB&utm_source=shortlink&utm_medium=shortlink&utm_campaign=numericalrecipes.

[67] I.N. Bronshtein et al. *Handbook of mathematics, sixth edition*. Springer Verlag, Jan. 2015. ISBN: 978-3-662-46220-1. DOI: 10.1007/978-3-662-46221-8.

[68] Dunham Jackson. "On Approximation by Trigonometric Sums and Polynomials". In: *Transactions of the American Mathematical Society* 13.4 (1912), pp. 491–515. ISSN: 00029947. URL: http://www.jstor.org/stable/1988583.

[69] G. Vidal. "Class of Quantum Many-Body States That Can Be Efficiently Simulated". In: *Phys. Rev. Lett.* 101 (11 2008), p. 110501. DOI: 10.1103/PhysRevLett.101.110501.

[70] I. P McCulloch and M Gulácsi. "The non-Abelian density matrix renormalization group algorithm". In: 57.6 (2002), pp. 852–858. DOI: 10.1209/epl/i2002-00393-0.

[71] Ian McCulloch. "From density-matrix renormalization group to matrix product states". In: *J. Stat. Mech. Theory Exp* 2007 (Jan. 2007). DOI: 10.1088/1742-5468/2007/10/P10014.

[72] F. Verstraete, D. Porras and J. I. Cirac. "Density Matrix Renormalization Group and Periodic Boundary Conditions: A Quantum Information Perspective". In: *Phys. Rev. Lett.* 93 (22 2004), p. 227205. DOI: 10.1103/PhysRevLett.93.227205.

[73] Peter Pippan, Steven R. White and Hans Gerd Evertz. "Efficient matrix-product state method for periodic boundary conditions". In: *Phys. Rev. B* 81 (8 2010), p. 081103. DOI: 10.1103/PhysRevB.81.081103.

[74] B. Pirvu, F. Verstraete and G. Vidal. "Exploiting translational invariance in matrix product state simulations of spin chains with periodic boundary conditions". In: *Phys. Rev. B* 83 (12 2011), p. 125104. DOI: 10.1103/PhysRevB.83.125104.

[75] Jutho Haegeman et al. "Time-Dependent Variational Principle for Quantum Lattices". In: *Phys. Rev. Lett.* 107 (7 2011), p. 070601. DOI: 10.1103/PhysRevLett.107.070601.

[76] Maarten Van Damme et al. "Real-time scattering of interacting quasiparticles in quantum spin chains". In: *Physical Review Research* 3.1 (2021). ISSN: 2643-1564. DOI: 10.1103/physrevresearch.3.013078.

[77] Laurens Vanderstraeten et al. "Quasiparticles in Quantum Spin Chains with Long-Range Interactions". In: *Physical Review Letters* 121.9 (2018). ISSN: 1079-7114. DOI: 10.1103/physrevlett.121.090603.

[78] Ashley Milsted et al. *Collisions of false-vacuum bubble walls in a quantum spin chain*. 2021. arXiv: 2012.07243 [quant-ph].

[79] Amandeep Singh Bhatia and Mandeep Kaur Saggi. *Implementing Entangled States on a Quantum Computer*. 2019. arXiv: 1811.09833 [quant-ph].

[80] F. Barratt et al. "Parallel quantum simulation of large systems on small NISQ computers". In: *npj Quantum Information* 7.1 (2021). ISSN: 2056-6387. DOI: 10.1038/s41534-021-00420-3.

[81] Shi-Ju Ran. "Encoding of matrix product states into quantum circuits of one- and two-qubit gates". In: *Phys. Rev. A* 101 (3 2020), p. 032310. DOI: 10.1103/PhysRevA.101.032310.

[82] G. Vidal. "Classical Simulation of Infinite-Size Quantum Lattice Systems in One Spatial Dimension". In: *Phys. Rev. Lett.* 98 (7 2007), p. 070201. DOI: 10.1103/PhysRevLett.98.070201.

[83] I. P. McCulloch. *Infinite size density matrix renormalization group, revisited*. 2008. arXiv: 0804.2509 [cond-mat.str-el].

[84] "Fractal decomposition of exponential operators with applications to many-body theories and Monte Carlo simulations". In: *Physics Letters A* 146.6 (1990), pp. 319–323. ISSN: 0375-9601. DOI: https://doi.org/10.1016/0375-9601(90)90962-N.

[85] Masuo Suzuki. "General theory of fractal path integrals with applications to many-body theories and statistical physics". In: *Journal of Mathematical Physics* 32.2 (1991), pp. 400–407. DOI: 10.1063/1.529425.

[86] F. Verstraete, J. J. García-Ripoll and J. I. Cirac. "Matrix Product Density Operators: Simulation of Finite-Temperature and Dissipative Systems". In: *Phys. Rev. Lett.* 93 (20 2004), p. 207204. DOI: 10.1103/PhysRevLett.93.207204.

[87] Adrian E. Feiguin and Steven R. White. "Finite-temperature density matrix renormalization using an enlarged Hilbert space". In: *Phys. Rev. B* 72 (22 2005), p. 220401. DOI: 10.1103/PhysRevB.72.220401.

[88] Michael Zwolak and Guifré Vidal. "Mixed-State Dynamics in One-Dimensional Quantum Lattice Systems: A Time-Dependent Superoperator Renormalization Algorithm". In: *Phys. Rev. Lett.* 93 (20 2004), p. 207205. DOI: 10.1103/PhysRevLett.93.207205.

[89] Claudio Altafini. "Representing multiqubit unitary evolutions via Stokes tensors". In: *Phys. Rev. A* 70 (3 2004), p. 032331. DOI: 10.1103/PhysRevA.70.032331.

[90] Claudio Altafini. "Commuting multiparty quantum observables and local compatibility". In: *Physical Review A* 72 (May 2005). DOI: 10.1103/PhysRevA.72.012112.

[91] Robert N. C. Pfeifer et al. *NCON: A tensor network contractor for MATLAB*. 2015. arXiv: 1402.0939 [physics.comp-ph].

[92] Anders Sandvik. "Computational Studies of Quantum Spin Systems". In: *AIP Conference Proceedings* 1297 (Jan. 2011). DOI: 10.1063/1.3518900.